Aston University

Some pages of this thesis may have been removed for copyright restrictions.

If you have discovered material in Aston Research Explorer which is unlawful e.g. breaches copyright, (either yours or that of a third party) or any other law, including but not limited to those relating to patent, trademark, confidentiality, data protection, obscenity, defamation, libel, then please read our Takedown policy and contact the service immediately (openaccess@aston.ac.uk)

SEPARATION OF N-PARAFFINS BY SELECTIVE ADSORPTION

BY

ALI MOHAMMED AL-DAMKHI

A Thesis Submitted to the University of Aston in Birmingham for the degree of Doctor of Philosophy

Department of Chemical Engineering
University of Aston in Birmingham

January 1986

ACKNOWLEDGEMENTS

I wish to express my deepest gratitude to Professor G.V. Jeffreys for his supervision, valuable guidance and advice.

Thanks are due to Dr. C.J. Mumford for his constructive criticism and supervision, and to Dr. R.S. Al-Ameeri for his kind supervision throughout the study.

The sincere gratitude and thanks are extended to Dr. Abdul Rahman Al-Awadi, Minister of Public Health and Planning, Mr. Ibrahim M. Hadi, the Director of EPD, Dr. Mostafa El Desouky, the Technical Advisor to EPD, and Dr. Mahmood Yousef, Deputy Director of EPD, for their encourangement without which the performance of this work would not have been possible.

The continuous encourangement of His Excellency Sheikh Salem Al-Ali Al-Sabah, Chief of the National Guard, is highly appreciated.

Special thanks are due to Dr. Fathi Owaysi of KISR for his kind cooperation and valuable comments throughout the study, to Prof. Mohammed Fahim for his valuable suggestions, and to Eng. Imad Abu Naba'a of KISR for his assistance.

My deepest thanks and appreciation are presented to the late Director of EPD, Mr. Mejren Al-Shallal for his approval of the scholarship, before his untimely death.

Thanks are also extended to all members of the EPD, and especially to Mr. Adel Al-Natour, for his continuous help and to Mr. P. Chandran for his neat typing and exacting of the text.

To My Beloved Country, KUWAIT

My Parents, Wife, and Lovely Daughters

Isra'a and Tahani

THE UNIVERSITY OF ASTON IN BIRMINGHAM

"Separation of n-Paraffins by Selective Adsorption"

Ali Mohammed Al-Damkhi

Ph.D. January 1986

SUMMARY

A study has been undertaken of the vapor-phase adsorptive separation of n-alkanes from Kuwait kerosene (Kuwait National Petroleum Company, heavy kerosene) using zeolite molecular sieves.

Due to the shortage of information on the adsorption of multicomponent systems in the open literature, the present investigation was initiated to study the effect of feed flowrate, temperature, and zeolite particle size on the height of mass transfer zone (MTZ) and the dynamic capacity of the adsorbent for multicomponent n-alkanes adsorption on a fixed-bed of zeolite type-5A. The optimum operating conditions for separation of the n-alkanes has been identified so that the effluent would also be of marketable quality. The effect of multicycle adsorption-desorption stages on the dynamic behaviour of zeolite using steam as a desorbing agent has been studied and compared with n-pentane and n-hexane as desorbing agents.

The separation process comprised one cycle of adsorption using a fixed-bed of zeolite type-5A. The bed was fed with vaporized kerosene until saturation had been achieved whereby the n-alkanes were adsorbed and the denormalized material eluted. The process of adsorption-desorption was carried out isobarically at one atmosphere.

A mathematical model has been developed to predict the breakthrough time using the method of characteristics. The results were in a reasonable agreement with the experimental values. This model has also been utilized to develop the equilibrium isotherm.

Optimum operating conditions were achieved at a feed flowrate of 33.33×10^{-9} m^3/s, a temperature of 643 K, and a particle size of $(1.0 - 2.0) \times 10^{-3}$ m. This yielded an HMTZ value and a dynamic capacity of 0.206 m and 9.653×10^{-2} kg n-alkanes/kg of zeolite respectively. These data will serve as a basis for design of a commercial plant. The purity of liquid-paraffin product desorbed using steam was 83.24 wt%. The dynamic capacity was noticed to decrease sharply with the cycle number, without intermediate reactivation of zeolite, while it was kept unchanged by intermediate reactivation. Normal hexane was found to be the best desorbing agent, the efficiency of which was mounted to 88.2%.

Key words: Normal Alkanes
Adsorption
Molecular Sieve
Normal Paraffins
Zeolite

CONTENTS

		Page
CHAPTER 1	INTRODUCTION	1
CHAPTER 2	APPLICATION AND PROPERTIES OF NORMAL-PARAFFINS	6
2.1.	Introduction	6
2.2.	Physical Properties	6
2.3.	Chemical Structure	11
2.3.1.	Normal-Alkanes	12
2.3.2.	Iso-Alkanes and Naphthenes	12
2.3.3.	Aromatic Hydrocarbons	13
2.3.4.	Sulphur-Organic Compounds	16
2.4.	Application of Normal-Paraffins	16
CHAPTER 3	ZEOLITE MOLECULAR SIEVE	24
3.1.	Introduction	24
3.2.	Historical Background	24
3.3.	Zeolite Crystal Structure	25
3.4.	Classification of Zeolite	33
3.5.	Physico-Chemical Properties	34
3.6.	Industrial Applications of Zeolite	38
3.6.1.	Zeolite as Adsorbent	38
3.6.2.	Zeolite as Catalysts	44
3.6.3.	Zeolite as Ion Exchangers	45
3.7.	Uses of Zeolite in Industrial Processes	45
3.7.1.	Drying of Gases and Liquids	46
3.7.2.	Separation and Purification of Industrial Streams	47
3.7.2.1.	Purification of Air Prior to Liquefaction	47
3.7.2.2.	Natural Gas Purification	48
3.7.2.3.	Oxygen Enrichment of Air	48
3.7.3.	Pollution Control Applications	49
3.7.4.	Nonregenerative Applications	50
3.7.5.	Hydrocarbon Separation Processes	51

		Page
3.7.5.1.	N-Paraffins Separation	51
3.7.5.2	p-Xylene Separation (V.O.P.'s Parex Process)	53
3.7.2.3.	Olefin Separation (U.O.P.'s Olex Process)	53
CHAPTER 4	NORMAL PARAFFINS SEPARATION METHODS	55
4.1.	Introduction	55
4.2.	Alternative Separation Methods	55
4.2.1.	Separation by Fractional Distillation	55
4.2.2.	Separation by Fractional Crystallization	56
4.2.3.	Separation by Elution Chromatography	57
4.2.4.	Separation by Thin Layer Chromatography	58
4.2.5.	Separation by Adduct Formation with Urea	58
4.3.	Separation by Adsorption on Molecular Sieves	62
CHAPTER 5	NORMAL PARAFFINS SEPARATION BY ADSORPTION ON ZEOLITE	66
5.1.	Commercial Separation Processes	66
5.2.	Normal Paraffins Adsorption Studies on Zeolite	70
CHAPTER 6	ADSORPTION DESIGN THEORY	81
6.1.	Introduction	81
6.2.	Mass-Transfer Front	82
6.3.	Bed Breakthrough	85
6.4.	Analyzing Column Operation	86
6.5.	Resistance to Mass Transfer	87
6.6.	Analyzing Mass-Transfer Waves	88
6.7.	Assumptions of the Model	90
6.8.	Mathematics of the Model	91
6.9.	Analyzing Commercial Units	97
6.10.	Heat Effects and Space Velocity	100
6.11.	Development of a Mathematical Model	101
CHAPTER 7	MATERIALS AND EXPERIMENTAL APPARATUS	107
7.1.	Materials	107
7.1.1.	Molecular Sieve Adsorbent	107

		Page
7.1.2.	The Hydrocarbon Feed	108
7.1.3.	Desorbent Materials	108
7.2.	Experimental Apparatus	111
CHAPTER 8	EXPERIMENTAL PROCEDURES AND ANALYTICAL TECHNIQUES	118
8.1.	Molecular Sieves Preparation Procedures	118
8.2.	Adsorption Separation Process Procedures	119
8.3.	Desorption Process Procedures	122
8.4.	Multi-cycle Adsorption Process	124
8.4.1.	Multi-cycle Adsorption without Intermediate Reactivation of Zeolite	124
8.4.2.	Multi-cycle Adsorption with Intermediate Reactivation of Zeolite	124
8.5.	Analysis of Hydrocarbon Fractions	125
8.5.1.	N-Alkanes Analysis by Gas-Liquid Chromatography	125
8.5.2.	Aromatic Hydrocarbon Analysis by Ultra-Violet Spectrophotometry	130
CHAPTER 9	RESULTS AND DISCUSSIONS	134
9.1.	One Cycle Adsorption Processes	134
9.2.	Multicycle Adsorption Processes	181
9.3.	Desorption Processes	189
9.4.	Analysis	199
9.5.	Mathematical Modelling	214
CONCLUSIONS		**220**
RECOMMENDATIONS FOR FURTHER WORK		**224**
APPENDICES		**226**
NOMENCLATURE		**301**
LIST OF REFERENCES		**306**

LIST OF FIGURES

		Page
Figure 1.1	Sterioscan/microphotograph of the structure of Zeolite Type-5A.	5
Figure 2.1.	Applications of Liquid Paraffins for Production of Surfactants, Detergents and Others.	17
Figure 3.1.	Line Drawings of 5A-Zeolite Framework.	28
Figure 3.2.	Position of the Silicon and Aluminum Atoms in the Basic Truncated Octahedron Cell of the Molecular Sieves.	31
Figure 3.3.	Position of the Silicon and Aluminum Atoms in Type A Molecular Sieves.	32
Figure 3.4.	Typical Adsorption and Desorption Isotherms for Water Vapor on Molecular Sieve, Silica Gel, and Alumina.	40
Figure 4.1.	Method for Separation of the n-Alkanes and iso-Alkanes Content in Macrocrystalline and Microcrystalline Paraffin Waxes by Urea Adduct.	60
Figure 6.1.	Analysis of Adsorbent and Effluent from Adsorption Column Operation.	83
Figure 6.2.	Stoichiometric Front Used to Analyze Real Mass-Transfer Fronts.	89
Figure 6.3A.	Progress of a Stable Mass-Transfer Front Through an Adsorbent Bed.	92
Figure 6.3B.	Progress of the Stoichiometric Front Through an Adsorbent Bed.	93

		Page
Figure 6.3C.	Position of the Stoichiometric Front Relative to the Stable Mass-Transfer Front During Dynamic Adsorption.	94
Figure 6.4.	The Relationship Between the Relative Bed Length and the Use of Total Bed Equilibrium Capacity.	99
Figure 6.5.	Material Mass Balance around an element of the Adsorption Column	106
Figure 7.1.	Schematic Diagram of the Experimental Apparatus.	113
Figure 7.2.	Photograph of the Experimental Apparatus.	116
Figure 7.3..	Photograph of the Molecular Sieve Adsorbent Type-5A Used in This Study.	117
Figure 8.1.	Calibration Between Pump Efficiency and Actual Flowrate.	121
Figure 8.2.	Schematic Diagram of the GLC Used for Determination of n-Paraffins Content.	127
Figure 8.3.	UV-Spectra for Heavy Kerosene.	133
Figure 9.1.	Agreement Between n-Paraffins Concentration as Determined by GLC and Refractive Index Reading @ 298 K (25°C).	136
Figure 9.2.	Calibration Curve Between Refractive Index Reading @ 298 K and n-Paraffins Concentration as Determined by GLC.	137
Figure 9.3.	BT-Curve of Adsorption of n-Paraffins from HK by Zeolite Type-5A at a Feed Flowrate of 16.66×10^{-9} m^3/s, a Temperature of 643 K, and a Particle Size of $(1.0 - 2.0) \times 10^{-3}$m.	139

Page

Figure 9.4. BT-Curve of Adsorption of n-Paraffins from HK by Zeolite Type-5A at a Feed Flowrate of 22.22×10^{-9} m^3/s, a Temperature of 643 K, and a Particle Size of $(1.0 - 2.0) \times 10^{-3}$m. 140

Figure 9.5. BT-Curve of Adsorption of n-Paraffins from HK by Zeolite Type-5A at a Feed Flowrate of 33.33×10^{-9} m^3/s, a Temperature of 643 K, and a Particle Size of $(1.0 - 2.0) \times 10^{-3}$m. 141

Figure 9.6. BT-Curve of Adsorption of n-Paraffins from HK by Zeolite Type-5A at a Feed Flowrate of 44.44×10^{-9} m^3/s, a Temperature of 643 K, and a Particle Size of $(1.0 - 2.0) \times 10^{-3}$m. 142

Figure 9.7. BT-Curve of Adsorption of n-Paraffins from HK by Zeolite Type-5A at a Feed Flowrate of 50.00×10^{-9} m^3/s, a Temperature of 643 K, and a Particle Size of $(1.0 - 2.0) \times 10^{-3}$m. 143

Figure 9.8. Effect of Feed Flowrate on the BT-Curves of n-Paraffins Adsorption from HK by Zeolite Type-5A, at a Temperature of 643 K, and a Particle Size of $(1.0 - 2.0) \times 10^{-3}$m. 144

Figure 9.9. BT-Curve of Adsorption of n-Paraffins from HK by Zeolite Type-5A at a Temperature of 603 K, a Feed Flowrate of 33.33×10^{-9} m^3/s, and a Particle Size of $(1.0 - 2.0) \times 10^{-3}$m. 147

Figure 9.10. BT-Curve of Adsorption of n-Paraffins from HK by Zeolite Type-5A at a Temperature of 623 K, a Feed Flowrate of 33.33×10^{-9} m^3/s, and a Particle Size of $(1.0 - 2.0) \times 10^{-3}$m. 148

Page

Figure 9.11. BT-Curve of Adsorption of n-Paraffins from HK by Zeolite Type-5A at a Temperature of 643 K, a Feed Flowrate of 33.33 x 10^{-9} m^3/s, and a Particle Size of (1.0 - 2.0) x 10^{-3}m. 149

Figure 9.12. BT-Curve of Adsorption of n-Paraffins from HK by Zeolite Type-5A at a Temperature of 663 K, a Feed Flowrate of 33.33 x 10^{-9} m^3/s, and a Particle Size of (1.0 - 2.0) x 10^{-3}m. 150

Figure 9.13. BT-Curve of Adsorption of n-Paraffins from HK by Zeolite Type-5A at a Temperature of 683 K, a Feed Flowrate of 33.33 x 10^{-9} m^3/s, and a Particle Size of (1.0 - 2.0) x 10^{-3}m. 151

Figure 9.14. Effect of Temperature on the BT-Curves of n-Paraffins Adsorption from HK by Zeolite Type-5A at a Feed Flowrate of 33.33 x 10^{-9} m^3/s, and a Particle Size of (1.0 - 2.0) x 10^{-3}m. 152

Figure 9.15. BT-Curve of Adsorption of n-Paraffins from HK by Zeolite Type-5A at a Particle Size of (2.0 - 3.0) x 10^{-3}m, a Temperature of 643 K, and a Feed Flowrate of 33.33 x 10^{-9} m^3/s. 155

Figure 9.16. BT-Curve of Adsorption of n-Paraffins from HK by Zeolite Type-5A at a Particle Size of (0.5 - 1.0) x 10^{-3}m, a Temperature of 643 K, and a Feed Flowrate of 33.33 x 10^{-9} m^3/s. 156

Figure 9.17. BT-Curve of Adsorption of n-Paraffins from HK by Zeolite Type-5A at a Particle Size of (1.0 - 2.0) x 10^{-3}m, a Temperature of 643 K, and a Feed Flowrate of 33.33 x 10^{-9} m^3/s. 157

Page

Figure 9.18. BT-Curve of Adsorption of n-Paraffins from HK by Zeolite Type-5A at a Particle Size of $<0.5 \times 10^{-3}$m, a Temperature of 643 K, and a Feed Flowrate of 33.33×10^{-9} m^3/s. 158

Figure 9.19. Effect of Particle Size on the BT-Curves of n-Paraffin Adsorption from HK by Zeolite Type-5A, at a Feed Flowrate of 33.33×10^{-9} m^3/s, and a Temperature of 643 K. 159

Figure 9.20. The Effect of Feed Flowrate on the Dynamic Properties of Adsorption of n-Paraffins from HK by Zeolite Type-5A. 168

Figure 9.21. The Effect of Temperature on the Dynamic Properties of Adsorption of n-Paraffins from HK by Zeolite Type-5A. 169

Figure 9.22. The Effect of Particle Size on the Dynamic Properties of Adsorption of n-Paraffins from HK by Zeolite Type-5A. 170

Figure 9.23. Effect of Nitrogen Flowrate on the BT-Curve of Adsorption of n-Paraffins from HK by Zeolite Type-5A at a Feed Flowrate of 33.33×10^{-9} m^3/s, a Temperature of 643 K, and a Particle Size of $(1.0 - 2.0) \times 10^{-3}$ m. 173

Figure 9.24. Equilibrium Adsorption of Multicomponent n-Alkanes from HK by Zeolite Type-5A as Derived from the Adsorption Breakthrough Data at a Feed Flowrate of 33.33×10^{-3} m^3/s, a Temperature of 643K, and a Particle Size of $(1.0 - 2.0) \times 10^{-3}$ m. 175

		Page
Figure 9.25	Effect of Feed Flowrate, Adsorption Temperature and Zeolite Particle Size on the Diffusion Coefficient of n-Paraffins Adsorption from HK on Zeolite Type-5A.	182
Figure 9.26	Effect of Repeated Desorption with Steam Without Intermediate Reactivation on the BT-Curve of Adsorption of n-Paraffins from HK at a Feed Flowrate of 33.33×10^{-9} m^3/s, a Temperature of 643 K, and a Particle Size of $(1.0 - 2.0) \times 10^{-3}$ m.	184
Figure 9.27	Variation of the Dynamic Capacity of Zeolite with the Cycle Number at the Optimal Conditions of Adsorption of n-Paraffins from HK Using Steam as the Desorbing Agent.	187
Figure 9.28	Effect of Desorption Temperature on the Amount of n-Paraffins Desorbed Using Steam as the Desorbing Agent at the Optimal Adsorption Conditions of n-Paraffins from HK on Zeolite Type-5A.	190
Figure 9.29	Effect of Desorbent Agent on the Percentage of n-Paraffins Desorbed at the Optimum Adsorption Conditions of n-Paraffins from HK by Zeolite Type-5A.	193
Figure 9.30	Effect of Desorbent Agent Type on the Equilibrium Desorption Time of n-Paraffins Adsorbed from HK on Zeolite Type-5A.	196
Figure 9.31.	Effect of Repeated Desorption Cycles (Without Intermediate Reactivation of Zeolite) on the Desorption Time Using Steam at Different Flowrates.	197

Page

Figure 9.32. Distribution of n-Alkanes as Determined by the Gas-Liquid Chromatography. 200

Figure 9.33. N-Alkanes Peaks as Determined by GLC for n-Paraffins Product. 203

Figure 9.34. N-Alkanes Peaks as Determined by GLC for Denormalized Kerosene. 204

Figure 3.35. N-Alkanes Peaks as Determined by GLC for Heavy Kerosene. 205

Figure 3.36. Graphical Solution of Fixed-Bed Adsorption using the BET-Equilibrium . 219

LIST OF TABLES

		Page
Table 2.1.	Structure and Physical Constants of n-Alkanes.	7
Table 2.2.	Melting Points of Various Normal and Branched Alkanes Found in Waxes.	9
Table 2.3.	Composition of Aromatic Hydrocarbons in Liquid Paraffin which is Isolated by Different Methods.	14
Table 2.4.	Content of Sulphur Compounds in Liquid Paraffin which is Isolated from Diesel-Cut by Carbamide Method.	15
Table 2.5.	Consumption of Liquid Paraffins (in 100 Tons) in Japan for Different Aplications (1969-1973).	22
Table 2.6.	The Prospective Requirement of Quality of Liquid Paraffin According to Applications.	23
Table 3.1.	Basic Types of Commercially Available Molecular Sieves.	30
Table 3.2.	Classification of Zeolite.	35
Table 3.3.	Physical Properties of Typical "Linde" Molecular Sieves Type-A and Type-X.	36
Table 3.4.	Basic Types of "Linde" Molecular Sieve.	39
Table 7.1.	Physico-Chemical Properties of 5A-Molecular Sieves Used in Adsorption Separation of n-Paraffins From Heavy Kerosene.	109
Table 7.2.	Physico-Chemical Properties of Heavy Kerosene.	110

Page

Table 8.1. Operating Conditions of Gas-Liquid Chromatograph for Determination of n-Paraffins in Heavy Kerosene, Denormalized Kerosene, and n-Paraffins Product. 128

Table 8.2. The Retention Time for each n-Alkane Present in the Standard Solution Under the Specified Conditions Mentioned in Table 8.1. 129

Table 9.1. Variation of the Exhaustion and the BT-Time with the Feed Flowrates. 146

Table 9.2. Variation of the Exhaustion and the BT-Time with the Adsorption Temperatures. 154

Table 9.3 Variation of the Exhaustion and the BT-Time with the Zeolite Particle Sizes. 161

Table 9.4. The Effect of Feed Flowrate on the Dynamic Properties of Adsorption of n-Paraffins from HK by Zeolite Type-5A. 163

Table 9.5. The Effect of Temperature on the Dynamic Properties of Adsorption of n-Paraffins from HK by Zeolite Type-5A. 165

Table 9.6. The Effect of Particle Size on the Dynamic Properties of Adsorption of n-Paraffins from HK by Zeolite Type-5A. 166

Table 9.7. The Effect of Nitrogen Flowrate on the Dynamic Properties of Adsorption of n-Paraffins from HK by Zeolite Type-5A. 172

Page

Table 9.8. Variation of the Diffusion Coefficient of n-Paraffins Adsorption from HK on Zeolite Type-5A at Different Flowrates, a Temperature of 643 K, and a Particle Size of $(1.0 - 2.0) \times 10^{-3}$m. 178

Table 9.9. Variation of the Diffusion Coefficient of n-Paraffins Adsorption from HK on Zeolite Type-5A at Different Temperatures, a Feed Flowrate of 33.33×10^{-9} m^3/s, and a Particle Size of $(1.0 - 2.0) \times 10^{-3}$m. 179

Table 9.10. Variation of the Diffusion Coefficient of n-Paraffins Adsorption from HK on Zeolite Type-5A at Different Particle Size, a Temperature of 643 K, and a Feed Flowrate of 33.33×10^{-9} m^3/s. 180

Table 9.11. Variation of HMTZ for the Adsorption of n-Paraffins from HK with Different Cycles of Adsorption. 185

Table 9.12. Variation of the Dynamic Capacity of Zeolite with the Cycle Number at the Optimum Conditions of Adsorption of n-Paraffins from HK using Steam as the Desorbing Agent. 188

Table 9.13. Effect of the Desorption Temperature on the Amount of n-Paraffins Desorbed Using Steam. 192

Table 9.14. Effect of Desorbing Agent on the Amount of n-Paraffins Desorbed. 195

		Page
Table 9.15.	Effect of Repeated Desorption Cycles (Without Intermediate Reactivation of Zeolite) on Desorption Time Using Steam at Different Flowrates.	198
Table 9.16.	Distribution of the Normal Alkanes present in the Original Feed, Isolated Liquid Paraffins, and Denormalized Kerosene as Determined by the Gas-Liquid Chromatography.	201
Table 9.17.	Total Material Balance of Adsorption Separation of n-Paraffins from HK on zeolite Type-5A at a Feed Flowrate of 33.33×10^{-9} m^3/s, a Temperature of 643 K, and a Particle Size of $(1.0 - 2.0) \times 10^{-3}$ m.	208
Table 9.18.	Aromatic Content of Original Feed, Isolated Liquid Paraffins, and Denormalized Kerosene as Determined by the Ultra-Violet Spectrophotometry.	209
Table 9.19	Physico-Chemical Properties of Original Feed, Isolated Liquid Paraffins, and Denormalized Kerosene.	211
Table 9.20.	Surface Area and Pore Volume Data for Used and Regenerated Molecular Sieves Zeolite Type-5A.	212

CHAPTER ONE

INTRODUCTION

CHAPTER ONE

INTRODUCTION

Normal paraffins, comprise straight-chain organic compounds with the general formula C_nH_{2n+2}, and have many industrial applications. Large volumes of n-paraffins are used as feedstocks for the production of chlorinated paraffins, which in turn are used industrially such as lubricating oil, additives, plasticizers, flame retardants, coating materials, paints, surfacants, etc. A potential outlet for the consumption of n-paraffins is in the production of biodegradable detergents and paraffin sulfonates which act as anionic surface active agents [1]. Single cell protein is produced from n-paraffins by fermentation.

All distillate fractions of petroleum contain varying amounts of n-paraffins; other constituents being olefins, branched-chain paraffins, aromatics, cycloparaffins, naphthenes, etc. Chandra et al. [2] analyzed the n-paraffin contents of straight-run kerosenes derived from different crudes. The middle distillates from the Ankleshwar field were found to contain 30 to 38% n-paraffins, those from the Assam field 0 to 6%; and kerosenes derived from the Middle East crudes 15 to 20% n-paraffins.

Normal paraffins are of commercial importance within the Arabian Gulf because of the large volume of imported detergents. Recovery of these n-paraffins from refining streams might eliminate

the need for importation, and therefore provide a boost to n-paraffin- based-industries. Heavy kerosene from Kuwait National Petroleum Company (KNPC) appears to be a very promising feedstock for this purpose because of its relatively high n-paraffin content (18.75 wt%) and high smoke point (0.024 m), and, was therefore chosen for this study.

Since the range of boiling points of n-paraffins overlaps with that of other hydrocarbons, fractional distillation is completely unsuitable method of separation [3]. The most extensively used techniques for the separation of n-paraffins are urea adduction and molecular sieve adsorption, both of which exhibit great selectivity for the size of molecules. The normal or straight-chain molecules of paraffins, which have smaller radii than other hydrocarbons i.e. of the order of 4.9Å, can selectively enter the openings in urea adducts or zeolite crystals and become occluded in their cavities [4]. Urea selectively crystallizes around organic compounds with long chains to make a solid, filterable complex or adduct. This urea crystal forms a channel large enough to accommodate straight chain hydrocarbon molecules, but not cyclic or branched chain hydrocarbons. Only low n-paraffin content petroleum fractions are suitable for urea adduction. Other fractions produce a thick paste with urea, with associated processing and transfer difficulties. Because of the high operating costs, the method is not a much favoured one nowadays [3]. Separation using molecular sieves is based upon the principle of selective, Van der Waal type adsorption of n-paraffins on natural zeolites, as first reported by Barrer [5].

The dehydrated zeolite particles have as much as 43% porosity. All of the pores are approximately of the same size as shown in Fig. 1.1. Of particular interest, is the Linde Molecular Sieves (LMS)-5A which have opening of 5Å size. The n-paraffin molecule have a mean cross-sectional diameter of 4.9Å while iso-paraffins and cyclic molecules have a minimum cross-sectional diameter of 5 to 6Å. Due to the sieving effect in addition to polarity, out of a mixture of different hydrocarbons, the n-paraffins will be selectively adsorbed, which can then be recovered by desorption by a suitable fluid. Because of the adsorption-desorption cycles involved, the process is essentially "batchwise" in nature [3]. The purity of n-paraffins separated by molecular sieves is higher than those separated by urea adduction. For example, the purity of n-alkanes separated from straight-run kerosene by molecular sieves is 96.33%, while this purity is reduced to 85.01% using urea adduction [1]. It has been shown that the breaking of adducts is cumbersome, and some non-normal paraffins that participate in the adduct formation are also separated with the normal type [4].

Several studies have been made on the vapor-phase adsorption of pure and binary paraffins on molecular sieves. For example, those of Ruthven [6] and Ruthven et al. [7]. Sundstrom and Krautz [8] report data on liquid-phase adsorption of n-heptane, n-decane, n-dodecane, and n-tetradecane on Linde 5A molecular sieves, albeit mainly for binary systems of these paraffins. Zeolite type X was used by Benachrelli [9] to isolate aromatics from naphtha-kerosene

and diesel cuts in the gas phase. Avery (10) used a constant-pressure process for separating n-paraffins from a hydrocarbon vapor feed using molecular sieve adsorbent.

All commercial processes for n-paraffins recovery are based upon fixed-bed of molecular sieves. As discussed in Chapter 5, these include the British Petroleum, the Isosiv, the Molex, the Texaco, the Parex, and the Ensorb processes. All, except the Molex Process, apply the vapor-phase adsorption.

In the present work the vapor-phase adsorption on fixed-bed molecular sieve type-5A has been applied to separate a multicomponent mixture of n-paraffins from Heavy Kerosene. It covered the effect of feed flowrate, temperature, and zeolite particle size on the height of mass transfer zone (MTZ) and the dynamic capacity of the adsorbent.

FIG.1.1 Sterioscan/microphotograph of the Structure of Zeolite Type-5A .

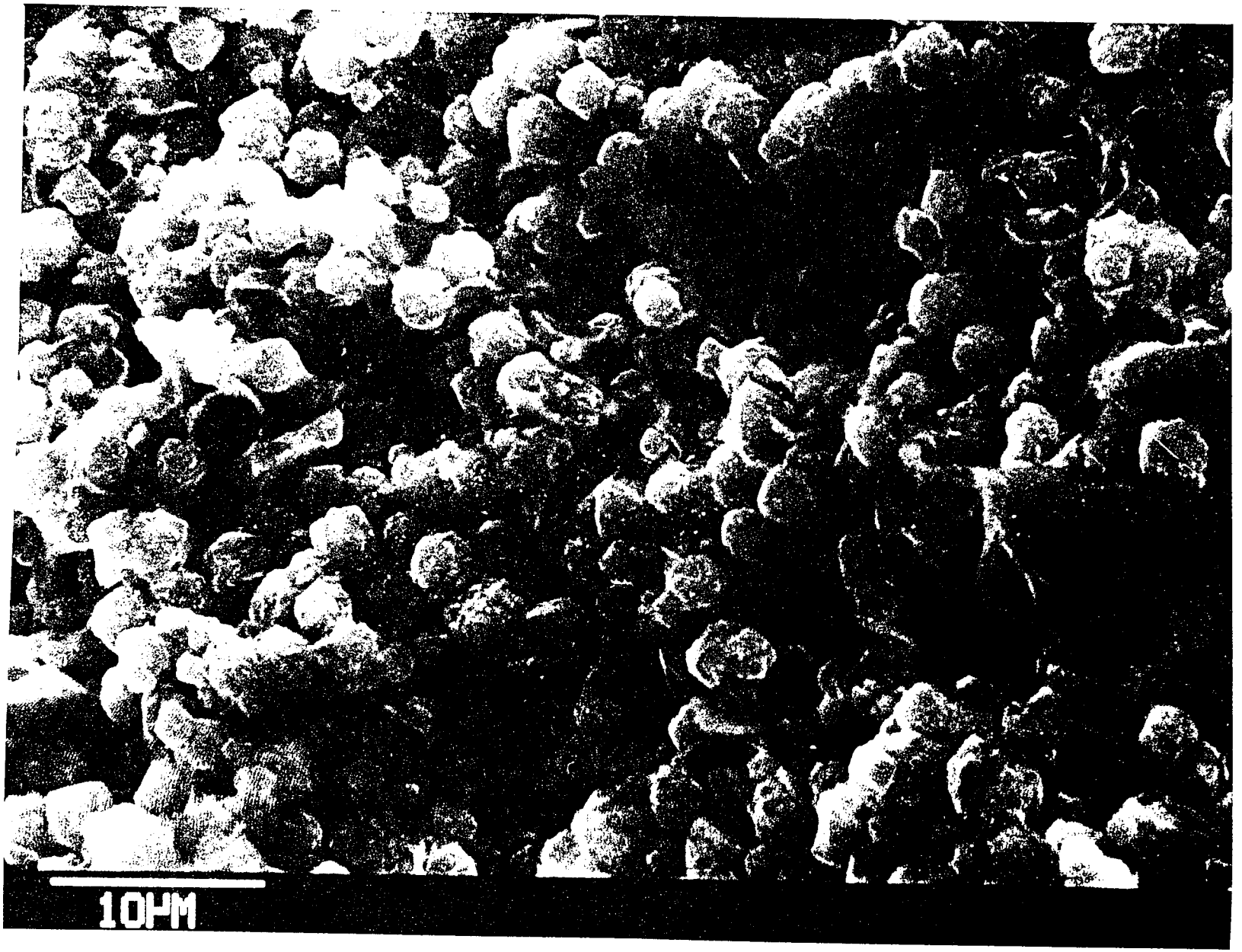

CHAPTER TWO

APPLICATIONS AND PROPERTIES OF NORMAL PARAFFINS

CHAPTER TWO

APPLICATIONS AND PROPERTIES OF NORMAL PARAFFINS

2.1 Introduction:

N-Paraffins are important raw materials for the synthesis of biodegradable detergents, plasticizers and a variety of medicinal grade paraffins, acids, alcohols and aldehydes. Besides, n-paraffins are excellent low cost feedstock for single cell protein manufacture.

Adduct formation with urea and adsorption on molecular sieves are the most commonly used techniques for separation of n-paraffins from various petroleum fractions (4)

2.1 Physical Properties:

N-Paraffins are saturated hydrocarbons with the general formula C_nH_{2n+2}. They are often referred to as alkanes with normal structure. Liquid paraffins have a melting point lower than 318 K (45°C). Commercial liquid paraffins contain 92-99.5% wt. of normal alkanes (1).

The quality of liquid paraffins depend mainly on the structure and properties of n-alkanes and the nature and quantity of impurities. Some important physical properties of n-paraffins,

Table (2.1) Structure and physical constants of n-alkanes (11).

Hydrocarbon	Formula	Temperature K (@ 1 atm)		Density (kg/m^3) @ 293 K	Refractive Index @ 293 K
		Melting Point	Boiling Point		
Octane	C_8H_{18}	216.2	398.7	702.6	1.3974
Nonane	C_9H_{20}	219.3	423.8	717.7	1.4054
Decane	$C_{10}H_{22}$	243.3	447.1	730.1	1.4119
Undecane	$C_{11}H_{24}$	247.4	468.9	740.2	1.4172
Dodecane	$C_{12}H_{26}$	263.3	489.3	748.7	1.4216
Tridecane	$C_{13}H_{28}$	267.0	508.4	756.3	1.4256
Tetradecane	$C_{14}H_{30}$	278.5	526.6	762.7	1.4290
Pentadecane	$C_{15}H_{32}$	283.0	543.6	768.4	1.4319
Hexadecane	$C_{16}H_{34}$	291.1	559.8	773.3	1.4345
Heptadecane	$C_{17}H_{36}$	295.0	574.9	776.7*	1.4367
Octadecane	$C_{18}H_{38}$	301.0	589.1	776.7*	1.4388
Nonadecane	$C_{19}H_{40}$	305.0	604.5	777.6*	1.4350*
Eicosane	$C_{20}H_{42}$	309.4	615.1	777.7*	1.4360*
Heneicosane	$C_{21}H_{44}$	313.4	631.4	778.2*	1.4352*
Docosane	$C_{22}H_{46}$	317.4	640.0	778.2*	-
Hexacontane	$C_{60}H_{122}$	371.5-372.3	-	-	-
Heptacontane	$C_{70}H_{142}$	378.0-378.5	-	-	-
Hectane	$C_{100}H_{202}$	388.1-388.4	-	-	-

* At melting point

liquid or solid at ambient temperature, are summarised in Table 2.1.

On the basis of inter-relation between different properties of paraffins, the quality of paraffins can be determined. The type of n-alkanes and iso-alkanes affect the physico-chemical properties of liquid paraffins. The melting point of n-alkanes increases with molecular weight. The melting point of hectane, the highest molecular weight normal alkane isolated in a pure state, is 388 K. Over the carbon atom number range from C_9 to C_{25}, the relationship between the melting point and the carbon atom number cannot be described with one single function for even-numbered and odd-numbered n-alkanes, i.e., the melting points are higher and lower, respectively, than the average values calculated from even - and odd - numbered n-alkane melting points [11].

It should be stressed that the branching of the carbon chain, at identical molecular weights, results in an important decrease of the melting point, since high melting points are inseparable from high symmetry of the crystals, and this condition will be satisfied above all in the case of straight-chain alkanes. The melting points of various normal and branched paraffins are presented in Table 2.2. For example, it may be seen, that among $C_{26}H_{54}$ alkanes, the melting point of n-hexacosane is 329.4 K as compared to 273 K for 11-n-butyldocosane [11].

The boiling points of identical molecular weight straight-chain and branched alkanes also differ, but to a much

Table (2.2) Melting points of various normal and branched alkanes found in waxes.

Hydrocarbon	Melting point by Capillary Tube Method K
$C_{24}H_{50}$	
n-Tetracosane	324.5
2-Methyltricosane	315.0
2,2-Dimethyldocosane	307.6
5-n-Butyleicosane	281.0
$C_{26}H_{54}$	
n-Hexacosane	329.4
5-n-Butyldocosane	293.8
7-n-Butyldocosane	276.2
9-n-Butyldocosane	274.3
11-n-Butyldocosane	273.0
$C_{28}H_{58}$	
10-Nonylnonadecane	268-267
$C_{44}H_{90}$	
22-Methyltritetracontane	339.6-339.7

lesser degree than the melting points. In the C_{24}-C_{28} range, the boiling point of the branched alkanes is lower by only 4 to 15°C (depending on the number, length and position of the side chains) than that of the corresponding n-alkane.

No definite relationship between the viscosities of normal and branched paraffinic hydrocarbons can be established. While alkanes with one side chain often have lower viscosities than that of the normal alkane, the viscosity of alkanes with two or three side chains is higher than that of the corresponding normal alkanes.

The temperature coefficient of the viscosity of normal alkanes decreases with increasing molecular weight. Among isomeric branched alkanes the temperature coefficient of viscosity is highest for the compound with the shortest side chain, while this coefficient is substantially lower for alkanes with long side chains and for normal alkanes.

Paraffin liquids at ambient temperature and melts of paraffins solid at ambient temperature behave as Newtonian systems. For certain applications, the viscosity of macrocrystalline and microcrystalline paraffin waxes, above all in the 373-423 K temperature range, is of importance. The density of paraffin increases with their melting point. The refractive index is a physical property frequently used for identifying substances and for determining their compositions. The refractive index of light-molecular weight normal paraffins is usually measured 293 to

298 K while that of paraffin waxes is measured @ 353 to 358 K.

The relationship between density, refractive index (both measured at the same temperature) and molecular weight is given by the Lorentz-Lorenz formula (11).

$$M_r = \left[\frac{n^2 - 1}{n^2 - 2} \right] \frac{M}{d} \qquad (2.1)$$

where M_r is molar refraction, n refractive index, M molecular weight and d density.

The molar refraction of the compounds can be calculated, with a knowledge of the molecular weight, by using the following relationship (11):

$$M_r = 0.33063 \ M + 1.6165 \qquad (2.2)$$

2.3 Chemical Structure:

Liquid paraffins contain impurities such as naphthenes, aromatics, isoparaffins and sulfur compounds.

There are several methods for determination of the content and composition of different types of hydrocarbons in liquid paraffins (11). These methods include distillation, crystallization, adsorption on zeolite and other types of adsorbents, chromatography, mass spectroscopy, nuclear magnetic resonance (NMR), and other different mathematical methods. The chemical structure has been frequently determined using a separation

method to produce narrow fractions so that the group structure of fractions can be determined. From these narrow fractions the different types of hydrocarbons can be segregated, then the individual hydrocarbon structure can be determined.

The chemical structure of liquid paraffins as determined by the different studies are grouped mainly under n-alkanes, iso-alkanes and naphthenes, aromatic hydrocarbons, and sulfur-organic compounds [12].

2.3.1 N-alkanes: The main content of a liquid paraffin is different depending on the methods of isolation and purification of the liquid paraffin. The range of purity of liquid paraffin is 90-99.5% by wt. Liquid paraffin isolated by using selective solvents method has n-alkanes of 93-95% wt, and 96% wt of n-alkanes can be isolated from diesel petroleum cuts using alcohol carbamide solution method. The liquid paraffin isolated from kerosene diesel cuts by zeolite contains about 97-98% n-alkanes which will be further purified to obtain pure liquid paraffin free from carcinogenic agents (i.e. 0.01-0.3% by wt of aromatic hydrocarbons).

2.3.2 Iso-alkanes and Naphthenes: Some authors [13, 14] have reported that an increase in the molecular weight of the feed leads to an increase in the content of naphthenic hydrocarbons in the liquid paraffin. The number of rings in the molecule of naphthenic hydrocarbons is 1-4. Determination of the composition of liquid paraffin which is isolated from diesel cuts using the carbamide

method shows that the content of naphthenic hydrocarbons is approximately 0.4% wt (15). After the purification of liquid paraffin, it is found that it contains 1.84% wt iso-alkanes and 0.431% cyclohexanes (15).

2.3.3 Aromatic hydrocarbons: It is important to know the content and structure of aromatic hydrocarbons existing in liquid paraffin. This can be determined by dearomatization of the liquid paraffin using different methods. The content and the composition of aromatic hydrocarbon depend on the method of isolation of liquid paraffin (13). Liquid paraffin which is isolated using alcohol diluted carbamide has a content of aromatic hydrocarbons of 2.6% wt. This content is obtained after hydrodesulphurization of diesel cuts. The content of aromatic hydrocarbon in liquid paraffin which is isolated using adsorbent (type A molecular sieves) is 1-2% wt. The main aromatic types which can be found in the liquid paraffin are alkylbenzene, naphthenes and anthracinic hydrocarbons. The quantitative and qualitative analysis of liquid paraffin structure can be determined using gas-liquid chromatography and mass spectroscopy. A study (12) has shown that increasing the molecular weight of the petroleum fraction leads to an increase in the boiling point range of hydrocarbons and that high content of aromatics can be found in light boiling point fractions. There is a sharp decrease of aromatic hydrocarbons in petroleum fractions with boiling point higher than 573 K. The composition of aromatic hydrocarbons in liquid paraffin depends on the boiling point of fractions and the method of separations. Table 2.3 illustrates the

Table (2.3) Composition of aromatic hydrocarbons in liquid paraffin which are isolated by different methods (12).

Compounds	Method of isolation of liquid paraffin		
	Crystallic carbamide (473-593 K)	Alcohol-solution carbamide (513-623 K)	Molecular Sieves Zeolite (473-593 K)
Alkylbenzene	9.5	32.2	47.3
Alkyltetralene	12.5	10.8	9.6
Alkylnaphthalene	16.0	28.5	10.3
Indens	13.5	7.1	15.6
Alkyl acyto-naphthalene	18.0	7.1	5.3
Diphenyls	17.5	10.8	5.5
Tricyclo-compounds	-	-	-

Table (2.4) Content of sulphur compounds in liquid paraffin which is isolated from diesel-cut by carbamide method.

Compounds	Type of feedstock	
	High sulphuric	Hydrodesulphurized
Mercaptane	0.004-0.009	-
Sulfides	0.001-0.007	0.0-0.007
Disulfides	-	-
The rest	0.194-0.296	0.010-0.073
Total	0.22-0.31	0.010-0.080

composition of aromatic hydrocarbons of liquid paraffins which are isolated from diesel cuts by different methods.

2.3.4 Sulphur-organic compounds: The sulphur-organic compound content depends on the type of feedstock, also on the method of isolation and purification of liquid paraffin. For example, the liquid paraffin which is isolated by the carbamide method has values of sulphur-organic compounds as shown in Table 2.4. (12).

In many countries normal paraffins are currently obtained mainly using urea adduction or molecular sieves. Small amounts of liquid paraffin are also being produced in commercial crystallization units with selective solvents (12).

2.4. Applications of Normal Paraffins:

Liquid paraffin is used in the petrochemical industry on a large scale, especially in the manufacture of synthetic fatty acids (SFA), secondary alcohols, α-olefins, chloroparaffins and in the production of single cell protein (SCP), speciality oils and additives. Paraffin is also used in the manufacture of paper and packing materials, electro-technical goods, automobile tires, polishing artificial leather and textiles. Other uses of liquid paraffin are in the manufacture of matches, milk cartons, candles, shoe polish, cosmetics, pharmaceutical materials, etc (16, 8, 17).

In Kuwait, industries for some of the above-mentioned

Fig. 2.1 The Different Applications of Liquid Paraffins for Production of Surfactants, Detergents and Others

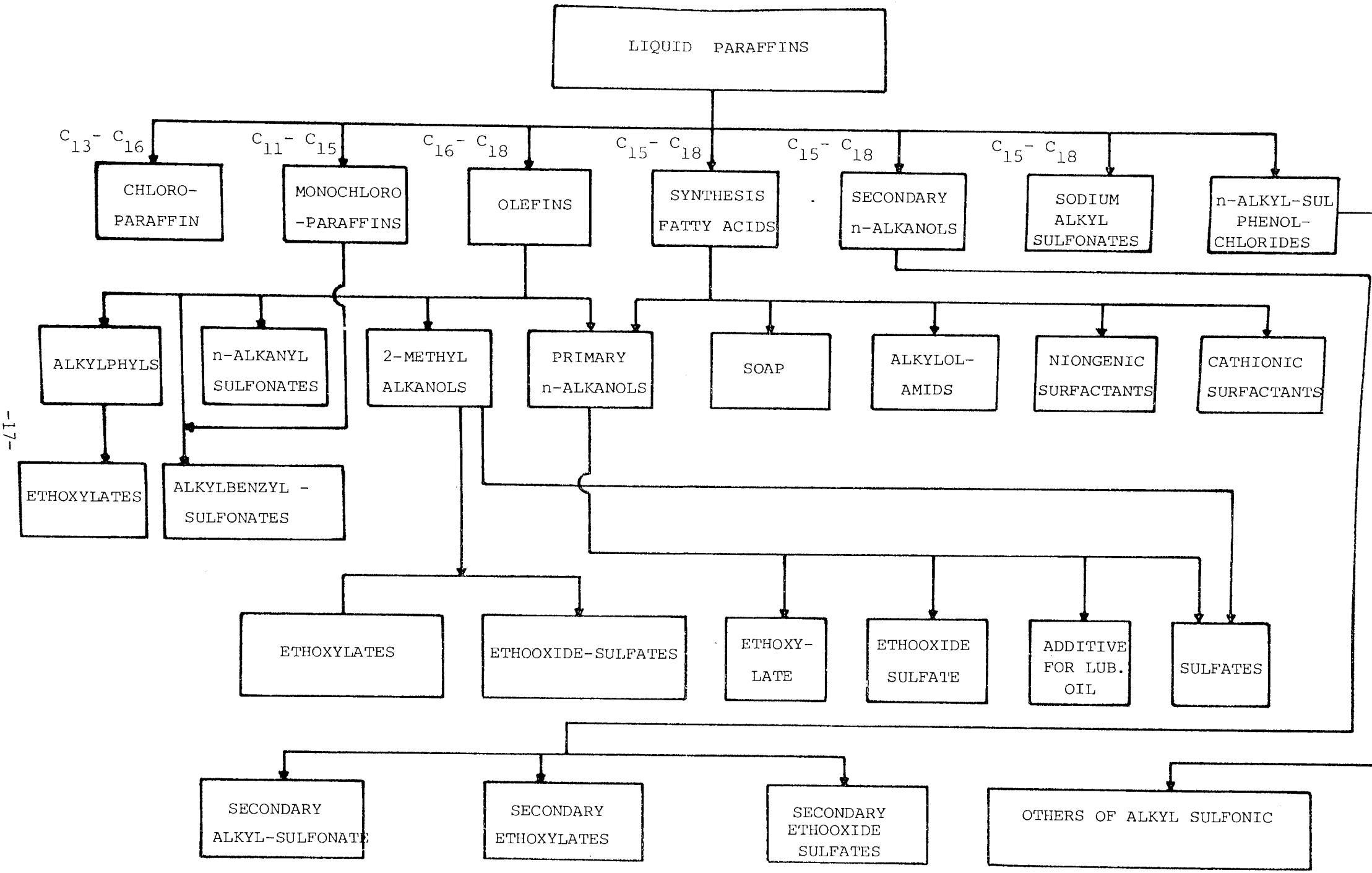

products are already established or under study. For this purpose, liquid paraffin and waxes are important for developing the petrochemical industries in Kuwait. On the other hand, the separation of liquid paraffin from kerosene-diesel cuts, heavy kerosene cuts and diesel cuts results in an improved kerosene and diesel cut with low pour point which can be marketed as by-products.

Studies on the demand for paraffin in Kuwait have shown that the fields of application will be extended (12). Figure 2.1 illustrates the different applications of liquid paraffin for production of surfactants, detergents and others.

A discussion of each end-use area of some of the application mentioned in Fig.(2.1) is as follows (18):

a. Single cell protein: It may be produced from n-paraffins by fermentation. This process has been used in Scotland and U.S.S.R., the products have been used for animal feeds.

b. Chlorinated paraffin: The average chlorine content of chlorinated paraffin products based on C_{10}-C_{18} range n-paraffins is believed to be about 55%. The major end use for chlorinated paraffins are lubricating oil additives, plasticizers, and flame retardants in plastic and coating materials. Chloroparaffins are very effective as extreme-pressure additives in gear oils and metal working lubricants. Chloroparaffins are used as secondary plasticizers

in paints, adhesives-caulk and sealant compounds, flexible polyvinylchloride (PVC), rubber inks, and in paper and textile coating.

c. Alkyl sulfonates (linear alkyl benzene and linear alkyl-benzene sulfonates): The largest application for n-paraffins has been for the production of linear alkyl benzene (also known as linear detergent alkyllate or LAB). LAB is the raw material for the production of linear alkylbenzene sulfonates (LAS) which is employed as a surfactant in numerous household and industrial detergent formulations. LAS applications are strictly industrial (e.g., as an emulsifier in pesticide and agricultural chemical formulations). A potential outlet for consumption of n-paraffins is in the production of normal paraffin sulfonates, which are anionic surface-active agents, and liquid dishwashing detergents.

d. Synthesis fatty alcohols: They are used as surface-active agents and liquid washing materials.

e. Synthesis fatty acids: They are used in detergent industries.

In 1978, the world production of surfactants was about 8 million tons. Out of this, 1.5 million tons of surfactants were produced in the USA alone [19]. Large amounts of surfactants are produced in England, France, West Germany, India and other countries. The main product of surfactant is alkylbenzene sulfonate

(ABS), then alkyl sulfates. The two products can be produced by sulfochlorination and sulfo-oxidation of paraffins. The second prospective application of liquid paraffin is in the microbiological industries for protein production. In France, Japan, England and the USSR the demand for production of single cell protein is increasing.

Applications of liquid paraffin depend on its structure, especially the number of carbon atoms in the molecule of n-alkanes. Liquid paraffin which contains C_6-C_{13} can be used for production of special solvents. Liquid paraffin which is isolated from kerosene petroleum cuts can be used for surfactants materials and single cell protein production. Liquid paraffins containing C_{12}-C_{13} can be used as antidetonation additives; C_{10}-C_{17} can be used as plasticizers, C_{10}-C_{20} for synthesis of fatty acids; C_{20} and higher can be used as additives for lubricating oils [20]. Consumption of liquid paraffin worldwide will increase in particular for the detergent industries and for single cell protein production. The demands for each grade of paraffin will not increase to the same extent. For example, the relative fraction of paraffin to be used as feedstock for the detergent industry is expected to be more than the liquid feedstock for single cell protein production. Table (2.5) illustrates the consumption of liquid paraffins for different applications in Japan from 1969-1973 [19].

In recent years there has been an increase in the demand of high purity liquid paraffin, in particular liquid paraffin for

microbiological industries. Table (2.6) illustrates the prospective requirements of quality of the liquid paraffin according to its applications (12).

Liquid paraffin is very important for pharmaceutical, food and microbiological industries in which the content of aromatic hydrocarbons should be less than 0.01% wt. Liquid paraffin, which is used for the preparation of secondary alcohols, and detergents should have aromatic hydrocarbons not exceeding 0.5% wt. (21).

This process is of vital importance to the area of the Arabian Gulf because of the large volumes of imported detergents. These detergents could be made locally if the separation of hydrocarbons as outlined above could be achieved. These hydrocarbons could be the basis for a detergent industry that will meet the future growing needs of Kuwait and the neighbouring countries.

Table (2.5) Consumption of liquid paraffins (in 100 tons) in Japan for different applications (1969- 1973)

Products	1969	1970	1971	1972	1973
Alkylbenzene	52	62	71	82	95
Chloroparaffin	6	6	8	9	10
Single-cell protein (SCP)	-	-	135	300	390
Total	58	68	214	391	495

Table (2.6) The prospective requirement of quality of liquid paraffin according to applications

Indicator	Synthesis fatty acids	Sulfonates methanol sulfochloronation	Sulfonol method of sulfo-oxidation	Chloroparaffin	Olefins	Single cell-protein
b.p.range (K)	543-643	493-613	463-533	523-583	533-643	473-593
n-alkanes	95	97	-	-	-	99
Aromatic h.c.content (wt%)	0.3	0.3	0.2	0.5	4.5	.05-.01
Sulfur content(wt%)	0.05	0.005	0.01	0.01	0.01	0.01
Pour point (not more K)	300	-	268	283	-	-

CHAPTER THREE

ZEOLITE MOLECULAR SIEVE

CHAPTER THREE

ZEOLITE MOLECULAR SIEVE

3.1 Introduction

Because of their diverse properties zeolites have found numerous applications [22]. Examples include drying, separating, and purifying of gases and liquids. Research work on zeolites is continued and more novel practical applications for these versatile materials are expected, e.g. in the air pollution control field [23].

3.2 Historical Background

Zeolites, are naturally occurring minerals and, were discovered two centuries ago by Baron Cronstedt who observed that certain mineral crystals when heated appeared to melt and boil at the same time [24, 25]. Therefore, he coined the term zeolite from Greek zeo, to boil, and lithos, stone. The earliest zeolite was found in 1756 and is called stilbite; chabazite and faujasite were subsequently found and then merlineite, in 1976. There are now about 30 recognized, naturally-occurring, zeolites. Mostly they are found in alkaline-rich rocks scattered around the world [22]. These zeolites are the minerals now termed 'crystalline alumino silicates'. In 1954, Linde Air Co. introduced synthetic zeolites under the trade name 'Molecular Sieves' [22] and in 1959, the

Davison Chemical Division of W.R. Grace and Co. initiated production and distribution of crystalline alumino silicates under the trade mark of 'Microtrap' (25). Different trade names are applied in other countries, for example in East Germany Molecular Sieve 'Zeosorb 5 AM' is used in the parex process for the recovery of n-paraffins from petroleum fractions, and the Czechoslovak product is known as 'Calsit-5' (22).

Commercial interest in zeolites arose from the discovery that they could act as sieves with the ability to separate mixtures of molecules according to their size and shape. Such zeolites can actually 'sieve' molecules, either rejecting or retaining them, in an analogous manner to a mechanical mesh for separating finer particles from coarser ones. Thus the name 'molecular sieves' was coined for these zeolites. Mc Bain is the first who use the term molecular sieves (22). The pioneering work in this field is done by Barrer (26) in late 1940's. Since massive deposits of appropriate zeolites were unknown at that time, scientists began to synthesize zeolites with specific molecular sieving properties. In 1946 Barrer reports the successful synthesis of a molecular sieve, thus heralding a new era of synthetic zeolites which has revolutionized adsorption technology ever since (27).

3.3 Zeolite Crystal Structure:

In all zeolite research a knowledge of the structure and framework of the crystal is essential for a thorough understanding

of its behaviour. Exhausting reviews of the structure and properties of zeolites are reported (28, 29, 30, 31, 32, 33, 34). The structure and properties of synthetic zeolite type A are first reported by Breck et al in 1956 (27). Here, a description of the lattice framework of the 5A sieves is presented. A line drawings of 5A-zeolite framework is shown in Fig. (3.1).

The zeolite crystal is a three dimensional arrangement of SiO_4 and AlO_4^- tetrahedra, which are linked together at their vertices by shared oxygen ions, to form ordered lattices. This arrangement of the tetrahedra forms interconnected cavities of varying sizes, at regular intervals throughout the crystal lattice. Because of the net negative charge on the AlO_4^- tetrahedron, a cation, is required for each tetrahedron to maintain electrical neutrality in the lattice. The general formula for a unit cell of the zeolite crystal is given by:

$$M\ x/n\ [(AlO_2)x(SiO_2)y].Z\ H_2O \quad , \text{where}$$

M is an alkali metal such as sodium and potassium, or alkaline earth metals like calcium, magnesium, strontium, etc. Both x and y are integers and n is the valence of the cation. Z is the number of moles of water of crystallization.

The unit structure of the zeolite lattice is the sodalite cage in the shape of a truncated octahedron, which is formed by the combination of silica and alumina tetrahedra, totalling twenty-four in number.

As shown in the schematic drawings of Fig. 3.1, this sodalite cage encloses a cavity (β -cage) which has eight, six-membered oxygen rings (6MR) and six, four-membered oxygen rings (4MR). The diameter of a 6MR is 2.3Å and that of the β -cage is 6.6Å. In the 5A zeolites, the framework consists of a tetrahedral arrangement of eight sodalite cages linked by twelve 4MR, all of which together define a roughly spherical cavity (α-cage) of 11.4Å in diameter. This arrangement of the sodalite cages leads to the formation of six, eight-membered oxygen rings (8MR), which are the entrances to the α -cage. These 8MR apertures form the links between other $\alpha\beta$ cages. The size of the 8MR apertures is of importance because it determines the maximum dimensions of the molecules that can enter the crystal lattice. Aperture openings are a direct function of the Si/Al ratio and the type of cations. The Si/Al ratio determines the number of cations in a unit cell, and the size of the cation, which is associated with the 8MR, fixes the diameter of the aperture. Table 3.1 shows the basic types of commercially available molecular sieve with the nominal pore diameter, the available form, the cation and the theoretical SiO_2/Al_2O_3 for each type [35]. In the Linde 5A zeolite which has a formula for a unit cell of:

$$Ca_{4.5}Na_3\ (AlO_2)_{12}\ (SiO_2)_{12}\ 30H_2O$$

there are 60% calcium ions and 40% sodium ions which results in an aperture of 4.2Å in diameter. Sodium ions, accessible to the intracrystalline voids or pores, undergo cation exchange readily in aqueous solution. Replacement of sodium ions by calcium ions effectively enlarges the pore openings. The adsorption properties of zeolite type A are strongly dependent on the number and type of

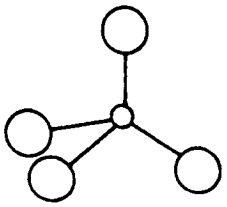

Skeletal Tetrahedron

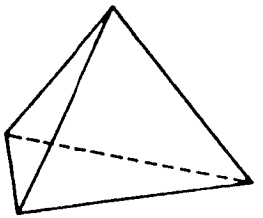

Solid Tetrahedron

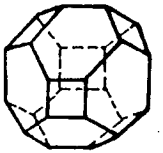

Truncated Octahedron

(sodalite β-cage)

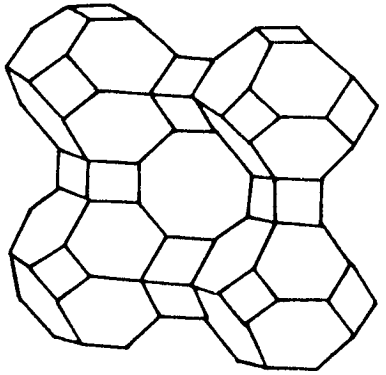

Face of Cubic Array of

Truncated Tetrahedron

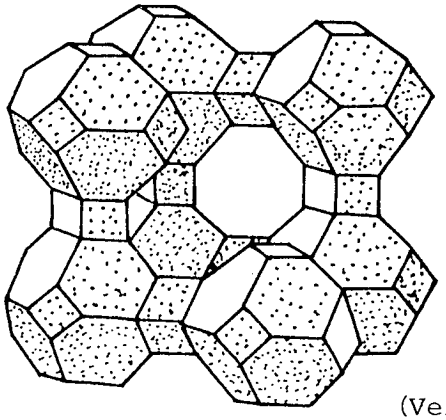

A Unit Cubic Cell

Forming an α-Cage

(Vertices represent Si or Al atoms and lines represent oxygen atoms)

Fig. 3.1 Line Drawings of 5A-Zeolite Framework.

cations in the structure. This allows molecules with effective diameters up to 5Å to squeeze through the apertures into α-cages (32, 33, 34). Fig. (3.2) shows the position of the silicon and aluminum atoms in the basic truncated octahedron cell of the molecular sieves, while Fig. (3.3) shows the positions of the silicon and aluminum atoms in type A molecular sieve (27).

Normal paraffin molecules which have an effective diameter of 4.86Å can easily penetrate the crystal lattice and be adsorbed on the surface of an α-cage. Larger molecules of the branched paraffins and aromatic hydrocarbons cannot enter the lattice because their effective diameter is larger than 5Å. However, benzene is known to penetrate some of the α-cages existing near the surface of the crystal (34), for which case 2% of the α-cages are available.

Apart from hydrocarbons, smaller molecules such as water and oxygen can enter the α-cages and also diffuse into the smaller β-cages. This additional characteristic is reflected in the zeolites' high affinity for water.

In the zeolite diffusion process, the diffusing molecule first enters the crystal through the interstitial space to an empty or partially filled α-cage, where it is adsorbed on the surface. Some molecules may by-pass a partially filled cavity and seek out an empty one while others may displace adsorbed molecules, thus facilitating further penetration of the crystal.

Table 3.1 Basic types of commercially available molecular sieves

Basic Type	Nominal Pore Diameter, Å	Available Form	Cation	Theoretical SiO_2/Al_2O_3
3A	3	Powder, 1/8", 1/16" Pellets, 4x8, 8x12 beads	K^+	2/1
4A	4	Powder, 1/8", 1/16" pellets, 4x8, 8x12 beads, mesh	Na^+	2/1
5A	5	Powder, 1/8", 1/16" Pellets, 4x8, 8x12 beads, mesh	Ca^{++}	2/1
10X	8	Powder, 1/8", 1/16" Pellets	Ca^{++}	2.5/1
13X	10	Powder, 1/8", 1/16" Pellets, 4x8, 8x12 beads, mesh	Na^+	2.5/1
Y	7 to 9	Powder, 1/8", 1/16" Extrudates	Varying	3 to 6/1
AW-300	3 to 4	1/8", 1/16" Pelllets	Mixed	10/1
AW-500	4 to 5	1/8", 1/16" Pellets 4x8, 8x12 beads	Mixed	4 to 6/1
Mordenite	7 to 9	Powder 1/8", 1/16" Pellets, mesh	Na+ or H^+	10/1

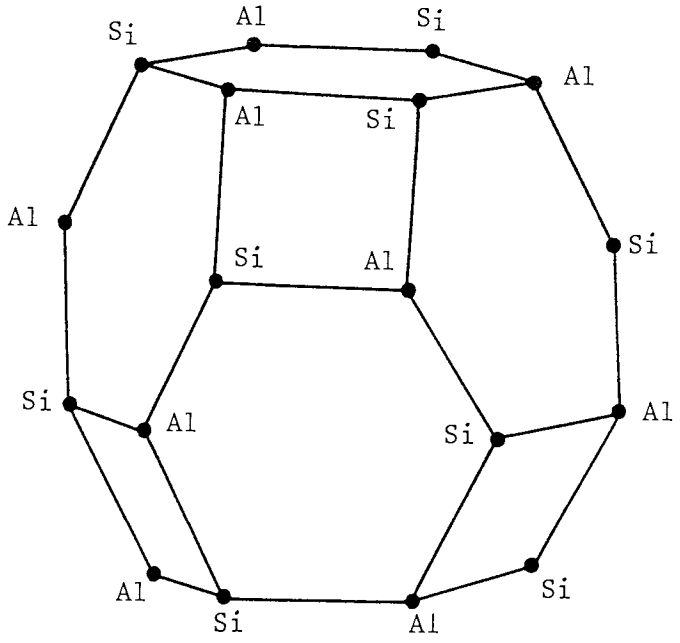

Fig. 3.2 Position of the Silicon and Aluminum Atoms in the Basic Truncated Octahedron Cell of the Molecular Sieves.

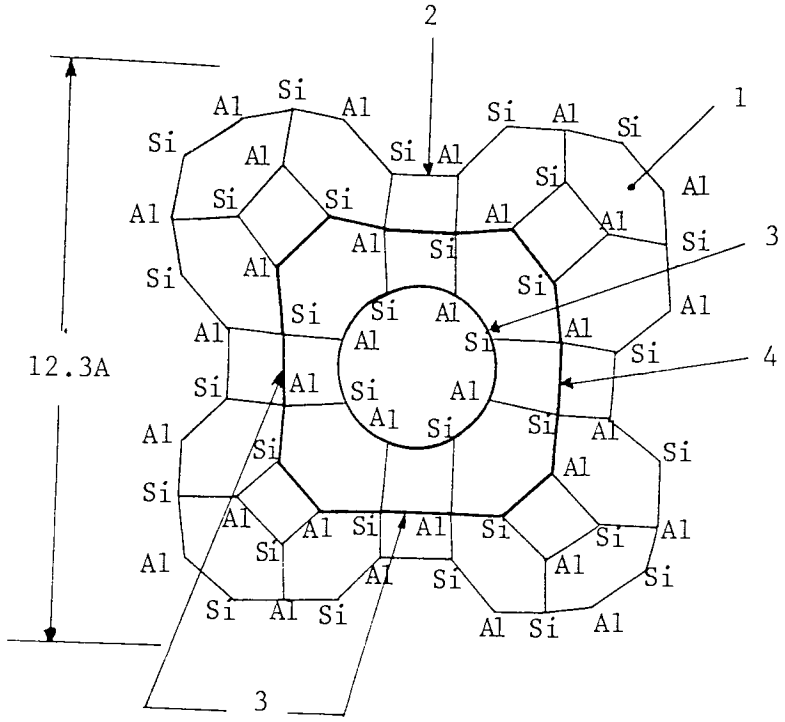

Fig. 3.3 Position of the Silicon and Aluminum Atoms in Type A Molecular Sieves.

1- Basic truncated octahedron cell.

2- Cube junction between basic cells.

3- Inlet of pores.

4- Contour line of a pore.

Whatever the phenomenon for transport, the diffusing molecules generally show a high degree of interaction with the zeolite lattice framework. It is this interaction which is of primary interest in molecular sieve research (34). Of secondary, yet vital interest, is the influence of other molecules, both solute and solvent, on the behaviour of a diffusing molecule.

3.4 Classification of Zeolite:

Zeolites are usually grouped into any of the Analcime, Natrolite, Heulandite, Erionite, Mordenite, Faujasite or A groups. There are many zeolites in each group, so we will not discuss all these various groups, but will confine our discussion to the more commercially important molecular sieves, Type A and Type X. Table 3.2 shows the classification and types of zeolite under each group and the free aperture of the main channels for each type (35). These zeolites are manufactured usually be digesting a mixture of silica, alumina and caustic soda in the correct mol ratio at the boiling point of the mixture for several hours till the mixture crystallizes out (22). In type A molecular sieve, the tetrahedron are grouped to form a truncated octahedron (also called a cubo-octahedron) with a silica or alumina tetrahedron at each point. This gives rise to what is known as a sodalite cage which is mentioned previously. When a number of sodalite cages join together, the result is a net work of cavities with about 11.4Å in diameter (22). A sodalite cage structure is illustrated in Fig. (3.1). The openings to the cavities are on the six sides,

surrounded by eight oxygen ions. In the sodium form having the chemical formula

$$Na_{12}\ [(AlO_2)_{12}\ \ (SiO_2)_{12}].xH_2O$$

diameter of the opening window is 4.2Å. Thus only molecules of diameter 4.2Å or less can enter these cages or cavities. These zeolites are therefore called 4A molecular sieves (22).

It has been pointed out earlier that zeolites have exchangeable cations. If part of the Na^+ ions are replaced by K^+ ions, for example, the window diameter will be decreased from 4Å to 3Å. If, on the other hand, Ca^{++} ions are exchanged the opening becomes 5Å in diameter (22). Hence it is possible to alter window diameters of molecular sieves by selecting appropriate cations.

Another type of molecular sieves, Type-X has the formula

$$Na_{86}\ [(AlO_2)_{86}\ \ (SiO_2)_{86}].xH_2O$$

where $x \leqslant 276$. The crystal architecture is built by the same sodalite cages in a tetrahedral stacking. The six membered oxygen atom ring provides an opening of 10Å in diameter. As in Type A, the cations can be exchanged to provide different window openings. Some physical properties of typical "Linde Molecular Sieves" of both Type A and Type X are given in Table 3.3.

3.5 Physico-Chemical Properties:

Synthetic zeolites have large surface areas, in the order of 700-800 m^2/gram and the zeolite pellets which are the main

Table 3.2 Classification of zeolites

Name	Free Aperture of main channels, Å
Group 1	
Analcine	2.6
Phillipsite	4.2 - 4.4
Paulingite	3.9
Yugawaralite	3.5
Group 2	
Erionite	3.6 - 4.8
Offerlite	3.6 - 4.8 a axis; 6.3 c axis
Omega	7.5
T	3.6 - 4.8
Group 3	
A	4.2
P	3.5
Group 4	
Faujasite	7.4
X	7.4
Chabazite	3.7 - 4.2
Gmelinite	3.4 - 4.1 a axis; 6.9 c axis
ZK - 5	3.9
L	7.5
Group 5	
Natrolite	2.6 - 3.9
Thowsomite	2.6 - 3.9
Edingtonite	3.5 - 3.9
Group 6	
Mordenite	6.7 - 7.0 c axis; 2.9 - 5.9 b axis
Dachiardite	3.7 - 6.7 b axis; 3.6 - 4.8 c axis
Epistilbite	3.6 - 6.3 a axis; 4.9 - 6.3 c axis
Group 7	
Henlamdite	3.9 - 5.4 a axis; 4.2 - 7.1 c axis
Stilbite	4.1 - 6.2 a axis; 2.7 - 5.7 c axis

Table 3.3 Physical properties of typical "Linde molecular sieves" type A and type X

Type	Pellet Size, m x 10^3	Bulk Density, kg/m^3	Particle Diameter, m x 10^3	Crush Strength, kg	Heat of Adsorption, kJ/kg H_2O	Equilib. H_2O Capacity @ 298 K wt%
3A	1.6	641.3	1.5 - 2.0	2.91	4186.8	20
3A	3.2	641.3	3.0 - 3.5	6.58	4186.8	20
4A	1.6	657.3	1.5 - 2.0	4.72	4186.8	22
4A	3.2	657.3	3.0 - 3.5	9.53	4186.8	22
5A	1.6	700.0	1.5 - 2.0	2.63	4186.8	21.5
5A	3.2	700.0	3.0 - 3.5	5.72	4186.8	21.5
13X	1.6	609.2	1.5 - 2.0	5.45	4186.8	28.5
13X	3.2	609.2	3.0 - 3.5	11.35	4186.8	28.5

commercial product are made of microcrystals of zeolites about 1.0 micron in diameter embedded in a dried clay binder (36). The basic unit of the type-5A molecular sieve is a zeolite crystal with an open structure consisting of a large number of adsorption cavities roughly spherical in shape. As generally prepared the type A zeolite crystals are cubic with edges averaging from 1-5 micron in length (29). The individual adsorption cavities are about 11.5Å in diameter and are connected to adjacent cavities by apertures having an effective diameter of 5Å. The unit cell has a dimension of 12.3Å. Since the average zeolite crystal size is about 20,000Å, a molecule must diffuse through approximately 1000 cavities to reach the center of the crystal. Such diffusion within the crystal is referred to as zeolite diffusion (37). Molecules like benzene which have an effective diameter of 6.5Å, cannot penetrate the 5Å apertures of the crystal lattice, while a normal paraffin molecule, with an effective diameter of 4.86Å, can squeeze through these apertures. Table (3.4) shows the basic types of "Linde" molecular sieves with the nominal pore diameter in Å, and the molecules that are adsorbed or excluded by each type(35). The intercrystalline void spaces within the pellet are of the same magnitude as the crystal size and are referred to as macropores. The macropores occupy about 31% of the total particle volume. The macropore size distribution is found to peak sharply at 10,000Å, and that less than 10% volume of the macropores have a radius of less than 1000Å (37). The cavities and pores within the zeolite crystals are precisely uniform in size, and normally contain water molecules. But when the sieves are heated, this water of hydration is driven off, leaving

voids that comprise nearly 50% of the total volume of the crystals[36]. The water content and the crystal density of fully hydrated type-A are found to be 22.2 wt% and 1.990 ± 0.004 gram/cm^3 respectively. Type A crystals are isotropic with a refractive index of 1.463 for the hydrated crystals diminishing to 1.385 when the adsorbed water is removed. As shown by x-ray diffraction patterns, the basic type A structure remains intact after heating in air at 623 K and one atmosphere for 475 hours and in vacuum at 623 K for 350 hours [29]. Although uneffected by heating in air at one atmosphere and 973 K for 6 hours, zeolite type A recrystallizes at 1073 K in air in less than two hours to an α -crysto-balite-like structure [29]. The greater ease of adsorption in 5A zeolite is primarily due to crystal structure. Each of the spherical 5A adsorption cavities has a volume of 770Å^3 compared to the 400Å^3 available in the narrow cylindrical cavity of erionite. Further more, n-paraffins can move in a straight line, fairly unhindered path through the 5Å cavities but must bend in a tortuous manner to accommodate themselves to the cylindrical cavities in erionite[38].

3.6 Industrial Applications of Zeolites:

Most of the industrial applications of molecular sieves depend on their ability to adsorb, catalyse or exchange cation[22].

3.6.1 Zeolites as adsorbents:

Adsorption on molecular sieves takes place in the innumerable

Table 3.4 Basic types of "Linde" molecular sieves

Basic Type	Nominal Pore Diameter, Å	Molecules Adsorbed*	Molecules Excluded
3A	3	Molecules with an effective diameter <3Å, including H_2O and NH_3	Molecules with an effective diameter >3Å, e.g. ethane
4A	4	Molecules with an effective diameter <4Å, including ethanol, H_2S, CO_2, SO_2, C_2H_4, C_2H_6, and C_3H_6	Molecules with an effective diameter >4Å, e.g. propane
5A	5	Molecules with an effective diameter <5Å, including $n\text{-}C_4H_9OH$*, $n\text{-}C_4H_{10}$*, C_3H_8 to $C_{22}H_{46}$, R-12.	Molecules with an effective diameter >5Å, iso compounds and all 4 carbon rings
10X	8	Iso paraffins and olefins, C_6H_6, molecules with an effective diameter <8Å	Di-n-butylamine and larger
13X	10	Molecules with an effective diameter <10Å	Molecules with an effective diameter >10Å, e.g.,$(C_4F_9)_3N$

* Each type adsorbs listed molecules plus those of preceding type.

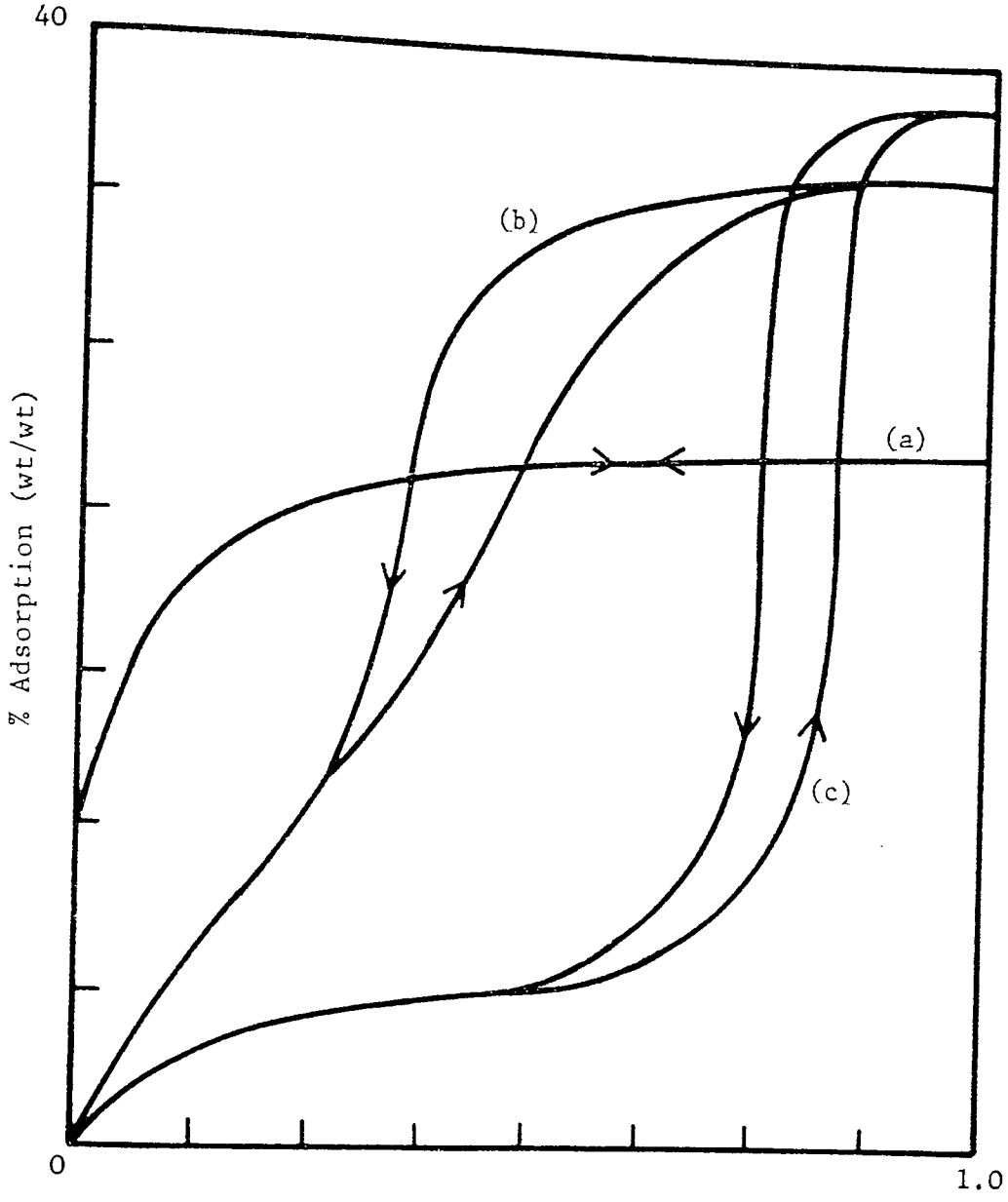

Fig. 3.4 Typical Adsorption and Desorption Isotherms for Water Vapor on :
(a) Molecular Sieve
(b) Silica Gel
(c) Alumina

cages or cavities through physical forces of the van der Waals type. If polar adsorbents are involved, ion-dipole type attractive forces are also operative. Generally, polar or polarizable molecules like H_2O, H_2S, NH_3, amines, aldehydes, alcohols etc. are strongly adsorbed by molecular sieves (22). Adsorption is mainly of the Langmuir type, whereby a monomolecular adsorbed layer is formed. Langmuir in presenting the first model of adsorption in 1916, assumes that a molecule can get adsorbed only on one site on the adsorbent surface. The langmuir theory is later modified by Br nauer, Emmett and Teller to accommodate adsorbed molecules of many layers thick, now popularly called the BET multilayer adsorption model (22, 27). Fig.(3.4) shows typical adsorption and desorption isotherms of water vapor on moleular sieves. For comparison, isotherms for two other most commonly used adsorbents silica gel, and activated alumina are also given. The differences are obvious from the graph. In the case of molecular sieves, adsorption is very strong at low relative vapor pressure and is almost complete at about 0.2. However, silica gel and alumina go on adsorbing as the vapor pressure is increased. Adsorption uptake at saturation pressure is also lower for molecular sieve. The shape of adsorption isotherms as shown in Fig. (3.4) points out the fact that there is uniform pore size for molecular sieves. The pores of which are micro with diameters less than 20Å. Silica gel and alumina, on the other hand, have distribution of pore sizes. Some are micro, many are transitional (20-200Å) and some are macro (more than 200Å). Multilayer adsorption is facilitated in silica gel and alumina unlike in molecular sieves. For example, in silica gel having a

predominant pore diameter of 30Å, about 10 layers of water molecules can be adsorbed, whereas in a molecular sieve of 4Å pore size, only a single layer can get adsorbed remembering that the effective diameter of a water molecule is 3.2Å (22). Another interesting feature in comparing the isotherms of molecular sieve with those of silica gel and alumina is the absence of hysteresis in the former. In silica gel and alumina, adsorption and desorption isotherms are not coincident thereby forming what is called a hysteresis loop. The implication of adsorption hysteresis is that at a given relative vapor pressure, more adsorbate is held by the adsorbent during desorption than that held during adsorption. Among other reasons hysteresis is caused by the presence of irregular "ink-bottle" shaped cavities. Adsorption hysteresis is of much theoretical and practical interest in surface chemistry, so it will not be discussed here in detail. The most versatile property which distinguishes zeolites from all other adsorbents is their ability to sieve and sort molecules according to their size and shape. Thus, n-paraffins from a mixed refinery stream containing branched and cylic hydrocarbons can be seperated. Hydrogen sulfide and carbon dioxide from natural gas are removed by using Type A molecular sieve, for removal of mercaptans, 13 X molecular sieve is used because of the large molecular diameter of mercaptans. A 5A molecular sieve similarily separates straight chain hydrocarbons from iso-compounds, either in the vapor phase or liquid phase. Zeolites are now widely used for "sweetening" (i.e., removing H_2S and other sulfur compounds) liquefied petroleum and natural gas.

The separation of para-xylene, which is used in the manufacture of polyester, from mixed xylenes and ethyl benzene is now successfully done in large scale by employing zeolite adsorbents. Pressure-swing adsorption process using molecular sieves now separates oxygen of 95% purity from air in a cheaper and more efficient way than conventional cryogenic separation routes (22). Such processes are also used in the manufacture of pure hydrogen by steam-reforming from a mixture of CO_2, CO, H_2O, CH_4 and N_2 which are much strongly adsorbed than H_2. Because of their high adsorptive selectivity and high adsorption capacity at low pressures, molecular sieves have now replaced other adsorbents in drying and purification of gases. One of the first industrial applications of molecular sieves since they were commercially introduced in the late 1950's is the dehydration of natural gas and air. For the cryogenic extraction of helium from natural gas, zeolites have distinctive advantages over other conventional adsorbents. Ethane recovery from natural gas, drying of cracked gases prior to low temperature fractionation, drying of ethylene, propylene and acetylene, are some other applications of molecular sieves. They are the only adsorbents which can produce effluent dew points as low as $-65^{o}C$, an important property in efficient ultimate drying.

A new class of acid-resistant molecular sieves has recently become available commercially for the drying of natural gas and refinery gas streams containing corrosive vapors of H_2S, Cl_2, HCl, SO_3 and NO_x (22). Conventional adsorbents like silica gel and alumina deteriorate rapidly in a corrosive acidic environment.

Molecular sieves are also equally efficient in dehydration in the liquid phase. Applications include the drying of alkylation feed, isomerization feed, kerosene, solvents, aromatics, halogenated hydrocarbons, etc.

3.6.2 Zeolites As Catalysts:

In the 1960's some zeolites were found to possess cracking activity far greater than any conventional silica-alumina catalysts. The centers responsible for the catalytic activity of zeolites are the so-called Bronstd acid centres (22). These reactive centres can result in the formation of carbonium ions as reactive intermediates responsible for cracking. Zeolites as cracking catalysts are first introduced in the market in 1962, and they have displaced other cracking catalysts ever since. They are far superior in their performance; they give less coking, increased production capacity and improved gasoline yields. These characteristics are too important in an energy-starved world. A marvellous property of zeolite cracking catalysts is that they can sieve as well as catalyse at the same time. For example, n-paraffins from a mixture of branched chain or cyclo-paraffins can be selectively adsorbed and cracked while others are left unchanged. This combination of molecular sieving and catalytic properties of zeolites is opening up a variety of new applications in petrochemical industry which were hitherto impossible (22).

3.6.3 Zeolites As Ion Exchangers:

Zeolites are capable of exchanging cations. It has been seen earlier that by exchanging cations, the window diameters are controlled. Synthetic ion exchange zeolites, however, are not as well developed commercially as zeolite adsorbents or catalysts. Some potential applications of zeolites as cation exchangers include removal of ammonium ions from sewage and agricultural waste, isolation of radio-active by-products of nuclear reactions for collection or disposal, ion-sieving, and separation of isotopes etc.

3.7 Uses of Zeolite in Industrial Adsorption Processes:

Many unique uses of zeolite have been developed over the years. Some of these uses include the drying of pyrolysis gas, separation of hydrogen isotopes, vacuum drying of iodine, drying of low molecular weight fatty acids, separation of lithium isotopes, adsorption of heavy water, and the drying of dimethyl formamide and acrylonitrile. Zeolites have been suggested as cigarette filters, packing desiccants, dessicants for fast drying cements, and as encapsulation of volatile or poison gases and liquids.

The major industrial adsorption processes using zeolite adsorbents may be classified as follows [39]:

1. Drying of gases and liquids.
2. Separation and purification of industrial streams.

3. Pollution Control applications.

4. Non regenerative applications.

5. Hydrocarbon separation processes.

3.7.1 Drying of Gases and Liquids:

All zeolites have a highly hydrophillic surface and are very efficient dessicants. Contrary to other nonzeolitic dessicants such as silica gel and activated alumina, zeolite adsorbents have a high water adsorption capacity at low concentration of water. To obtain extremely dry gases and liquids, therefore, zeolite adsorbents are strongly preferred over amorphous dessicants. The 3A molecular sieve adsorbent in particular has the additional advantage of selective adsorption for water because of its small pore size, and it is very useful in drying polar liquids and gases.

Ethylene and propylene are two of the most important petrochemical raw materials today. They are manufactured by a thermal cracking of ethane, propane, or naptha. One of the important separation - purification steps in the production of ethylene and propylene is the removal of water before low temperature separation. Although alumina has been the most commonly used dessicant in drying cracked gas in the past, 3A molecular sieve adsorbents have an overall economic advantage, and many cracked gas plants are using the 3A molecular sieve today. The main advantages of 3A molecular sieve over alumina and silica gel are its higher capacity and, therefore, smaller adsorption tower size and its

longer service life. The degradation of 3A molecular sieve in cracked gas drying is not from a chemical destruction of zeolites crystals but rather from an accumulated deposit of carbon material on the zeolite. Since a regular 3A, i.e. potassium exchanged type A, is not thermally stable enough to withstand normal carbon burn-off operation, it is replaced with a fresh charge of 3A molecular sieve when it has accumulated excessive carbon and other hydrocarbons derivatives. A rare earth containing 3A zeolite having sufficient thermal stability to withstand normal carbon burn-off conditions. This should prolong the service life of the zeolite adsorbents and, therefore, enhance the advantage of zeolite adsorbents in cracked gas drying over non-zeolitic dessicants.

3.7.2 Separation and Purification of Industrial Streams:

3.7.2.1 Purification of Air Prior to Liquefaction:

Separation of air by cryogenic fractionation processes requires removal of water vapor and carbon dioxide to avoid heat exchanger freeze up. Many plants today are using a 13X (NaX) molecular sieve adsorbent to remove both water vapor and carbon dioxide from air in one adsorption step. Since there is no necessity for size selective adsorption, 13X molecular sieves are generally preferred over type A molecular sieves. The 13X molecular sieves have not only higher adsorption capacities but also faster rates of CO_2 adsorption than type A molecular sieves. The rate of CO_2 adsorption in a commercial 13X molecular sieves seems to be

controlled by macropore diffusion. The optimum operating temperature for CO_2 removal by 13X molecular sieves is reported as 160-190K (39).

3.7.2.2 Natural Gas Purification:

Natural gas containing water vapor, sulfur compounds (mostly hydrogen sulfide), and CO_2 is purified by molecular sieve adsorbents. Since, with the exception of feed preparation for LNG, the complete removal of CO_2 is usually not necessary, the molecular sieve bed is used mainly to remove water vapor and sulfur compounds. The adsorption step is continued even after the carbon dioxide breakthrough. 4A and 5A molecular sieves are generally used to remove water and hydrogen sulfide from natural gas although 13X can be used when the natural gas contains a significant amount of large sulfur compounds. There is, however, some evidence that NaX can produce COS catalytically from H_2S and CO_2. Other important applications of molecular sieves in natural gas purification include purification of pipeline natural gas for liquefication, drying of natural gas prior to cryogenic hydrocarbon recovery using a turbo expander, and sweetening natural gas feed to ammonia plants.

3.7.2.3 Oxygen Enrichment of Air:

Recent developments in application of oxygen or oxygen-rich air in biological waste water treatment plants generate a necessity for a low cost, on-site oxygen generator. Many waste-water

treatments in the U.S. require less than 100 tons per day of contained oxygen. For the low-to-intermediate range, the pressure swing adsorption process using zeolite adsorbents is competitive with, or advantageous over, the conventional cryogenic air separation process. Commercial processes known today are: Esso Research and Engineering Processes, the W.R. Grace process, the Union Carbide Process, the L'Air Liquids Process, the Bayer-Mahler Process, and the Nippon Steel process. Differences between these processes are type of zeolites used, number of adsorbent beds, operating pressures, and cyclic operating steps. The pressure swing adsorption process can produce up to 95% oxygen, the remainder mainly argon, and is definitely advantageous over the cryogenic air separation process at below 25 tons-per-day capacity. Other potential applications of oxygen rich air produced by pressure swing adsorption processes are pollution control in the pulp and paper industry, secondary smelting plants, river and pond aeration, feed gas to ozone generators, medical applications and chemical oxidation processes.

3.7.3 Pollution Control Applications:

Zeolite adsorbents can effectively remove pollutants such as SO_2, H_2S and NO_x from industrial off-gas streams at near ambient temperature. Since water vapor usually exists along with these acidic compounds, an acid-stable or acid-resistent zeolite adsorbent is necessary for a long service life. Union Carbide developed three processes for pollution control [39]. They are the PuraSiv-Hg

process for mercury vapor removal, the PuraSiv-N process for NO_x removal from nitric acid plant off gas, and the PuraSiv-S process for SO_2 removal from sulfuric acid plant off-gas. A recent British patent describes a process using a molecular sieve bed preadsorbed with 0.1-10 wt% of ammonia before the gas stream containing acidic gases is introduced.

3.7.4 Nonregenerative Applications:

Applications of zeolite adsorbents are not limited to the fixed-bed, cyclic operation discussed above. Some applications involve no regeneration and therefore no cyclic operation. Important non regenerative applications are drying Freon-type refigerants and manufacture of dual-pane windows. Every refrigerator and air conditioner using halogenated hydrocarbon refrigerants require a dessicant cartiridge to keep the refrigerants super dry. The 3A molecular sieves can effectively dry refrigerants, but its catalytic activity to decompose refrigerant should be suppressed. In the dual-pane windown application, zeolite adsorbents are often used together with other adsorbents such as silica gel to keep the vapor pressure of gases inside the dual-pane windows sufficiently low. It is important to remove water vapor and organic solvent vapors from the sealing compound to avoid fogging in winter months.

3.7.5 Hydrocarbon Separation Processes:

These processes include n-paraffin, p-xylenes and olefins separation. This thesis will concentrate on n-paraffins separation by adsorption on zeolite type-5A which will be discussed in the subsequent Chapters.

3.7.5.1 n-Paraffin Separation:

n-paraffins are separated from a mixture of paraffins by using a CaA molecular sieve which has a Ca effective pore diameter of about 5A. Because of its pore size, a Ca-A molecular sieve adsorb only n-paraffins, and the effluent from a molecular sieve bed contains mainly isoparaffins and a small amount of aromatics existing in the feed stream. The adsorbed n-paraffins are later desorbed from the bed and recovered. Major commercial processes in n-paraffin separation are the Molex process, the British Petroleum process, the Isosiv process, the Texaco Selective Finishing process, the Ensorb process, and the Parex process. Except for the Molex process which operates under liquid phase, all and others operate under vapor phase and use the fixed-bed, cyclic adsorption technology. The processes are different, however, in operating conditions. Most processes operate under isothermal and isobaric conditions with desorption of n-paraffins by displacement. Displacement agents often mentioned in patent literature are low boiling n-paraffins such as n-pentane and n-hexane, and ammonia or alkylamines. Inert gases such as nitrogen are mentioned also, but

they may serve as carrier gases rather than displacement agents. Some processes utilize a pressure swing operation, especially for separating low carbon number n-paraffins. In pressure swing operation, the adsorption pressure is substantially higher than the desorption pressure to furnish enough driving force for a reasonably fast mass transfer. In cases where product purity is important, an intermediate step (purge step) is used after adsorption steps. Purging removes iso-paraffins existing in the void space between molecular sieve adsorbents and macropores within each adsorbent particle prior to desorption step. Because most impurities can be removed from the adsorbent bed in the purging step, the n-paraffins recovered in the subsequent desorption would be relatively pure. The operating temperature for vapor-phase process must be above the highest boiling point of the feed stream but generally lower than 700 K (427°C) to avoid cracking. Desorption of n-paraffins is achieved by displacement. The rate of n-paraffin desorption generally controls the overall production rate. The diffusion of n-paraffins in commercial 5A molecular sieve is reported to be controlled by either micropore diffusion or macropore diffusion or both, depending on the molecular sieve crystal size and macropore size distribution of the adsorbent. A 5A molecular sieve adsorbent with smaller crystal size and optimum macropore size distribution would have a faster adsorption-desorption rate and, therefore, a higher effective capacity.

3.7.5.2 p-Xylene Separation (V.O.P.'s Parex Process):

The continued rapid increase in the p-xylene demand as a raw material for poly[illegible] products in recent years necessitates the development of a new xylene separation process for separating p-xylene from a C_8-aromatics mixture containing xylenes and ethyl benzene. The hardware for the Parex process seems to be similar to that for the U.O.P.'s Molex process for n-paraffin separation, and it uses the continous liquid phase, simulated moving bed operation. This process, in a pilot-plant operation, demonstrates that it can separate p-xylene from various types of feedstocks with 99.5% purity and recovery as high as 98.4% (40). The high p-xylene recovery in particular is believed to be a significant improvement over conventional crystallization processes. Patents issued to U.O.P. in regard to aromatic separation suggest that the adsorbent used is a synthetic faujasite (41). Recent literature (39) also claims that sodium mordenite and modified type-Y zeolite containing predominantly potassium ions can separate p-xylene from a xylene mixture and a C_8-aromatic mixture, respectively. However, neither is known to be commercialised yet.

3.7.5.3 Olefin Separation (U.O.P.'s Olex Process):

U.O.P's other hydrocarbon separation process developed recently - i.e., the Olex process- is used to separate olefins from a feed stock containing olefins and paraffins. The zeolite adsorbent used, according to literature, is a synthetic

faujasite (39). The Olex process is also believed to use the same simulated moving-bed operation in liquid phase as U.O.P'S other hydrocarbon separation process i.e. the Molex and Parex processes.

CHAPTER FOUR

NORMAL PARAFFINS SEPARATION METHODS

CHAPTER FOUR

NORMAL PARAFFINS SEPARATION METHODS

4.1 Introduction:

The common techniques used for separation of n-paraffins are urea adduction and molecular sieve adsorption. Each of these processes exhibits a selectivity according to the size of molecules. The normal or straight-chain molecules of paraffins have smaller radii than other hydrocarbons and hence can selectively enter the openings in urea adduct or zeolite crystals and become occluded in their cavities. Urea adduction has been used selectively but has some disadvantages; the breaking of adduct can easily occur and some non-normal paraffins also could participate in adduct formation (4). These disadvantages do not exist in case of adsorption by molecular sieves. Other separation methods include fractional distillation, fractional crystallization, elution chromatography, and thin layer chromatography (11).

Whilst this study is concerned with separation of n-paraffins from multicomponent mixture by molecular sieves, brief summaries of alternative processes are given.

4.2 Alternative Separation Methods:

4.2.1 Separation by Fractional Distillation:

Separation by distillation is based on the differing boiling

points of the components. This separation method is limited, since the boiling points of the successive members of the n-alkane series, particularly in the case of compounds containing more than 25 C-atoms, are very close to one another and there is a danger in intense cracking of the products at the temperature required for distillation. Therefore, preparative separation by distillation is effective mainly in the case of $<C_{20}$ n-alkanes. This separation method is difficult to apply to iso-alkanes and cycloalkanes, since the boiling points of the members of these two homologous series overlap.

If a mixture of pure n-alkanes has been first separated, by some method, from the material to be analyzed, the distribution of the compounds in the mixture can be determined by distillation.

Clearly separation by distillation is much less effective in the case of microcrystalline paraffin waxes than in the case of liquid paraffins and macrocrystalline paraffin waxes.

4.2.2 Separation By Fractional Crystallization:

A successful method for the separation of microcrystalline paraffin waxes is fractional crystallization based on differential solubility. Ketones, mixture of ketones and aromatics, halogenated hydrocarbons and different gasoline grades have been used as solvents in research up to the present. Fractional crystallization

yields fractions of both macrocrystalline and microcrystalline paraffin waxes differing in molecular structure and molecular dimension. At higher temperatures of crystallization, fractions containing higher molecular weight and less branched alkanes, as well as cycloalkanes with long side chains will crystallize. With successive lowering of the temperature, the fractions will contain more and more iso-alkanes and cycloalaknes with shorter side chains; simultaneously the average molecular weight of the fractions will decrease. A further disadvantage is that the process is slow and therefore a large equipment investment would have to be made for a large-scale manufacture.

4.2.3 Separation By Elution Chromatography:

For chemical group analysis of liquid paraffins and macro- and microcrystalline paraffin waxes, column chromatographic separation methods are used. Silica gel or activated alumina is preferably used as adsorbent. The ratio of adsorbent to sample is between 20:1 and 30:1 which has a limiting effect on such a process. The sample is introduced in the form of a dilute solution in gasoline or hexane. The succession of the eluents is that of the increasing polarity, e.g. hexane, mixture of hexane and benzene, benzene, methanol and chloroform. This method allows separation of saturated hydrocarbons, and mono-, bi- and tricyclic aromatics with satisfactory sharpness.

4.2.4 Separation By Thin Layer Chromatography:

Separation of macro- and microcrystalline paraffin waxes by thin-layer chromatography has been developed, among others, by Dietsche (11). They use a 250 micrometer silica gel support layer impregnated with 40% urea. To avoid recrystallization of the urea, a small amount of sorbite is applied. The paraffin wax to be studied is applied in a 1% solution in benzene, at 323 to 333.K (50-60°C). The solvent used for runs is a mixture of carbon tetrachloride and ethanol saturated with urea. By using appropriate conditions and simultaneous runs with reference standard materials, they could determine the ratio of n-alkanes and iso-alkanes in macrocrystalline paraffin waxes.

4.2.5 Separation By Adduct Formation with Urea:

n-Alkanes can also be separated from iso- and cycloalkanes by urea adduct formation. X-ray studies have shown that the long chains of n-alkanes as well as long chains, if present, of iso- and cycloalkanes are enclosed in the tubular channels of the adduct, and this results in a hexagonal urea lattice. Urea crystallizes in the hexagonal system only when an adduct is formed, its normal crystal system being tetragonal. Straight-chain derivatives of n-alkanes, e.g. carboxylic acids, alcohols, esters, amines, etc., are also capable of adduct formation.

Adduct formation between n-alkanes and urea takes place in

solutions of the former in gasoline, benzene or halogenated hydrocarbons when solid urea or an aqueous or alcoholic urea solution is added. When solid urea is applied, a small amount of a wetting agent, i.e. water, alcohol or some other substance with a similar effect is necessary.

Adduct formation is inhibited by resins, bituminous substance, sulfur compounds, etc. It is, therefore, important to remove such substances from the material before adduct formation, by elution chromatography or some other method.

Adduct formation is an equilibrium reaction, the equilibrium being dependent on temperature, concentration of urea and adduct-forming components, and nature of the solvent.

The following method is used by Hessler and Meinhart (11). Dilute solutions of macro- and microcrystalline paraffin waxes in carbon tetrachloride are prepared, methyl alcohol saturated with urea is added and the mixture vigorously agitated. The crystalline precipitate formed is filtered, washed with alcohol and dried. The decomposition of the adduct is carried out with distilled water at 343 K (70°C). A diagram of the urea adduct method developed in the Hungarian Oil and Gas Research Institute is shown in Fig. 4.1.

As well as urea, thiourea can also successfully be used for studying the chemical composition of complex mixtures of hydrocarbons and thin derivatives. This urea forms adducts most

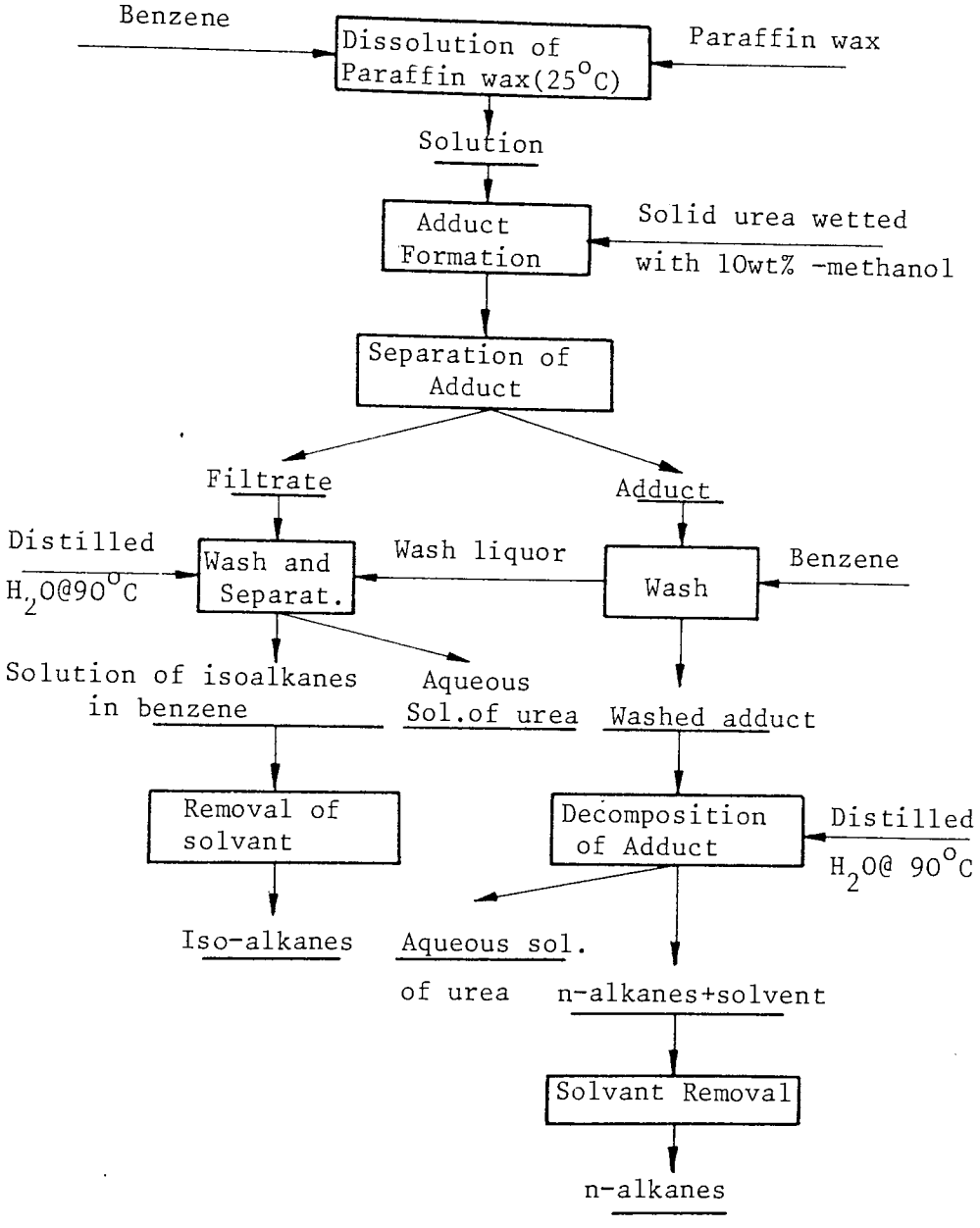

Fig. 4.1 Method for Separation of the n-Alkanes and Iso-Alkanes Content in Macrocrystalline and Microcrystalline Paraffin Waxes by Urea Adduct .

readily with branched compounds (11).

Urea adduct deparaffinization process of different petroleum cuts has been studied by Dorodnova et al. (42). Separation of paraffins from kerosene-diesel and diesel cuts using urea has been commercially used (12). The liquid paraffin produced by deparaffinization of kerosene-diesel and diesel cuts with water/alcohol solution of urea contains at least 93-95% n-alkanes. Other deparaffinization of kerosene-diesel cuts process can be achieved with saturated aqueous soulution of urea and with crystalline urea in the presence of methanol as an activator. The low purity of liquid paraffin isolated by urea adduct could be attributed to the coadsorption of normal paraffins by iso-alkanes and some of the aromatic hydrocarbons. In a study conducted recently, Owaysi and Al-Ameeri (1) separated n-paraffins from two feedstocks by the urea adduct technique. The reported purities of n-paraffins isolated from straight-run kerosene and naphtha-kerosene blend were 85.01% and 91.40% respectively. Thus in the case of urea adduct, the purity of n-paraffins depended strongly on the composition of the hydrocarbon feedstock from which they were separated. In addition, these purities were lower than the corresponding purities obtained in the case of separation by adsorption on molecular sieves. The two separation techniques are quite different in nature. While the molecular sieve process is simply a physical adsorption process, urea adduct formation is an equilibrium exothermic reaction whose heat of reaction increases as the alkane chain becomes longer. Hence the longer the

adduct-forming molecular chain, the greater the stability of the adduct (i.e., the greater the degree of its recovery). Short-chain n-alkanes form adducts only at low temperatures, and these products will readily decompose. Compounds, such as alkylbenzene, which are too large to enter the zeolite micropores, form adduct with urea, thus contributing to the impurities present in the separated n-paraffins.

4.3 Separation by Adsorption on Molecular Sieves

Molecular sieves are zeolites consisting of aluminium, calcium, alkali and hydrogen orthosilicates. Their characteristic feature is the ready compensation of the negative charges of their tetrahedral SiO_4^{-4} and AlO_4^{-4} crystal lattices by cation exchange. The interconnected voids in their lattices contain combined water that can reversibly be removed by heating. Dehydrated zeolite is capable of binding molecules having suitable dimensions to fit into the voids.

For the separation of n-alkanes from hydrocarbon mixtures, synthetic molecular sieves of type-5A are most suitable. The average diameter of their pores is 5Å, their chemical composition is $Ca_{4.5}\ Na_3\ [(AlO_2)_{12}\ (SiO_2)_{12}].\ 30\ H_2O$. Separation using adsorption on molecular sieves is adapted in this study for the separation of n-alkanes from heavy kerosene.

For production of pure liquid paraffins in industry this

process is carried out in general on three stages: feedstock distillation followed by zeolite adsorption then oleum treatment for removal of aromatic concentrate and regeneration of acid tar. In liquid paraffin process, the feedstock has to be in the range of 463-593 K. The yield recovery of liquid paraffin from kerosene-diesel cuts using molecular sieves is in the range of 97-98%, aromatics content in liquid paraffin after oleum treatment is not greater than 0.4-0.1% wt (43).

Sodhi and Chandra (24) mentioned several basic adsorption process cycles which involve adsorption and desorption. These can be classified as thermal swing, pressure swing, purge gas stripping, displacement and a combination cycle.

Thermal Swing Cycle:

This process employs different temperature levels for adsorption and desorption. The desorption temperature is always higher than the adsorption temperature. An upper limit to the adsorption temperature is in any case imposed by the thermal stability of the adsorbed material.

Pressure Swing Cycle:

Adsorption processes can be operated at a constant temperature by conducting adsorption under pressure and desorption under reduced pressure or vacuum.

Frequently, the above two techniques are combined i.e. low temperature and high pressure being used in the adsorption step and high temperature and low pressure in the desorption step.

Purge Gas Stripping Cycle:

The effect of purging an adsorbent with a non-adsorbable gas is similar to desorption by reduction of the total pressure. In such a case the purge gas reduces the partial pressure of the adsorbate in the void space surrounding the adsorption surface.

Displacement Cycle:

This cycle uses the difference in affinity of the adsorbent for different molecules: thus, desorption occurs by introducing an adsorbable fluid which displaces all or part of the previously adsorbed material. If a more strongly adsorbed fluid is used, it will be adsorbed and displace the less strongly adsorbed material on the adsorbent. When a less strongly adsorbed fluid is used, desorption is due to both displacement and partial pressure stripping.

Displacement can be effected by steam or other polar molecules (e.g. H_2S or CO_2) or higher or lower n-paraffins. The preferred purge gases are normal paraffins having at least 4 carbon atoms per molecule. Esso's Ensorb process uses ammonia for desorbing normal paraffins (44).

Separation using adsorption on molecular sieve type-5A is adopted in this study for isolation of n-paraffins from heavy kerosene (b.p. 505-588 K).

CHAPTER FIVE

NORMAL PARAFFINS SEPARATION BY ADSORPTION ON ZEOLITE

CHAPTER FIVE

NORMAL PARAFFINS SEPARATION BY ADSORPTION ON ZEOLITE

Separation based upon adsorption with the zeolitic molecular sieves compares favourably with the urea adduction process from the point of view of economics. The product from the adsorption process is of high purity, i.e. >96%, and operating costs are lower.

5.1 Commercial Separation Processes

The Isosiv process developed by the Linde Company operates on an isothermal pressure swing cycle as described in Section 3.7.5(45, 46, 47, 48). Originally it produced lower n-paraffins (C_5-C_{12}) but later the process was extended to separate higher n-paraffins (C_{10}-C_{16}). For the separation of lighter n-paraffins, two adsorption columns are used, working alternatively under pressure. One adsorbs whilst the other is desorbed and regenerated. For the separation of C_{10}-C_{16} n-paraffins more adsorbers are used in series. Adsorption is carried out in the vapor phase and is very flexible, giving 90% yield of n-paraffins of 95% purity.

The British Petroleum M.S. Process makes use of an isothermal isobaric cycle for the extraction of n-paraffins from C_{10}-C_{18} (from gas oil) (48, 49). Adsorption takes place in the vapor phase and desorption is accomplished with a boiling paraffin. The molecular

sieves are loaded under pressure (9.5 atm) since the adsorption rate of molecular sieve increases substantially with increasing pressure. In order to avoid cracking, evaporation is carried out in the presence of nitrogen as carrier gas. By connection of several adsorbers in parallel, the discontinous operation of a single adsorber is converted to fully continous operation. Products in the C_{13}-C_{17} range typically have a n-paraffin content of 97% weight, while product in the C_{10}-C_{17} range may be of 98% purity or better.

The Molex Process, was first developed in 1959 for improving the anti-knock properties of gasoline, and was later extended by UOP for the separation of detergent range normal paraffins (49, 50, 51, 52, 53, 54, 55). The adsorption of n-paraffins takes place in the vapor phase. Operation is isothermal and continous, in that feed and products enter and leave the process at a constant rate and with constant composition. Pressures are moderate, of the order of 1 atm and temperatures do not exceed the atmospheric boiling points of the charge stocks. The system has made it possible to use a single stationary bed of solid adsorbent in a way which produces the desired results. The desorbent used is a low boiling hydrocarbon fraction. The recovery of n-paraffins is 85%, the purity being 96%. Feedstocks are straight run petroleum fractions which have been fractionated to include the C_{11}-C_{14} hydrocarbons. These feeds are catalytically hydrotreated into the Molex unit.

The Texaco Selective Finishing Process is employed for improving the octane number of light catalytic reformates, light

straight run napthenes and isomeric stocks (56, 57).

The Parex Process developed by VEB Leuna Works "Walter Ulbricht", East Germany for the production of C_{10} to C_{18} n-paraffins from petroleum fractions boiling in the range of 453 to 593 K consists of three stages (58, 59, 60). In the first the n-paraffins are adsorbed on a specially modified molecular sieves type-5A in the presence of an auxiliary gas at 573-673 K and 5-15 atm; these temperatures and pressures are maintained throughout the entire process. In the second stage, a gas is used to remove material adsorbed in the secondary pore structure. Finally, the n-paraffins are desorbed with n-pentane. Prehydrofining of the feed is sometimes necessary if the sulfur content of the feed is more than 300 ppm and olefins are more than 1.0 wt%. Additional swing adsorbers are used for oxidative regeneration of the molecular sieves during operation.

The Ensorb Process developed by ESSO Research and Engineering Co. is designed for the recovery of high purity n-paraffins using ammonia as desorbing agent (5 . Paraffins upto C_{33} have been recovered by this process in pilot plant equipment. Since the heats of adsorption of C_{10}^{+} n-paraffins are typically above 41.87 kJ/mole, cycles involving desorption by depressuring are effective only at very low pressures. Desorption by ammonia at a convenient pressure (1.0-3.4 atm) overcomes this high heat of adsorption of normal paraffins. The heat of adsorption of ammonia on the molecular sieves type-5A (41.87-50.24kJ/mole) balances the

energy required to desorb n-paraffins. Ammonia is also added to hydrocarbon feed during adsorption step to assist in vaporizing the heavier components. The addition of ammonia into the feed is claimed to improve product quality. The process is operated at constant temperature (533-643 K) and constant pressure (1.0-3.4 atm). Adsorption takes place in the vapor phase. By employing two beds of adsorbents, one for adsorption and one for desorption at all times, continuous flow of the feed and ammonia stream is maintained. A large Ensorb unit has been in operation at Bayton, Texas, since January 1965, with the feedstocks in the C_9/C_{10} boiling range. The purity of the n-paraffin is greater than 98 wt%. Regeneration is accomplished by exposing the molecular sieve beds to a controlled amount of oxygen in air and is undertaken about once a year, thus prolonging sieve life. Since provision is made for regeneration, the need for feed pre-treatment by hydrofining is reduced.

The commercial processes described above are used not only for the separation of n-paraffins, which are valuable for the manufacture of synthetic detergents but also for low boiling straight run distillates and reformates. The objectives then are; to increase the octane number by removal of paraffins and, on the other hand, to recover n-paraffins for use as fuel for aeronautic purposes. Low boiling n-paraffins are of interest to the chemical industry as raw materials for the production of acids, aldehydes and alcohols. Cracking of normal paraffins to olefins may also be possible by the combination of aromatic extraction, molecular sieves and isomerisation processes and offers interesting possibilities for

the future.

5.2 N-Paraffins Adsorption Studies on Zeolites

Avery [10] disclosed an isobaric process for separating n-paraffins from a hydrocarbon vapor feed mixture (containing either or both kerosene with 10-15 C or gas oil with 15-25 C atoms/molecule, b.p. 447-543.5 K) by selective adsorption of the normals in a crystalline calcium zeolitic molecular-sieve, type 5A, in the form of 1/8" pellets. N-hexane vapor was used as a desorbing agent. The n-paraffins were separated from the desorbate by a fractional condensation method. An efficient separation by this method is obtained with a high heat transfer coefficient which is furnished by an isobaric operation. The inventor gave a comparison between an isobaric and pressure swing desorption. He discovered that in contrast to the pressure swing gasoline feedstock-molecular sieve selective adsorption process, minimum deactivation rate (i.e. minimum loss of adsorption capacity) of molecular sieves material is achieved in his isobaric process with kerosene feedstock when the adsorption-desorption temperature is relatively low, between about 574-630 K (the operable range for the process is between 533-700 K). The higher desorption pressure used in this isobaric process (1.4-4.4 atm) decreases the deactivation rate more rapidly as compared to vacuum desorption, moreover it increases the effectiveness of the n-hexane as a desorbing agent. The adsorption-desorption process are performed at substantially constant temperature. The optimum performance is achieved in the

temperature range of 589-608 K.

A process involving a vapor-phase adsorption separation of n-paraffins by five beds of 5A-zeolite from a kerosene range fraction of average carbon number of C_{11} boiling in the range 423-523 K has been reported by Grebbell (61) to permit the purity of n-paraffins to be increased. The process comp rises three stages of adsorption, washing and desorption, all conducted at constant temperature (623-673 K). The pressure of the first two stages was in the range 0.34-3.4 atm while the desorption pressure was in the range of 1.3×10^{-4} - 263×10^{-4} atm (this has been achieved by direct condensation with recycled n-paraffins product). Toluene or benzene (being a mononuclear aromatic hydrocarbon) was used as a washing agent to remove non-normal materials from the void spaces in the adsorbent and macroporous structure of the sieves. The feed is passed into the bed until 90-110% of the break through volume has been passed (within 1-2 minutes) and the washing stage is continued until 40-80% of the bed volume of benzene or toluene has been passed (in 30 seconds). The preferred duration of desorption stage was found to be (3-8 minutes). The feed flow rate was in the range (1-2 v/v/hr). The result achieved was a desorption effluent containing 98.5 weight % n-paraffins; 0.6% aromatics and 0.9% other materials. This was obtained at a rate of 0.75% sieve weight/cycle. This relatively high purity can be attributed to the efficient desorption method adopted by Grebbell (61), i.e. pressure reduction since n-paraffins found in kerosene (in contrast to that in gasoline feedstocks) are more strongly adsorbed by molecular sieves material

and can only be effectively desorbed by this very low pressure range.

Anstey & Macnab (62) disclosed an adsorption separation process similar to the process performed by Grebbel (61) to some extent by which kerosene fraction containing 25.6% weight of n-paraffins in the C_{10}-C_{15} range (b.p. 447-543 K) and contacted with five beds of 5A molecular sieve. Such a process comprises stages of adsorption, purging and desorption respectively, all being conducted isothermally at 653 K, purging and desorption being affected by pressure variation alone. Purging was carried out simultaneously from both ends of the sieve bed at 0.102 atm, desorption being conducted only from the end opposite to that at which the feed was introduced at a pressure of 6.8×10^{-3} atm. The feed flow rate was 0.5 v/v/hr and a duration of 4, 1.5, 6.5 minutes for the three stages was timed respectively. The n-paraffins yield was 3.0% sieve weight/hr with a purity of 97.5% weight and the carbon number distribution substantially the same as the feed. By desorbing from both ends of the bed simultaneously , the n-praffins yield was increased to 3.5% sieve weight/hr.

The process of Turnbull & Gilbert (63) involves passing a vaporized kerosene fraction (boiling range 453-513 K) over a bed of 5A-molecular sieve at a temperature of 644 K and at elevated pressure (2.5 atm) until the sieve was substantially saturated with n-paraffins. The pressure in the purge stage was then reduced to 0.112 atm by partial vacuum drawn by passing the effluent vapor up a

condenser column countercurrent to a flow of quench liquid. This condenser column was provided with a baffle arrangement to improve the vapor-liquid contact. Then by the same manner the pressure was further reduced to 5.3×10^{-3} atm in the desorption stage. In this process the kerosene vapor was fed to the top of the sieve bed in the adsorption stage of the cycle and it passed out under the pressure control at the base of the adsorber. In the purge stage the adsorber was opened through any combination of three valves at its top, middle and base to the purge condensers causing reduction of the adsorber pressure and transfer of material to the condenser. Similarly in the desorption stage, material was withdrawn through the same adsorber evacuation manifold to the desorption condenser. The feed flow rate was 5.485×10^{-3} kg/s. The n-paraffin yield to the desorption condenser was 0.58% wt. sieve/cycle and the purity of normal paraffin content was 98% by weight.

One method by which the n-paraffins (in the kerosene or gas oil range) can be desorbed is by pressure reduction. Turnbull & Gilbert (63) proposed to effect the pressure reduction by directly condensing the effluent vapors from the adsorbent bed with a quench liquid. However, when the effluent vapors are hydrocarbons in (a gasoline fraction boiling in the range 303-473 K), in order to get a low enough pressure to effect the desorption it is necessary to cool the recycling liquid below ambient temperature. This involves a large capital and operating cost for refrigeration plant. Wanless (64) therefore invented a process that avoided this disadvantage by which the pressure reduction for the desorption stage is effected by

means of an ejector which is a jet pump (65) that uses either gas or liquid for either motive or entrained fluid and discharges at a pressure intermediate between the motive pressure and the suction pressure. By treating a feed stock of C_7-C_9 range at an isothermal temperature of 633 K and a flow rate of 12.03 kg/hr using this technique the cyclic yield to the desorption condenser was 1.81% sieve weight and contained 94.5% n-paraffins. The pressure at the end of adsorption, purge and desorption stages were 11.5 atm, 1.0 atm and 7.9×10^{-2} atm respectively.

Powers & Corer (66) disclosed a method for purifying the normal paraffins desorbed from a bed of molecular sieve. The invention contemplated passing a vaporized n-paraffin-containing hydrocarbon stream boiling in the kerosene range in contact with a bed of 5A molecular sieve. This was carried out at about 1.34 atm and 616 K until from about 4.54×10^{-3} - 0.091 kg of n-paraffin in the feed stream has been passed per kg of sieve in the bed. The bed was then purged with ammonia vapor to displace the adsorbed normal paraffins by the action of the ammonia gas which was passed in contact with the bed until about 0.02 kg of NH_3 gas per kg of bed has been employed. The temperature of the desorption was about 616 K at a pressure of 1.34 atm. Vapors from the sieve bed were then passed through a condenser to liquefy the hydrocarbons and to remove the ammonia as a non-condensable gas stream. Powers et al. (66) suggested that the first portion of the hydrocarbons may be withdrawn during the initial stages of the desorption step and segregated for recycle. The second portion (about 88% of the total

desorbed hydrocarbons) was recovered as desorbate product believed to contain about 96-97% n-paraffins, 1.0-1.5% isoparaffins, 1.5-2.0% cycloparaffins, and about 1.0-2.0% aromatics. The desorbate product was then fractionated to obtain a product of C_{11} to C_{14} n-paraffins of 98% purity and containing a lower percentage of aromatic hydrocarbons than were present in the desorbate. This was accomplished by precise fractionation to obtain a final product boiling within the range of (477-525 K).

Lauder & Rolfe [67] proposed a cylic, vapor-phase, pressure swing process for the separation of n-paraffins from a kerosene feed stock fraction of average carbon number of C_{11}. Such a process comprises the steps of adsorption, purging and desorption. Purge effluent was recycled through a bed of 5A molecular sieves in an adsorption stage and an effluent of reduced n-paraffin content was recovered. The bed was purged to remove surface adsorbed and interstitial matter by reducing the pressure in the bed by direct contact condensation with fresh feed introduced at or near ambient temperature. A purge effluent was recovered for recycle to stage one. The bed was then desorbed to recover n-paraffins by further reducing the pressure in the bed. The operating temperature of the process was in the range of 623-673 K, an adsorption pressure of 0.34-3.4 atm, a purge pressure of 6.6×10^{-3} - 0.2 atm, and a desorption pressure in the range of 1.3×10^{-4} - 2.6×10^{-2} atm. No more details were reported about the yield and product purity or even the dynamic capacity of such a process.

Savage et al. [68] encountered the problem of bed lifting in a cyclic molecular sieve adsorption-desorption process wherein desorption was effected with a displacing agent, such as ammonia, by making use of a co-current adsorption-desorption cycle at temperatures between 658 and 680 K and pressure between 1.0-3.4 atm. After the bed was loaded with displacing agent and fresh feedstock was passed into the system, bed lifting occurred because the displacing agent was desorbed so rapidly that it caused the bed of molecular sieve to rise up suddenly with explosive force. This resulted in a considerable breakthrough of adsorbable feed material. By the proposal mentioned previously, bed lifting was prevented, impurities were not found when adsorbed component was desorbed from the sieve and temperatures were sufficiently low to prevent cracking in the feed stock. These proposals are claimed to be applicable to the removal of normal paraffins from kerosene feedstocks in order to recover normal paraffins for use in biodegradable detergents, whilst simultaneously improving the characteristics of the kerosene by reducing the cloud and pour points.

Phillips [69] presented a method for predicting the behaviour of the desorption step in a vapor-phase adsorption process of normal paraffins from a fixed bed of type 5A molecular sieves. This is important since it determines the amount of product recovered per cycle and, as a consequence, the capacity of the bed for the next adsorption step. An attempt was made to define a relationship between the amount of heavy normal paraffin desorbed as a function of quantity and nature of the purge material, temperature, and

pressure. This relationship is usually obtained from experiments. It was shown, in the case where the purge material is a lower molecular weight normal paraffin (e.g., pentane C_5 or hexane C_6), that the desorption curve may be calculated from knowledge of the adsorption behaviour of the individual components, provided that the desorption step is regarded as an equilibrium process. The experiments were carried out for normal tridecane (C_{13}) to represent the heavy normal paraffin feed material and three different purge materials (n-C_5, n-C_6, and n-C_7) at two temperatures 561 and 616 K and three pressure levels (2, 1, and 0.13 atm). As a conclusion, it was found that, as might be expected the desorption process is generally favoured by higher temperatures, lower pressures, and increasing molecular weight purge. Also, it has been shown that, after about 0.036 kg purger/kg sieve, desorption becomes a linear function of purge quantity.

The vapor-phase desorption of normal paraffins from a fixed bed of type-5A molecular sieves was the object of considerable interest. In the usual case, the desorption is accomplished by displacing normal paraffins previously adsorbed on the bed by a purge material, which can then be separated from the normal paraffins by conventional means. For the important case in which the purge material is a normal paraffin of lower molecular weight, Phillips [70] gave three case studies which describe the desorption process. The first two studies were semi-theoretical in nature and consist primarily of calculation procedures for predicting desorption or elution curves. The third study contains some rather

extensive experimental results. Direct comparisons were made for the three studies at 2.50 atm total pressure, n-tetradecane originally on the bed, n-hexane purge material and two temperatures 644 and 700 K. Agreement between the data and predicted results was good in both cases.

O'Connor and Norris (71) described a procedure for recovering the adsorbed normal paraffins from the 5A molecular sieves by desorption with n-pentane. The mechanism of recovery appeared to be a diffusion-controlled process, with the rates of desorption varying inversely with the molecular weight.

Barton and Hajnik (72) examined the feasibility of the combination process of volatility amplification of non-volatile mixtures by the addition of supercritical fluids followed by contacting the vapor with molecular sieves to separate specific materials from the mixtures. C_{16}-C_{32} wax distillate was separated into n-paraffin and denormal oil fractions by vapor-phase contact with type-5A molecular sieves. 2,2,4-trimethylpentane (iso-octane), 2,2-dimethylbutane and 2-methylpentane were each used as the supercritical fluid. Recovery of n-paraffins from the molecular sieves was accomplished by contacting the molecular sieves with nitrogen or ammonia gas. It appeared that temperatures in the range of 500 to 670 K for the adsorption of n-paraffins in the 560-740 K boiling range on type-5A molecular sieves should be considered for investigating the combination of supercritical fluid volatility amplification and vapor phase molecular sieve process.

Sinha et al. [73] investigated the feasibility of using steam as a desorbent for n-paraffins adsorbed on Linde Molecular Sieve Type-5A. The feedstock was kerosene obtained from Gujrat Refinery and experiments were conducted at two different temperatures (473 and 523 K) for a fixed feed rate. Desorption with steam has been carried out repeatedly for a number of cycles without intermediate reactivation. Substantial decrease in adsorption capacity of the sieves was observed. On reactivation, the sieve regained its original capacity. Performance of steam was compared with n-pentane as desorbent and it was concluded that the adsorption capacity of 5A-zeolite decreases with cycle number when using steam as a desorbent for recovering the n-paraffins adsorbed and the decrease is larger at lower temperatures, also the reactivation at 673 K restores the original capacity of the sieves to adsorb n-paraffins. Compared to n-pentane, more time was required for desorption with steam. The performance of n-pentane, was found to be superior to that of steam. However, it was proposed that if the molecular sieves can be modified to reduce the equilibrium loading of water at desorption temperature, then steam can be recommended on grounds of lower cost and easier separation from the product.

Equipment for adsorption separation of n-paraffin from Gujarat kerosene (Baroda refinery, straight run of b.p. ranging from 413-573 K) using molecular Sieves (LMS-5A) was designed by Shukla et al. [4] to identify optimum operating conditions (pressure, flow rate, temperature, etc) for the recovery of normal paraffins from kerosene so that the remaining stock could also be of marketable

quality. The optimum operating conditions were identified as 14.3 atm (at 653 K) and 2.5 x 10^{-7} m^3/s. Under these conditions a recovery of 6.83 x 10^{-8} m^3/s kg of adsorbent was obtained. The purity of recovered n-paraffins was above 94%. The equilibrium loading at the optimum conditions was 54 x 10^{-6} m^3 for 0.63 kg of adsorbent and it increased with pressure. Ammonia was seen to be the best desorbent agent compared with N_2 and LPG.

To sum-up all commercial processes operate on an adsorption-purging-desorption cycles. The majority of cases use a low-boiling n-alkane or ammonia for the desorption step. When steam is used as the desorbing agent a regeneration step is required since a considerable loss of zeolite dynamic capacity is noticed.

Except for the molex process all the commercial processes for n-paraffins recovery apply vapor-phase adsorption.

CHAPTER SIX

ADSORPTION DESIGN THEORY

CHAPTER SIX

ADSORPTION DESIGN THEORY

6.1 Introduction:

In fixed-bed, dynamic adsorption systems, a gas or liquid feed that is rich in the adsorbable component flows through a bed, or zone, containing adsorbent particles. The contact time between adsorbent and fluid is limited by the rate of flow and the geometry of the bed, and therefore both rate and capacity considerations are involved in adsorber design.

The rate of adsorption in fixed-bed, dynamic systems may be characterised by either a mass transfer coefficient approach or using a mass transfer zone concept.

When the design is based on mass-transfer coefficients which might be considered as a "micro" approach, it is necessary to consider each of the resistances encountered as molecules are transferred from the bulk fluid to a film on the adsorbent particles and eventually to the adsorbed phase. Mass-transfer coefficients provide insight into the mechanisms by which adsorption occurs, but they can be difficult to determine and uncertain to use in design calculations.

The mass-transfer-zone concept is a "macro" approach to mass

transfer, expressed in terms of an amount of unused adsorbent, which is necessary to saturate the adsorbent bed. The mass-transfer-zone concept - originally suggested by Michaels [74] for fixed-bed ion-exchange columns - provides a simple and effective method for considering rate phenomena in fixed-bed adsorption systems. The concept is particularly amenable to rapid determination and correlation of rate data and to simple design procedures [75, 76]. Therefore this chapter will be directed solely to the mass-transfer-zone concept, because it is simpler and more reliable to apply in process design analysis.

6.2 Mass-Transfer Front:

Consider an adsorbent bed with feed fluid entering at the top, and effluent - lean in adsorbable component - leaving at the bottom. (The mathematical treatment would be identical if flow directions were reversed). To facilitate the discussion, the adsorbent bed will be shown resting on its side (as in Fig. 6.1), recognizing, however, that flow in a vertical direction is important for proper flow distribution in commercial adsorbers. Directly below the diagram of the adsorbent bed is a series of graphs. In each graph, the adsorbent loading, X, is plotted as ordinate, and distance from the inlet end of the bed, L, as abscissa.

Initially, the adsorbent is highly activated, and the initial adsorbate loading (designated X_o) is low. (This is indicated in Fig. 6.1a). At some starting time, which shall be designated as θ_o,

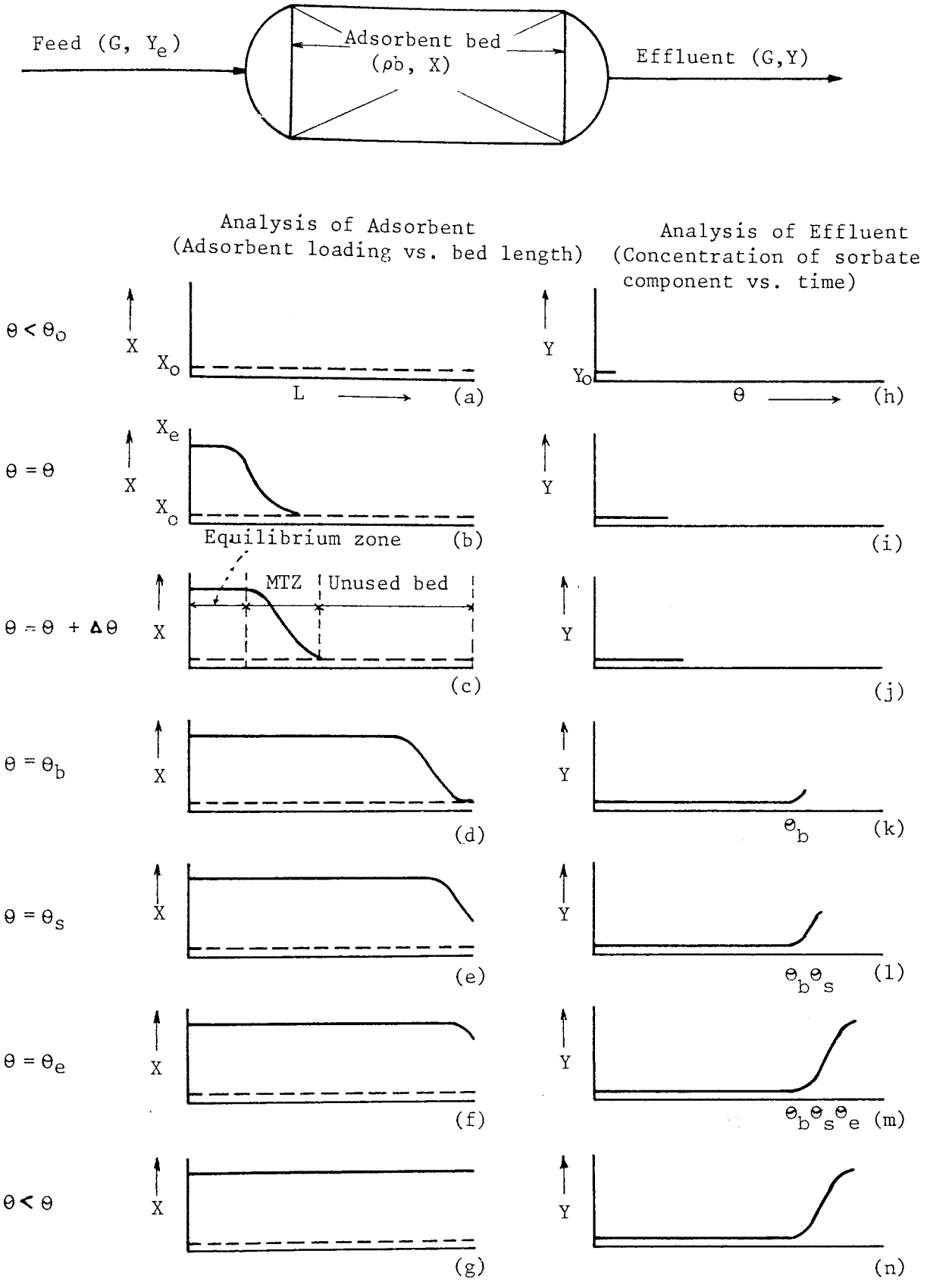

Fig. 6.1 Analysis of Adsorbent and Effluent from Adsorption Column Operation.

feed at a mass flow rate, G, with uniform concentration of adsorbable component is fed to the activated adsorbent bed. As the fluid passes through the bed, the adsorbable component diffuses to and is adsorbed on the adsorbent.

Flow continues under steady-state conditions. At some later time, Θ, an analysis of uniformly spaced samples taken from the effluent leaving the bed would show an adsorbate loading curve similar to that shown in Fig. 6.1b.

At the inlet end of the bed, the adsorbate loading would be X_e, the equilibrium loading corresponding to the concentration of the adsorbable n-paraffin in the feed. That portion of the bed whose adsorbate loading is equal to X_e is defined as the Equilibrium Zone.

Toward the effluent end of the bed, the adsorbate loading would be X_e, essentially the same as it was when the fluid was first admitted to the bed. That portion of the bed whose adsorbate loading is equal to X_o is defined as unused bed.

In some intermediate zone, the adsorbate loading changes from saturation, X_e, into the initial adsorbate loading, X_o and this is represented by the "S-shaped wave" in Fig. 6.1b. It is in this zone that the adsorbable component is being transferred from the bulk fluid to the adsorbate phase. That portion of the bed in which the adsorbate concentration transition occurs is defined as the

mass-transfer zone, abbreviated "MTZ". The S-shaped wave in a concentration "X" -vs- height "L" plot is defined as the X-L mass-transfer-wave or front.

6.3 Bed Breakthrough:

As flow continues, the mass-transfer wave moves through the bed in a steady-state fashion, at uniform velocity. If absorbent samples were analyzed at time $\Theta + \Delta\Theta$, the X-L mass transfer wave would be identical to the wave obtained at time Θ, but displaced a distance ΔL in the L direction as shown in Fig. 6.1c.

Breakthrough refers to the condition when the leading edge of the mass-transfer wave just reaches the effluent end of the bed as shown in Fig. 6.1d. However the breakthrough concentration is defined as the minimum detectable concentration, i.e. 5% greater than the initial concentration of the adsorbate in the feed. The saturation concentration on the other hand, is defined as the maximum allowable concentration of the adsorbate in the effluent from the bed, i.e. C/Co approaches 95% of the adsorbate concentration in the feed.

The time at which breakthrough occurs is termed the breakthrough time, and designated θ_b. If flow is continued, the time at which the trailing edge of the mass-transfer wave reaches the effluent end of the bed is called the exhaustion time, and designated θ_e. This is shown in Fig. 6.1f. At time θ_e, all of the

adsorbent in the bed is at saturation with the concentration of adsorbable component in the feed, the adsorbent capacity is completely spent; and the bed is said to be at saturation. No discernable changes occur if flow continues beyond time θ_e (as shown in Fig. 6.1g).

6.4 Analyzing Column Operation:

Analyzing the adsorbent samples taken from various positions in the bed presents a difficult, although not insurmountable, problem. A simpler method of determining the shape of the mass-transfer front involves measuring the concentration of adsorbable component in the effluent. Often, this can be accomplished with a continuous analyzer-recorder, as shown schematically in Fig. 6.1h through 6.1n. A curve similar to that shown in Fig. 6.1n results. The concentration of adsorbable component in the fluid, designated Y, is plotted as the ordinate, and time, Θ, as the abscissa.

Initially, the concentration of adsorbable component in the effluent is equal to Y_o, a low value relative to the concentration, Y_e, in the feed. Y_o is the equilibrium concentration corresponding to X_o, the adsorbate loading at the effluent end of the bed.

From time $\Theta = \Theta_o$, until the breakthrough time, θ_b, the concentration of adsorbate component in the effluent remains equal to Y_o. At time θ_b, when the leading edge of the X-L mass-transfer

wave reaches the effluent end of the bed, the concentration of adsorbable component in the effluent begins to increase.

From time θ_b until time θ_e, the concentration of adsorbable component in the effluent increases until it is equal to the Y_e. The smooth S-shaped wave in the Y-Θ plot is defined as the Y-Θ mass-transfer wave or front.

If the bed length were increased by some amount ΔL, and the experiment repeated with all other parameters held constant, the Y-Θ mass-transfer wave would be identical to that previously obtained, but displaced in the Θ direction. A comparison of the X-L and Y-Θ mass-transfer waves shows that they are similar but inverted.

In a steady-state system, X and Y are related by equilibrium requirements, and it can be shown that time onstream and bed length are equivalent parameters.

6.5 Resistance to Mass Transfer:

The fact that real mass-transfer waves are S-shaped is evidence of resistance to mass transfer. As the resistance to mass transfer increases, the gradient of the wave decreases whereas, as mass transfer resistance decreases, the wave gradient of the wave increases. In the ultimate, "ideal" case, the curve becomes a vertical, straight line (HMTZ = 0). The "ideal" mass-transfer wave is called the stoichiometric wave or front.

An adsorber bed with a stoichiometric front is comprised solely of an equilibrium zone and unused bed, because the length of the mass-transfer zone is zero. At breakthrough under ideal conditions, the concentration of adsorbate component in the effluent would change instantaneously from Y_o to Y_e, and the entire bed would be loaded to saturation capacity. Breakthrough time under the ideal conditions of no mass-transfer resistance is defined as the stoichiometric time, and designated θ_s.

6.6 Analyzing Mass-Transfer Waves:

All real mass-transfer waves can be analyzed in terms of an equivalent stoichiometric front. Consider the geometry of the transfer waves in Fig. 6.2. The area under the X-L wave (a,g,d,b,a) represents used adsorbent capacity; the area above the wave (a,g,d,e,a), unused adsorbent capacity. Thus, the ratio of the area under the wave to the total area of the rectangle (a,b,d,e,a, which just enclose the mass-transfer wave) is the fraction "f" (see Chapter 9) of used adsorbent in the mass transfer zone.

In a Y-θ diagram, geometric considerations are reversed. The area below the wave (a,g,d,e,a) reflects unused adsorbent capacity. The ratio of the area above the wave (a,g,d,b,a) to the total area of a rectangle (a,b,d,e,a, which just encloses the wave) is the fraction of used adsorbent in the mass-transfer zone.

In either plot, a vertical straight line drawn through the

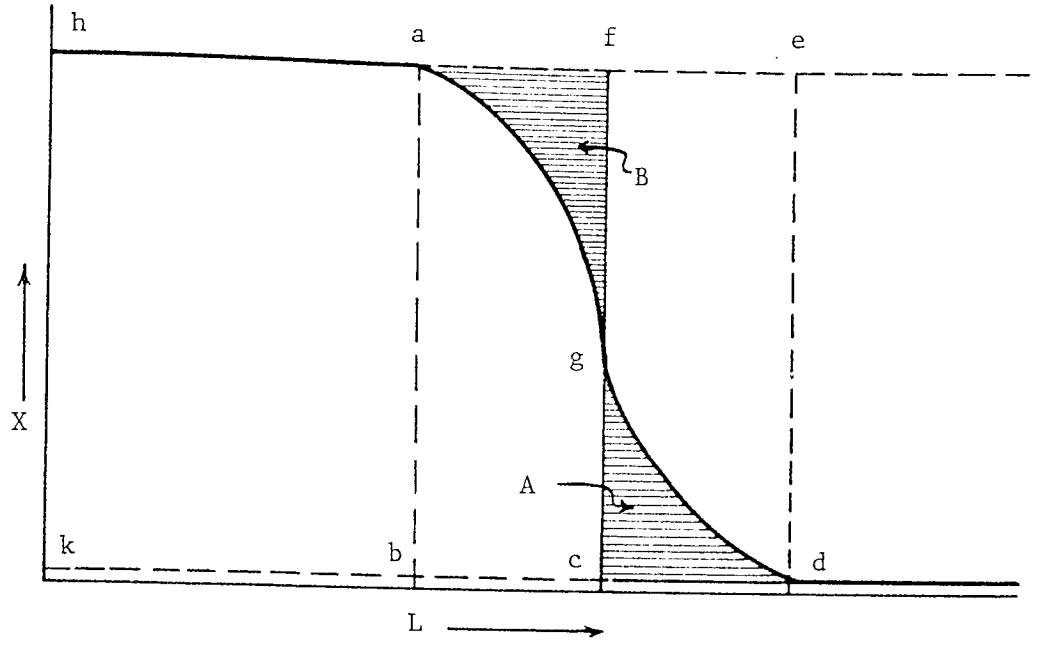

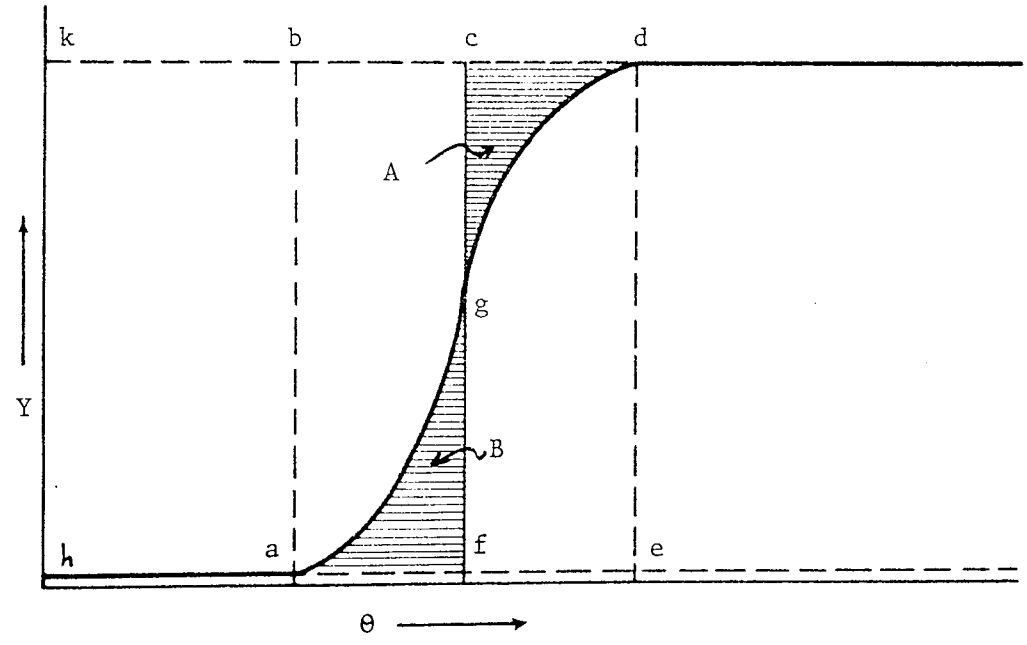

Fig. 6.2 Stoichiometric Front Used to Analyze Real Mass-Transfer Fronts.

mass transfer wave at g - such that the area a,f,c,b,a, is equal to the area a,g,d,b,a; and the area f,e,d,c,f is equal to the area a,g,d,e,a - yields an equivalent stoichiometric front for the particular system. Then the entire rectangle h,f,c,k,h corresponds to adsorbent at its equilibrium loading Y_e, and is defined as the equivalent equilibrium section. It is specified in terms of the length of equivalent equilibrium section, LES, or weight of equivalent equilibrium section, WES:

$$WES = LES \left(\pi D^2/4\right) \rho_B \qquad (6.1)$$

The area f,e,d,c,f corresponds to adsorbent at its initial loading, X_o, and by definition, it is equivalent unused bed, or briefly called unused bed. It is specified in terms of the length or weight of unused bed, LUB or WUB:

$$WUB = LUB \left(\pi D^2/4\right) \rho_B \qquad (6.2)$$

In accordance with this model, an adsorbent bed at breakthrough consists of an equilibrium zone and a mass-transfer zone (MTZ); or it is hypothetically comprised of an equivalent equilibrium section (WES or LES) plus equivalent unused bed (WUB or LUB), and this is tantamount to a bed with stoichiometric front. The WES can be calculated directly from equilibrium data and the quantity of adsorbable component to be removed from the feed. The WUB is developed from dynamic data obtained in a fixed-bed adsorption system.

6.7 Assumptions of the Model:

The important assumptions implicit in the development of this

model are [75]:

(1) The bed is uniformly packed.

(2) The absorbent temperature and initial adsorbate loading are uniform throughout the bed.

(3) The feed rate, feed temperature and feed composition are constant.

(4) There are no radial temperature, concentration or flow-rate gradients.

(5) The temperatures of both the fluid and adsorbent are essentially equal.

(6) The fluid does not undergo a phase change.

(7) Adsorption heat effects are negligible.

(8) Chemical reactions do not occur.

Caution should be exercised if this model is applied to systems involving chemisorption reactions, high concentrations of adsorbable component (i.e., bulk separation), large heat effects, or non-steady-state conditions.

6.8 Mathematics of the Model:

Consider the adsorber shown schematically in Fig. 6.3. Fig. 6.3A depicts a stable mass-transfer zone moving at uniform velocity, U, through an adsorber vessel. In Fig. 6.3B, the bed is shown with stoichiometric fronts only, and in Fig.6.3C, the stoichiometric transfer front is superimposed over the actual transfer front.

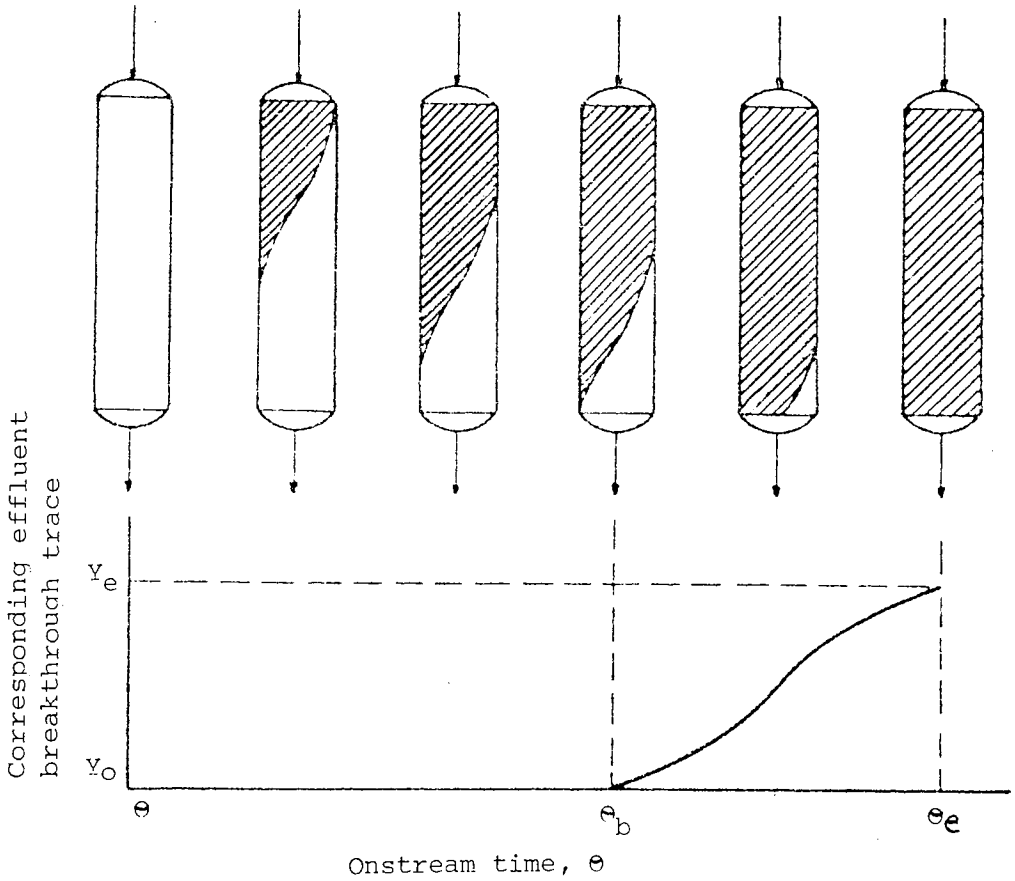

Fig.6.3A Progress of a Stable Mass-Transfer Front Through an Adsorbent Bed (Stable Mass-Transfer Front).

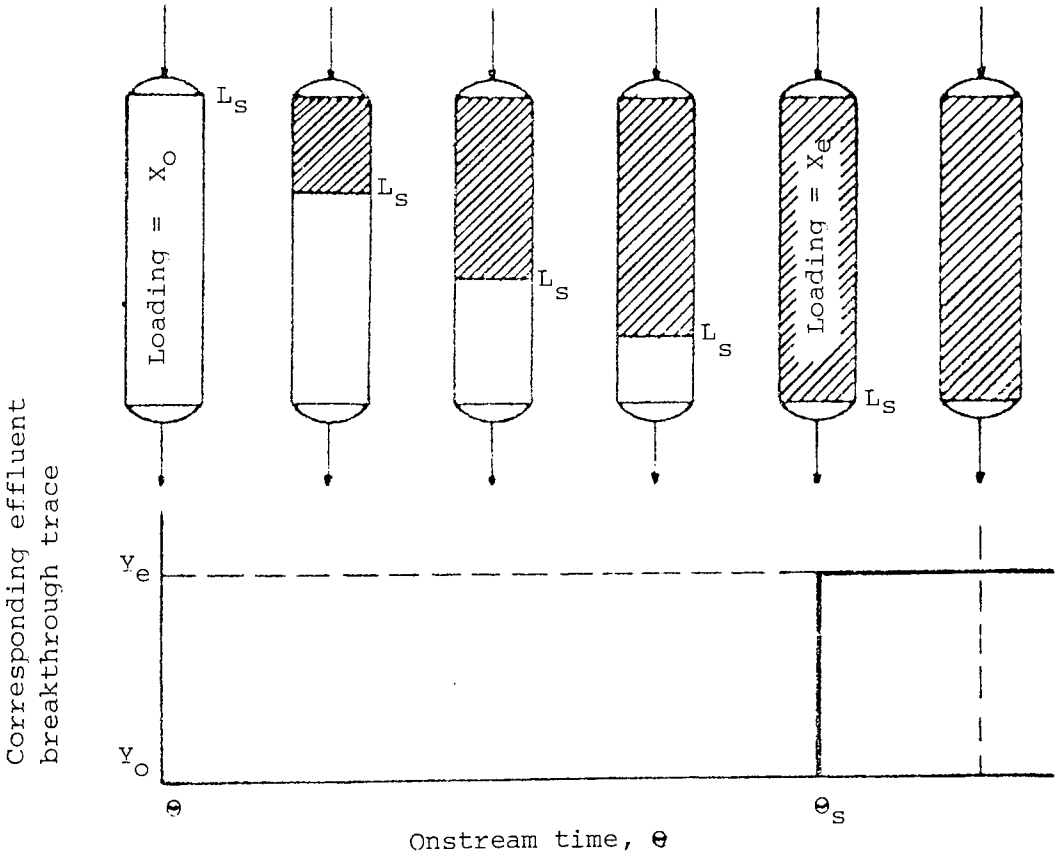

Fig. 6.3B Progress of the Stoichiometric Front Through an Adsorbent Bed (Stoichiometric Transfer Front)

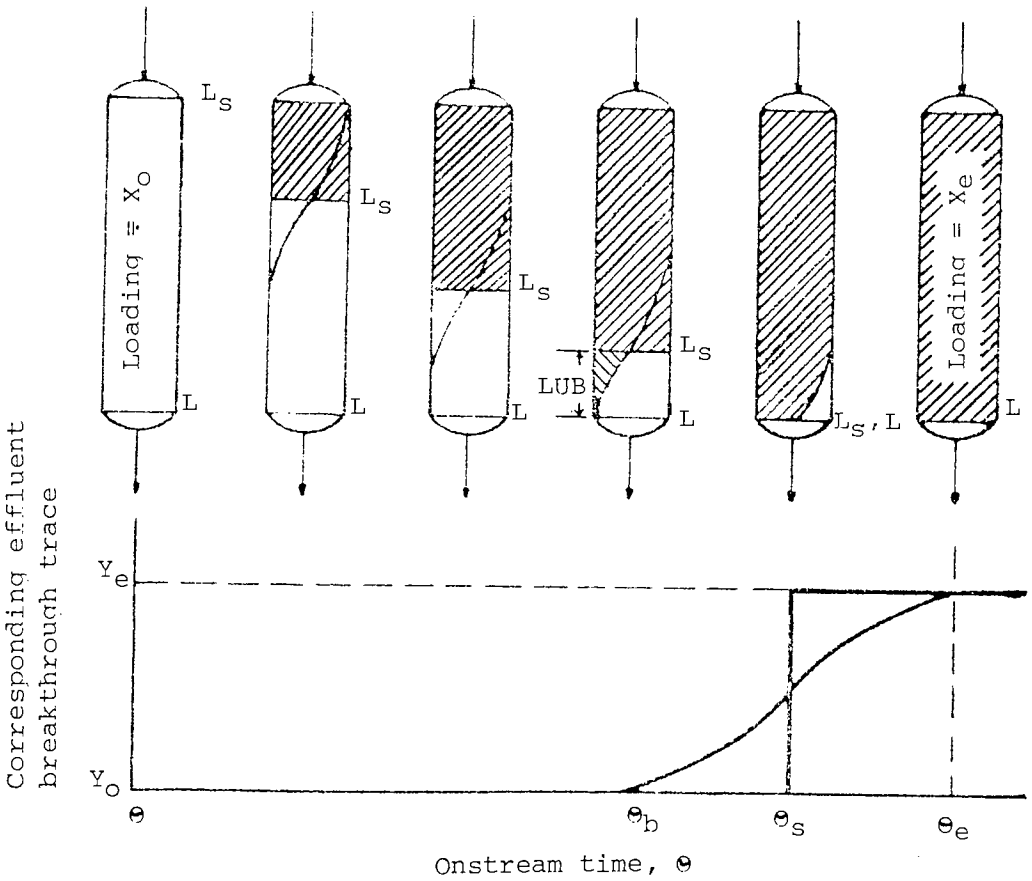

Fig. 6.3C Position of the Stoichiometric Front Relative to the Stable Mass-Transfer Front During Dynamic Adsorption (Stable Front Relative to Stoichiometric Front)

The total amount of adsorbable component, w, removed from the bulk fluid between time θ and time $(\theta + \Delta\theta)$ is expressed by Eq. (6.3):

$$w = G\,(Y_e - Y_o)\,A_z\,\Delta\theta \qquad (6.3)$$

As w kgs of adsorbable component are adsorbed on the bed, the shape of the mass transfer wave is unaltered although its position changes. Thus, the tangible effect of adsorbing w on the bed is an increase in length, ΔL of either the equilibrium zone or equivalent equilibrium section, LES, as expressed by Eq. (6.4):

$$w = (\Delta L)\,A_z \rho_B\,(X_e - X_o) \qquad (6.4)$$

where ρ_B is the bulk density of the adsorbent bed.

Therefore:

$$(\Delta L)\,A_z\,\rho_B\,(X_e - X_o) = G\,(Y_e - Y_o) A_z \Delta\theta \qquad (6.5)$$

Rearranging,

$$\Delta L = (G\,\Delta Y/\rho_B\,\Delta X)\,\Delta\theta \qquad (6.6)$$

Or,

$$\Delta L = U\,\Delta\theta \qquad (6.7)$$

During steady-state operation, the values of G, ρ_B are fixed, and $\Delta X = \Delta Y$. Thus, the expression $(G\,\Delta Y/\rho_B\,\Delta X)$ is a constant having the units of velocity at which the equilibrium zone expands as the mass transfer wave moves through the bed.

The velocity of a steady state mass-transfer wave depends only on the fluid mass velocity, the bulk density of the adsorbent and the terminal conditions. Local mass transfer rates within the

front have no effect on the front velocity, although they do affect the shape of the front.

At any time, θ, the position of the stoichiometric front is given by Eq. (6.8):

$$L_s = U\theta \tag{6.8}$$

By definition, at time, θ_b:

$$L_s = LES \tag{6.9}$$

Therefore,

$$LES = U\,\theta_b \tag{6.10}$$

By definition, at time θ_s:

$$L_s = L \tag{6.11}$$

Therefore,

$$L = U\,\theta_s \tag{6.12}$$

However,

$$LUB = L - LES \tag{6.13}$$

Or, combining Eq. (6.10), (6.12) and (6.13):

$$LUB = U\,(\theta_s - \theta_b) \tag{6.14}$$

Combining Eq. (6.12) and (6.14), by eliminating U:

$$LUB = L\ (\theta_s - \theta_b/\theta_s) \tag{6.15}$$

Thus, simple breakthrough curves provide the data required for the correlation of rate data in dynamic systems. Eq. (6.15) is the basic equation used for analyzing breakthrough data.

6.9 Analyzing Commercial Units:

Industrial adsorbers are never operated beyond the breakthrough point.

Therefore combining:-

$U = (G\,\Delta Y/\,\rho_B\,\Delta X)$ (the velocity front) with Eq. (6.12) gives:

$$\theta_S = L/U = L_S\,(\rho_B\,\Delta X/G\,\Delta Y) \qquad (6.16)$$

Then, combining Eq. (6.14) and (6.15) gives:

$$LUB = L - (G\,\Delta Y/\,\rho_B\,\Delta X)\,\rho_B \qquad (6.17)$$

Eq. (6.17) enables an estimate to be made of LUB when the adsorption step must be stopped at breakthrough. The LUB so calculated is sensitive to the value of ΔX. (An accurate value of ΔX is often difficult to obtain from an industrial unit that has "cycled" for an extended period of time.).

The development of this model depends on assumptions that the adsorbent bed is of sufficient length to contain a steady-state mass-transfer zone, and that a steady-state mass-transfer zone exists from time $\Theta = 0$. The fact that some finite period of time at the beginning of an adsorption step is required for the formation of the steady-state MTZ does not complicate the model, provided that the bed is long enough to contain a steady-state MTZ. An equivalent stoichiometric front can be considered to exist from time $\Theta = 0$ provided that the finite period at the beginning of the adsorption step is known. However, if the adsorbent bed is shorter than an MTZ

breakthrough will occur earlier than predicted by this model.

The question of bed size and its relation to a steady-state MTZ is important. Lukchis [75] defines a short bed as one that will not contain a steady-state MTZ under specified operating conditions. If Rosen's analysis [77] is restated in terms of the MTZ model, it can be shown that the breakthrough conditions for a short bed are approximated by Eq. (6.18) and (6.19):

$$\Theta_{b_{SB}} = (W_{SB}/W_{MTZ})^2 \Theta_{MTZ} \qquad (6.18)$$

Or,

$$(\Delta X)_{SB} = (W_{SB}/W_{MTZ})^2 (\Delta X)_{MTZ} \qquad (6.19)$$

From the previous analysis of the MTZ and its relationship to LUB, it is readily apparent that the average change in adsorbate loading in the MTZ is approximately half that of the equilibrium zone (see Section 6.8), i.e. adsorbent used in the MTZ is approximately 50%. Eq.(6.19) suggests that the adsorbent used falls off rapidly as bed size is reduced below that required to contain an MTZ. For example, if W_{SB} reduces from 0.7 to 0.6 in a process for which $W_{MTZ} = 1.5$, X_{SB} is reduced by more than 32%.

Increasing the bed size beyond the length of the MTZ adds equilibrium capacity - adsorbent that provides 100% use. An approximate relationship between capacity and bed length is shown in Fig. 6.4. Bed length is expressed in terms of the length of an MTZ. Capacity is expressed in terms of overall, average adsorbent use, in which equilibrium zone ΔX is defined as 100%.

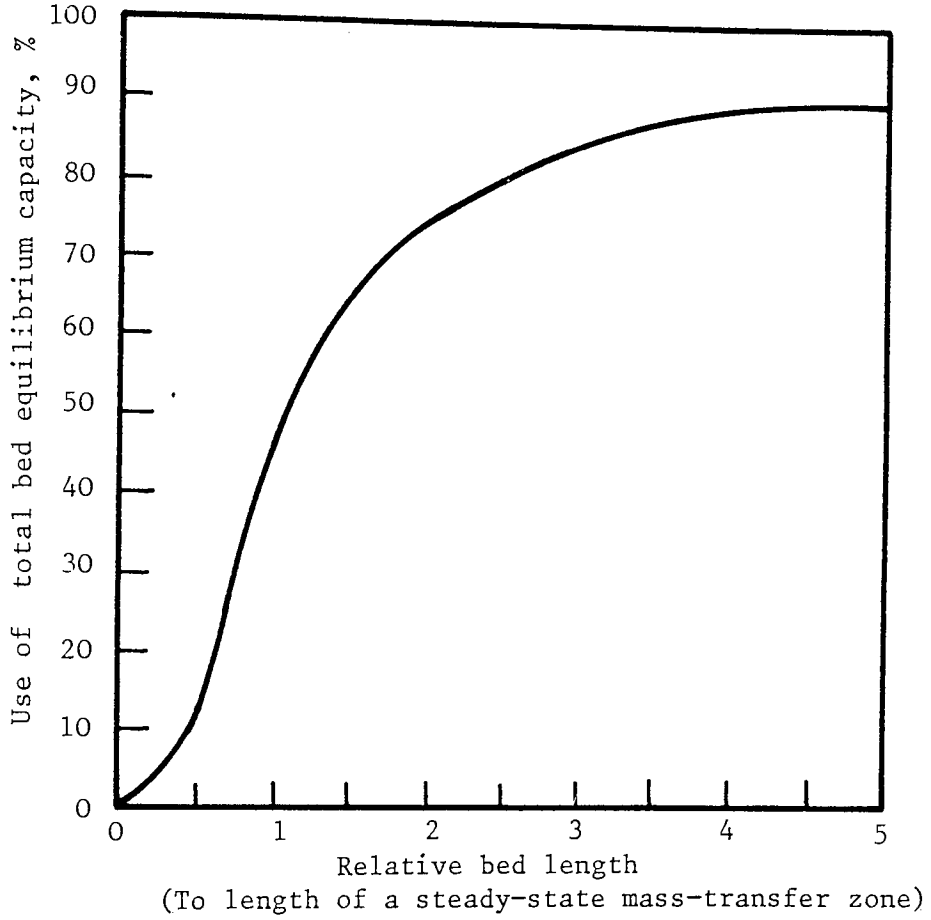

Fig. 6.4 The Relationship Between the Relative Bed Length and the Use of Total Bed Equilibrium Capacity.

If adsorbent cost is a major factor influencing the design of an adsorbent bed, one would deduce from Fig. 6.4 that the preferred bed length would be 1.5 to 3 times the size of the MTZ.

The majority of reported adsorption breakthrough data have been obtained in short columns [75]. In some instances, the conclusions based on these data led to downgrading the adsorption process because of apparent low adsorbate loadings. Had the data been analyzed in light of Fig. 6.4 or Eq. (6.19), the adsorption process might have appeared more attractive.

6.10 Heat Effects and Space Velocity:

Typically, the steady-state wave is inversely symmetrical. A skewing (or trailing) of the wave as attributed by Lukchis [75] is caused principally by the heat generated during adsorption. When the concentration of the adsorbable component is high, the heat generated can become large enough to grossly distort the mass-transfer wave. In extreme cases, the heat can even prevent formation of a stable mass-transfer wave.

Lukchis [75] stated that space velocity appears to be a poor design-parameter for an adsorption system that operates with steady-state mass-transfer zones. Space velocity is defined as: (vol. of feed fluid/hr.)/vol. of adsorbent bed. The definition implies that the entire volume of adsorbent is actively involved in

the adsorption process at all times, which contradicts observations of mass-transfer-zones.

6.11 Development of the Mathematical Model:

A differential fluid phase mass balance for an elementary volume of the adsorption column is the starting point for the development of the mathematical model.

Let a feed of heavy kerosene containing a fixed quantity of liquid paraffin (adsorbate component) to contact a given mass of zeolite packed in the adsorption column, and assume that the bed has a radius R, and the total depth of the bed is measured as L as shown in Fig. 6.5.

The mathematical complexity may be reduced by introducing the following assumptions:

1. The liquid paraffin is considered to be a single component.
2. Pressure drop across the adsorbent bed is negligible.
3. The bulk motion of the fluid phase is only in the axial direction with constant superficial linear velocity (plug flow).
4. The longitudinal diffusion is neglected.
5. There is no temperature gradience along and within the bed and the operation is isothermal.

The fundamental equations may be obtained from a differential

mass balance, which relates the adsorbate concentration in the adsorbent to that in the bulk fluid at any point in the column.

Consider an element of bed at a height Z from the base of the column and of thickness δZ as shown in Fig. 6.5, then a material balance on the element during the time interval δt will be:-

Let,

ϵ = Fractional void volume of the packed-bed

V = Velocity of fluid in interstices of bed, m/s

πR^2 = Cross-sectional area of the bed, m^2

C = Concentration of adsorbate in the fluid stream, moles/ m^3

Then,

n-paraffins into element :- $\pi R^2 V\epsilon C \delta t$

n-paraffins out of element :- $\pi R^2 V\epsilon \left[C + \frac{\partial C}{\partial Z} \delta Z\right] \delta t$

The change of concentration of the adsorbate with time in this cross-sectional area of the bed (the accumulative amount) is given by:

$$\pi R^2 \epsilon \delta Z \frac{\partial C}{\partial t} \delta t$$

and the adsorbate uptake of the adsorbent is given as:

$$\rho_B \delta Z \pi R^2 \frac{\partial q}{\partial t} \delta t$$

where

q = Solid-phase concentration of adsorbed material, moles/ kg of adsorbent

ρ_B = Bulk density, mass of solid phase ÷ volume of bed, kg/ m^3

Now,

The material conservation conditions demand that:

$$V\epsilon\pi R^2 \; C\,\delta t = \epsilon V \pi R^2 \left[C + \frac{\partial C}{\partial Z}\delta_Z \right]\delta t + \epsilon \delta Z \pi R^2 \frac{\partial C}{\partial t}\,\delta t + \rho_B \delta Z \; \pi R^2 \; \frac{\partial q}{\partial t}\,\delta t$$

Cancel common terms and divide all by $\pi R^2 \, \delta Z \, \delta t$ gives:-

$$V \frac{\partial C}{\partial Z} + \frac{\partial C}{\partial t} + \frac{\rho_B}{\epsilon} \frac{\partial q}{\partial t} = 0 \qquad (6.20)$$

The equilibria between the adsorbate and the gas in equilibrium can be written as:

$$\rho_B \frac{\partial q}{\partial t} . = ka \; F \; (C, \; q) \qquad (6.21)$$

Equation (6.21) expresses the rate of addition of solute to the solid phase in terms of the interphase mass-transfer coefficient, ka, and a driving force, F (q, c), to be selected. Following the procedure used for packed columns operating at steady state, k is based on a unit of exterior particle surface and a is the total surface in a unit volume of packed space.

Design of a fixed-bed column for adsorption requires solution of equations (6.20) and (6.21), given the fluid concentration at the entrance to the bed and the initial state of the fluid and solid in the bed. Sherwood et al. (81) mentioned that solutions have been obtained for a variety of situations. However they are moderately complex. Before some of the most important results are outlined it will be helpful to think about the behaviour of the packed bed in an extreme case in which k is infinitely great. Then local equilibrium

exists at all points and all times between the particles and the adjacent fluid. Under these conditions, $q = q^* = f(C)$, as expressed, for example, by Eq. (6.22).

$$\frac{q^*}{q_o} = \frac{r\,(C/Co)}{1+(r-1)\,(C/Co)} \qquad (6.22)$$

where

r = Equilibrium constant, equal to $(k + K_A Co)^{-1}$ for gas adsorption.

K_A = Adsorption equilibruim constant

Then Eq. (6.21) is not needed and Eq. (6.20) becomes:

$$\left[1 + \frac{\rho_B}{\epsilon} f'(C) \right] \frac{\partial C}{\partial t} + V \frac{\partial C}{\partial Z} = 0 \qquad (6.23)$$

Note that $\dfrac{\partial q}{\partial t} = \dfrac{\partial q}{\partial C} \cdot \dfrac{\partial C}{\partial t}$

$$\frac{\partial q}{\partial t} = f'(C) \frac{\partial C}{\partial t}$$

Equation (6.23) is a first order partial differential equation that is linear in the derivatives but has a variable coefficient because of $f'(C)$ and is most conveniently solved by establishing the characteristic with respect to C. Thus from Eq. (6.23),

$$\frac{\partial Z}{\partial t} = \frac{\partial C/\partial t}{\partial C/\partial Z} = \frac{V}{\left[1 + \frac{\rho_B}{\epsilon} f'(C) \right]} \qquad (6.24)$$

Equation (6.24) is a characteristic equation of (6.23) with respect to constant C_o · (the n-alkanes concentration in the feed).

This is equivalent to a linear equation of Z with respect to t

and of slope = $V / \left[1 + \frac{\rho_B}{\epsilon} f'(C) \right]$

There will be a number of characteristic equations for each feed concentration . All the values of the slope term are known, except the value of f'(C) which can be evaluated as follows:

Using the local-equilibrium theory for the adsorption curve, the method of characteristics shows that at each point

$$\frac{t}{Z} = \frac{1}{V^*} = \frac{1}{V}\left[1 + \frac{\rho_B}{\epsilon}\frac{dq^*}{dc}\right]$$

or,

$$f'(C) = \frac{dq^*}{dc} = \frac{\epsilon}{\rho_B}\left[\frac{Vt}{Z} - 1\right] \qquad (6.25)$$

Equation (6.25) has been applied in Appendix C to evaluate the equilibrium isotherm. Then, for any given value of t the LES can be estimated and checked with the experimental value. The results are shown in section 9.5. The detailed calculation of the values of $\frac{dq}{dc}$ are shown in Appendix C.

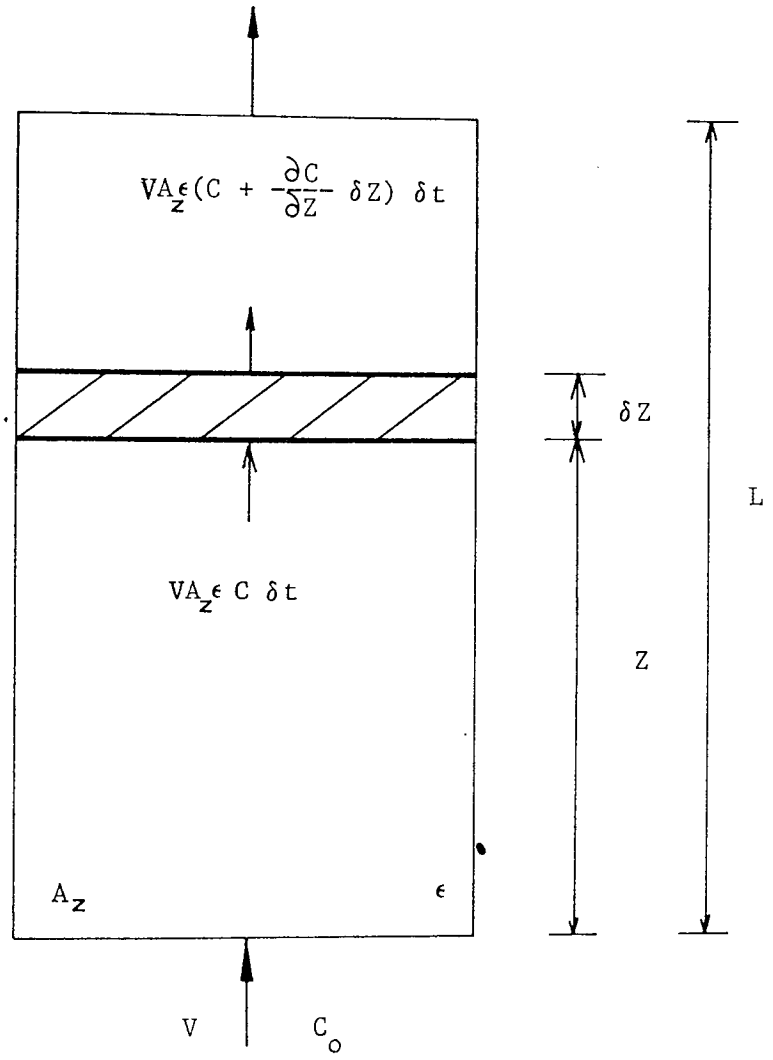

Fig. 6.5 Material Mass Balance around an Element of the Adsorption Column

CHAPTER SEVEN

MATERIAL AND EXPERIMENTAL APPARATUS

CHAPTER SEVEN

MATERIAL AND EXPERIMENTAL APPARATUS

The experimental adsorber used comprised Linde-5A molecular sieves in clay binders in the form of 1/8-inch extruded, cylindrical pellets. Heavy kerosene, characterized by its low sulfur content, was used as the feed in the experimental work. Generally steam was employed as desorbing agent, but occasionally n-pentane or n-hexane was used instead.

A description of these materials and the apparatus used in the experimental work are presented in the sections to follow.

7.1 Materials

7.1.1 Molecular Sieve Adsorbent:

The 5A-molecular sieves in the form of 1/8-inch cylindrical pellets were employed throughout this study. The average pellet length was approximately 0.48×10^{-2} m. The crystalline sieves themselves were evenly distributed within the macroporous clay matrix, and formed about 20% of the total weight of the pellet. Fig. 7.3 shows a photograph of the molecular sieves adsorbent Type-5A used in this study.

The physico-chemical properties of Type-5A molecular sieves

are summarized in Table 7.1.

7.1.2 The Hydrocarbon Feed:

The petroleum fraction utilized was a heavy kerosene supplied by the Kuwait National Petroleum Company (KNPC). This company stated that it contained 18.75% normal paraffins by weight and its smoke point and pour point were 0.024 m and 261 K respectively. Its boiling point range was 505.5 - 588 K. This fraction appeared to be a very promising feedstock because of its relatively high normal paraffin content, high smoke point and low sulfur content. High sulfur content is claimed to reduce the dynamic capacity of zeolite.

The physico-chemical properties of the hydrocarbon feed are summarized in Table 7.2 from which it was noticed that the sulfur content does not exceed 50 ppm.

7.1.3 Desorbent Materials:

Desorbent materials were selected to secure easy separation from the n-paraffins product. In desorbing the preferentially adsorbed components of the feed, both the desorbent and the desorbed components are removed from the adsorbent bed in admixture, and without a method of separation of these two materials the purity of the selectively adsorbed components of the feed would not be very high. Therefore, a desorbent with a significantly different boiling range to the feed mixture was preferred. This would allow

Table 7.1 Physico-chemical Properties of 5A-Molecular Sieves Used in Adsorption Separation of n-Paraffins from Heavy Kerosene[27].

Property	Value
Unit cell composition	$Ca_{4.5}Na_3[(AlO_2)_{12}(SiO_2)_{12}].30\ H_2O$
Pellet particle size, m	$<0.5 - 3.0 \times 10^{-3}$
Density, kg/m^3	700
Water content, wt%	<1.5
Inert binder, wt%	20.0
Porosity, %	43
Crushing strength, kg	5.63
Heat of Adsorption, kJ/kgH_2O	4186.8
Specific Heat, kJ/kgK	1.09
Type of Crystal	Simple Cubic
Adsorption Capacity for water vapor % (wt/wt)	22.2

Table 7.2 Physico-chemical Properties of Heavy Kerosene.

Properties	Units	Values
Molecular Weight	kg/kmole	215
Density @ 288 K	kg/m^3	826.1
Sulfur Content	ppm	50
Pour Point	K	261
Smoke Point	m	0.024
Refractive Index @ 293 K	-	1.4575
Distillation		
I.B.P.	K	505.5
5%	K	523
10%	K	528
20%	K	538
30%	K	542.5
40%	K	544
50%	K	546
60%	K	549
70%	K	555
80%	K	560
90%	K	566
95%	K	572
% Recovery	% Volume	98
Residue	% Volume	1.5
Losses	% Volume	0.5

fractionation, or some other separation method, to be used to separate the selectively-adsorbed feed component as a relatively pure product stream and allow recovery of the desorbent for possible reuse in the process.

The desorbents investigated were steam, n-pentane or n-hexane vapor in admixture with N_2 gas. Steam was always introduced into the top of the fixed-bed of zeolite at three different desorption temperatures of 623, 643 and 663 K. When the normal paraffins were used as desorbent these were also introduced into the top of the column at 623 K. The n-paraffin desorbents were purchased as pure grade chemicals with a guaranteed minimum purity of 99 mole % and were used directly from their containers without further purification. Nitrogen gas of 99.5% purity was used as a carrier and purging material.

7.2 Experimental Apparatus:

Adsorption of n-paraffins on the molecular sieves normally occurs rapidly. Desorption, on the other hand, is relatively slow[78]. The common techniques for desorption include pressure swing, thermal swing, purge gas stripping, displacement, or those which combine more than one of these mechanisms. The most popular is a combination of thermal swing and purge gas stripping as discussed in Section 4.3. Therefore, it was decided to construct a bench-scale, fixed-bed of zeolite molecular sieve Type-5A for adsorption; to use a counter current purge by nitrogen, and to

Fig. 7.1 Schematic Diagram of the Experimental Apparatus

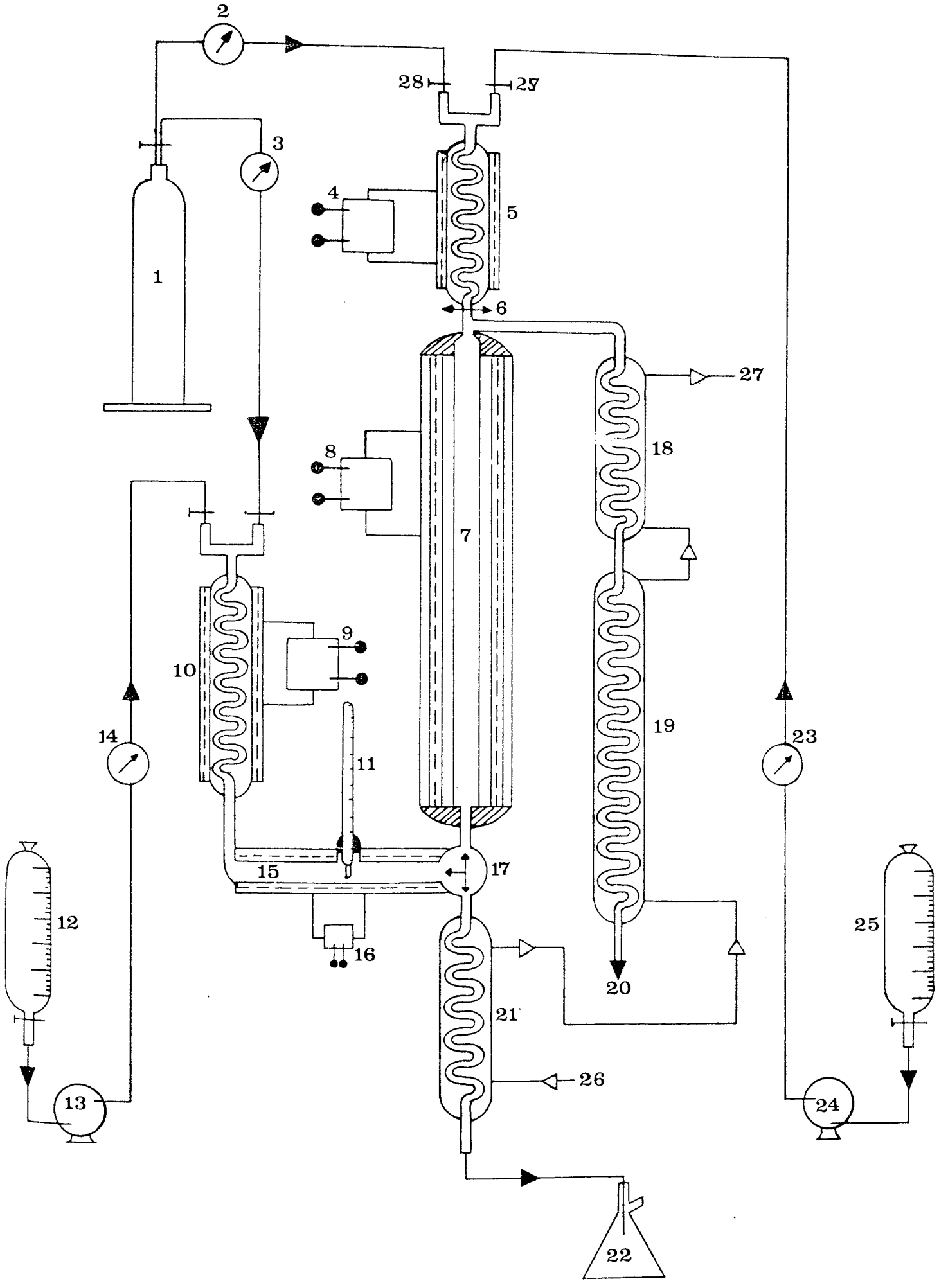

KEY TO NUMBERS OF FIG. 7.1

1	Nitrogen cylinder
5, 10	Preheaters
7	Adsorption column
6, 17, 20, 26, 27, 28, 29	Valves
18, 19, 21	Condensers
22	Vacuum pump
4, 8, 9, 16	Temperature controllers
15	U-shaped tube
13, 24	Pulsation pump
2, 3, 14, 23	Flow meter
12	Feed flask
11	Thermometer
25	Desorbent flask

adsorption column was connected to a condenser through a 3-way valve to condense the collected liquid paraffins removed from the molecular sieves. The preheater and the adsorption column were coupled by a preheated glass connection to which a thermometer was inserted as shown in Fig. 7.1 to indicate the temperature of the vaporized feed on entry to the adsorption column. The feedstock was fed to the bottom of the column from a 250 ml flask by means of a pulsation pump. The flowrate was controlled by reference to a calibrated rotameter. The desorbing agent was fed to the top of the column from another 250 ml flask by means of a pulsation pump with a calibrated rotameter to control the flowrate. A vacuum pump was connected to the bottom of the column through the condenser to enable the column to be freed of air during reactivation of the molecular sieves. Both flowrates were mixed with about 20:1 nitrogen to feedstock before entering the column thereby eliminating pulsation in the flow during adsorption and desorption.

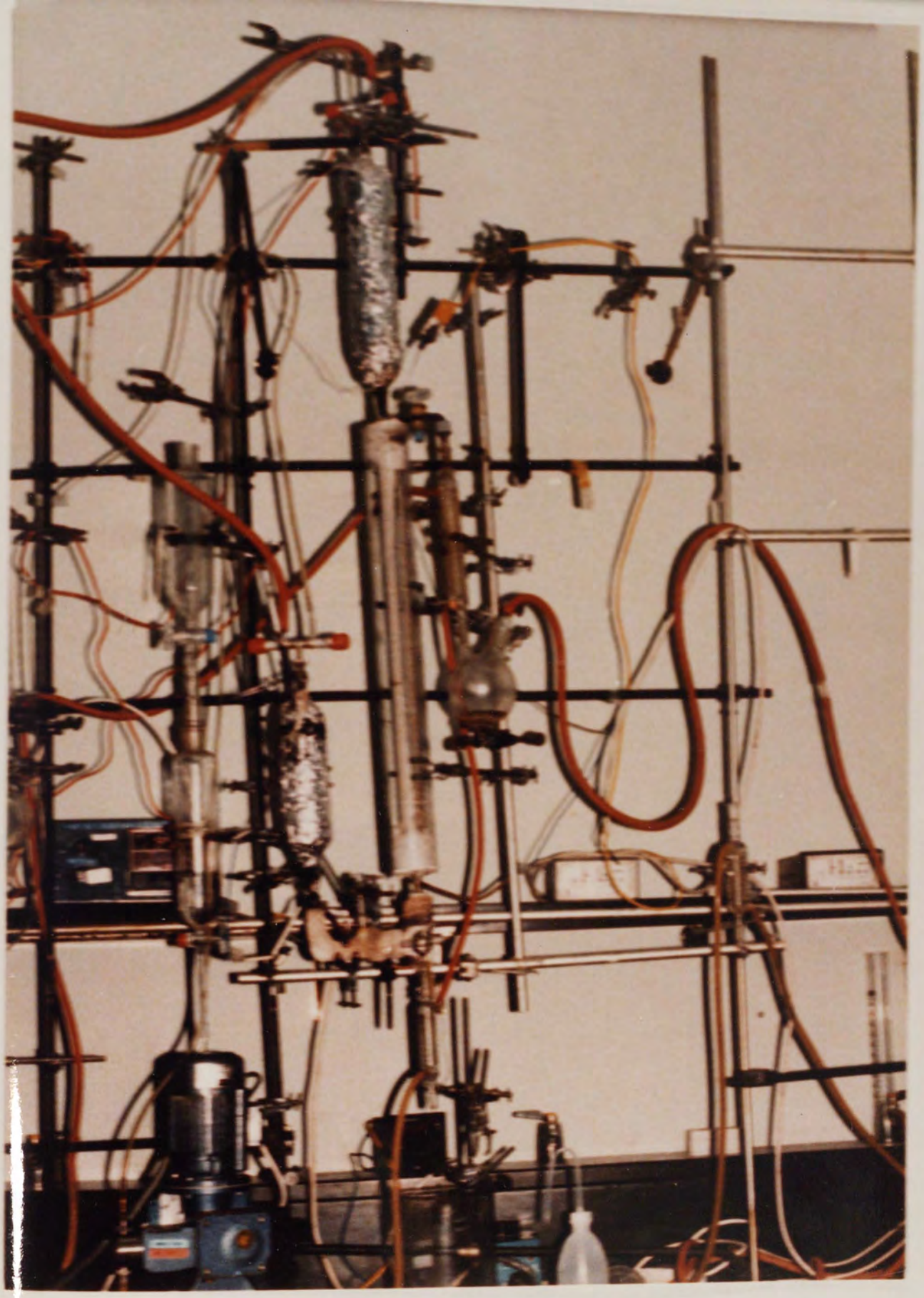

Fig. 7.2 A Photograph of the Experimental Apparatus Used in Separation of n-Paraffins from Heavy Kerosene.

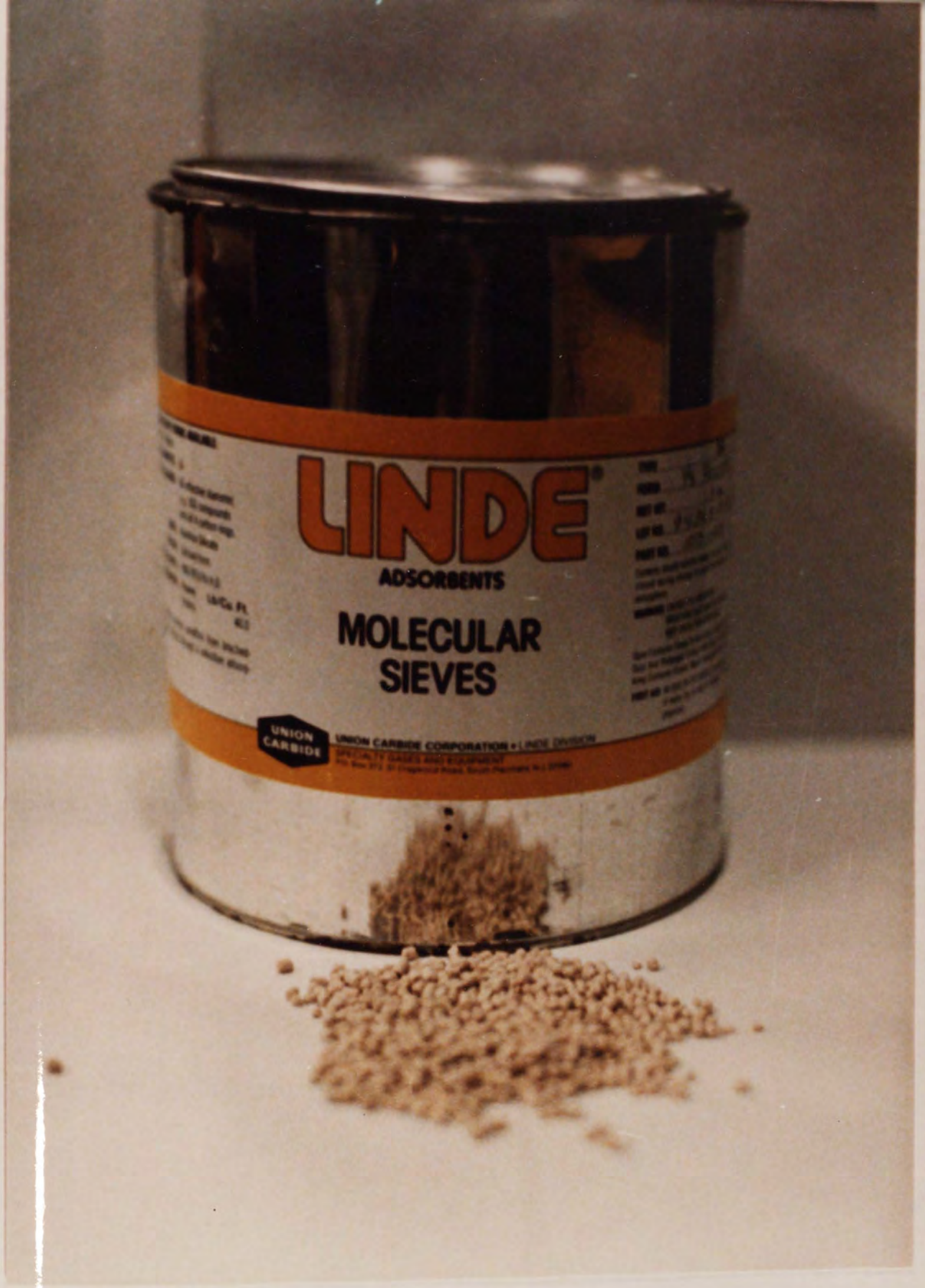

Fig. 7.3 A Photograph of the Molecular Sieves Adsorbent Type-5A Used for Separation of n-Paraffins from Heavy Kerosene.

CHAPTER EIGHT

EXPERIMENTAL PROCEDURES AND ANALYTICAL TECHNIQUES

CHAPTER EIGHT

EXPERIMENTAL PROCEDURES AND ANALYTICAL TECHNIQUES

Procedures for the preparation of the molecular sieves, the performance of adsorption-desorption experiments, and techniques for analysis of the hydrocrbon solutions using Ultra-Violet Spectrophotometry and Gas-Liquid Chromotagraphy are described in this chapter.

8.1 Molecular Sieves Preparation Procedures:

The following procedures were followed to ensure uniformity of adsorbent in successive experiments.

1. About 1.0 kg of molecular sieves (zeolite type-5A, 1/8") was crushed using a mortar and pestle.
2. The crushed zeolites were then sieved, using a (Fritsch) sieve shaker, to provide the following fractions: $<0.5 \times 10^{-3}$ m, $0.5\text{-}1.0 \times 10^{-3}$ m, $1.0\text{-}2.0 \times 10^{-3}$ m and $2.0\text{-}3.0 \times 10^{-3}$ m.
3. The different fractions of zeolites were distributed into crucibles such that each crucible contained approximately 0.03 kg of zeolites.
4. The crucibles with the zeolite were calcined in a muffle furnace (Carbolite-Eurotherm) at 773 K for 5 hours.
5. The crucibles were removed from the muffle and stored in a dessicator.

6. Procedures (1-5) were repeated several times to replenish the consumed crushed zeolites.

8.2 Adsorption Separation Process Procedures:

The process of adsorption separation of n-paraffins from Heavy Kerosene (HK) by zeolite type-5A comprised the following procedures:

1. The adsorption apparatus was prepared for evacuation by:
   (a) removing the preheater -5- and closing valve -6- at which it was connected to the column.
   (b) closing the tap valve -28- at the top of the column, and
   (c) connecting condenser -21- to column -7- and isolating preheater -10- using a three-way valve -17- at the lower end of the column.
2. A vacuum pump -22- (Genelac) was connected to condenser -21- at the lower end and was switched on.
3. The column temperature controller -8- was switched on until the temperature of the bed reached 423 K.
4. With the help of a funnel, column -7- was filled with the desired fraction of calcined molecular sieves. (This step was performed as rapidly as possible and usually took no more than one minute). Then, column -7- was closed with a piece of cotton and a stopper.
5. The temperature controller -8- was set at 673 K, and the emptied crucibles were weighed by a sensitive balance with

an accuracy of $\pm$ 0.0005 x 10^{-3}kg.

6. The vacuum pump -22- was stopped after three hours. The three-way valve -17- was closed at the lower end in such a way that the column was only connected to preheater -10-.

7. Using temperature controllers -9-, -16- and -8-, column -7-, preheater -10- and the U-shaped tube -15- temperatures were set to the predicted adsorption temperature in the individual experiment. Steady state was allowed to be attained. During this step the column temperature controller -8- was calibrated by means of the thermometer inserted inside the column.

8. The cooling water was circulated through condensers -18-, -19- and -21-. The water temperature was controlled by a water-bath.

9. Heavy kerosene was fed to the bottom of column -7- using a calibrated pulsation pump -13- (Netri-pump EI MK II) at the predicted flow rate in the individual experiment (See Fig. 8.1). The feed flowrate was measured by a rotometer -14- and controlled.

10. Valve -6- at the top of column -7- was opened so that condensers -18- and -19- were connected with the column.

11. Valve -20- was opened, and nitrogen was allowed to flow together with kerosene which was controlled by a flowmeter -3- at a fixed flowrate of 6.7 x 10^{-7} m^3/s.

12. The condensate of denormalized kerosene was collected at the bottom of condenser -19- at equal time intervals and samples taken for analysis.

Fig. 8.1 Calibration Between Pump Efficiency and Actual Flowrate

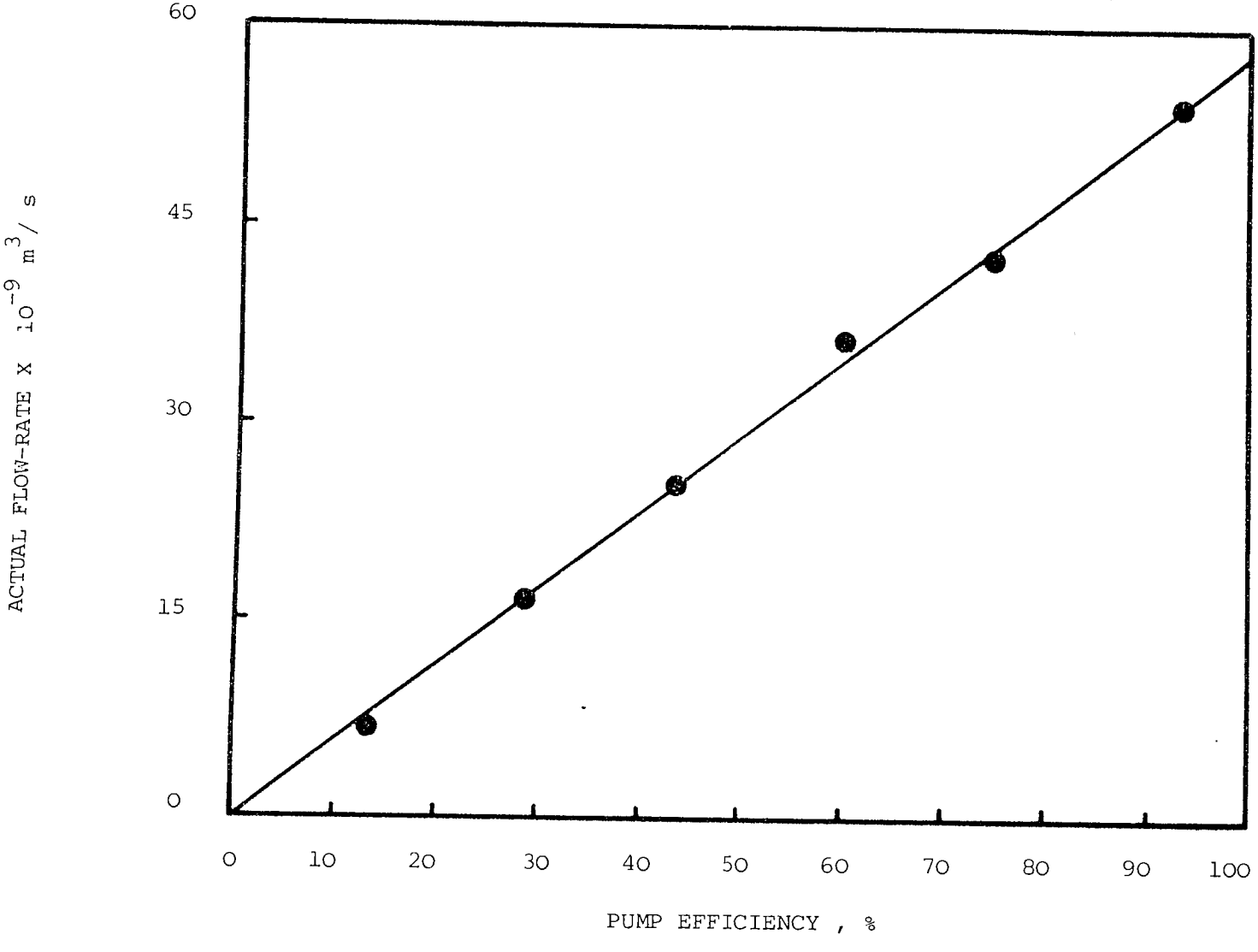

13. The refractive index for each sample of the collected condensate was estimated by Abbe-Refractometer which was connected to a water-bath of a temperature fixed at 298 K.
14. Step 13 was repeated until the refractive index of the condensate was the same as that of the feed.
15. Feed pump -13- was switched off and valve -28- was closed.
16. The distribution of n-alkanes in each condensate was found for one run using a GLC technique (Intersmat IGC-16), the results of which were used to calibrate the refractive index vs. n-paraffins concentration. These results are presented in Fig. 9.2.
17. Upon completion of the adsorption cycle, column -7- was purged with nitrogen gas for 120-300 s to sweep away the non-adsorbed component from the column.
18. Procedures (1 to 15) were repeated except that the nitrogen flow rate was doubled to 13.3 x 10^{-7} m^3/s to study the effect on the breakthrough curve of adsorption of n-paraffins from HK by zeolite type-5A.

8.3 Desorption Process Procedures:

The desorption of n-paraffins from the pores of zeolite crystals using steam as a desorbing agent comprised the following procedures:

1. Preheater -5- was installed in its position at the top of the column -7- and its temperature was set at 623 K by

temperature controller -4-.

2. Care was taken to sure that valves -6-, -17- through the preheater -5- to the column -7- and condenser -21- were opened and all the other valves were closed. The cooling water temperature was set at 298 K and it was made to flow through condenser -21-.
3. The feed flask -25- was filled with distilled water and the water was fed to the inlet of preheater -5- by means of a pulsation pump -24- at a flow rate of 2-3 x 10^{-3} kg/min which was controlled by flowmeter -23-.
4. Nitrogen valves -29- and -28- were opened so that nitrogen flowed together with the steam through the system.
5. The condensate of mixed n-paraffins and water was collected in a separating funnel.
6. The desorption process was terminated when the refractive index of the condensate was about the same as that of pure distilled water.
7. Pump -24- and temperature controllers -4- and -8- were switched off, and nitrogen valves -29-, -28- and cooling water valve -26- were closed.
8. The n-paraffins collected were separated from the water by drawing the aqueous layer from the separating funnel. The weight of n-paraffins measured represented the amount desorbed from the pores of zeolite.
19. The distribution of n-alkanes in the desorbed n-paraffins was determined using the GLC technique.
10. Procedures (1-8) were repeated using n-pentane or n-hexane -

in the vapor phase - as desorbent agents instead of steam. The n-pentane or n-hexane was separated from the desorbed n-paraffins by simple distillation. This was easily accomplished because of the large difference in the boiling point, i.e. 420-453 K between them.

8.4 Multi-Cycle Adsorption Process:

The multicycle adsorption process was investigated both with, and without, intermediate reactivation of the molecular sieves using steam as the desorbing agent.

8.4.1 Multicycle adsorption without intermediate reactivation of zeolite.

The process comprised the following procedures:

1. Steps (1-15) in section 8.2 and steps (1-7) in section 8.3 were repeated until a considerable decrease in the dynamic capacity of the zeolite was observed. This was clearly identifiable from breakthrough time in the adsorption process for each cycle.

8.4.2 Multicycle adsorption with intermediate reactivation of zeolite.

The process comprised the following procedures:

1. Steps (1-15) in section 8.2 and steps (1-7) in section 8.3 were repeated.
2. The adsorption column -7- was maintained under vacuum as mentioned in section 8.2.1 for three hours at a temperature of 673 K and 15 um vacuum.
3. Steps 1 and 2 were repeated for 5 cycles.

8.5 Analysis of Hydrocarbon Fractions:

The feed (heavy kerosene), the denormalized product and the desorbed n-paraffins were analyzed to determine the content of n-paraffins and aromatic hydrocarbons using the gas-liquid chromatography and the ultra-violet techniques respectively.

8.5.1 N-Alkanes Analysis by Gas-Liquid Chromatography:

The feed (HK), the denormalized product, and the normal paraffin product were analyzed for n-alkanes content using a gas-liquid chromatograph (Intersmat 1GC 16 equipped with flame ionization detector). The analysis was carried out on a fused silica column SE 30 of 50 m long and 0.35×10^{-3} m I.D. The column temperature was programmed to start at 393 K for 20 minutes and then to increase at a rate of 4^{o}C/minutes until it reached 493 K. The injection and the flame ionization detector temperatures were set at 503 K. Nitrogen was used as a carrier gas with a fixed flow rate of

1.5×10^{-6} m^3/min. The slope sensitivity, the chart speed and the attenuation were set at 126, 0.005 m/min and 1 respectively. The n-alkanes peaks were drawn using a Datasystem Integrator (Schimadzu C-R1A) connected to the GLC instrument. Fig. (8.2) shows a schematic diagram of the GLC apparatus. Table (8.1) represents the operating conditions of the GLC apparatus.

The procedures of analysis can be summarized as follows:

1. A standard solution of n-paraffins presented in the HK (C_{12}-C_{21}) was prepared.
2. The column of the GLC was prepared for analysis using the above mentioned conditions.
3. A sample of the standard solution (0.2×10^{-9} m^3) was injected into the column, where the retention time for each n-paraffin was reported (See Table 8.2).
4. A sample (0.2×10^{-9} m^3) of the first fraction of denormalized kerosene collected from the adsorption effluent was injected into the column, where the retention time of each n-paraffin present in the solution was compared with that of the standard solution.
5. For each retention time of n-paraffin shown on the sheet of the GLC, the concentrations were summed up to give the total concentration of n-paraffins in the fraction (wt%).
6. Step 4 and 5 were repeated for other denormalized fractions collected. The analysis of these fractions was carried out for two adsorption runs and calibrated with consecutive refractive indices.

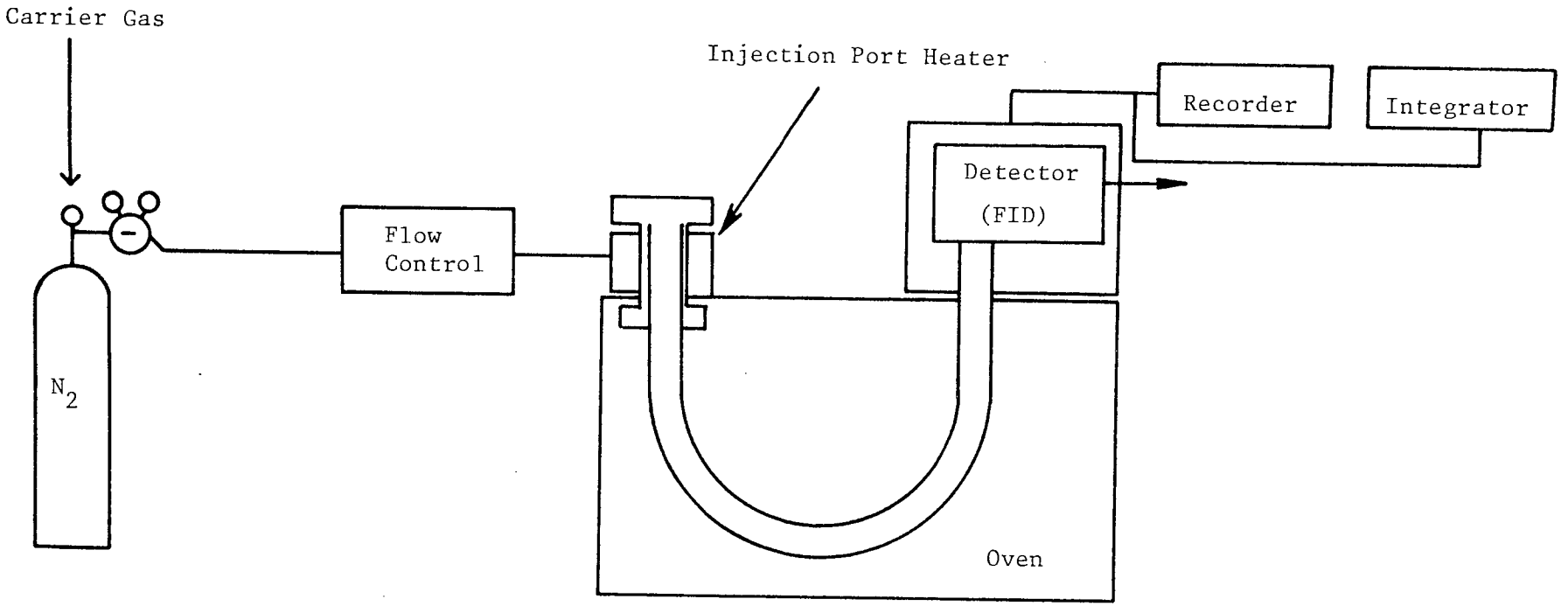

Fig. 8.2 Schematic Diagram of the GLC Used for Determination of n-Paraffins Content.

Table 8.1 Operating conditions of gas-liquid chromatograph for determination of n-paraffins in heavy kerosene, denormalized kerosene, and n-paraffins product.

Property	
Type of the column	Fused Silica Se-30
Length of the column	50 m
Diameter of the column	0.35×10^{-3} m
Type of detector	Flame Ionization Detector (FID)
Carrier gas	Nitrogen
Model	Intersmat I GC 16
Data system integrator	Shimadzu C-R1 A
Injection temperature	503 K (230°C)
Detector temperature	503 K (230°C)
Initial column temperature	393 K (120°C) for 20 min
Rate of temp. increase	4°C/min
Final column temperature	493 K (220°C)
Nitrogen flowrate	1.5×10^{-6} m^3/min
Attenuation	1
Chart speed	0.005 m/min
Slope sensitivity	126

Table 8.2 The retention time for each n-alkane present in the standard solution under the specified conditions mentioned in Table 8.1.

Normal Alkane	Retention Time (Min.)			
	1st Run	2nd Run	3rd Run	Average
n-Dodecane (C_{12})	16.92	16.41	16.65	16.66
n-Tridecane (C_{13})	22.86	22.42	22.55	22.61
n-Tetradecane (C_{14})	29.69	29.18	29.22	29.36
n-Pentadecane (C_{15})	35.79	35.26	35.30	35.45
n-Hexadecane (C_{16})	41.57	41.81	41.85	41.74
n-Heptadecane (C_{17})	45.82	45.88	45.82	45.84
n-Octadecane (C_{18})	51.64	51.83	51.60	51.69
n-Nonadecane (C_{19})	56.42	56.33	56.37	56.37
n-Eicosane (C_{20})	61.14	60.96	60.87	60.99

7. Procedures (1-5) were repeated for samples of original feed and product.

8.5.2 Aromatic-Hydrocarbon Analysis by Ultra-Violet Spectrophotometry:

The aromatics content of the original feed, denormalized kerosene, and n-paraffin product was monitored satisfactorily by measuring the optical density of the samples using UV spectrophotometer (Perkin-Elmer 402).

The procedures were as follows:

1. One milligram of the sample was weighed in a 10 millilit er of iso-octane solvent.
2. The unit cell of the UV Spectrophotometer was filled with the sample and compared to the pure solvent which was used as a reference (iso-octane).
3. The optical densities at different wavelengths: 200, 230 and 255 nm (nanometer) (i.e. optical density of mono-, di- and tri-aromatic rings) were recorded respectively.
4. The coefficients of adsorption at different wave lengths were determined.
5. The content of each aromatic type was calculated by using a system of equations set-up on the basis of average extinction coefficients for mono, di, and tri-aromatic rings of hydrocarbon. These equations were [79]:

$$C_{a_b} = + 0.212\ K_{200} - 0.040\ K_{230} - 0.063\ K_{255} \quad (8.1)$$

$$C_{a_n} = - 0.11\ K_{200} - 0.040\ K_{230} - 0.063\ K_{255} \quad (8.2)$$

$$C_{a_f} = - 0.002\ K_{200} - 0.007\ K_{230} + 0.732\ K_{255} \quad (8.3)$$

$$C_b = \frac{C_{a_b} \times M \times 0.87}{72} \quad (8.4)$$

$$C_n = \frac{C_{a_n} \times M \times 0.87}{120} \quad (8.5)$$

$$C_f = \frac{C_{a_f} \times M \times 0.87}{168} \quad (8.6)$$

Where:

- C_{a_b}, C_{a_n}, C_{a_f} : The content of benzene, naphthalene and phenanthrene nuclei (wt%).
- K_{200}, K_{230}, K_{255} : Specific extinction coefficients of sample adsorption in ranges 200, 230 and 255 nm wavelength and can be calculated from Eq. (8.7).

$$K = \frac{\overline{D}}{C.L} \quad (8.7)$$

Where

$\overline{D}$ = Optical density of the paraffin test sample.

C = Concentration of aromatic hydrocarbon remaining in the paraffin, g/L

L = Layer thickness, cm

- C_b, C_n, C_f : The content of benzene, naphthalene and phenanthrene hydrocarbons.
- M : Molecular weight of the sample.

- 72, 120, 168 : The total weight of atoms of carbon which exist in benzene, naphthalene, and phenanthrene nuclei respectively.
- 0.87 : The ratio of carbon in total molecular weight of the sample (average ratio).

Fig. (8.3) shows the ultraviolet spectroscopic analysis of the original feed of heavy kerosene.

The distribution of the different aromatic hydrocarbons is shown in Ch.9.

Fig. 8.3 UV-Spectra for Heavy Kerosene (HK)

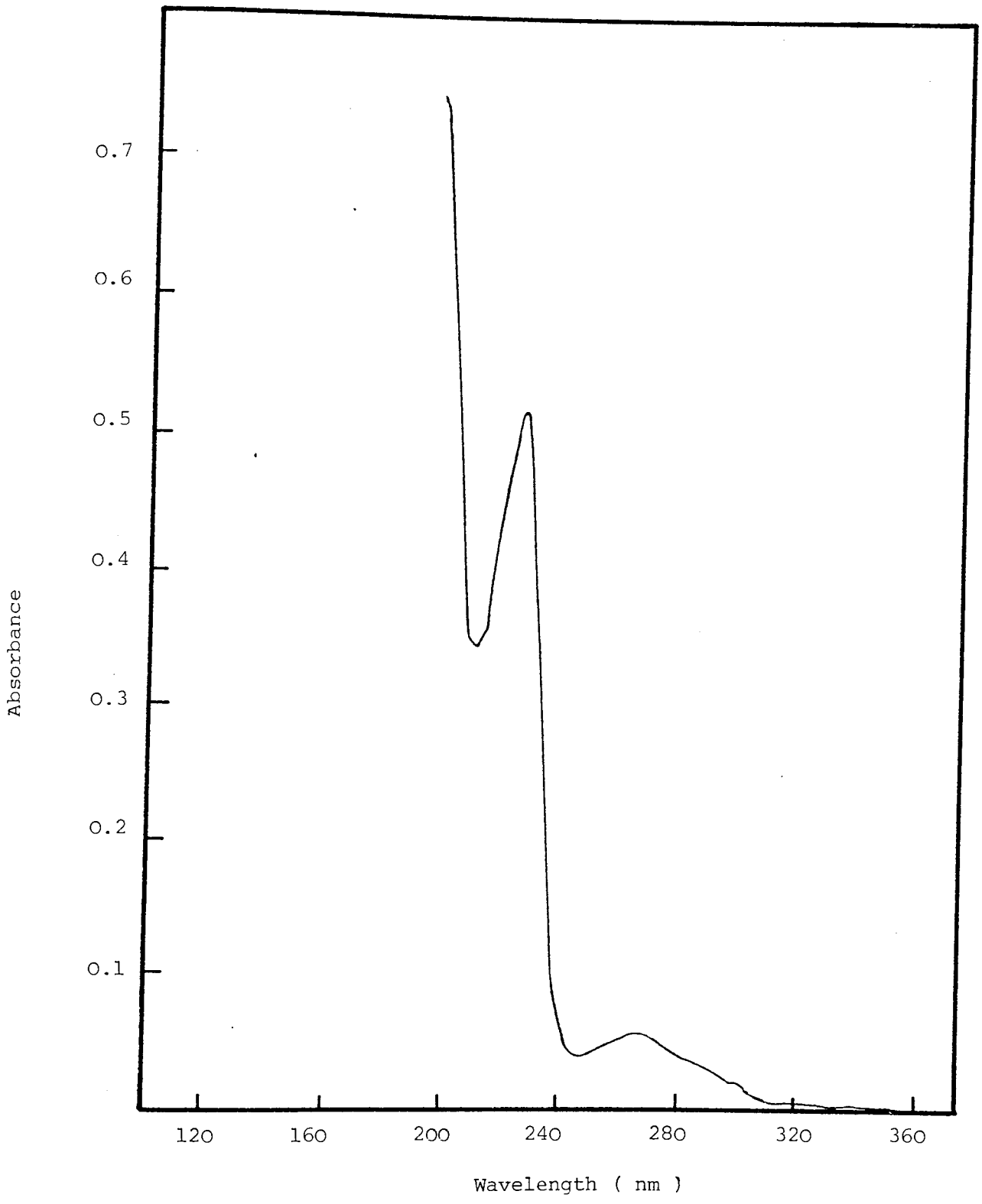

CHAPTER NINE

RESULTS AND DISCUSSION

CHAPTER NINE

RESULTS AND DISCUSSION

The experimental results are presented in this chapter in four separate sections. The first section deals with the dynamics and kinetics of the flow system using one-cycle of adsorption at different parameters. The second section describes the results of the desorption stage at the optimum adsorption conditions achieved using mainly steam as the desorbing agent. The results of the multi-cycle adsorption-desorption process are discussed in section three. Section four contains the results of the analysis of different hydrocarbon fractions and the measurement of the surface area and pore volume for fresh, regenerated and used zeolite.

9.1 One-Cycle Adsorption Process:

All the adsorption experiments were conducted in the vapor-phase using a fixed-bed of zeolite molecular sieves type-5A. By measuring the refractive index (RI) of the feedstock, namely 1.4580 at 298 K, and monitoring the refractive indices of the fractions collected (the by-product) from the adsorption process at equal intervals of time (180-600 s) the breakthrough curve for each run was established by plotting the RI versus time. By analyzing the n-paraffins content of each fraction collected from the adsorption process, the same breakthrough curve can be established by plotting C/Co in the vertices vs. time, where C is the

concentration of n-paraffin in wt% for each fraction and Co is the original concentration of n-paraffins in heavy kerosene which is mounted to 18.75 wt%. Figure (9.1) presents a comparison between the breakthrough curves established using the n-paraffins concentration and the refractive indices of the effluent from the adsorption process which is conducted at a feed flowrate of 33.33 x 10^{-9} m^3/s, an adsorption temperature of 643 K and a zeolite particle size of (1.0 - 2.0) x 10^{-3} m. The calibration curve between the refractive index at 298 K and the n-paraffins concentration in wt% is given in Fig. (9.2).

The adsorption of n-paraffins from heavy kerosene using zeolite type-5A was conducted in the vapor-phase over a range of different adsorption conditions. The variable parameters studied were the feed flowrate, the adsorption temperature and the particle size of zeolite. The height and internal diameter of the adsorption column, the concentration of n-paraffins in the original hydrocarbon feed and the nitrogen flowrate were fixed at 0.65 m, 0.016 m, 18.75 wt% and 6.7 x 10^{-7} m^3/s respectively ensuring that flowrates were well below incipient fluidization conditions. The feed flowrate studied was in the range of 16.66 x 10^{-9} to 50.00 x 10^{-9} m^3/s and the adsorption temperature was in the range of 603 to 683 K whereas the particle size of zeolite was ranged from less than 0.5 x 10^{-3} m to 3 x 10^{-3} m. Figure (9.3) through Fig. (9.7) show the breakthrough curves of adsorption of n-paraffins from HK using zeolites type-5A at feed flowrates of 16.66 x 10^{-9}, 22.22 x 10^{-9}, 33.33 x 10^{-9}, 44.44 x 10^{-9} and 50.00 x 10^{-9} m^3/s respectively at a

Fig. 9.1 Agreement between n-paraffins concentration as determined by GLC and refractive index reading @ 298 K ($25^{o}C$)

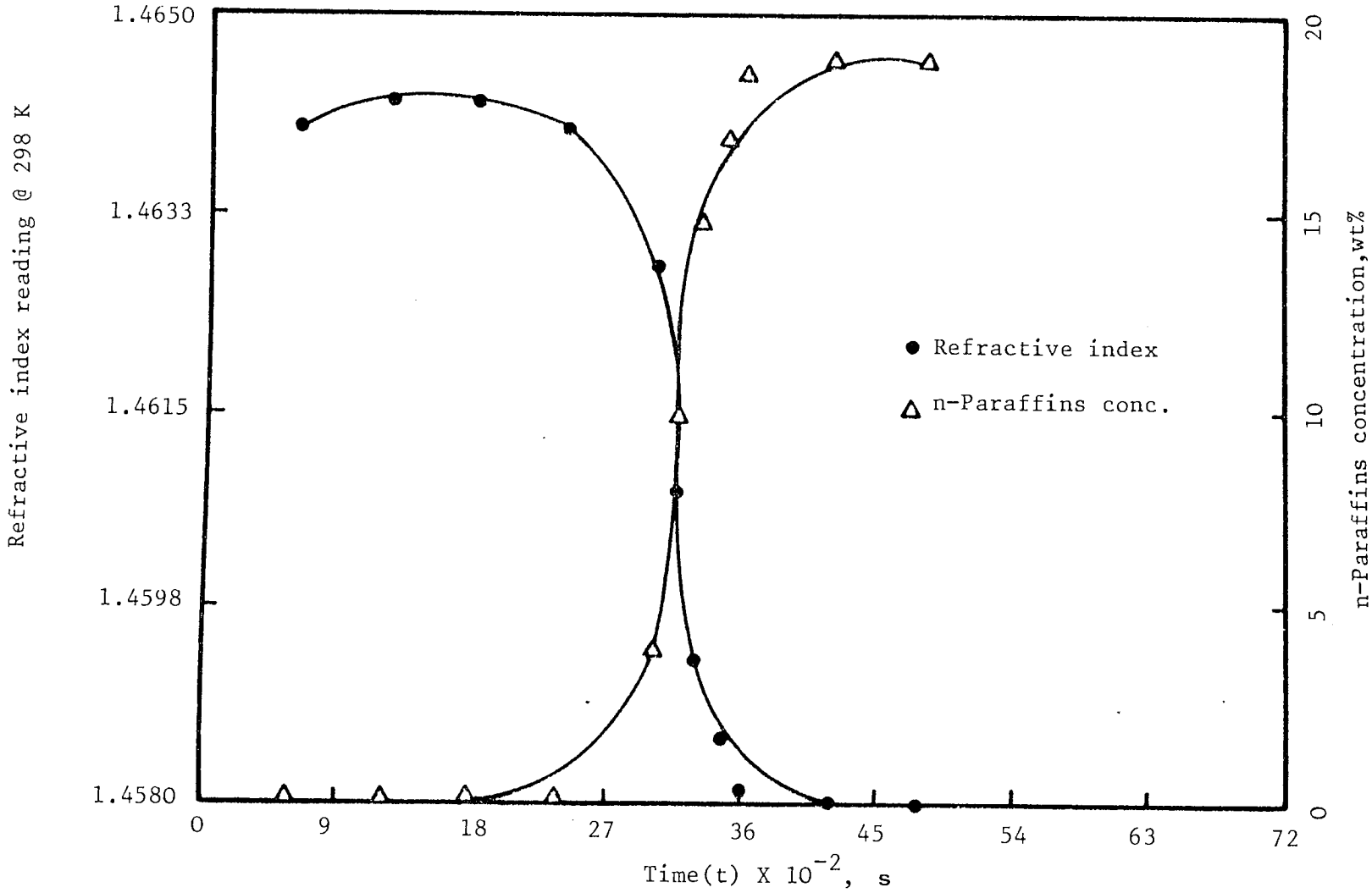

Fig. 9.2 Calibration curve between refractive index reading at 298 K and n-paraffins concentration as determined by GLC .

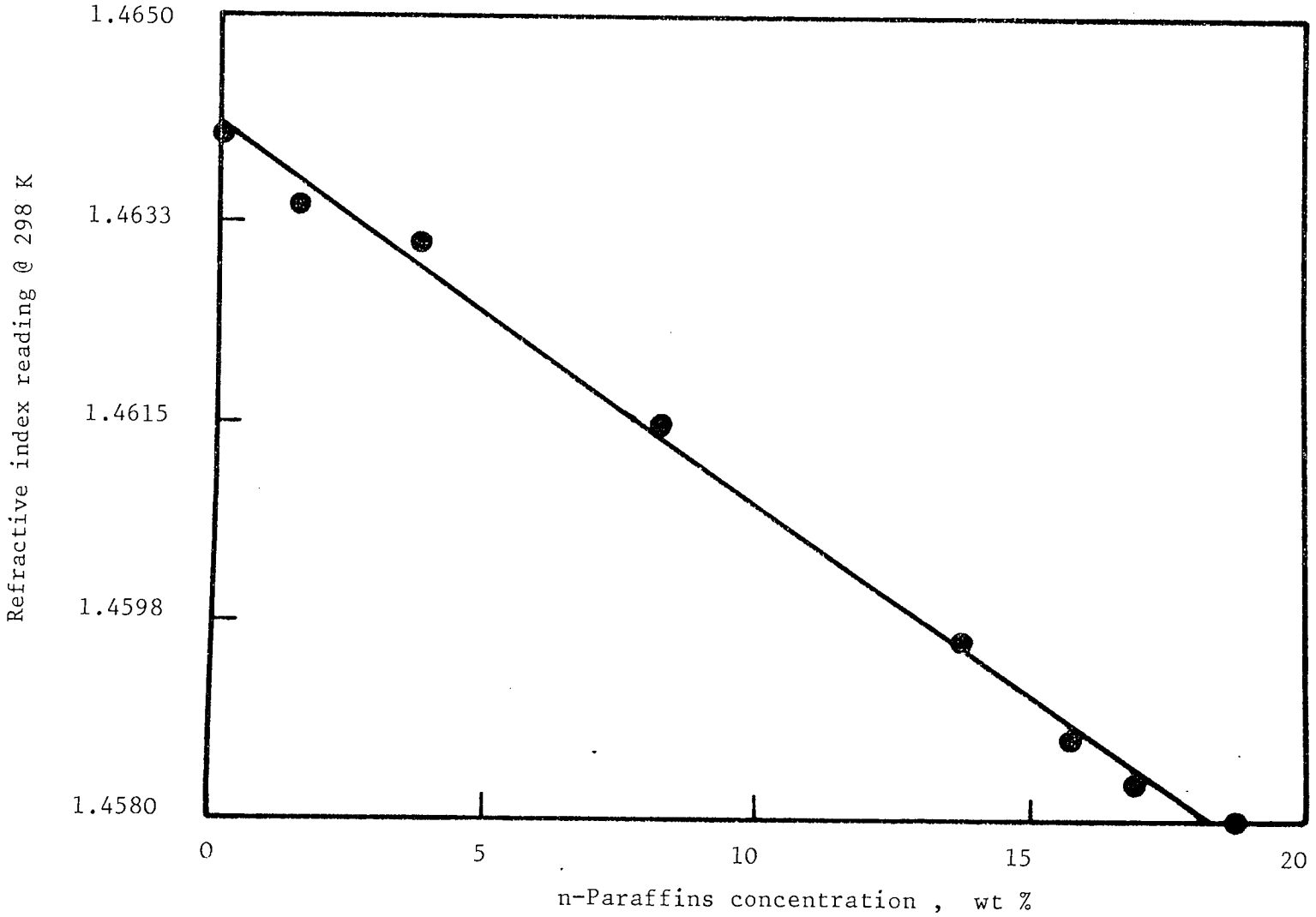

fixed adsorption temperature of 643 K and zeolite particle size of (1.0 - 2.0) x 10^{-3} m. The experimental data of these breakthrough curves which are plotted as the refractive indices vs. time are shown in Table (1) through Table (5) of Appendix (A). Figure (9.3) through Fig. (9.7) demonstrate that an increase in the feed flowrate leads to a decrease in the breakthrough time Θ_b. The breakthrough time at a flowrate of 16.66 x 10^{-9} m^3/s is 6600 s which means that 5% of the original n-paraffins concentration exists (or breaks through) in the effluent fraction of the adsorption process after a time period of 6600 s. By increasing the feed flowrate from 16.66 x 10^{-9} m^3/s to 22.22 x 10^{-9} m^3/s, the breakthrough time is reduced from 6600 s to 4500 s. By increasing the feed flowrate to 33.33 x 10^{-9} m^3/s, the breakthrough time is reduced by about 3900 s. At a feed flowrate of 50.00 x 10^{-9} m^3/s, the breakthrough time is reached after 1320 s from the beginning of the adsorption process. By using the calibration curve shown in Fig. (9.2) and the experimental data in Table (1) to Table (5) of Appendix (A), the breakthrough curves of adsorption of n-paraffins from HK at different feed flowrates are plotted as C/Co vs. time as shown in Fig. (9.8). It is seen that the difference between the exhaustion and the breakthrough times ($\Theta_e - \Theta_b$) is generally inversely proportional to the feed flowrate. These differences are 3180, 1500, 1020, 1230 and 660 s for the feed flowrates 16.66 x 10^{-9}, 22.22 x 10^{-9}, 33.33 x 10^{-9}, 44.44 x 10^{-9}, and 50 x 10^{-9} m^3/s respectively. An exception is noticed at the feed flowrates of 33.33 x 10^{-9} and 44.44 x 10^{-9} m^3/s suggesting that there is probably an optimum feed flowrate for the adsorption of n-paraffins from HK. The general trend, as shown in Fig. (9.8), is

Fig. 9.3 Breakthrough curve of adsorption of n-paraffins from HK by zeolite type-5A at a feed flowrate of 16.66×10^{-9} m^3/s, a temperature of 643 K, and a pellet particle size of $(1.0 - 2.0) \times 10^{-3}$ m.

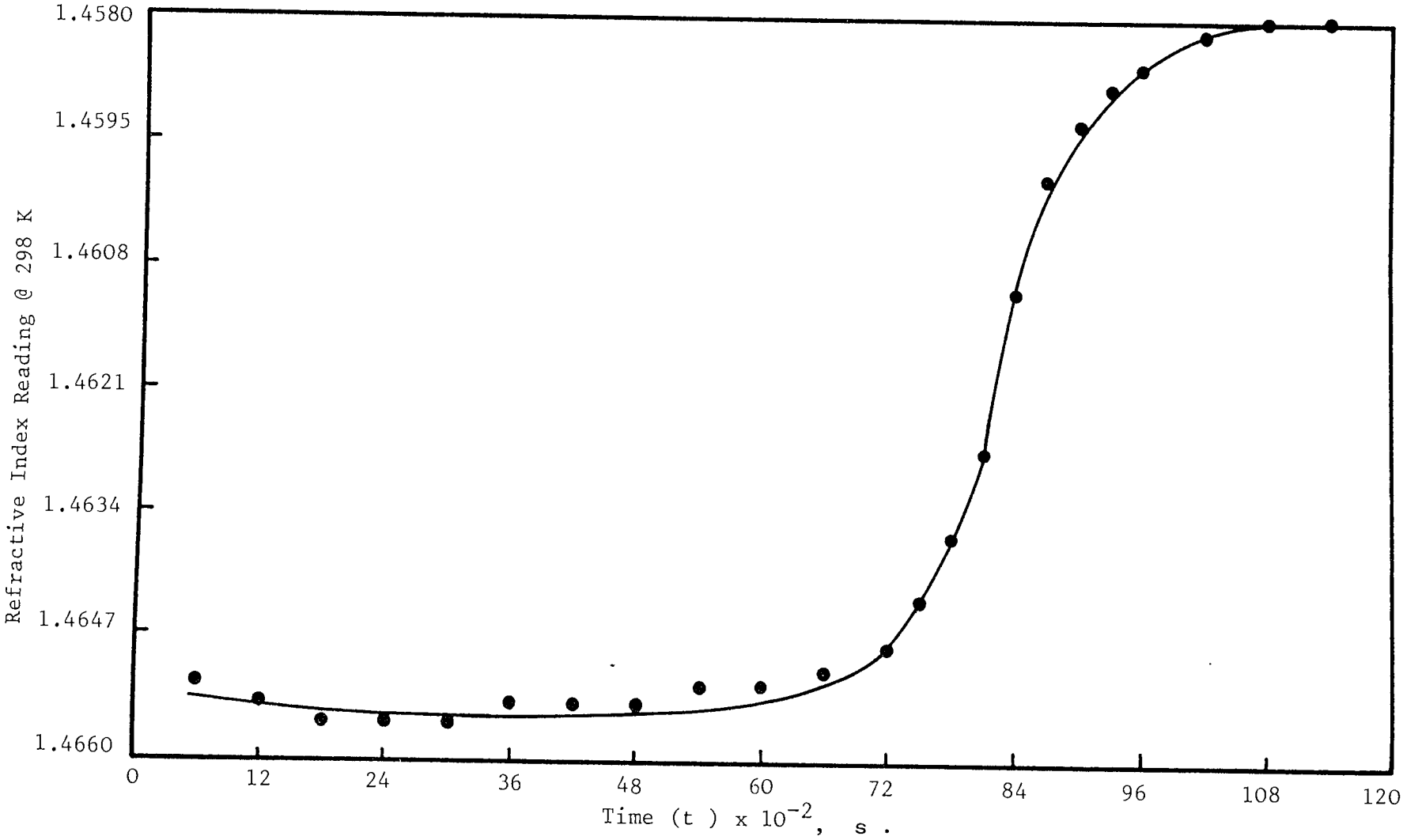

Fig. 9.4 Breakthrough curve of adsorption of n-paraffins from HK by zeolite type-5A at a feed flowrate of 22.22 x 10^{-9} m^3/s , a temperature of 643 K, and a pellet particle size of (1.0 - 2.0) x 10^{-3} m.

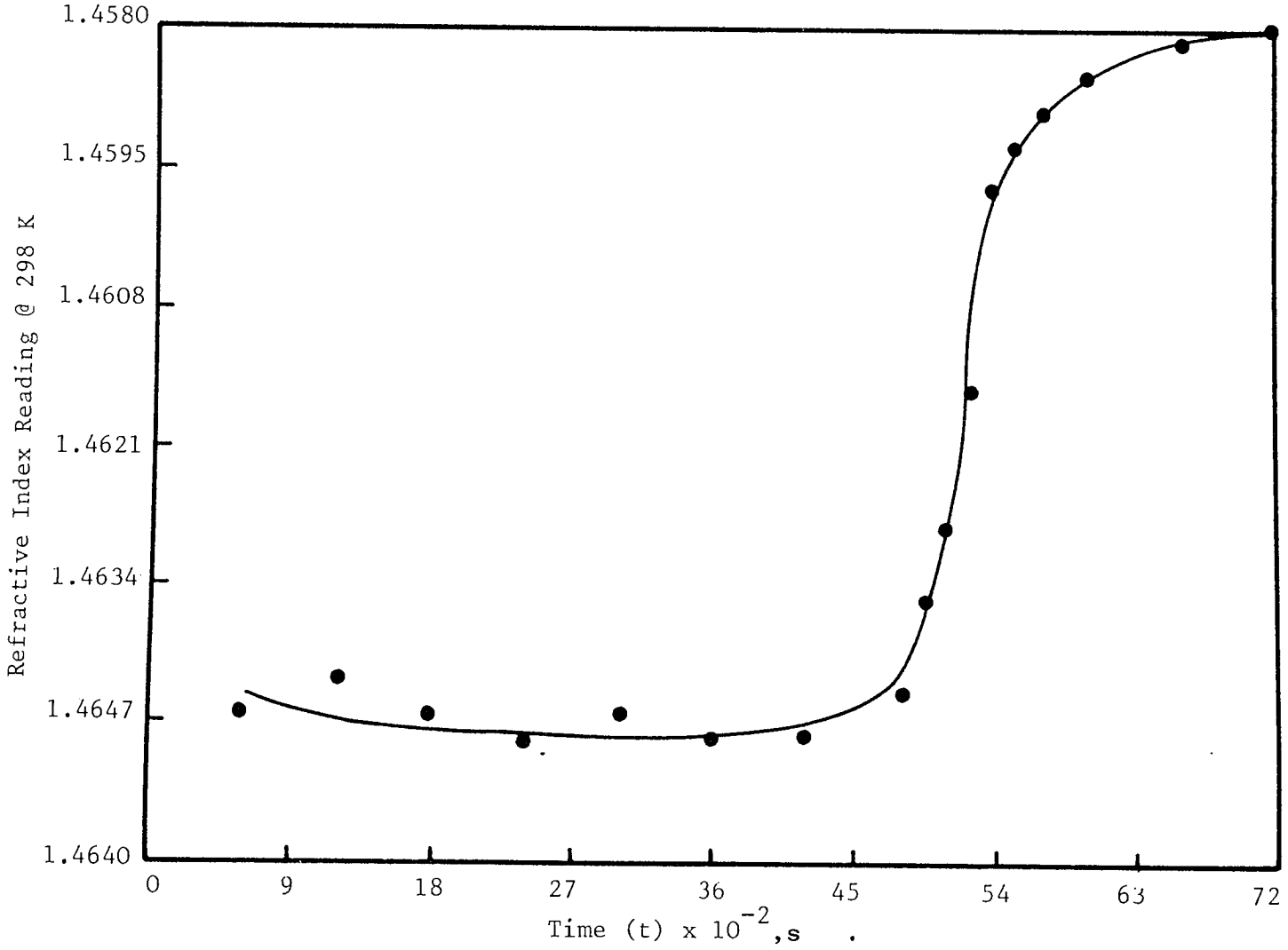

Fig. 9.5 Breakthrough curve of adsorption of n-paraffins from HK by zeolite type-5A at a feed flowrate of 33.33×10^{-9} m^3/s a temperature of 643 K, and a pellet particle size of $(1.0\text{-}2.0) \times 10^{-3}$ m .

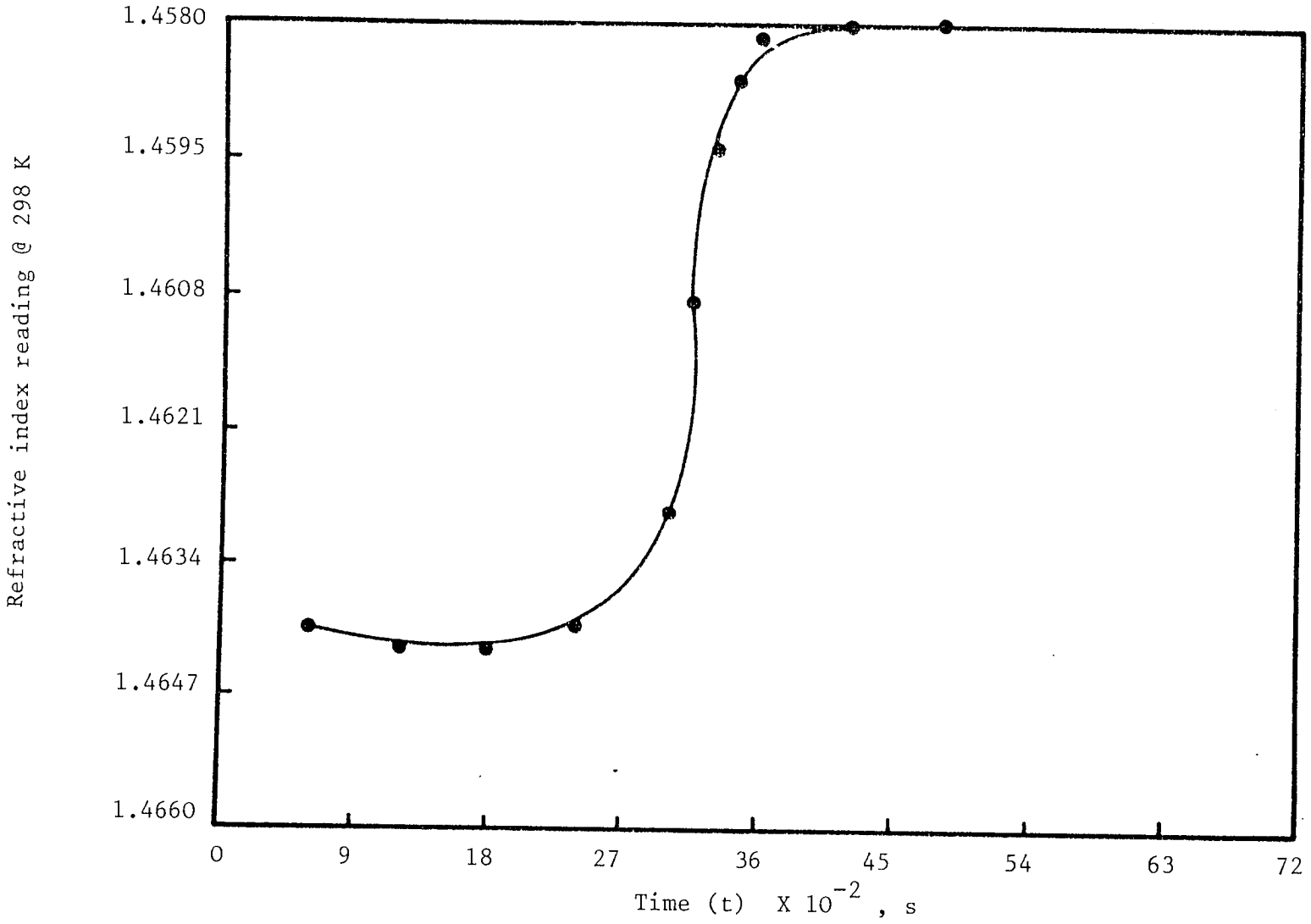

Fig. 9.6 Breakthrough curve of adsorption of n-paraffins from HK by zeolite type-5A at a feed flowrate of 44.44 x 10^{-9} m^3/s , a temperature of 643 K, and a pellet particle size of (1.0 - 2.0) x 10^{-3} m.

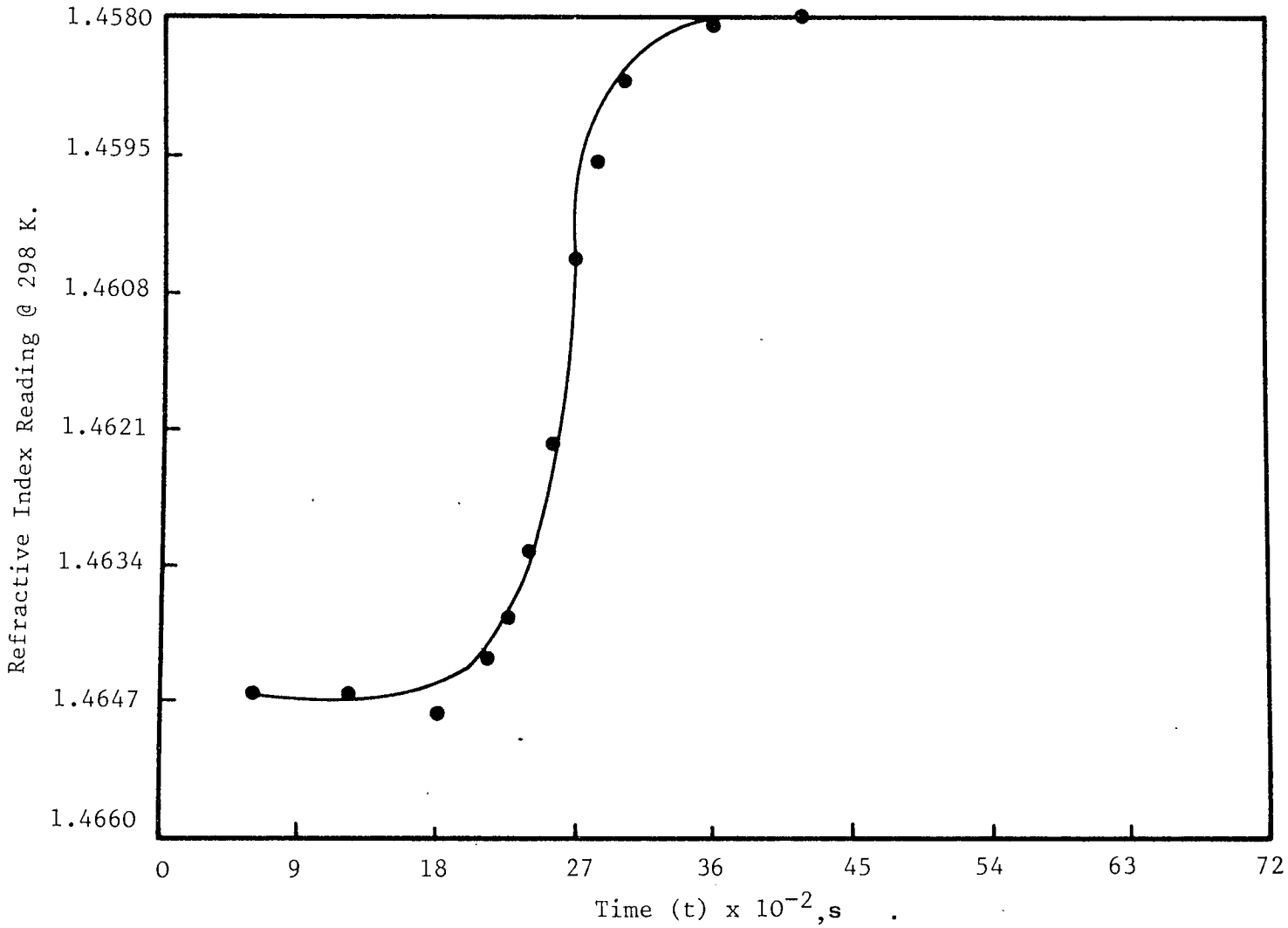

Fig. 9. 7 Breakthrough curve of adsorption of n-paraffins from HK by zeolite type-5A at a feed flowrate of 50.00 x 10^{-9} m^3/s , a temperature of 643 K, and a pellet particle size of (1.0 - 2.0) x 10^{-3} m.

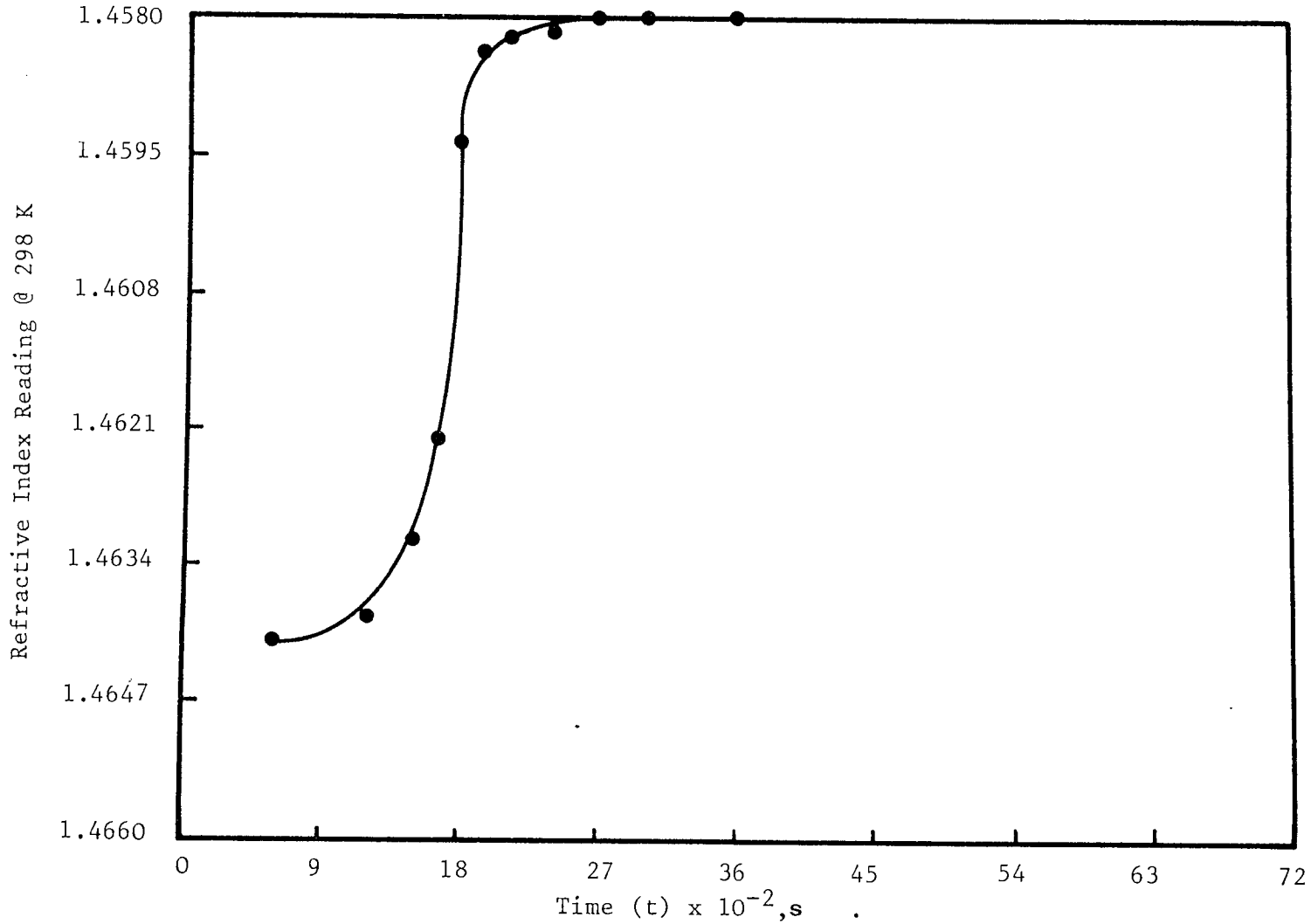

Fig. 9.8 Effect of feed flowrate on the breakthrough curves of n-paraffins adsorption from HK by zeolite type-5A , at a temperature of 643 K , and a pellet particle size of (1.0-2.0) X 10^{-3} m .

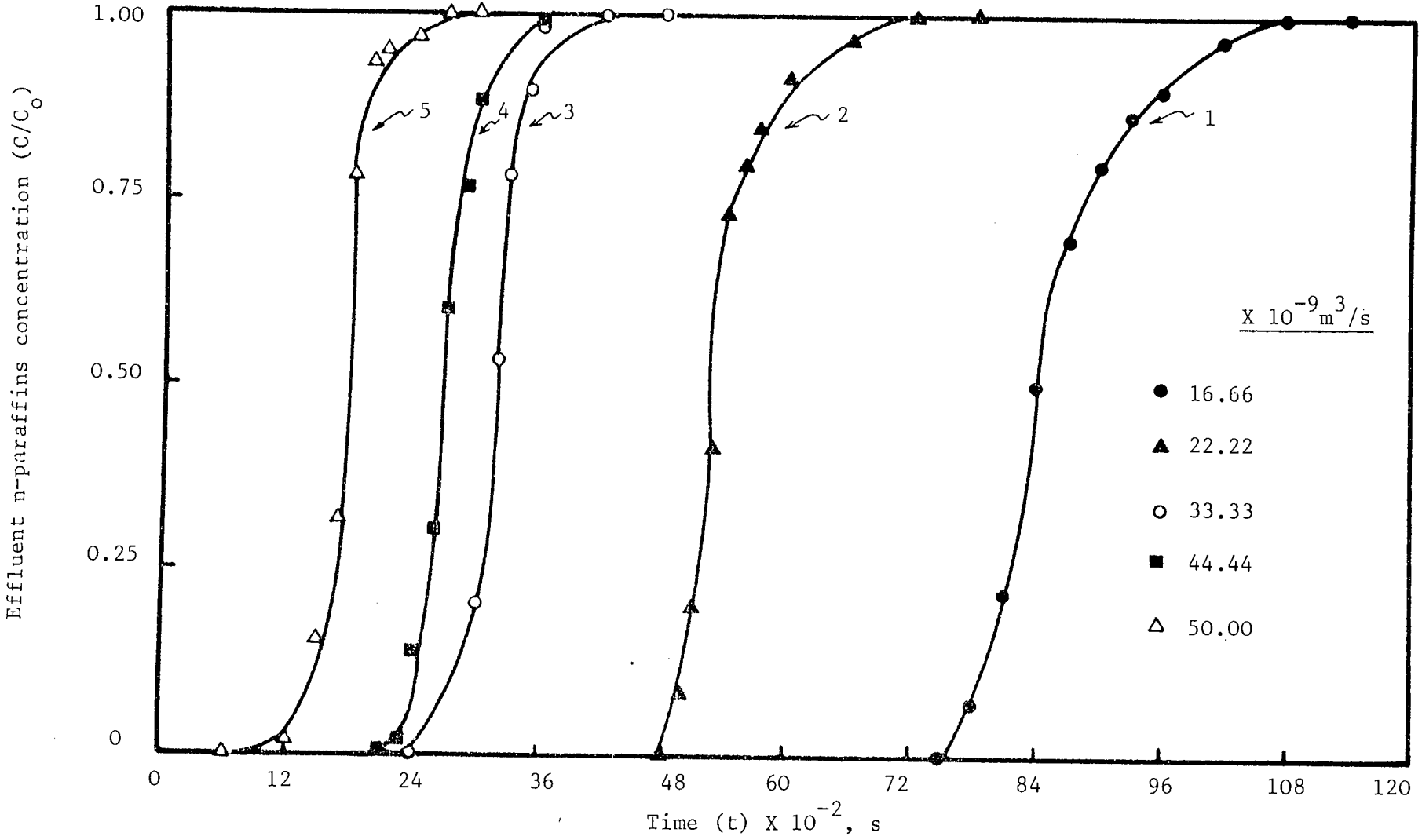

the sharpness of the (S-shaped) breakthrough curves and the faster occurrence of the breakthrough time with increasing the feed flowrate. Table 9.1 shows the variation of the exhaustion and the breakthrough times with the feed flowrates.

The second varying parameter investigated in this study was the adsorption temperature. Figure (9.9) through Fig. (9.13) show the breakthrough curves of adsorption of n-paraffins from HK using zeolite type-5A at adsorption temperatures of 603, 623, 643, 663 and 683 K respectively at a fixed feed flowrate of 33.33×10^{-9} m^3/s and zeolite particle size of $1.0 - 2.0 \times 10^{-3}$ m. The experimental data of these breakthrough curves, plotted as the refractive indices vs. time, are shown in Table (6) through Table (10) of Appendix (A). Again, by using the experimental data and Fig. (9.2), the breakthrough curves of n-paraffins adsorption from HK are plotted as the ratio C/Co vs. time at different adsorption temperatures as shown in Fig. (9.14). This figure shows an overlap of breakthrough curves at the different adsorption temperatures, especially in the range of 623 - 663 K where an optimum adsorption temperature is expected. The breakthrough time shown in Fig. (9.14) increases as the temperature is increased. This happens to a certain limit after which the brekathrough "BT" time decreases while the temperature is increased. For example, the BT-time is reached after 1350, 2040 and 2700 s at temperatures of 603, 623 and 643 K respectively while at 663 and 683 K the BT-time is reached at 2040 and 1860 s respectively. It will be seen that for both temperatures 623 and 663 K, the BT-time is reached at the same time, i.e. after 2040 s

Table 9.1 Variation of the exhaustion and the breakthrough times with the feed flowrate*

Flow-rate x 10^9 (m^3/s)	$\theta_E \times 10^2$ (s)	$\theta_B \times 10^2$ (s)	f
16.66	97.80	66.00	0.5121
22.22	60.00	45.00	0.4167
33.33	37.20	27.00	0.5015
44.44	32.40	20.10	0.4296
50.00	19.80	13.20	0.5233

* Conditions:

- Adsorption Temperature = 643 K
- n-Paraffins Conc. in the HK = 18.75 wt%
- Length of the Packed-Column = 0.650 m
- Particle Size of Zeolite = 1.0 - 2.0 x 10^{-3}m

Fig. 9.9 Breakthrough curve of adsorption of n-paraffins from HK by zeolite type-5A at a temperature of 603 K, a feed flowrate of 33.33×10^{-9} m^3/s , and a pellet particle size of $(1.0 - 2.0) \times 10^{-3}$ m.

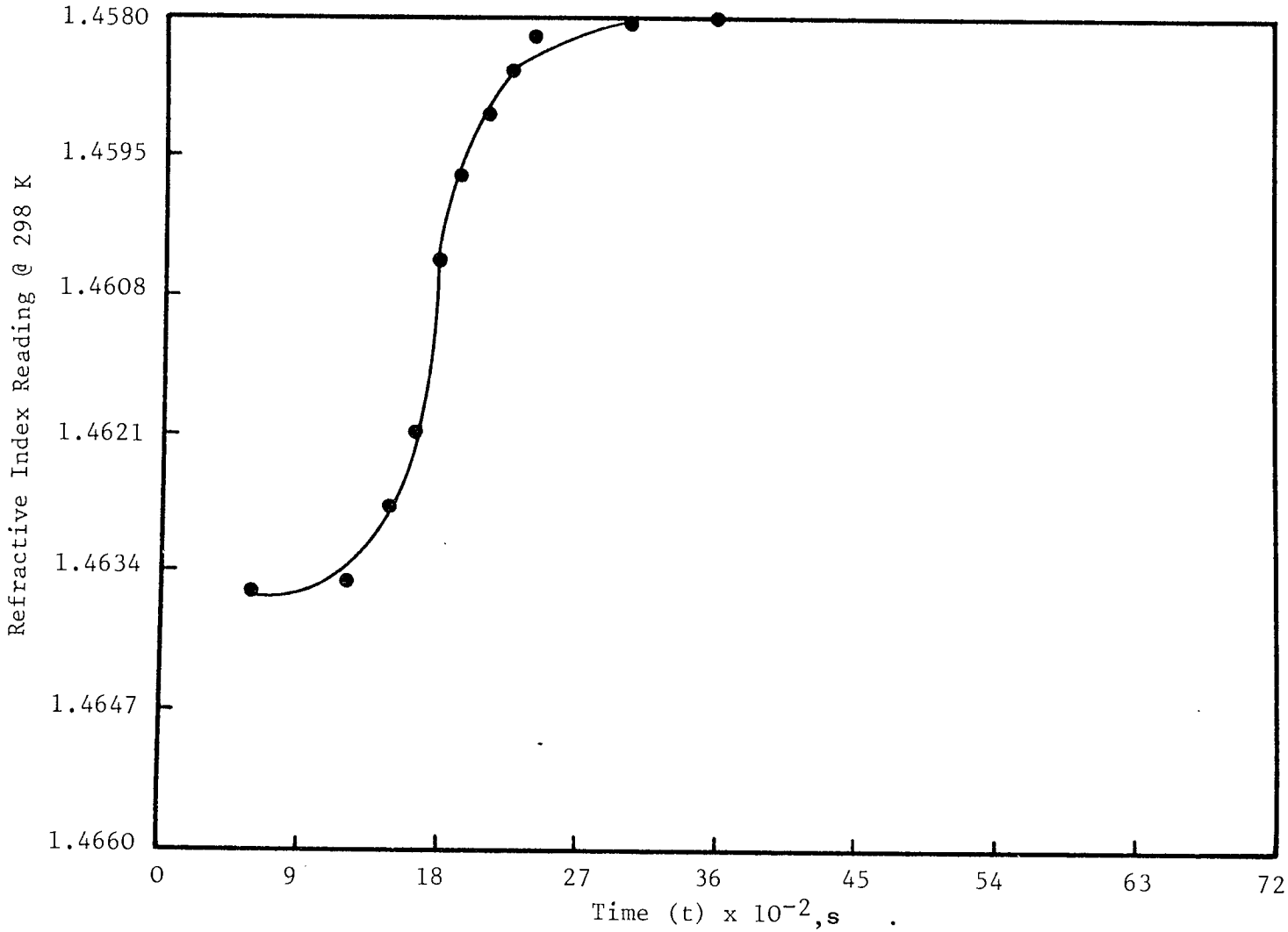

Fig. 9.10 Breakthrough curve o f adsorption of n-paraffins from HK by zeolite type-5A at a temperature of 623 K, a feed flowrate of 33.33×10^{-9} m^3/s , and a pellet particle size of $(1.0 - 2.0) \times 10^{-3}$ m.

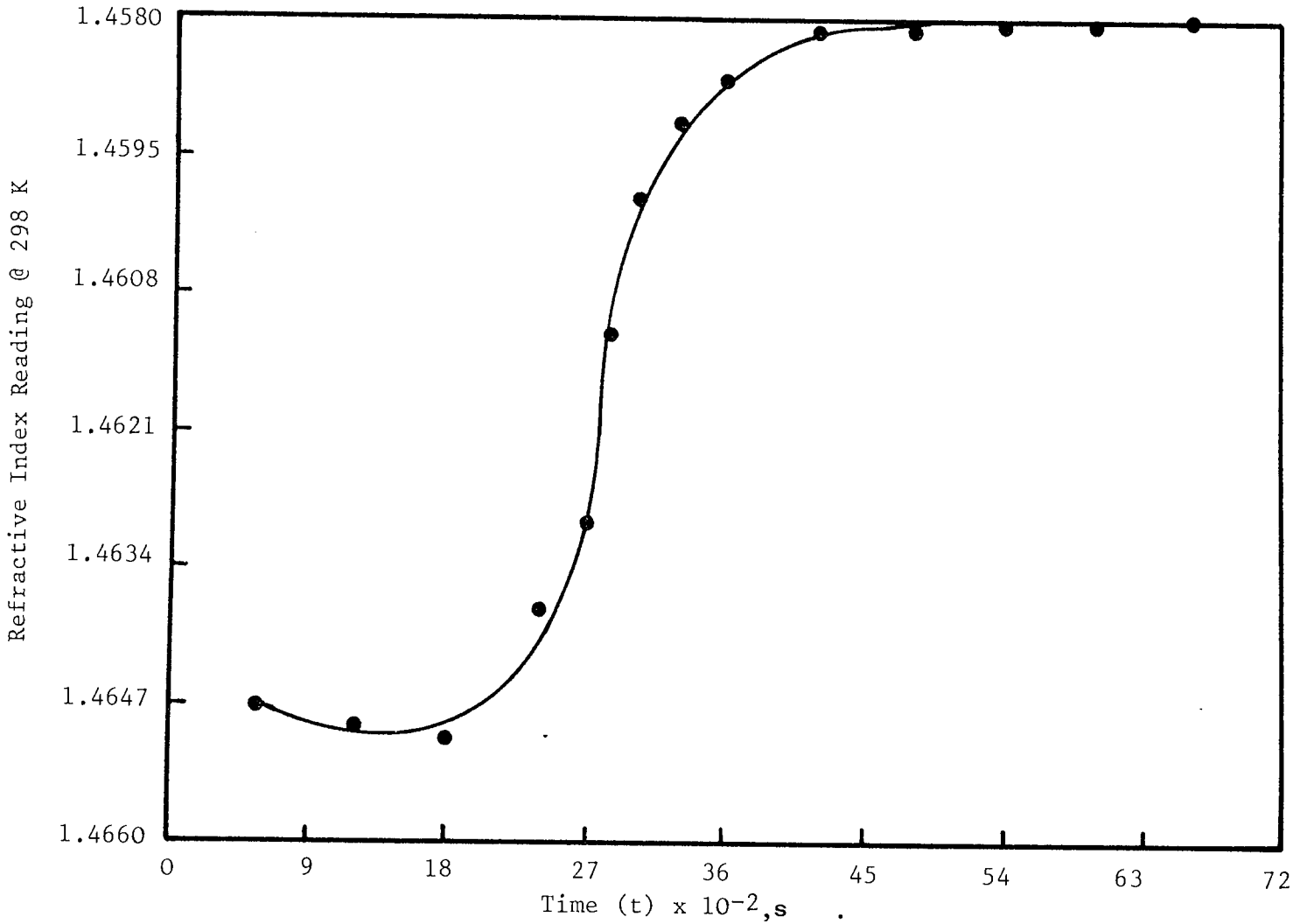

Fig. 9.11 Breakthrough curve of adsorption of n-paraffins from HK by zeolite type-5A at a feed flowrate of 33.33×10^{-9} m^3/s a temperature of 643 K, and a pellet particle size of $(1.0\text{-}2.0) \times 10^{-3}$ m .

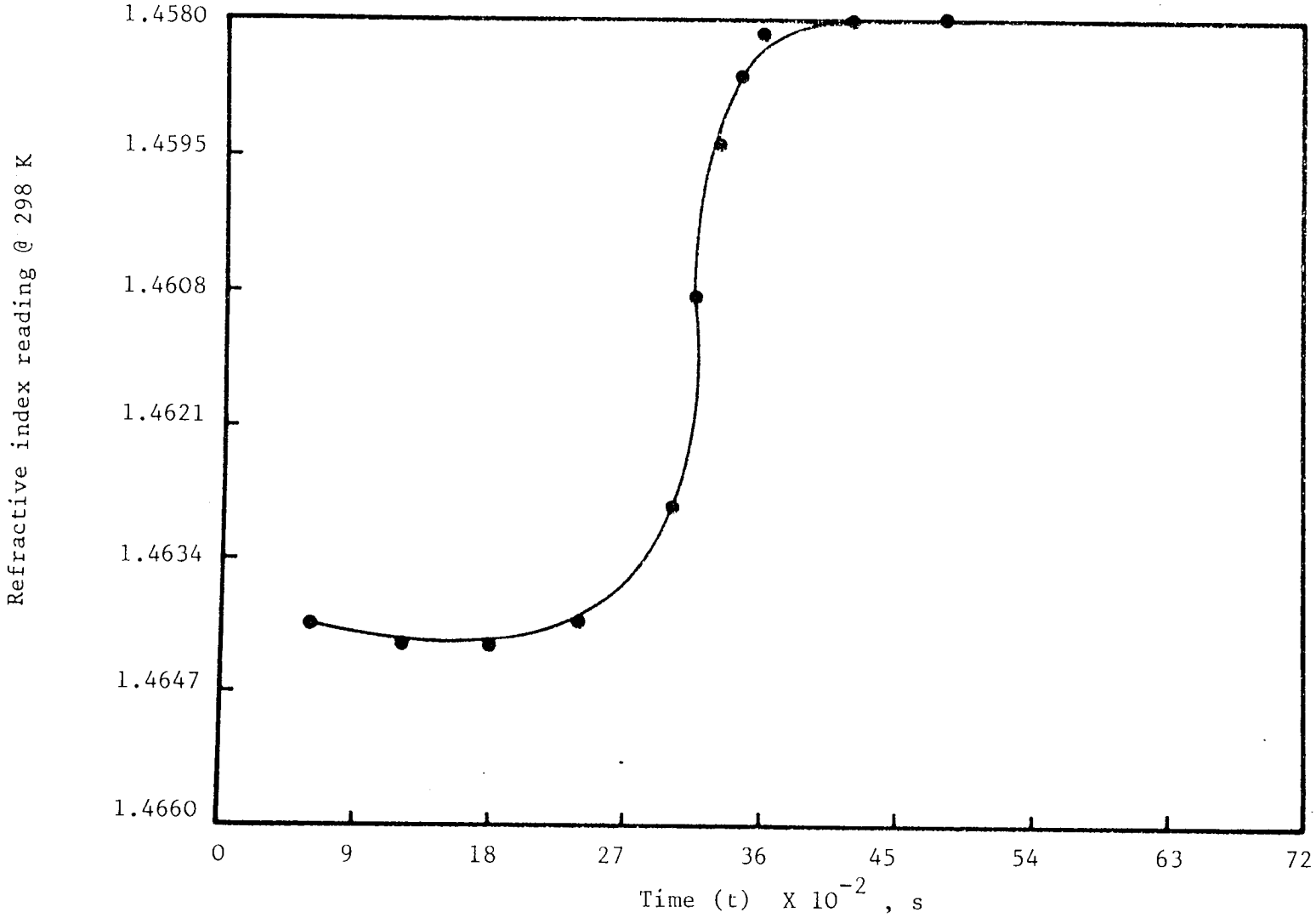

Fig. 9.12 Breakthrough curve of adsorption of n-paraffins from HK by zeolite type-5A at a temperature of 663 K, a feed flowrate of 33.33×10^{-9} m^3/s , and a pellet particle size of $(1.0 - 2.0) \times 10^{-3}$ m.

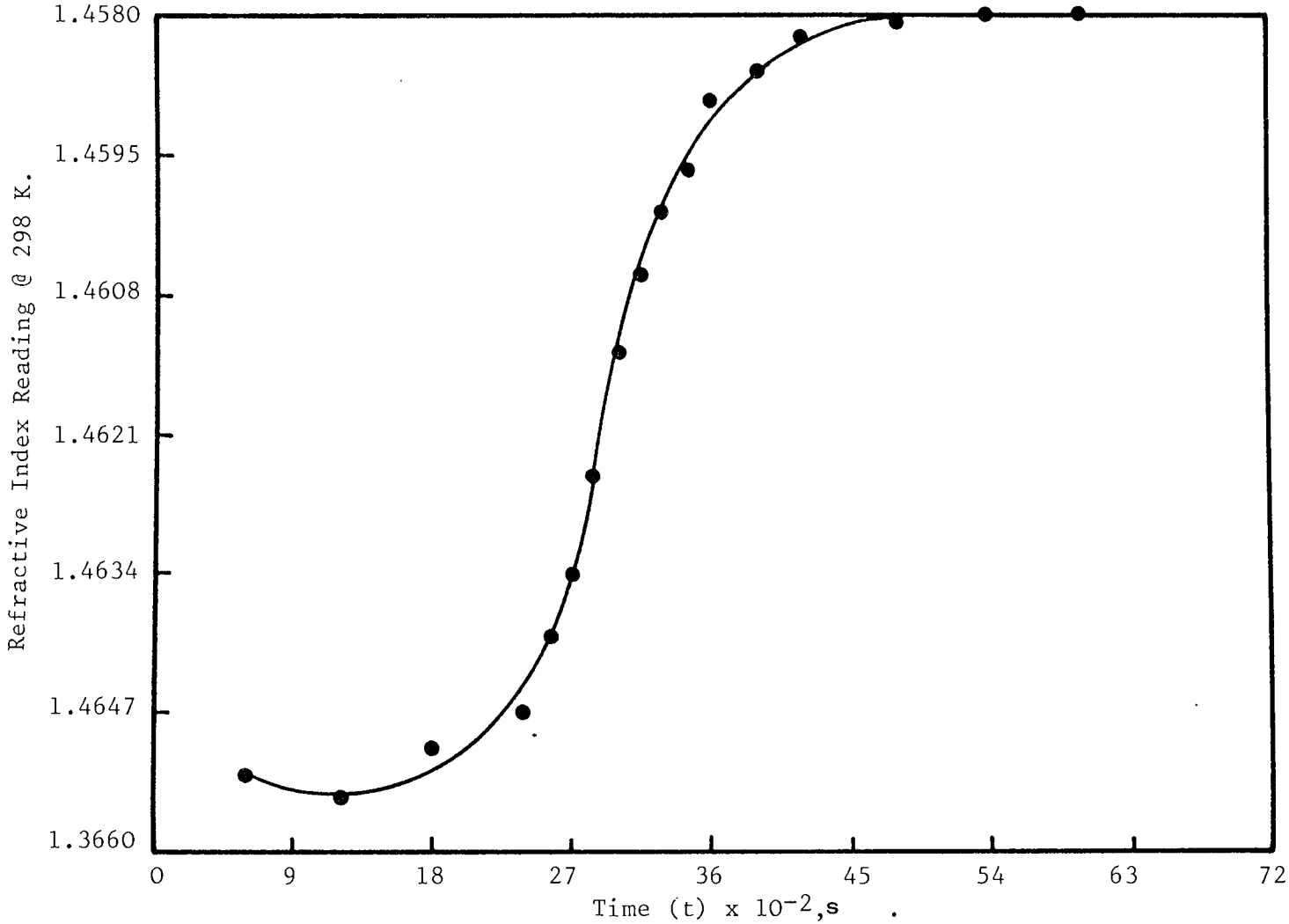

Fig. 9.13 Breakthrough curve of adsorption of n-paraffins from HK by zeolite type-5A at a temperature of 683 K, a feed flowrate of 33.33×10^{-9} m^3/s , and a pellet particle size of $(1.0 - 2.0) \times 10^{-3}$, m.

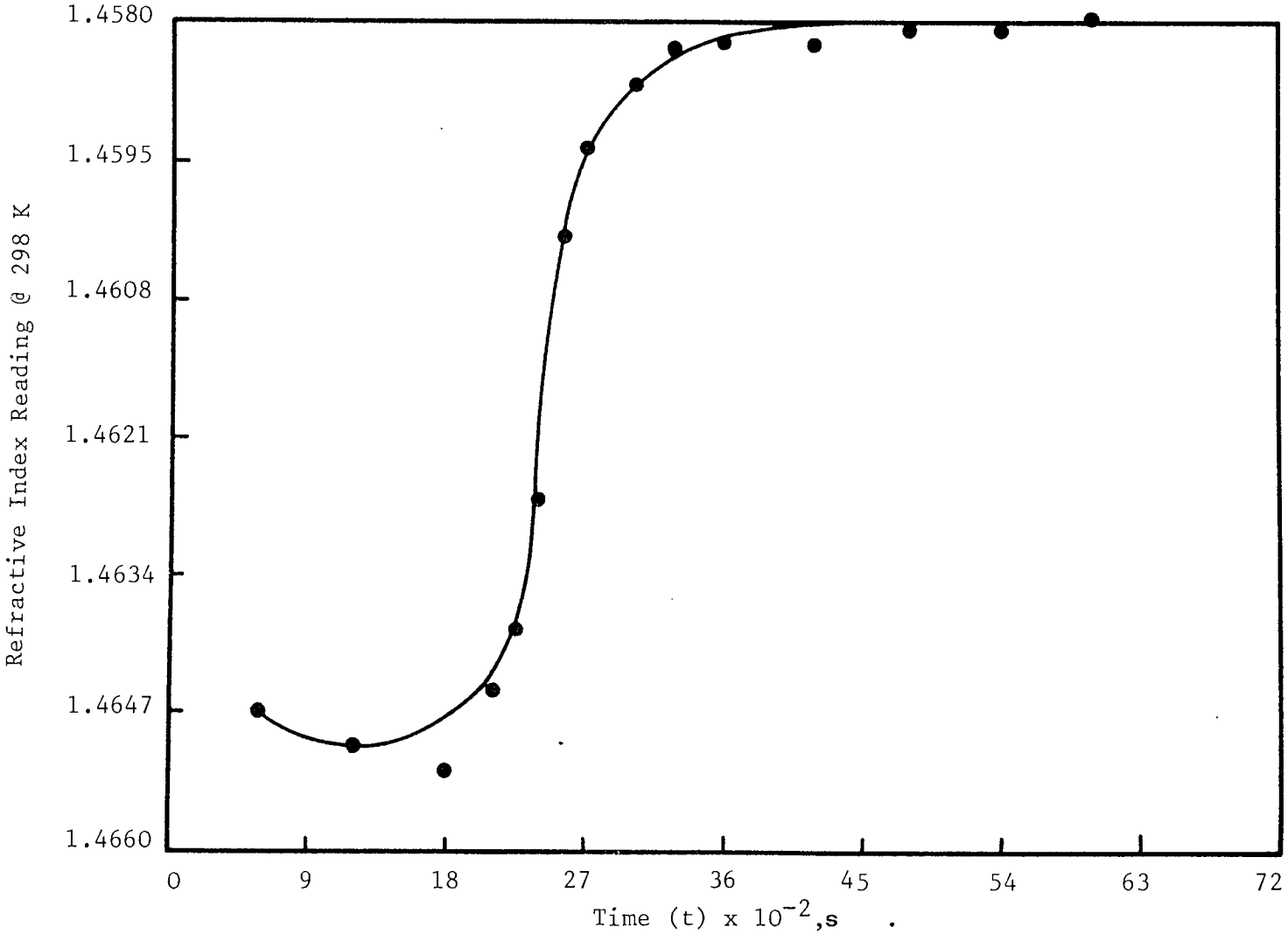

Fig. 9.14 Effect of temperature on the breakthrough curves of n-paraffins adsorption from HK by zeolite type-5A at a feed flowrate of 33.33×10^{-9} m^3/s , and a pellet particle size of (1.0-2.0) $\times 10^{-3}$ m .

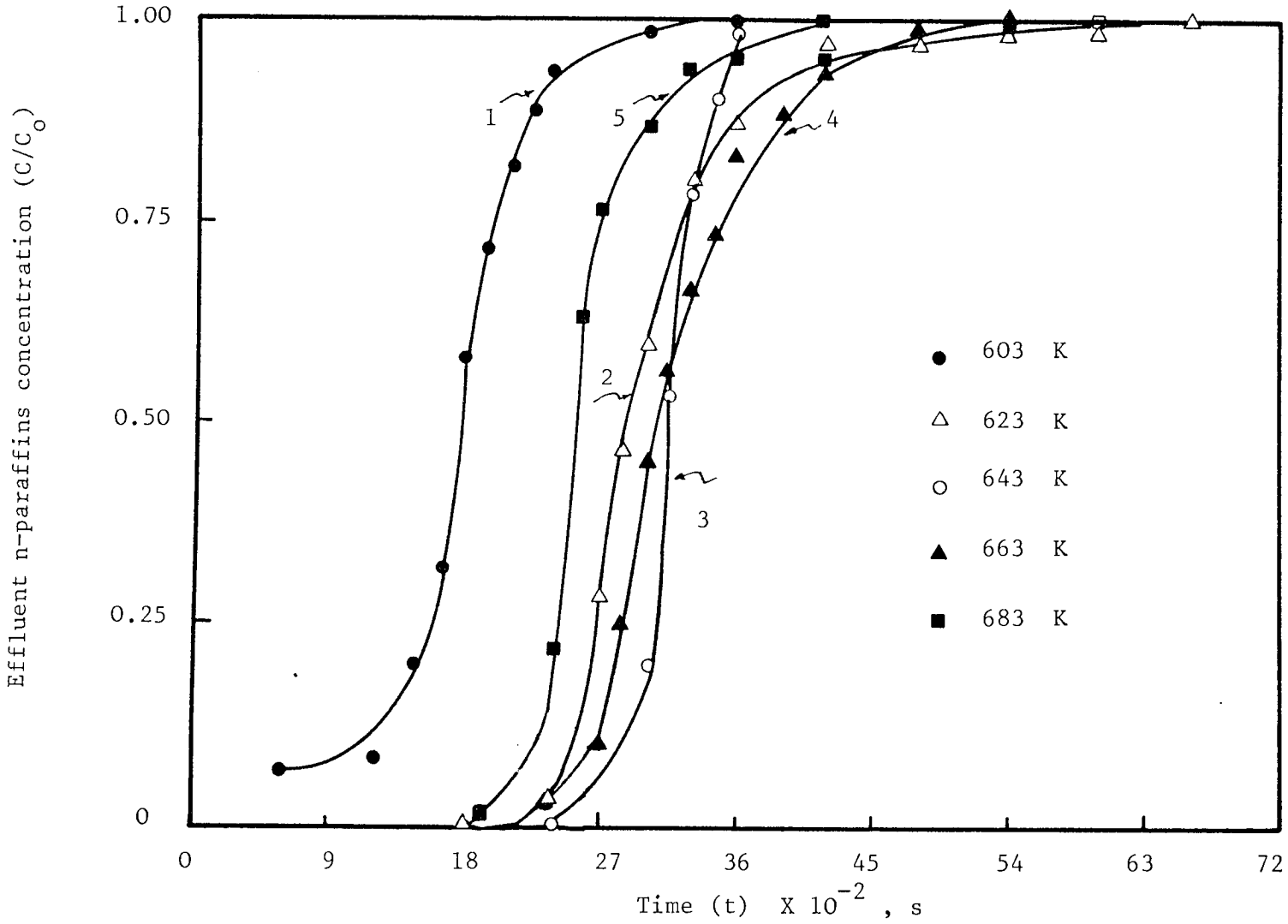

from the beginning of the adsorption process while the exhaustion time is reached faster in the case of 623 K by about 330 s. Table 9.2 shows the variation of the exhaustion and the BT-times with the adsorption temperatures.

The third variable parameter investigated was the particle size of zeolite. The breakthrough curves of adsorption of n-paraffins from HK at different particle sizes of zeolite type-5A are shown in Fig. (9.15) through Fig. (9.18). The particle sizes studied were pellets of diameter $<0.5 \times 10^{-3}$, $0.5 - 1.0 \times 10^{-3}$, $1.0-2.0 \times 10^{-3}$ and $2.0 - 3.0 \times 10^{-3}$ m while the adsorption temperature and the feed flowrate were fixed at 643 K and 33.33×10^{-9} m^3/s respectively. The experimental data of these BT-curves are presented in Table (11) through (14) of Appendix (A). Figure (9.19) shows the effect of different zeolite particle sizes on the adsorption of n-paraffins from HK in the form of BT-curves plotted as C/C_o vs. time. Curves 3 and 4 of Fig. (9.19) show that the BT-time reached by using particle sizes of $0.5 - 1.0 \times 10^{-3}$ and $<0.5 \times 10^{-3}$ m is about the same (i.e., 1590 and 1650 s respectively), but in the same time the n-paraffin content of the first fraction collected from the effluent of the adsorption process is different where the concentration of n-paraffins are 3.44 wt% and 7.5 wt% respectively. The saturation or the exhaustion points on the BT-curves of Fig. (9.19) are achieved at a time period of 2670, 2850, 3720 and 3480 s for particle sizes of $<0.5 \times 10^{-3}$, $(0.5 - 1.0) \times 10^{-3}$, $(1.0 - 2.0) \times 10^{-3}$ and $(2.0 - 3.0) \times 10^{-3}$ m respectively. The variation of zeolite particle sizes with the exhaustion and the

Table 9.2 Variation of the exhaustion and the BT-times with the adsorption temperatures *

Adsorption Temp.(K)	$\theta_E \times 10^{-2}$ (s)	$\theta_B \times 10^{-2}$ (s)	f
603	24.60	13.50	0.4206
623	39.00	20.40	0.4242
643	37.20	27.00	0.5015
663	42.30	20.40	0.4347
683	33.90	18.60	0.3979

* Conditions:

- Feed Flow-rate = 33.33×10^{-9} m^3/s
- n-Paraffins Conc. in the HK = 18.75 wt%
- Length of the Packed-Column = 0.650 m
- Particle Size of Zeolite = $1.0 - 2.0 \times 10^{-3}$m

Fig. 9.15 Breakthrough curve of adsorption of n-paraffins from HK by zeolite type-5A at a pellet particle size of (2.0 - 3.0) x 10^{-3} m, a temperature of 643 K, and a feed flowrate of 33.33 x 10^{-9} m^3/s .

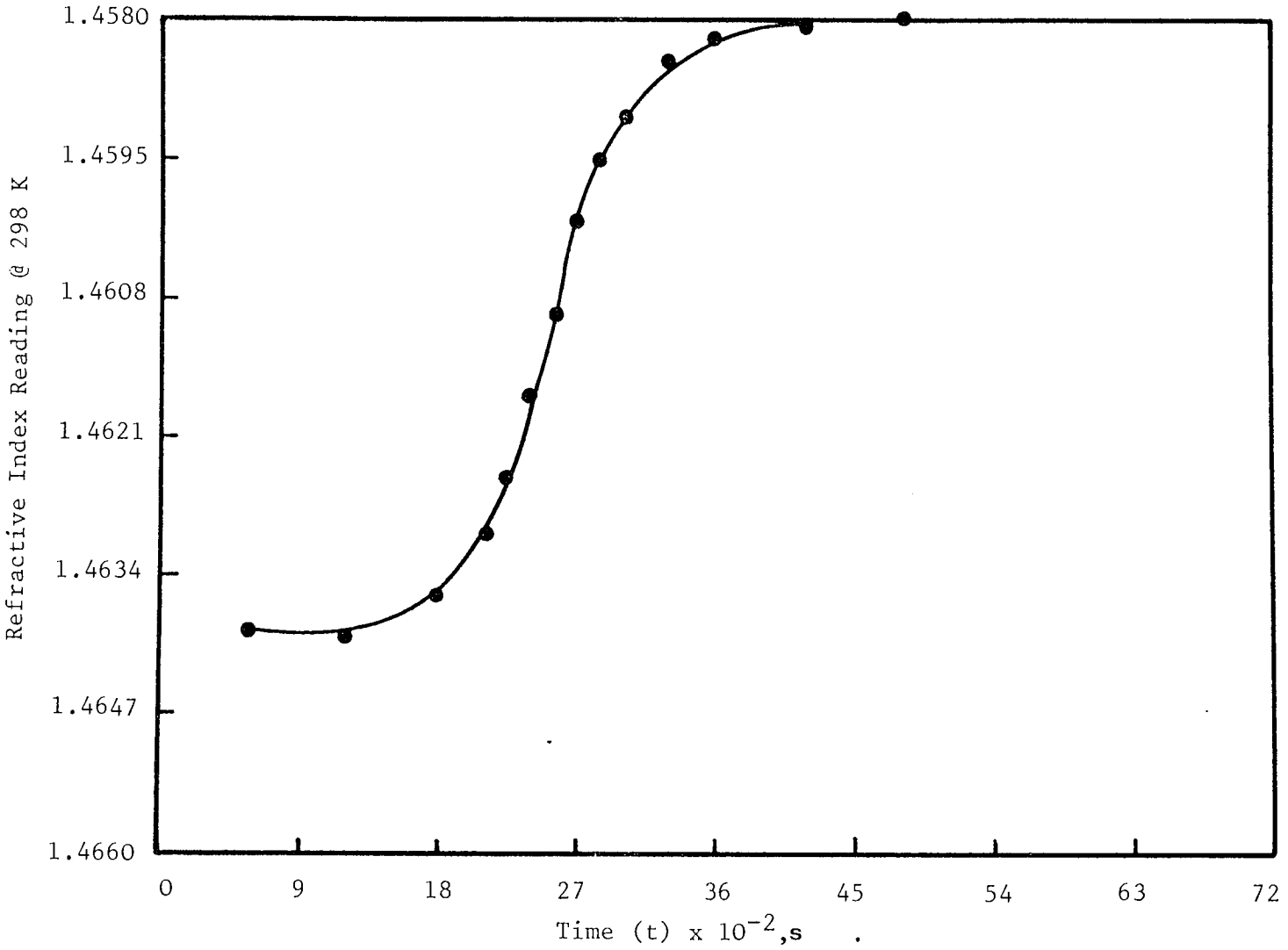

Fig. 9.16 Breakthrough curve of adsorption of n-paraffins from HK by zeolite type-5A at a temperature of 643 K, a feed flowrate of 33.33×10^{-9} m^3/s , and a pellet particle size of $(0.5 - 1.0) \times 10^{-3}$ m.

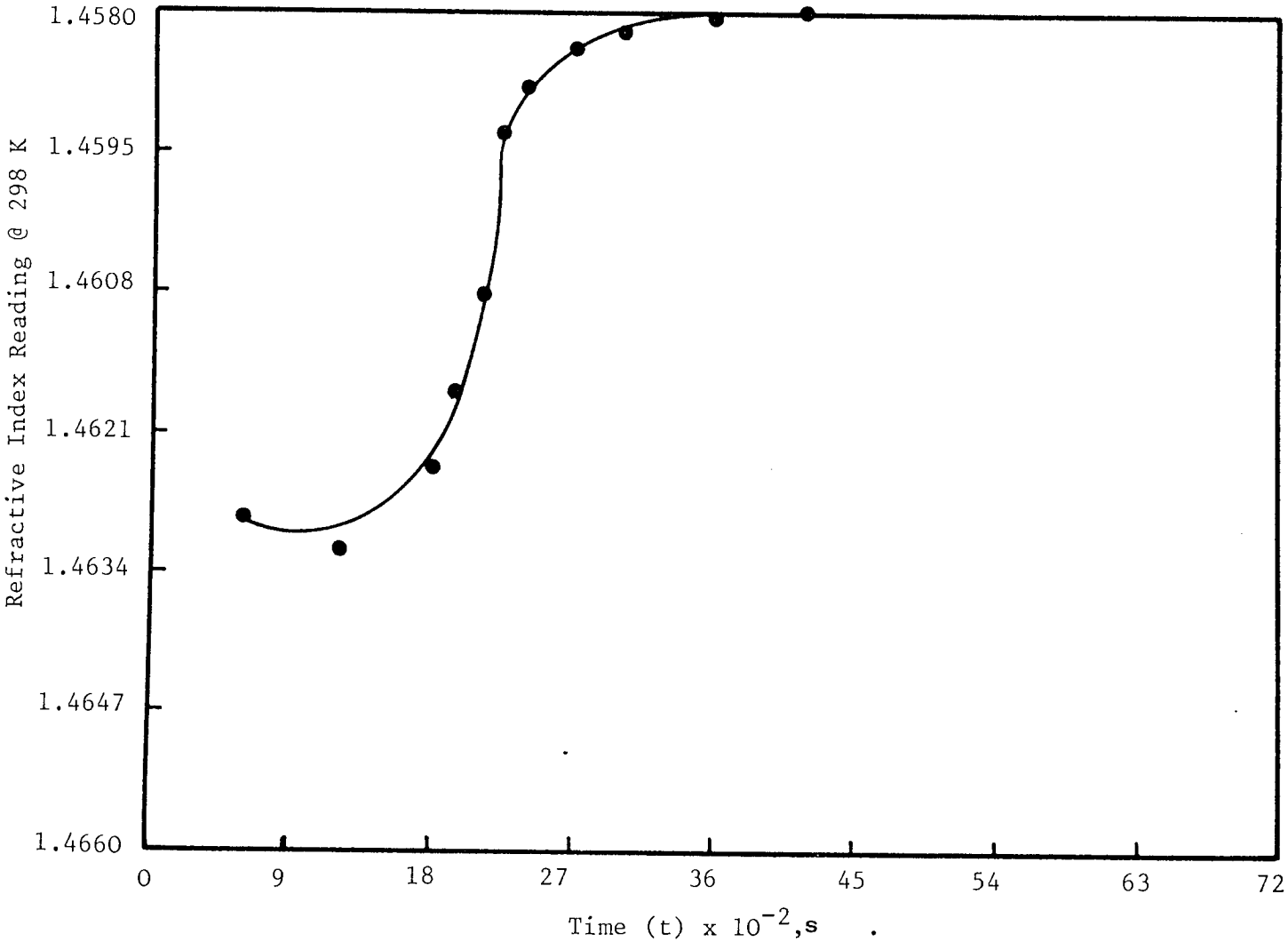

Fig. 9.17 Breakthrough curve of adsorption of n-paraffins from HK by zeolite type-5A at a feed flowrate of 33.33×10^{-9} m^3/s a temperature of 643 K, and a pellet particle size of $(1.0-2.0) \times 10^{-3}$ m .

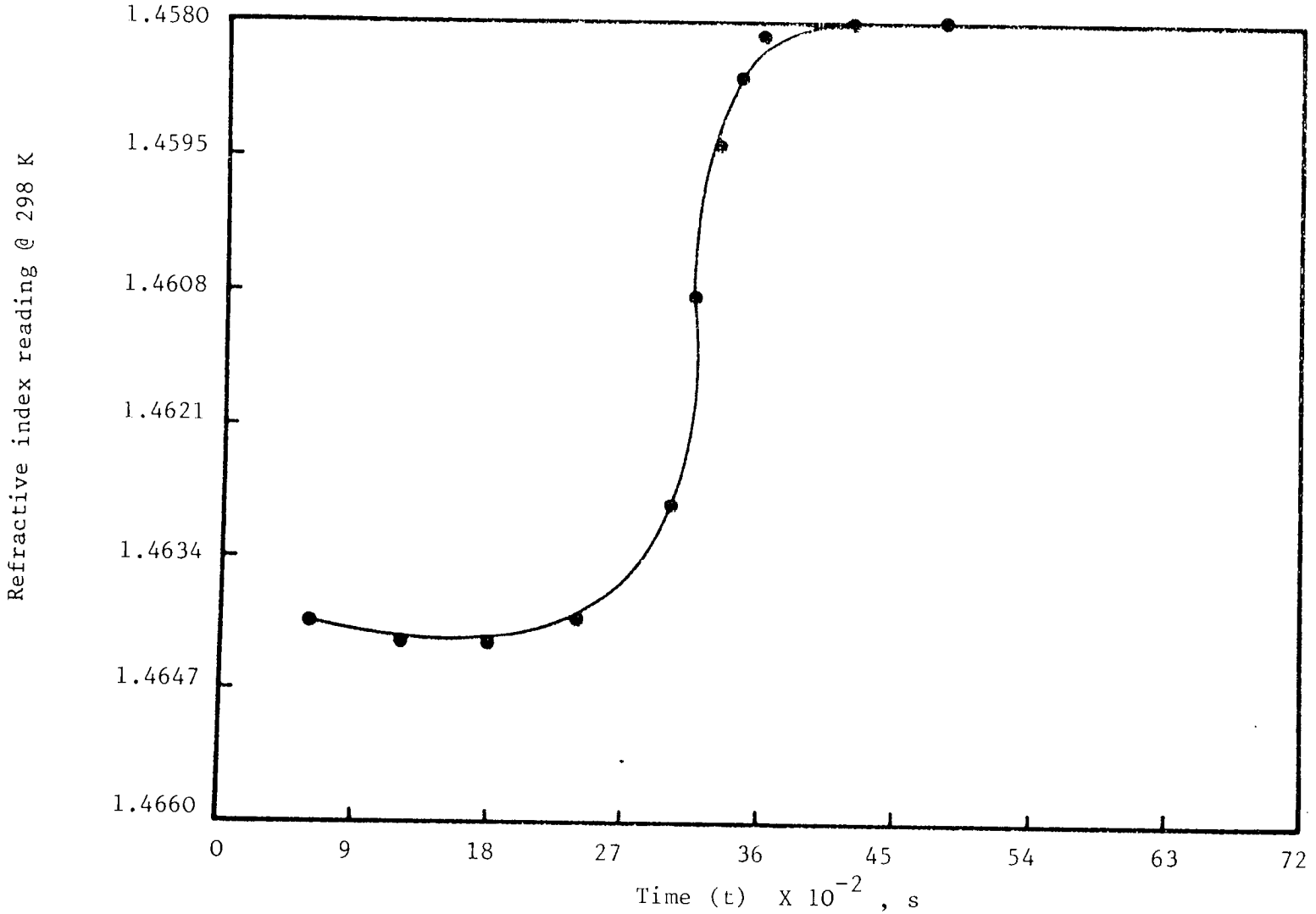

Fig. 9.18 Breakthrough curve of adsorption of n-paraffins from HK by zeolite type-5A at a temperature of 643 K, a feed flowrate of 33.33×10^{-9} m^3/s , and a pellet particle size of $(\prec 0.5) \times 10^{-3}$ m.

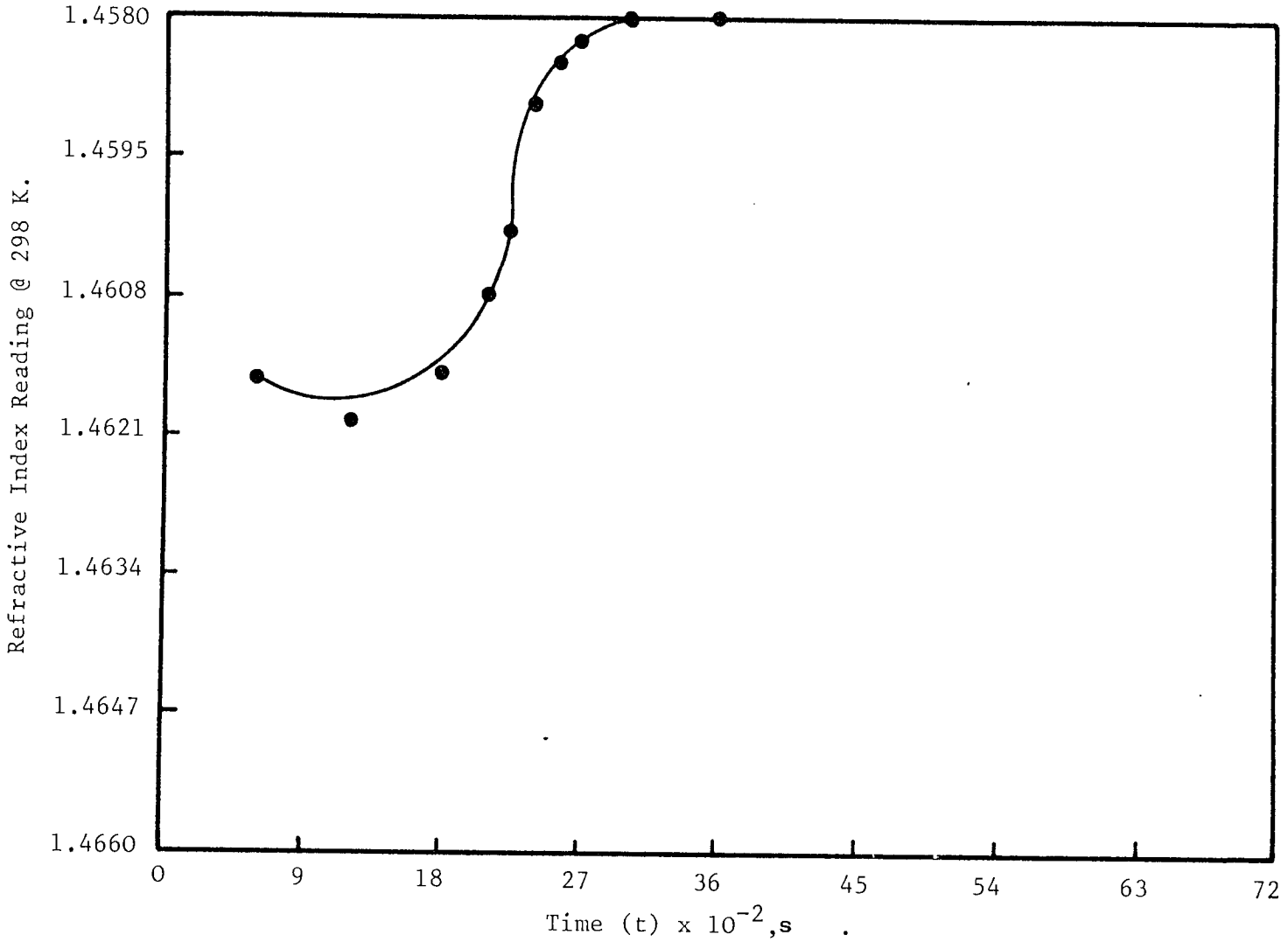

Fig. 9.19 Effect of pellet particle size on the breakthrough curves of n-paraffins adsorption from HK by zeolite type-5A, at a feed flowrate of 33.33 x 10^{-9} m^3/s , and a temperature of 643 K

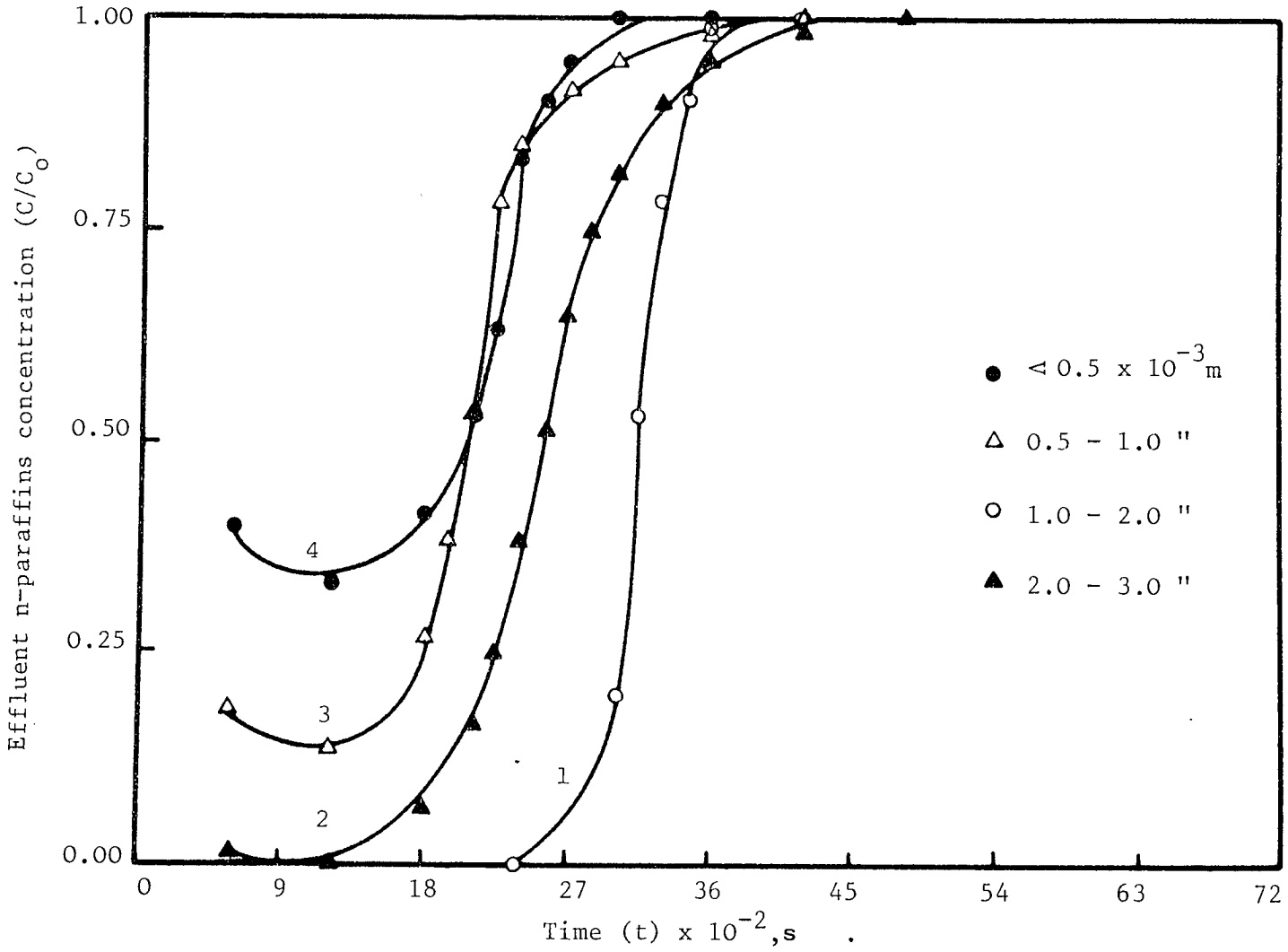

BT-times is presented in Table 9.3. It seems that there exists an optimum particle size of zeolite for the adsorption of n-paraffins from HK.

A study was made of the effect of the feed flowrate, the adsorption temperature and the zeolite particle size on the height of the mass transfer zone (HMTZ), and the equilibrium loading (Ad) or the dynamic capacity of zeolite. The HMTZ was estimated by analyzing the BT-curve of each run and using the following equation:

$$HMTZ = \frac{L\ (\theta_E - \theta_B)}{\theta_E - (1 - f)\ (\theta_E - \theta_B)} \qquad (9.1)$$

Equation (9.1) is based on a constant width, constant velocity adsorption zone and a zone formation time which is proportional to the fractional saturation of the adsorbent within the MTZ at the breakthrough point [74].

The dynamic capacity (Ad), namely the amount of n-paraffins adsorbed per unit weight of zeolite (usually estimated as grams of n-paraffins/100 gm of zeolite) was calculated using the following equation [80]:

$$Ad = \frac{\Sigma\ (C_o - C)\ m}{m_a} \qquad (9.2)$$

where C_o and C are the concentrations of n-paraffin before and after adsorption, m and m_a are the amount of solution and of adsorbent respectively. Tables (1) through (14) of Appendix (B) show the

Table 9.3 Calculation of the exhaustion and the breakthrough times with the zeolite particle sizes *

Particle Size x 10^3(m)	θ_E x 10^2 (s)	θ_B x 10^2 (s)	f
< 0.5	26.70	16.50	0.6857
0.5 - 1.0	28.50	15.90	0.4147
1.0 - 2.0	37.20	27.00	0.5015
2.0 - 3.0	34.80	18.00	0.4504

* Conditions:

- Feed Flow-rate = 33.33 x 10^{-9} m^3/s
- n-Paraffins Conc. in the HK = 18.75 wt%
- Length of the Packed-Column = 0.650 m
- Adsorption Temperature = 643 K

detailed calculation of the dynamic capacity of the zeolite at different feed flowrates, adsorption temperatures and zeolite particle sizes. The range of the parameters investigated was as mentioned previously, i.e. 16.66×10^{-9} - 50.0×10^{-9} m^3/s for feed flowrate, 603 - 683 K for adsorption temperature, and $<0.5 \times 10^{-3}$ - 3.0×10^{-3} m for zeolite particle size. As a general trend, the HMTZ was directly proportional to the feed flowrate, i.e. as the feed flowrate is increased the HMTZ increases also. For example, by increasing the flowrate from 33.33×10^{-9} to 44.44×10^{-9} m^3s the HMTZ is increased from 0.206 m to 0.315. The lowest value for HMTZ is calculated as 0.190 m at a flowrate of 22.22×10^{-9} m^3/s and the highest value was calculated as 0.315 m at a flowrate of 44.44×10^{-9} m^3/s. These lowest and highest values of HMTZ represents only 29.2% and 48.5% of the total bed height which was 0.65 m. This confirmed that the total height of zeolite bed was more than adequate for the experimental program. The dynamic capacity of zeolite varied significantly with the feed flowrate. For example, by increasing the flowrate from 16.66×10^{-9} to 33.33×10^{-9} m^3/s the dynamic capacity is increased from 7.513×10^{-2} to 9.653×10^{-2} kg n-paraffins per kg of zeolite while this capacity decreased to 7.676×10^{-2} kg n-paraffins per kg of zeolite with increased flowrate to 50.00×10^{-9} m^3/s. Table 9.4 shows the variation of HMTZ and Ad at different feed flowrates keeping the adsorption temperature and the particle size fixed at 643 K and $(1.0 - 2.0) \times 10^{-3}$ m respectively.

In Table 9.5, it can be seen that the dynamic capacity

Table 9.4 The effect of feed flow rate on the dynamic properties of adsorption of n-paraffins from HK by zeolite Type-5A *

Flow-rate 10^9x(m^3/s)	Height of MTZ (HMTZ) (m)	Effective Efficiency of the adsorbent column (γ) (%)	Dynamic Capacity of Zeolite (Ad) (10^2kg/kg) **
16.66	0.251	80.62	7.513
22.22	0.190	85.69	7.497
33.33	0.206	84.15	9.653
44.44	0.315	76.60	8.145
50.00	0.258	69.23	7.676

* Conditions:

- Adsorption Temperature = 643 K
- n-Paraffins Conc. in the HK = 18.75 wt%
- Length of the Packed-Column = 0.650 m
- Particle size of Zeolite = 1.0 - 2.0 x 10^{-3}m

** (10^2kg/kg) = 10^{-2}kg of n-Paraffins/kg of Zeolite Type-5A.

increases with increasing adsorption temperature upto a limit and then decreases with further increase of temperature. This indicates the existence of an optimum temperature. For example, the dynamic capacities calculated at the adsorption temperatures 603, 623 and 643 K are 6.617×10^{-2}, 8.269×10^{-2} and 9.653×10^{-2} kg n-paraffins/kg zeolite respectively, while this capacity is decreased to 7.772×10^{-2} kg n-paraffins/kg zeolite at a temperature of 663 K. The HMTZ estimated at different adsorption temperatures ranged from 0.397 m to 0.476 m, which represents 61 - 73% of the total bed height; an exception was noticed at an adsorption temperature of 643 K where the HMTZ was calculated to be only 0.206 m. Table 9.5 illustrates these variations at different adsorption temperatures. Similarly, in respect of the feed flowrate, the same behaviour of HMTZ and Ad was noticed at different zeolite particle sizes as shown in Table 9.6. The lowest value of dynamic capacity was calculated at a particle size of $(2.0 - 3.0) \times 10^{-3}$ m which was 6.199×10^{-2} kg n-paraffins/kg of zeolite while the highest value was calculated at a particle size of $(1.0 - 2.0) \times 10^{-3}$ m which was 9.653×10^{-2} kg n-paraffin/kg zeolite. The HMTZ seems to increase with increasing particle size. This is to be expected because the pore area per unit bulk volume has decreased; an exception was noticed at a particle size of $(1.0 - 2.0) \times 10^{-3}$ m where the value of HMTZ is 0.206 m. The HMTZ for zeolite particle sizes ranges between 0.282 - 0.427 m as calculated by analyzing the BT-curves and using Eq. 9.1.

The separation of n-paraffins from HK by selective adsorption

Table 9.5 The effect of temperature on the dynamic properties of adsorption of n-paraffins from HK by zeolite Type-5A *

Adsorption Temp. (K)	Height of MTZ (HMTZ) (m)	Effective Efficiency of the adsorbent column (γ) (%)	Dynamic Capacity of Zeolite (Ad) (10^2kg/kg) **
603	0.397	70.92	6.617
623	0.427	68.77	8.269
643	0.206	84.15	9.653
663	0.476	65.08	7.772
683	0.403	70.92	8.151

* Conditions:

- Feed Flow-rate = 33.33×10^{-9} m^3/s
- n-Paraffins Conc. in the HK = 18.75 wt%
- Length of the Packed-Column = 0.650 m
- Particle size of Zeolite = $1.0 - 2.0 \times 10^{-3}$m

** (10^2kg/kg) = 10^{-2}kg of n-Paraffins/kg of Zeolite Type-5A.

Table 9.6 The effect of pellet fraction-size on the dynamic properties of adsorption of n-paraffins from HK by zeolite Type-5A *

Pellet Particle Size 10^3 x (m)	Height of MTZ (HMTZ) (m)	Effective Efficiency of the adsorbent column (γ) (%)	Dynamic Capacity of Zeolite (Ad) (10^2kg/kg) **
< 0.5	0.282	76.46	7.449
0.5 - 1.0	0.388	71.54	8.284
1.0 - 2.0	0.206	84.15	9.653
2.0 - 3.0	0.427	68.15	6.199

* Conditions:

- Feed Flow-rate = 33.33×10^{-9} m^3/s
- n-Paraffins Conc. in the HK = 18.75 wt%
- Length of the Packed-Column = 0.650 m
- Adsorption Temperature = 643 K

** (10^2kg/kg) = 10^{-2}kg of n-Paraffins/kg of Zeolite Type-5A.

on zeolite type-5A was optimized by varying one of the three main parameters mentioned previously while keeping the other two constants, and then estimating the dynamic properties for each run from the individual BT-curves. These dynamic properties are the HMTZ, the effective efficiency of the adsorbent column and the dynamic capacity of zeolite. The optimum operating condition is achieved at the lowest value of HMTZ, the highest value of effective efficiency of the adsorbent column and the highest value of the dyn amic capacity (Ad) as illustrated in Fig. (9.20) through (9.22), but usually Ad is the most determining factor. The effective efficiency of the adsorbent column (γ) can be calculated from the following two equations:

$$LUB = L (\theta_S - \theta_B) / \theta_S \qquad (6.15)$$

$$\gamma = (L - LUB) / L \qquad (9.3)$$

where L is the total height of the adsorbent column. The optimum operating conditions are determined by the values inserted in equations 9.1, 9.2 and 9.3. Inspection of these equations show that optimization is dependent on the value of f in combination with the value of (θ_E - θ_B). Examination of Table 9.3 shows that while f is the lowest, its advantage is offset by the largest value of (Θ_E - Θ_B). Consequently the zeolite with the particle size (1.0 - 2.0) x 10^{-3} m emphasizing that the optimum is a combination of more than one factor. Table 9.4 through 9.6 list the dynamic properties for the adsorption of n-paraffins from HK at different feed flowrates, adsorption temperatures and zeolite particle size respectively. The optimum feed flowrate, as shown by Fig. (9.20), is at 33.33 x 10^{-9} m^3/s, while the optimum adsorption temperature is at 643 K as shown

Fig. 9.20 The effect of feed flowrate on the dynamic properties of adsorption of n-paraffins from HK by zeolite type-5A.

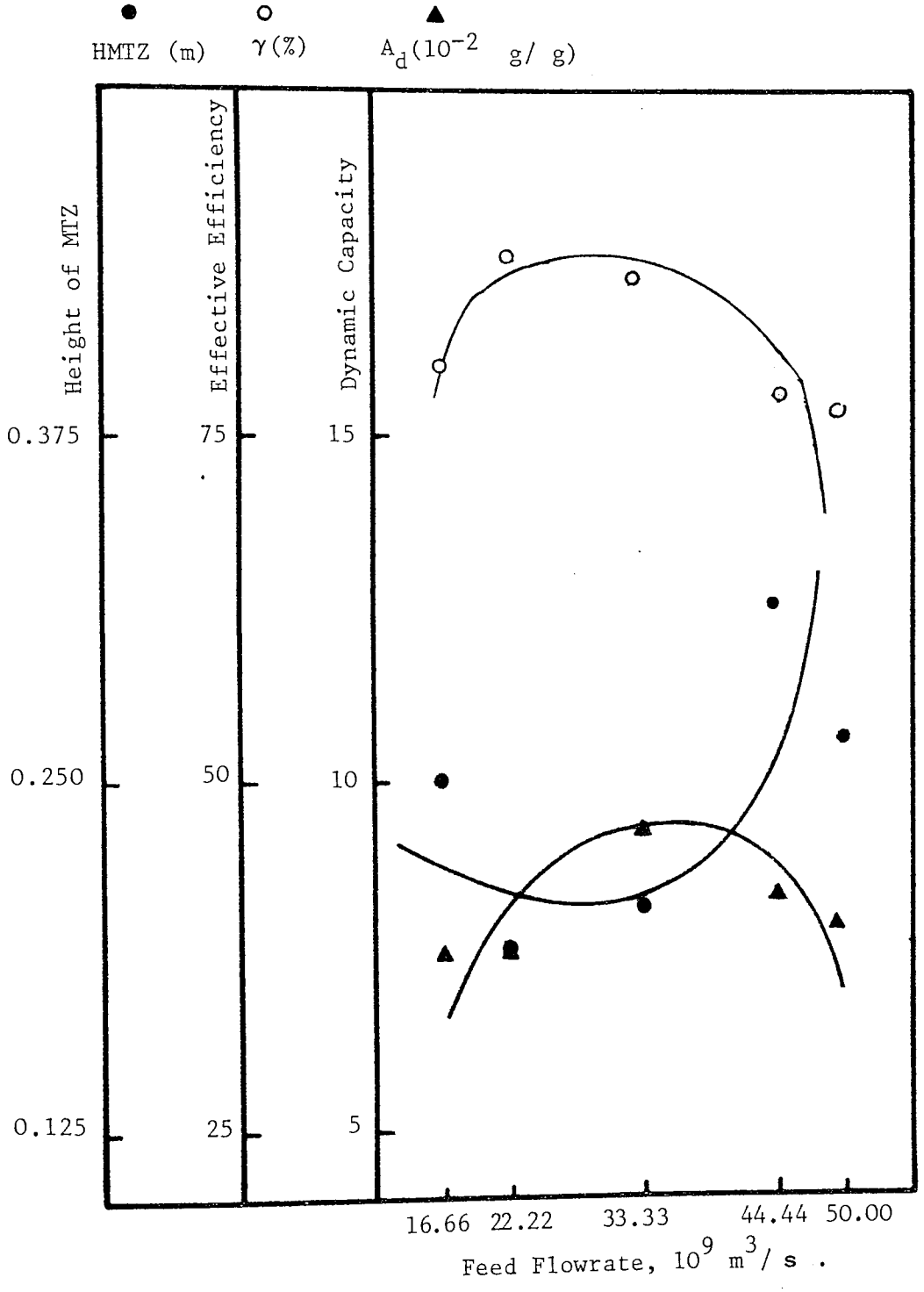

Fig. 9.21 The effect of temperature on the dynamic properties of adsorption of n-paraffins from HK by zeolite type-5A.

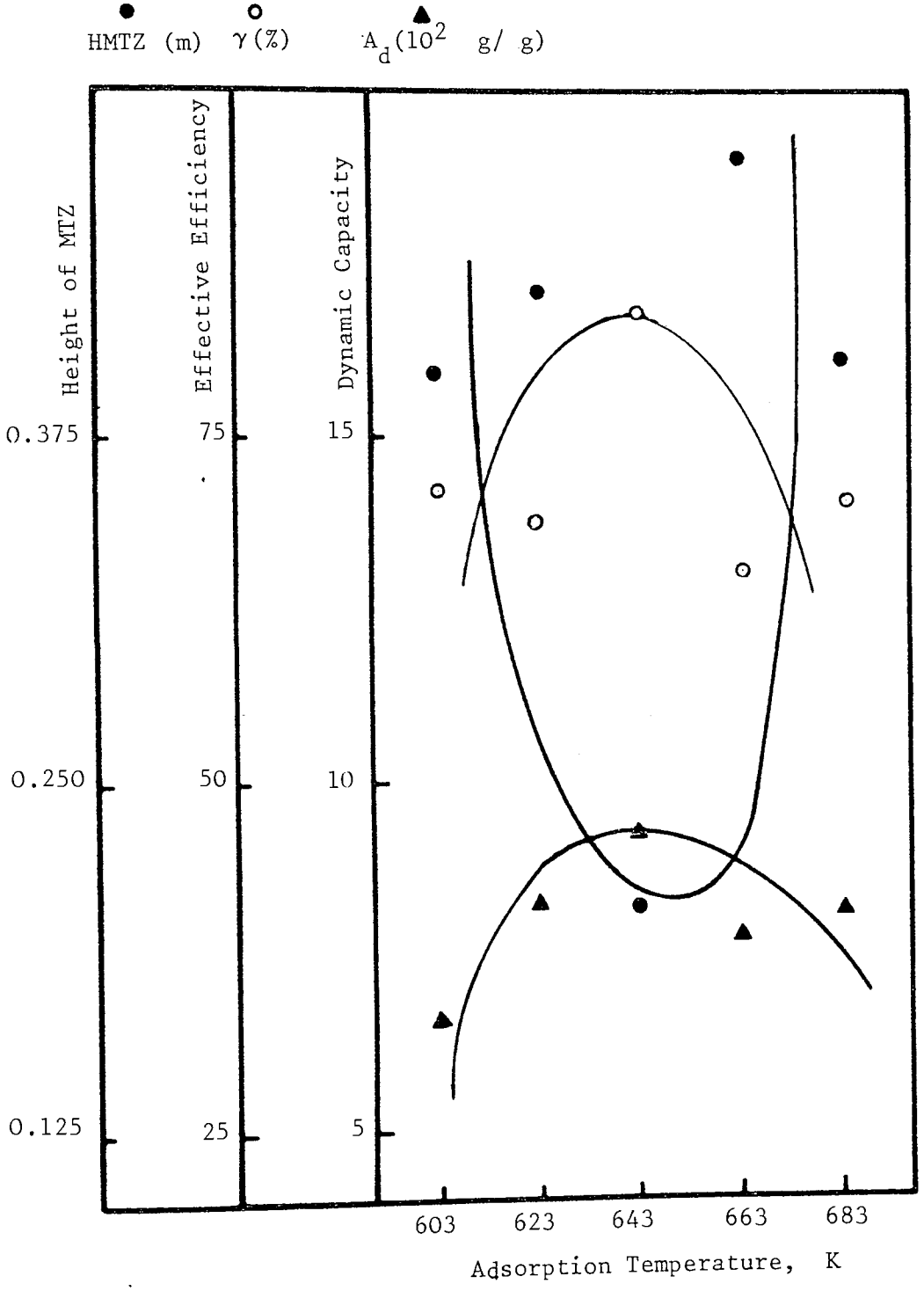

Fig. 9.22 The effect of pellet particle-size on the dynamic properties of adsorption of n-paraffins from HK by zeolite type-5A.

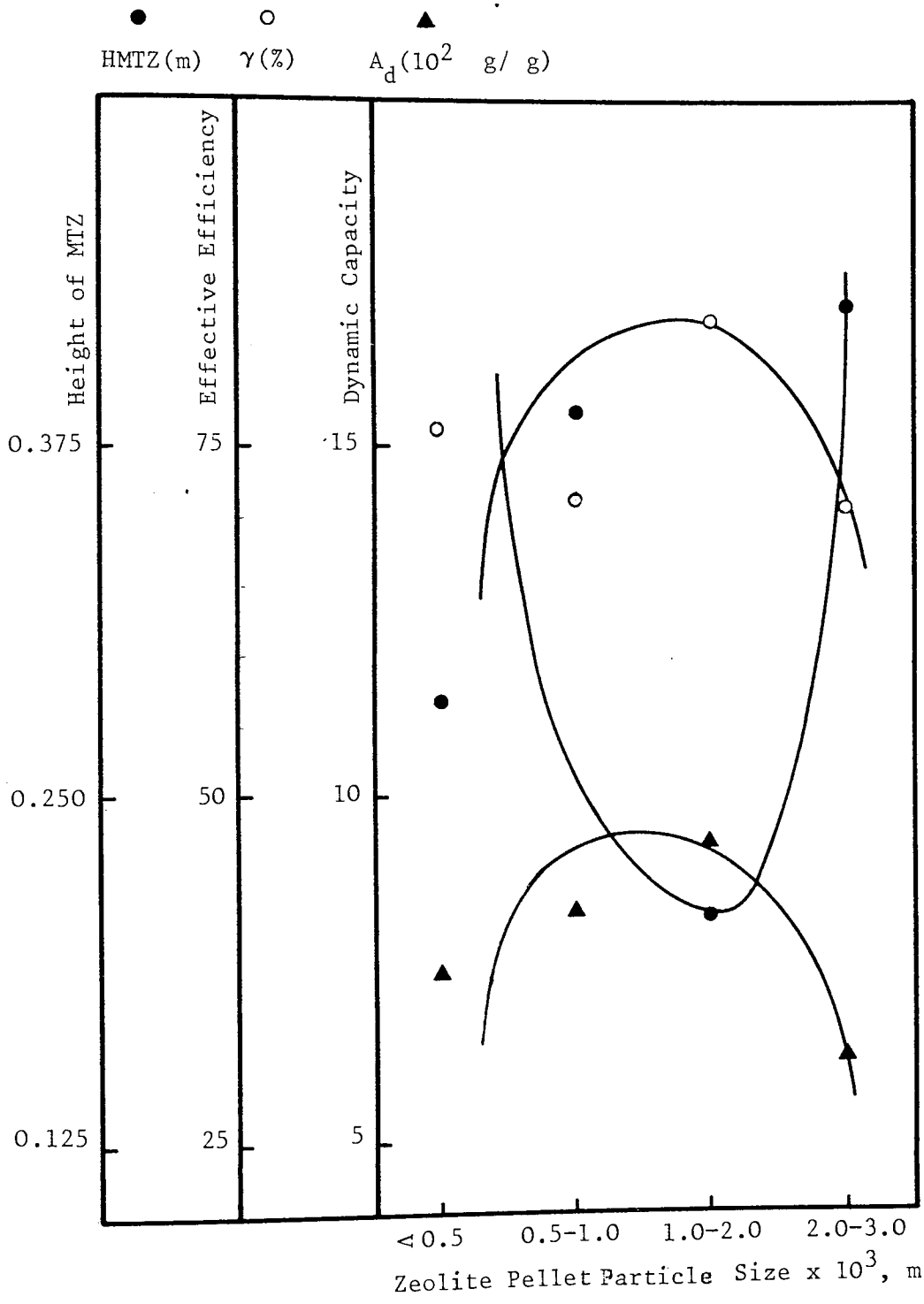

in Fig. (9.21). Figure (9.22) shows clearly that the particle size of (1.0 - 2.0) x 10^{-3} m is the optimum zeolite particle size for the adsorption separation of n-paraffins from Hk using zeolite type-5A.

The effect of nitrogen flowrate on the HMTZ and the dynamic capacity Ad was studied under the optimum operating conditions, i.e. at a feed flowrate of 33.33 x 10^{-9} m^3/s, an adsorption temperature of 643 K and zeolite particle size of (1.0 - 2.0) x 10^{-3} m. The nitrogen flowrate was controlled at 13.3 x 10^{-7} m^3/s, the effect of which on the BT-curve was compared with that of a nitrogen at a flowrate of 6.7 x 10^{-7} m^3/s at the same operating conditions. The BT-curves of adsorption of n-paraffins from HK at the two different nitrogen flowrates are shown in Fig. (9.23) and Table 9.7 where comparison between the HMTZ and the dynamic capacity at the two different nitrogen flowrates are presented. The BT-curves in Fig. (9.23) show that the BT-point is reached faster in the case of a nitrogen flowrate of 13.3 x 10^{-7} m^3/s than at 6.7 x 10^{-7} m^3/s which was expected. The two BT-curves are in a prallel S-shaped form. The n-paraffins content of the fractions collected from the adsorption process effluent using a nitrogen flowrate of 13.3 x 10^{-7} m^3/s is higher than that at a flowrate of 6.7 x 10^{-7} m^3/s at a certain time which affects in turn the dynamic capacity of zeolite. For example, by increasing the nitrogen flowrate from 6.7 x 10^{-7} to 13.3 x 10^{-7} m^3/s, the dynamic capacity of zeolite was reduced by 3.6% from 9.653 x 10^{-2} to 9.305 x 10^{-2} x 10^{-2} kg n-paraffin per kg of zeolite while the HMTZ was increased by about 0.079 m from 0.206 m to 0.285 m respectively. The experimental data of the BT-curve

Table 9.7 The effect of nitrogen flowrate on the dynamic properties of adsorption of n-paraffins from HK by zeolite Type-5A *

Nitrogen Flowrate 10^7 x (m^3/s)	6.7	13.3
Mass Transfer Zone Height (m)	0.206	0.285
Effective Efficiency of Adsorbent Column (%)	84.07	70.92
Dynamic Capacity of Zeolite x 10^2 (kg/kg)**	9.653	9.305
Diffusion Coefficient x 10^{10} (m^2/s)	1.387	1.067
Superficial Velocity (m/s)	0.34	0.41
($\Theta_E - \Theta_B$) (s)	1020	1305

* Conditions:

- Adsorption Temperature = 643 K
- n-paraffins conc. in the HK = 18.75 wt%
- Length of the packed-column = 0.650 m
- Particle size of zeolite = 1.0 - 2.0 x 10^{-3}m

** 10^{-2}kg of n-paraffins adsorbed/kg of zeolite

Fig. 9.23 Effect of nitrogen flowrate on the breakthrough curve of adsorption of n-paraffins from HK by zeolite type-5A, at a feed flowrate of 33.33×10^{-9} m^3/s, a temperature of 643 K, and a pellet particle size of $(1.0 - 2.0) \times 10^{-3}$ m.

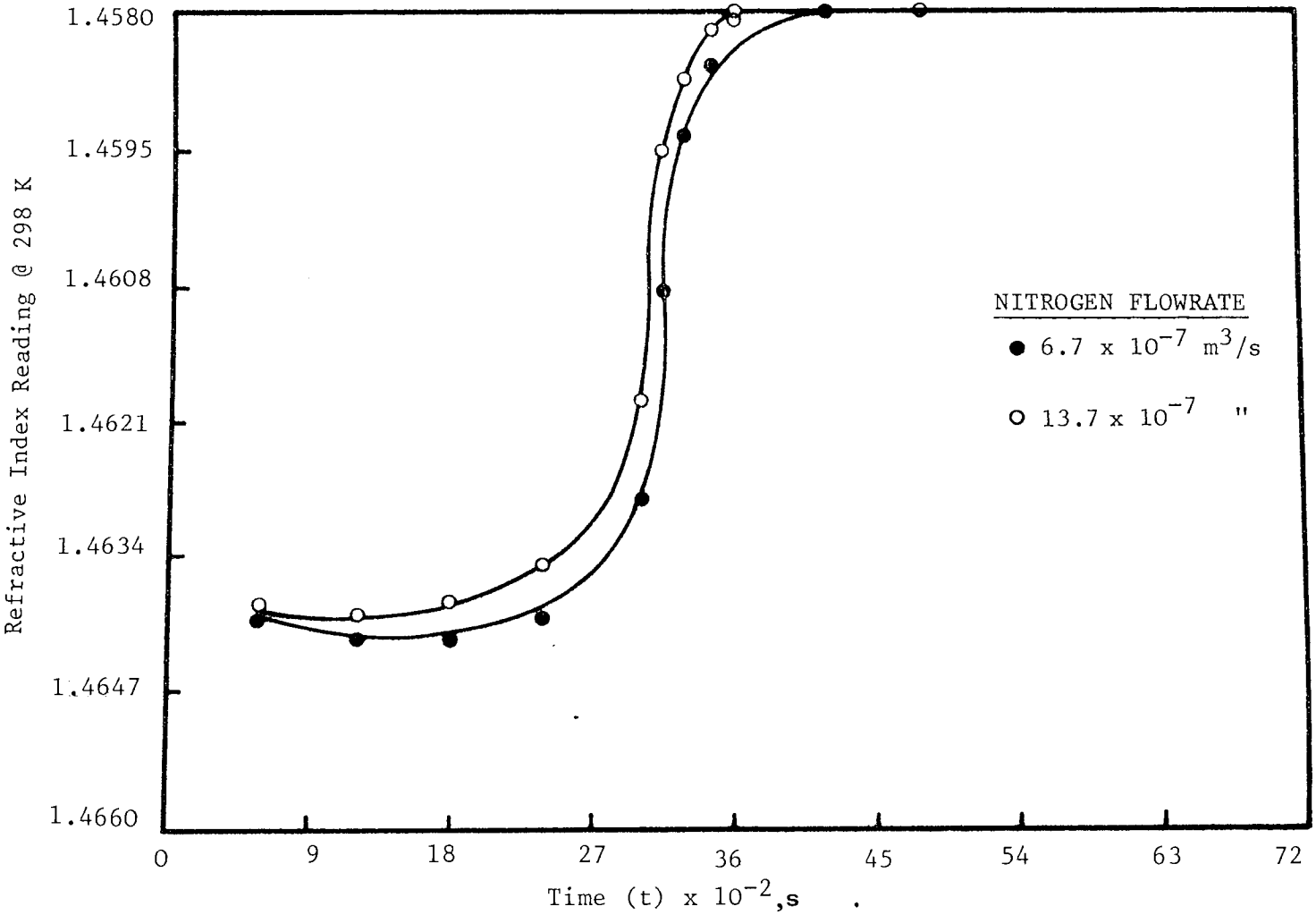

and the dynamic capacity calculation of adsorption of n-paraffins from HK at a nitrogen flowrate of 13.3 x 10^{-7} m^3/s is presented in Table (15) of Appendix (A) and Table (15) of Appendix (B) respectively.

The local-equilibrium theory (81) has been utilized to determine the adsorption isotherm of n-paraffins from HK on zeolite type-5A. The method of characteristics, as illustrated by Eq. (6.25), has been used to establish the equilibrium adsorption curve as shown in Fig. (9.24). This figure was derived from the adsorption breakthrough data at a feed flowrate of 33.33 x 10^{-9} m^3/s, a temperature of 643 K, and a pellet particle size of (1.0 - 2.0) x 10^{-3} m by abstracting the equilibrium amount adsorbed of n-paraffins (q^*) as a function of concentration (C). The detailed analysis of the calculations of the values of q^* and C is presented in Appendix (C). A regression program (see Appendix G) was used to predict the equilibrium adsorption curve. The results were in a very good agreement with the experimental curve.

The experimental equilibria of adsorption shown in Fig. 9.24 suggests that the isotherm is of Type I, i.e. of the Langmuir Type (81, 82). This means that Fig. 9.24 is a representative of the following equation:

$$q^* = q_m \frac{K_A C}{1 + K_A C} \qquad (9.4)$$

where q_m represents the capacity of the adsorbent, corresponding to complete coverage of the surface. Testing the experimental

FIG.9.24 Equilibrium adsorption of n-paraffins from HK on zeolite type-5A as derived from adsorption breakthrough data and the BET-equation .

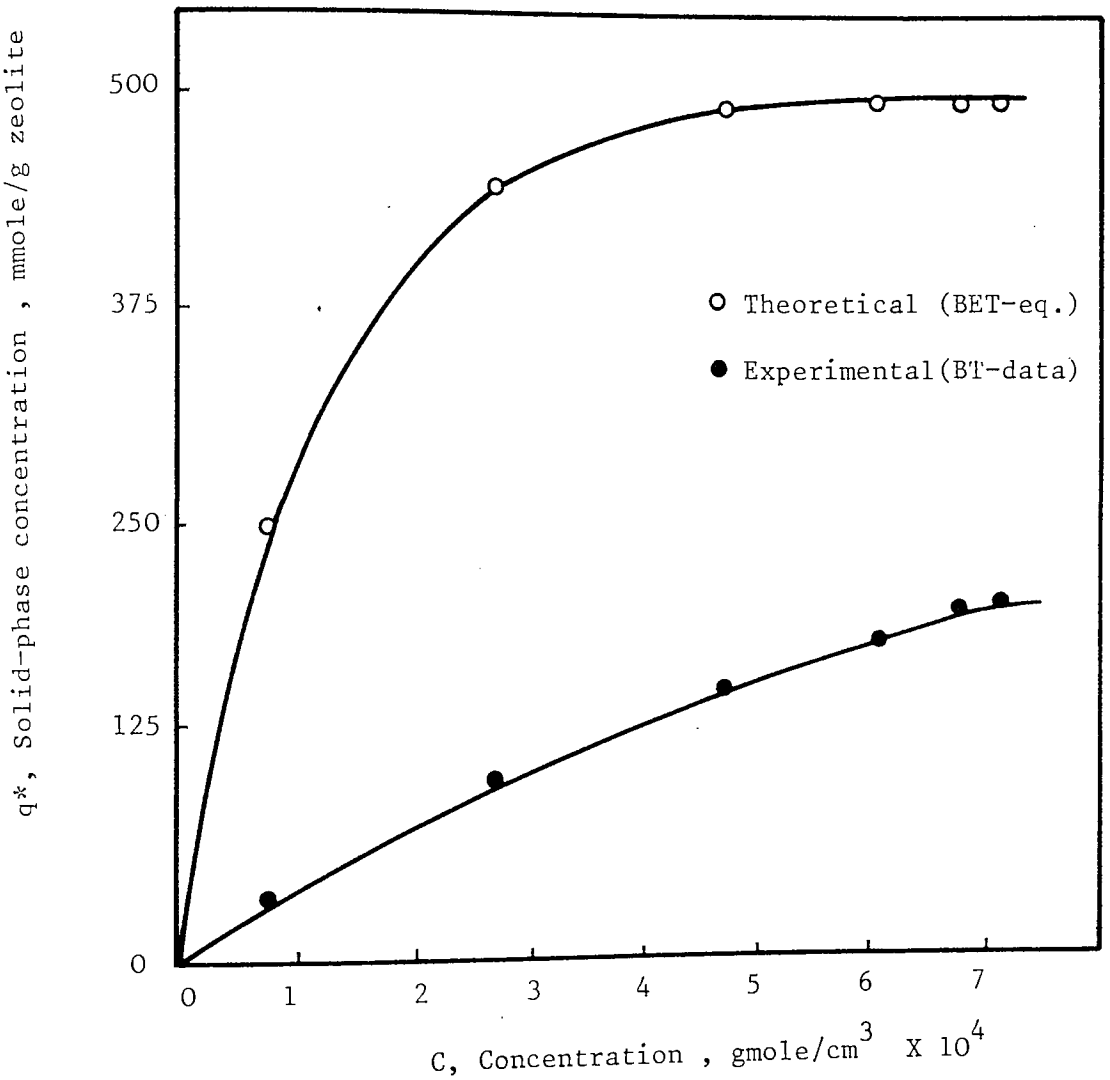

equilibria with the Langmuir equation (Eq. 9.4), the value of K_A was found to vary from 3000 - 75000 $cm^3/gmole$. This proves that the Langmuir equation is not applicable and hence suggesting the occurrence of multilayer adsorption.

The BET-equation (Eq. 9.5) suggested by Brunauer et al. (83) seems to be a suitable form for predicting the equilibrium isotherm of n-paraffins adsorption on zeolite Type-5A as shown in Fig. 9.24.

$$q = q_m \frac{\beta (F-1) X (1-X)}{1 + (\beta F - 1) X} \qquad (9.5)$$

The difference between the experimental and the predicted equilibrium isothermsshown in Fig. 9.24 can be attributed to the fact that the BET-equation is usually used for binary systems (83) whereas the system used in this study is complex, and consists of multicomponent n-paraffins. The equilibrium isotherm is usually obtained using batch system while in this study it was derived from the breakthrough data.

The detailed calculations of the equilibrium isotherm using the BET-equation is presented in Appendix (F).

The effective diffusion coefficients for n-paraffins adsorption on zeolite Type-5A were investigated in this study at different feed flowrates, adsorption temperatures and zeolite particle sizes. The formula of Barrer and Brooke (Eq. 9.6) (80) was used to calculate the effective diffusion coefficient. This formula is expressed as:

$$De = \left(\frac{\pi}{4\tau}\right)\left(\frac{V}{S_{ex}}\right)^2\left(\frac{Am}{Ad}\right)^2 \qquad (9.6)$$

where $\left(S_{ex}/V\right)$, the ratio of the external surface of a granule to its total volume, was taken as 20 cm^2/cm^3;

$$De^{-1} = \frac{6\tau(1-\epsilon)}{r^2} - \frac{12\,A_m}{C_o V r} \qquad (9.7)$$

The results were compared with those predicted by Eltekov's equation (Eq. 9.7). The detailed calculation of the diffusion coefficients using both equations, are shown in Tables (1) to (3) of Appendix (D) and Appendix E.3 respectively. The effect of feed flowrate, adsorption temperature and particle size on the diffusion coefficient as predicted by Barrer-Brooke's equation is shown in Fig. (9.25). Tables 9.8 through Table 9.10 present a comparison between the diffusion coefficients as predicted by Barr er-Brooke's and Eltekov's equations at different feed flowrates, adsorption temperatures and zeolite particle sizes respectively. The general trend for the diffusion coefficients are noticed to increase with increasing the flowrate. Table 9.8 shows that by increasing the feed flowrate from 16.66 x 10^{-9} to 33.33 x 10^{-9} m^3/s the diffusion coefficient is increased from 0.397 x 10^{-10} to 1.387 x 10^{-10} m^2/s. At a feed flowrate of 44.44 x 10^{-9} m^3/s, the diffusion coefficient is reduced to 1.0 x 10^{-10} m^2/s then increased to 1.8 x 10^{-10} m^2/s at a feed flowrate of 50 x 10^{-9} m^3/s. The diffusion coefficients as predicted by Eltekov's equation (Eq. 9.7) for the same flowrate are noticed to be about 1.5 times those predicted by Barrer-Brooke's equation (Eq. 9.6). For example, at a feed flowrate of 16.66 x 10^{-9} m^3/s, the diffusion coefficients are 0.397 x 10^{-10} and 0.517 x 10^{-10}

Table 9.8 Variation of the diffusion coefficient of n-paraffins adsorption from HK on zeolite Type-5A at different flow rates, a temperature of 643 K, and a pellet particle size of (1.0-2.0) x 10^{-3}m.

Flowrate x 10^9 (m^3/s)	De x 10^{10} (m^2/s) {Eq. 9.6}	De x 10^{10} (m^2/s) {Eq. 9.7}
16.66	0.397	0.517
22.22	1.008	1.096
33.33	1.387	1.612
44.44	1.000	1.337
50.00	1.800	2.492

Table 9.9 Variation of the diffusion coefficient of n-paraffins adsorption from HK on zeolite Type-5A at different temperatures, a feed flowrate of 33.33 x $10^{-9}m^3/s$, and a particle size of (1.0-2.0) x $10^{-3}m$.

Adsorption Temperature (K)	De x 10^{10} (m^2/s) {Eq. 9.6)	De x 10^{10} (m^2/s) {Eq. 9.7}
603	0.976	1.482
623	0.549	0.884
643	1.387	1.612
663	0.417	0.751
683	0.728	1.075

Table 9.10 Variation of the diffusion coefficient of n-paraffins adsorption from HK on zeolite Type-5A at different pellet particle size, a temperature of 643 K, and a feed flowrate of $33.33 \times 10^{-9} m^3/s$.

Zeolite Pellet Particle Size $\times 10^3$ (m)	De $\times 10^{10}$ (m^2/s) {Eq. 9.6}	De $\times 10^{10}$ (m^2/s) {Eq. 9.7}
< 0.5	0.949	0.179
0.5 - 1.0	1.111	0.326
1.0 - 2.0	1.387	1.612
2.0 - 3.0	0.579	2.720

m^2/s as predicted by Barrer-Brooke's and Eltekov's equations respectively. At the same adsorption temperature the diffusion coefficients, as predicted by Eltekov's equation, range from 1.2 - 1.8 times those predicted by Barrer-Brooke's equation. The situation is different at the different particle sizes of zeolite as shown in Table 9.10. For example, by using Barrer-Brooke's equation, the diffusion coefficients are shown to increase with increasing the particle size, except that at a particle size of (2.0 - 3.0) x 10^{-3} m, the value is reduced to 0.579 x 10^{-10} m^2/s. On the other hand, using Eltekov's equation, the diffusion coefficients are noticed to be directly proportional to the particle size of zeolite. Figure (9.25) shows that there exists an optimum value of diffusion coefficient, the conditions at which are shown to be the optimum operating conditions for adsorption separation of n-paraffins. In other words, the optimum value for the diffusion coefficient of n-paraffins on zeolite type-5A ranges between 1.387 - 1.612 x 10^{-10} m^2/s at a feed flowrate of 33.33 x 10^{-9} m^3/s, a temperature of 643 K and a particle size of (1.0 - 2.0) x 10^{-3} m. It is noteworthy to say that Eltekov's equation (Eq. 9.7) includes a parameter for the vapor mixture velocity which is in reality the superficial velocity. The detailed calculations of the superficial velocities at different operating conditions are shown in Tables (4) through (6) of Appendix (D).

9.2 Multicycle Adsorption Processes

A study was made of the effect of repeated adsorption cycles

Fig. 9.25 Effect of the feed-flowrate , adsorption temperature and zeolite pellet particle size on the diffusion coefficient of n-paraffins adsorption from HK on zeolite type-5A .

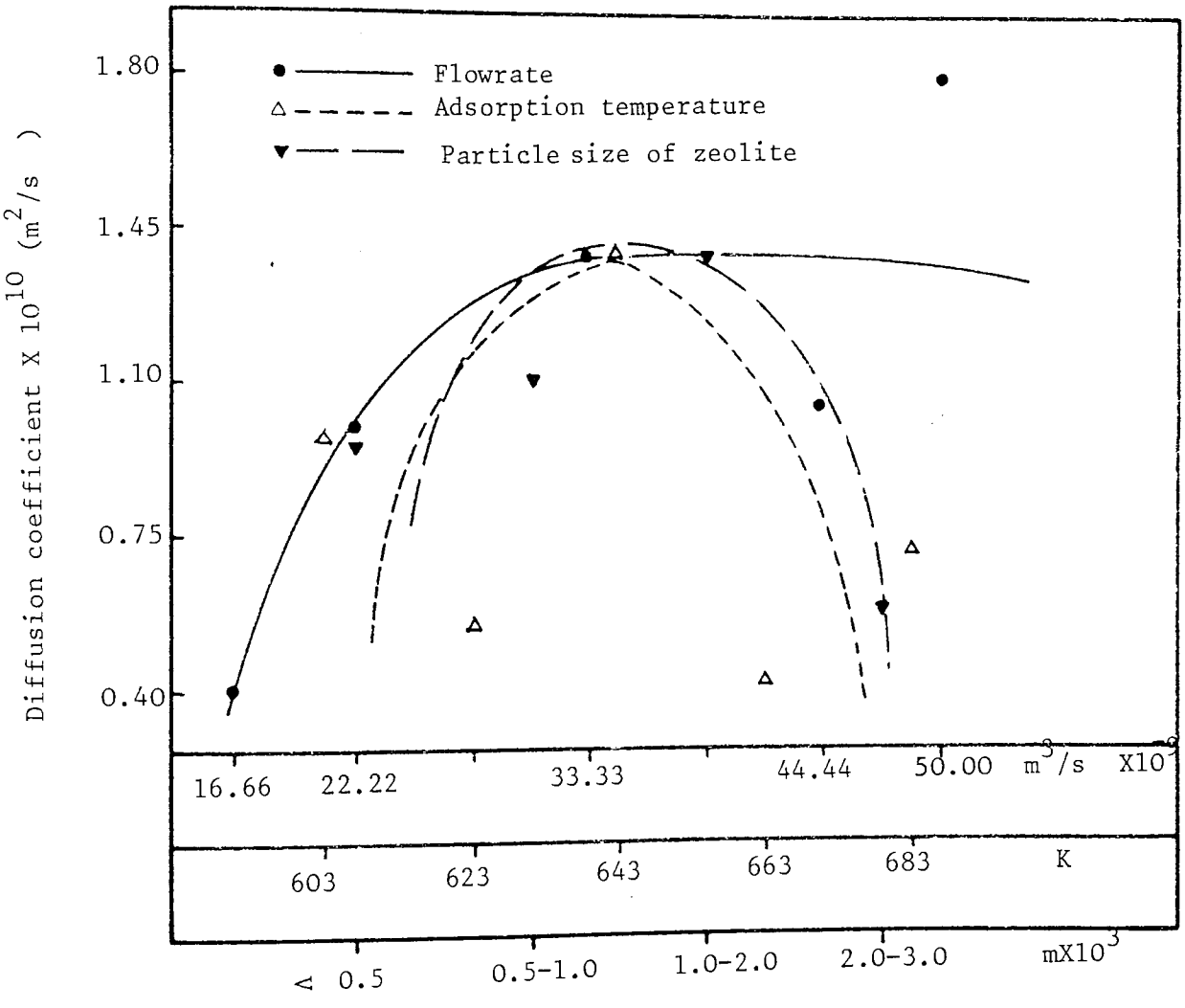

using steam as the desorbing agent, upon the BT-curves, HMTZ, and the dynamic capacity of the zeolite. All the adsorption cycles were conducted at the same operating conditions, namely, at a feed flowrate of 33.33×10^{-9} m^3/s, an adsorption temperature of 643 K, and a particle size of $(1.0 - 2.0) \times 10^{-3}$ m. Steam as the desorbing agent was fed into the column at a constant flowrate of 41.6×10^{-6} kg/s, and the desorption temperature was fixed at 643 K. The nitrogen gas flowrate at both adsorption and desorption cycles was regulated at 6.7×10^{-7} m^3/s. These cycles were repeated with and without intermediate reactivation of zeolite in the adsorption column. Figure (9.26) shows the effect of repeated adsorption cycles without intermediate reactivation of zeolite on the BT-curve of adsorption of n-paraffins from HK. The BT-curves plotted as refractive indices vs. time are shown only for cycles 1, 3, 5, and 8. It shows that the S-shaped BT-curves become more sharper as the adsorption cycle increases, i.e., the BT-time Θ_B and the exhaustion time Θ_E were reached faster as the number of adsorption cycle increased. For example, the BT-times were reached after 2700, 2025, 1350 and 820 s for cycles 1, 3, 5 and 8 respectively indicating that the effectiveness of zeolite for adsorption of n-alkanes is reduced by repeated cycling.

Table 9.11 shows the variation of the HMTZ with the cycle number of adsorption. The change in the HMTZ between successive cycleswas relatively small when intermediate reactivation of zeolite was carried out. For example the HMTZ was increased by about 6.8% and 14.6% in the third and the fifth cycles respectively relative to

Fig. 9.26 Effect of repeated desorption with steam without intermediate reactivation on the breakthrough curve of adsorption of n-paraffins from HK at a feed flowrate of 33.33 x 10^{-9} m^3/s , a temperature of 643 K, and a pellet particle size of (1.0 - 2.0) x 10^{-3} m.

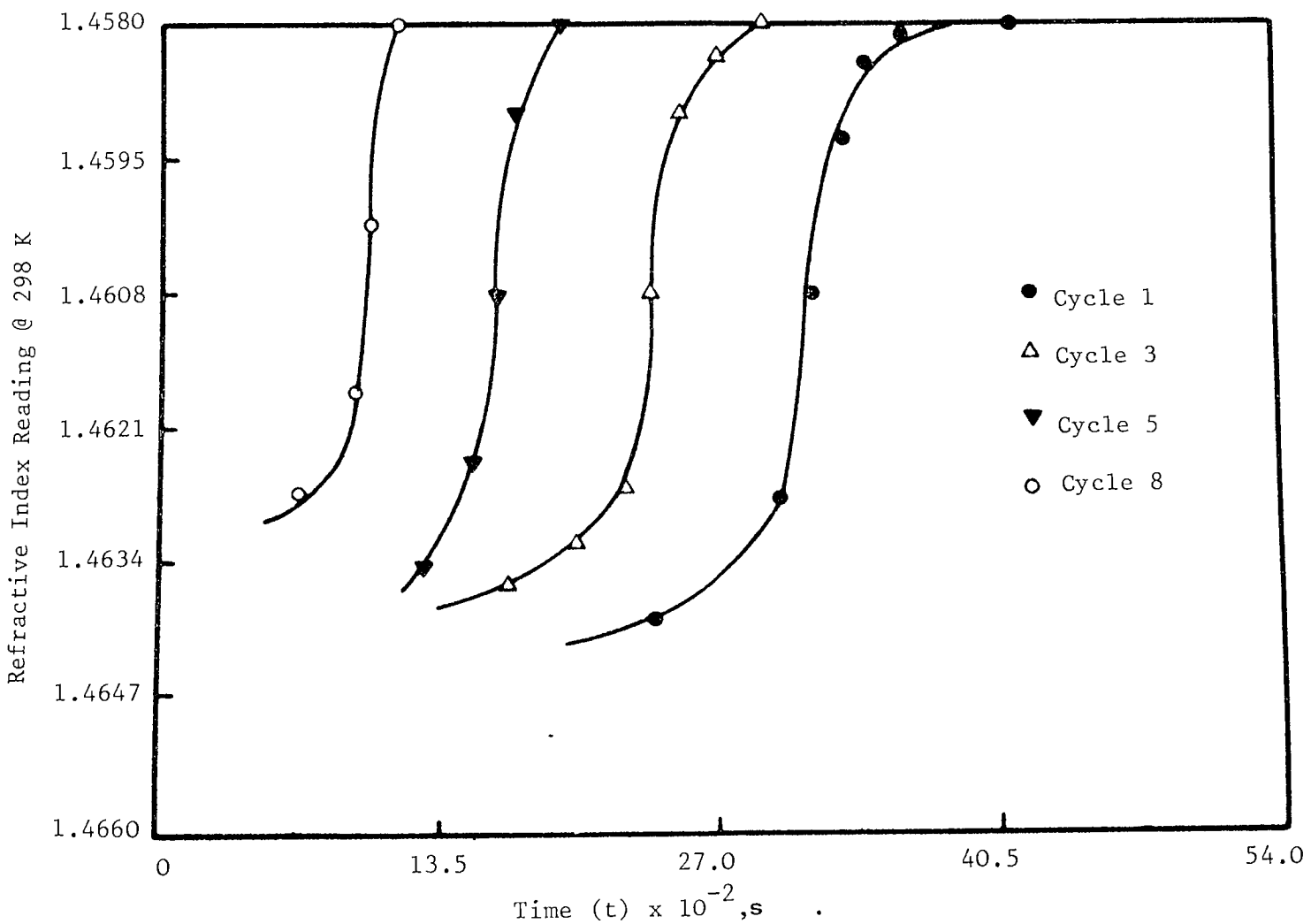

Table 9.11 Variation of the height of mass transfer zone (HMTZ) with the cycle number at the optimum conditions of adsorption of n-paraffins from HK using steam as the desorbent agent*.

Cycle No.	HMTZ (m) with intermediate reactivation	HMTZ (m) without intermediate reactivation
1	0.206	0.225
2	0.212	0.245
3	0.220	0.263
4	0.229	0.281
5	0.236	0.358
6	-	0.397
7	-	0.524
8	-	0.608

* Conditions of steam desorption:

- desorption temperature = 643 K
- steam flowrate = 41.6×10^{-6} kg/s

the first cycle. The average HMTZ was found to be 0.221 m for the five cycles investigated. The situation was rather different in the case where the adsorption cycles were carried out without intermediate reactivation of zeolite. For example, the HMTZ was increased by about 17% and 59% in the third and the fifth cycles respectively while the percentage was increased to 70% in the eighth cycle compared to the first one. The HMTZ was found to increase dramatically with increasing the cycle number where no intermediate reactivation of zeolite was carried out.

A similar trend was observed with the dynamic capacity of zeolite. Figure (9.27) shows the variation of the dynamic capacity of zeolite with the cycle number with, and without, intermediate reactivation of zeolite. The change of dynamic capacity with the cycle number in the case of intermediate reactivation of zeolite was very small compared to the cycle where no intermediate reactivation was carried out. In the latter case, the dynamic capacity decreased sharply as the cycle number increased which would be expected. Table 9.12 shows that the zeolite loses only about 3.5% and 4.8% of the original dynamic capacity at the third and the fifth cycles respectively with the intermediate reactivation of zeolite. In the case where no intermediate reactivation of zeolite is carried out, the zeolite loses about 11.2%, 37.1% and 63% of its original dynamic capacity at the third, the fifth and the eighth cycles respectively. In other words, the zeolite loses about one third of its dynamic capacity in the third cycle, while this loss is increased to two thirds in the eighth cycle.

Fig. 9.27 Variation of the dynamic capacity of zeolite with cycle number at the optimal conditions of adsorption of n-paraffins from HK using steam as the desorbing agent .

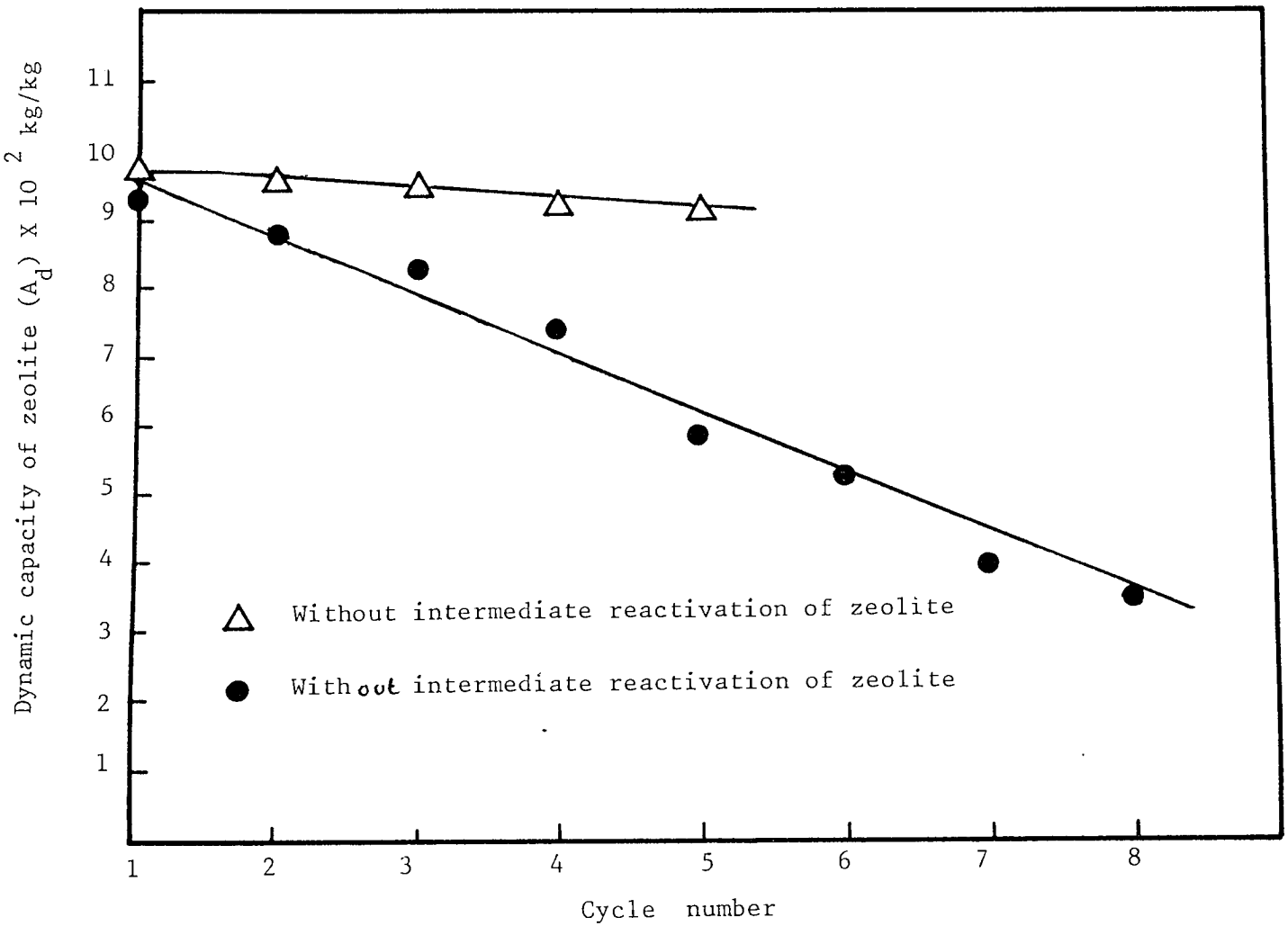

Table 9.12 Variation of the dynamic capacity of zeolite with the cycle number at the optimum conditions of adsorption* of n-praffins from HK using steam as the desorbing agent **

Cycle No.	Dynamic Capacity (10^2 kg/kg) with intermediate reactivation	Dynamic Capacity (10^2 kg/kg) without intermediate reactivation
1	9.653	9.278
2	9.401	8.754
3	9.311	8.240
4	9.247	7.604
5	9.188	5.832
6	-	5.259
7	-	3.987
8	-	3.433

* Optimum condition of adsorption:

- Feed flow rate = 33.33×10^{-9} m^3/s
- Temperature = 643 K
- Pellet particle size = $(1.0 - 2.0) \times 10^{-3}$ m.

** Condition of steam desorption:

- Desorption temperature = 643 K
- Steam flow rate = 41.6×10^{-6} kg/s

9.3 Desorption Processes

Steam was the main desorbing agent investigated in this study but some experiments were also performed with n-pentane or n-hexane for comparison purposes. This section presents the effect of the desorption temperature and the desorbing agent on the amount of n-paraffins desorbed. A comparison study was made among the three desorbing agents to investigate their effect on the saturation desorption time. The effect of repeated desorption cycles without intermediate reactivation of zeolite on the desorption time was studied using different steam flowrates.

The effect of the desorption temperature on the amount of n-paraffins desorbed was studied at the three different temperatures of 623, 643 and 663 K. Steam at a flowrate of 41.6×10^{-6} kg/s was used at the three desorption temperatures investigated while the adsorption processes for this investigation were conducted at a fixed feed flowrate, adsorption temperature and zeolite particle size of 33.33×10^{-9} m^3/s, 643 K and $(1.0 - 2.0) \times 10^{-3}$ m respectively. Figure (9.28) shows an increase in the amount of n-paraffins desorbed as the desorption temperature increases. The efficiency of steam, as a desorbing agent, is found to increase with increasing desorption temperature for the range investigated. By increasing the desorption temperature from 623 K to 663 K, the steam efficiency was increased from 46.01% to 53.76%, which correspond to 3.62×10^{-3} kg and 4.23×10^{-3} kg of n-paraffins desorbed at 623 K and 663 K respectively. The amount of n-paraffins adsorbed at

Fig. 9.28 Effect of desorption temperature on the amount of n-paraffins desorbed using steam at the optimal adsorption conditions*.

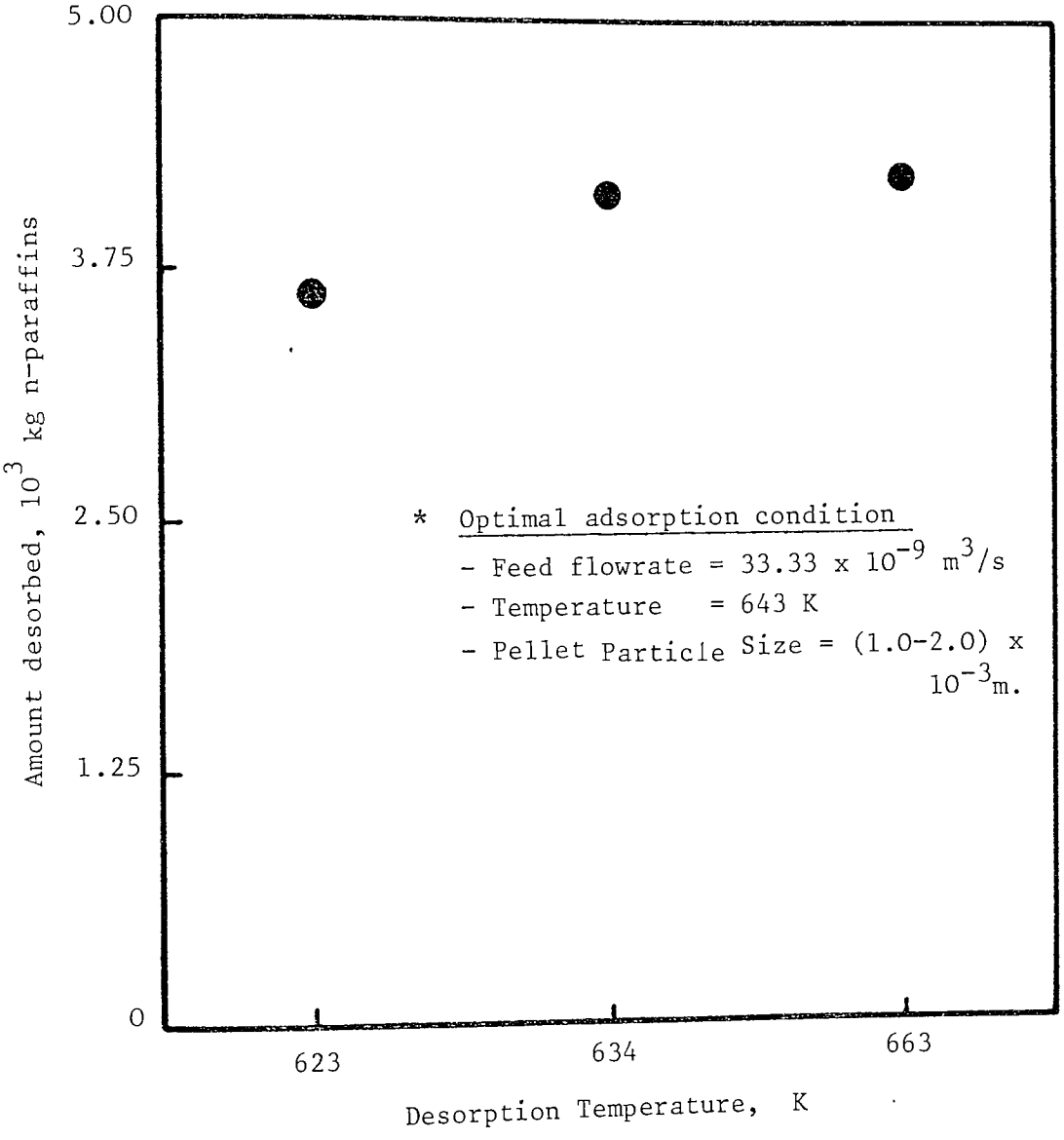

equilibrium was found to be 7.868×10^{-3} kg. Table 9.13 shows the variation of the desorption efficiency and the amount of n-paraffins desorbed with desorption temperature.

The effect of the desorbing agent on the amount of n-paraffins desorbed was also studied. The desorbing agents investigated were n-pentane and n-hexane in addition to steam. Figure (9.29) shows the effect of the desorbing agents on the percentage recovered of n-paraffins. By fixing the adsorption runs at the optimum conditions, the desorbents flowrate at 41.6×10^{-6} kg/s and the desorption temperature at 643 K, n-hexane was found to be the best desorbing agent. The amount of n-paraffins desorbed using n-hexane, n-pentane, and steam were 6.938×10^{-3}, 6.504×10^{-3} and 4.145×10^{-3} kg respectively. The desorption efficiency of steam was calculated as 52.36%, while this efficiency increased sharply to 82.66% using n-pentane and then slightly to 88.18% using n-hexane. The efficiency of steam as a desorbing agent was less by about 30% than that of n-pentane, while n-hexane was more efficient than n-pentane by about 5.5%.

The equilibrium desorption time required to desorb the n-paraffins from the pores of zeolite varied with the type of desorbent used. This time was recorded as 1500 s for steam while it was reduced to 900 s using n-pentane. The time recorded using n-hexane was 810 s. The desorption time difference using n-hexane and n-pentane was was 90 s, while this difference increased to 690 s using n-hexane and steam. In other words, more n-paraffins were

Table 9.13 Effect of the desorption temperature on the amount of n-paraffins desorbed using steam*. (At the optimum adsorption of n-paraffins from HK by zeolite Type-5A).**

Desorption Temperature (K)	623	643	663
Amount adsorbed @ equilibrium ** (10^3 kg n-paraffins)	7.868	7.868	7.868
Amount desorbed @ equilibrium (10^3 kg n-paraffins)	3.62	4.12	4.235
Desorption efficiency (%)	46.01	52.36	53.76

* Conditions:

- Steam flow rate = 41.6×10^{-6} kg/s

** Conditions:

- At optimum adsorption conditions
- Temperature = 643 K
- Feed flowrate = 33.33×10^{-9} m^3/s
- Pellet particle size = $(1.0 - 2.0) \times 10^{-3}$ m

Fig. 9.29 Effect of desorbent agent on the percentage of n-paraffins desorbed at the optimum adsorption conditions*.

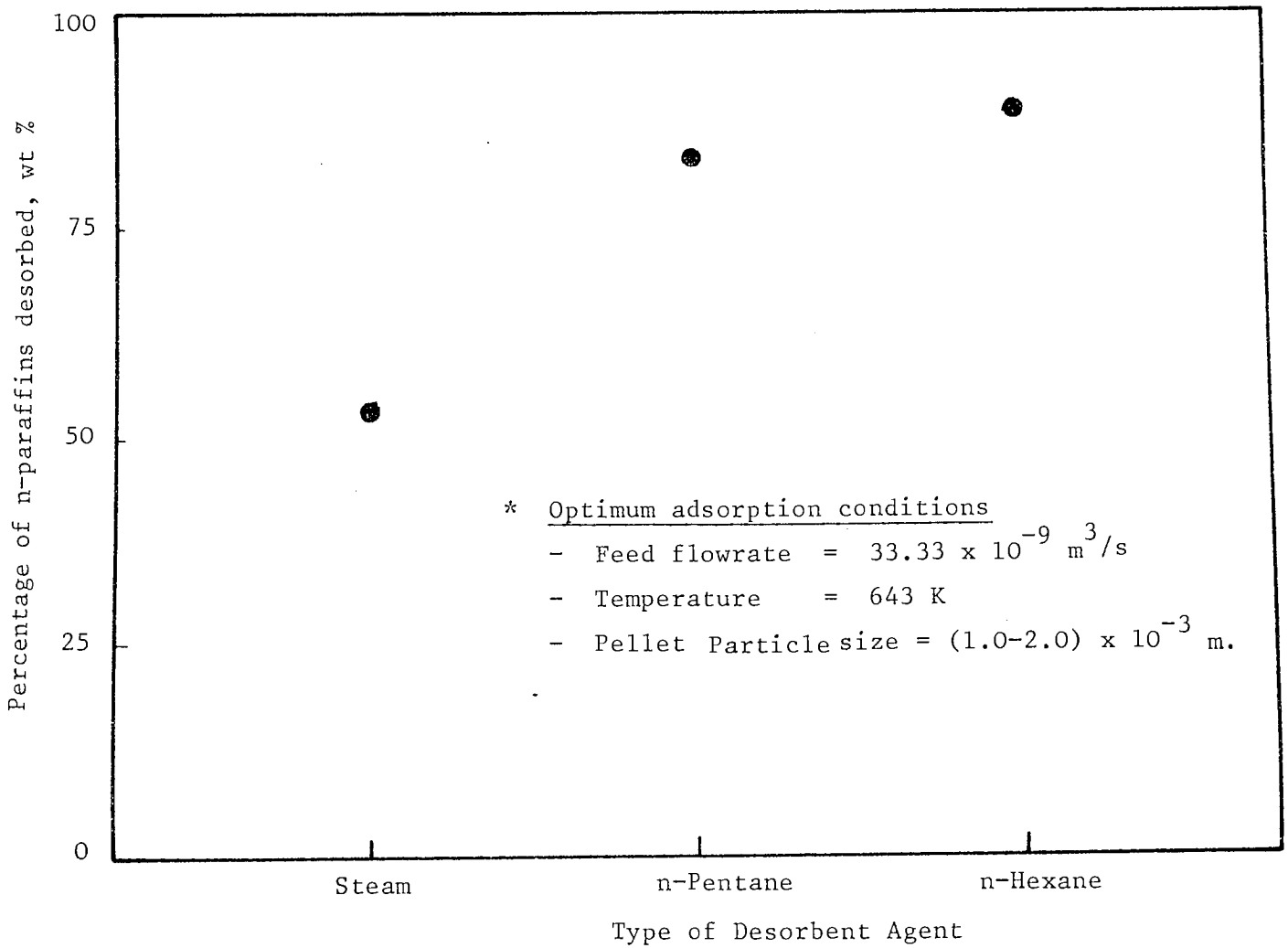

desorbed in a lesser time using n-hexane compared to n-pentane and steam. Table 9.14 shows the variation of the desorption efficiency and the amount desorbed with the types of desorbent. The variation of the desorption equilibrium time with the types of desorbent is shown in Fig. (9.30). Only the points were plotted and curves have not been reproduced because their shape cannot be envisaged with a limited amount of data produced.

The effect of repeated desorption cycles without intermediate reactivation of zeolite on the equilibrium desorption time was studied using steam as a desorbent at two different flowrates. The steam flowrates investigated were 41.6×10^{-6} kg/s and 75×10^{-6} kg/s. The desorption temperature was fixed for all the cycles at 643 K, while the adsorption runs were conducted at the optimum conditions. Figure (9.31) shows the variation of the desorption time with the cycle number at two different steam flowrates. As shown in this Figure, the desorption time decreases as the cycle number is increased. Table 9.15 shows that for cycle number one the equilibrium desorption time required to desorb the n-paraffins increased from 1500 s to 1720 s as the steam flowrate increased from 41.6×10^{-6} kg/s to 75×10^{-6} kg/s. At steam flowrate of 41.6×10^{-6} kg/s and at the fifth cycle, the desorption time was recorded as 900 s, meanwhile this time was recorded for the eighth cycle using a flowrate of 75×10^{-6} kg/s. This means that more equilibrium time is required to desorb the n-paraffins at the higher steam flowrate than the lower one for the same number cycle at the same desorption-adsorption condition. It seems from Fig. (9.31)

Table 9.14 Effect of desorbent agent on the amount of n-paraffins desorbed*. (At the optimum adsorption separation conditions** of n-paraffins from HK by zeolite Type-5A).

Desorbing Agent	n-Hexane	n-Pentane	Steam
Amount adsorbed @ equilibrium ** (10^3 kg n-paraffins)	7.868	7.868	7.868
Amount desorbed @ equilibrium (10^3 kg n-paraffins)	6.938	6.504	4.145
Desorption efficiency (%)	88.18	82.66	52.36
Desorption time (s)	810	900	1500

* Conditions:

- Desorbent flow rate = 41.6×10^{-6} kg/s
- Desorption temperature = 643 K

** Conditions:

- At optimum adsorption conditions
- Temperature = 643 K
- Feed flowrate = 33.33×10^{-9} m^3/s
- Pellet particle size = $(1.0 - 2.0) \times 10^{-3}$ m

Fig. 9.30 Effect of desorbent agent type on the equilibirium desorption time of n-paraffins adsorbed from HK on zeolite type-5A

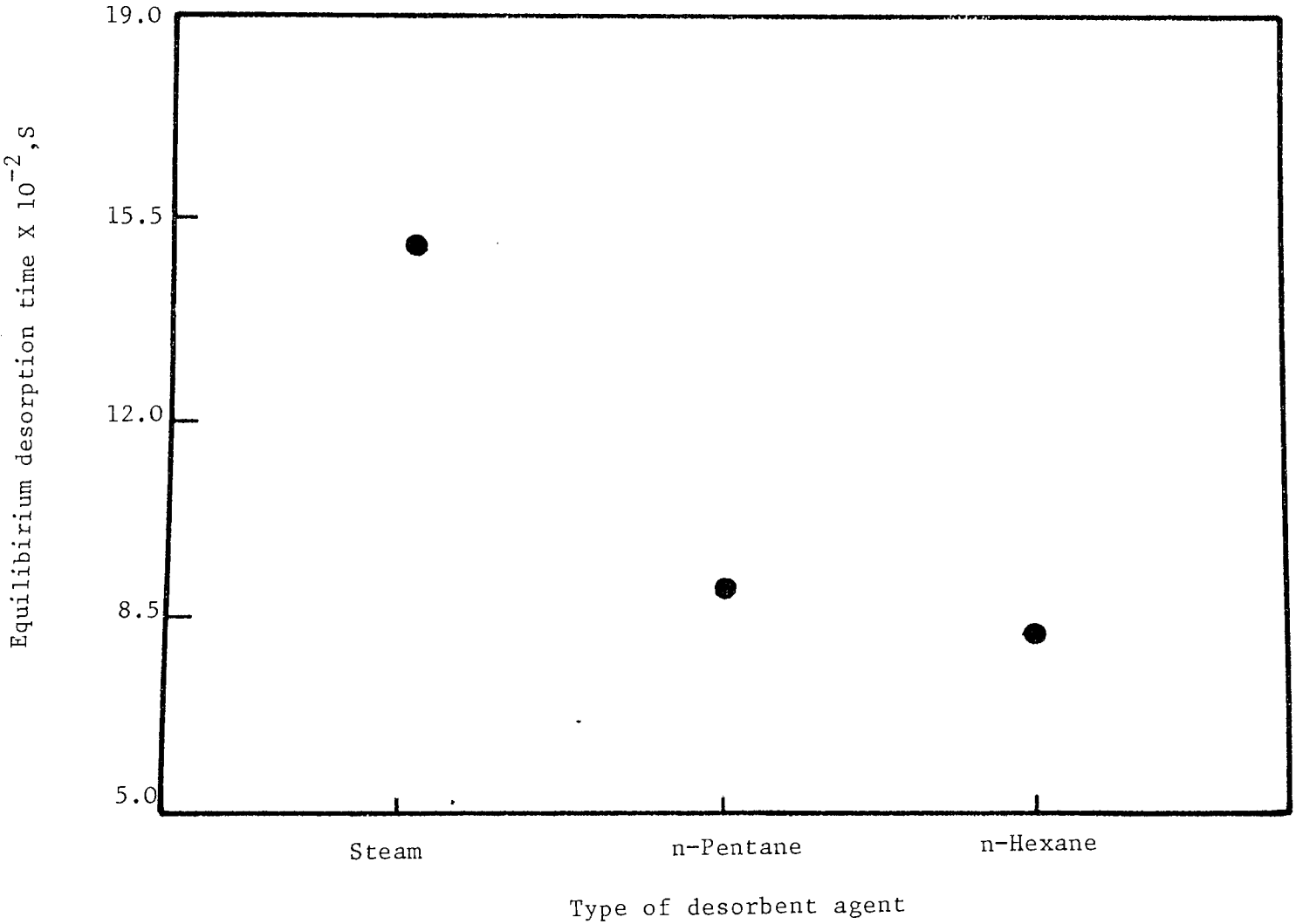

Fig. 9.31 Effect of repeated desorption cycles (without intermediate reactivation of zeolite) on desorption time using steam at different steam flowrate .

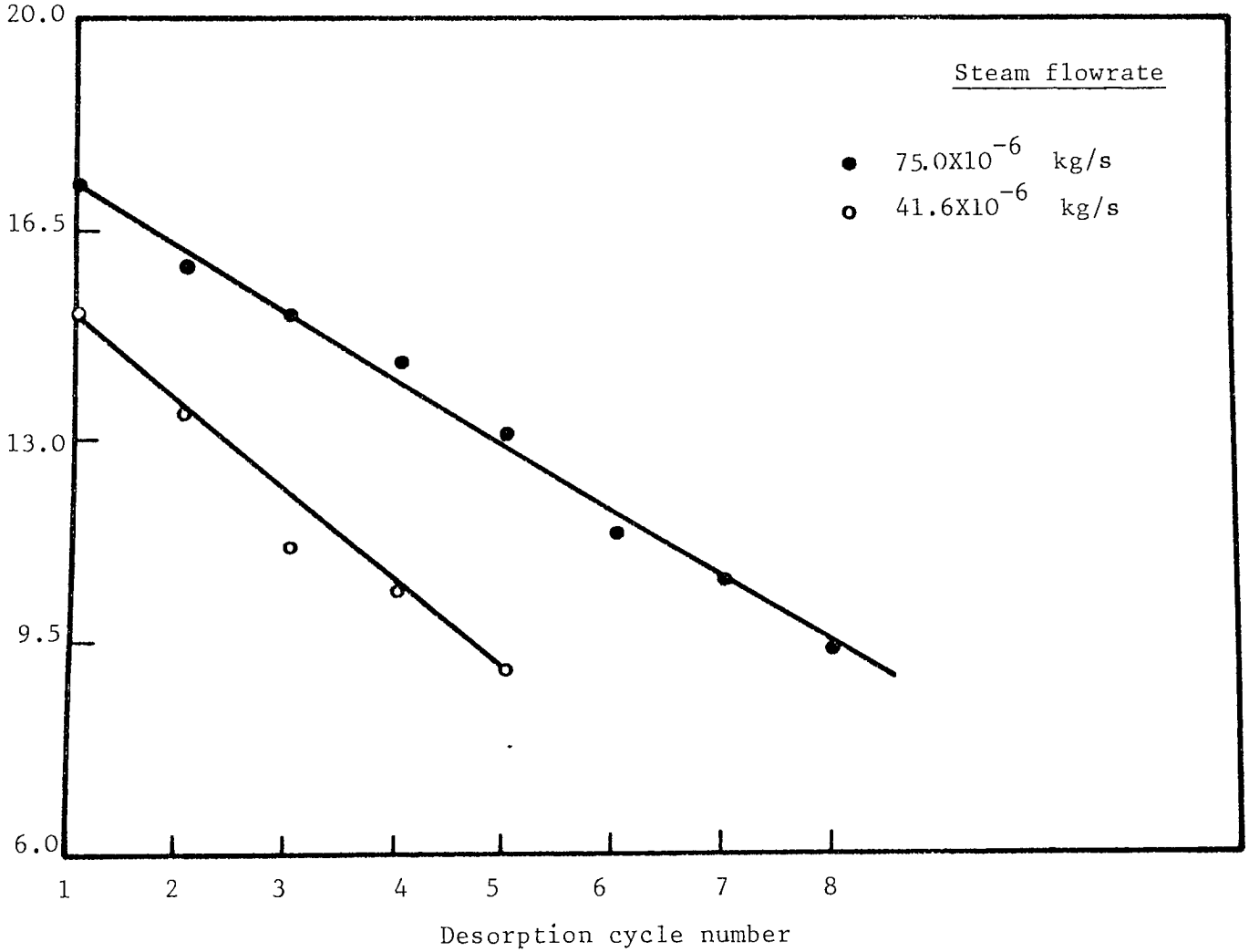

Table 9.15 Effect of repeated desorption cycles (without intermediate reactivation of zeolite) on desorption time using steam at different flow rate.*

Desorption Cycle Number	Desorption Time, s	
	Steam Flow rate 41.6×10^{-6} kg/s	Steam Flow rate 75×10^{-6} kg/s
1	1500	1720
2	1350	1600
3	1110	1510
4	1040	1430
5	900	1300
6	-	1190
7	-	1070
8	-	940

* At the optimum adsorption separation of n-paraffins from HK by zeolite Type-5A.

- 643 K
- 33.33×10^{-9} m^3/s
- $(1.0 - 2.0) \times 10^{-3}$ m

that the decrease of the desorption time with the number of cycle is slightly sharper in the case of the lower steam flowrate than that of the higher one.

9.4 Results of Analysis

This section presents the results of the analysis of the feed, the by-product, and the product for the n-paraffins and the aromatic hydrocarbons content. Some important physico-chemical properties of these compounds were measured. The fresh zeolite was compared with the reactivated and the used materials by measuring differences in the surface area and the pore volume.

The qualitative distribution of n-paraffins in the heavy kerosene, the denormalized kerosene (the by-product), and the isolated liquid paraffin (product) are presented in Figure (9.32). This Figure shows that the n-paraffins present in the feed peak at n-heptadecane (n-C_{17}), while in the denormalized kerosene they peak at n-pentadecane (n-C_{15}), and peak at n-hexadecane (n-C_{16}) in the isolated liquid paraffins. The general trend shown in Fig (9.32) is that the concentration of each individual n-paraffin is higher in the feed than that in the denormalized product, while in the case of the isolated liquid paraffin, the concentration of each individual n-paraffin is the highest which is expected. Table 9.16 shows the quantitative distribution of the n-paraffins present in the original feed, the denormalized kerosene, and the isolated liquid paraffins determined by the Gas-Liquid Chromatography technique. These

Fig. 9.32 Distribution of n-alkanes as determined by the gas-liquid chromatography.

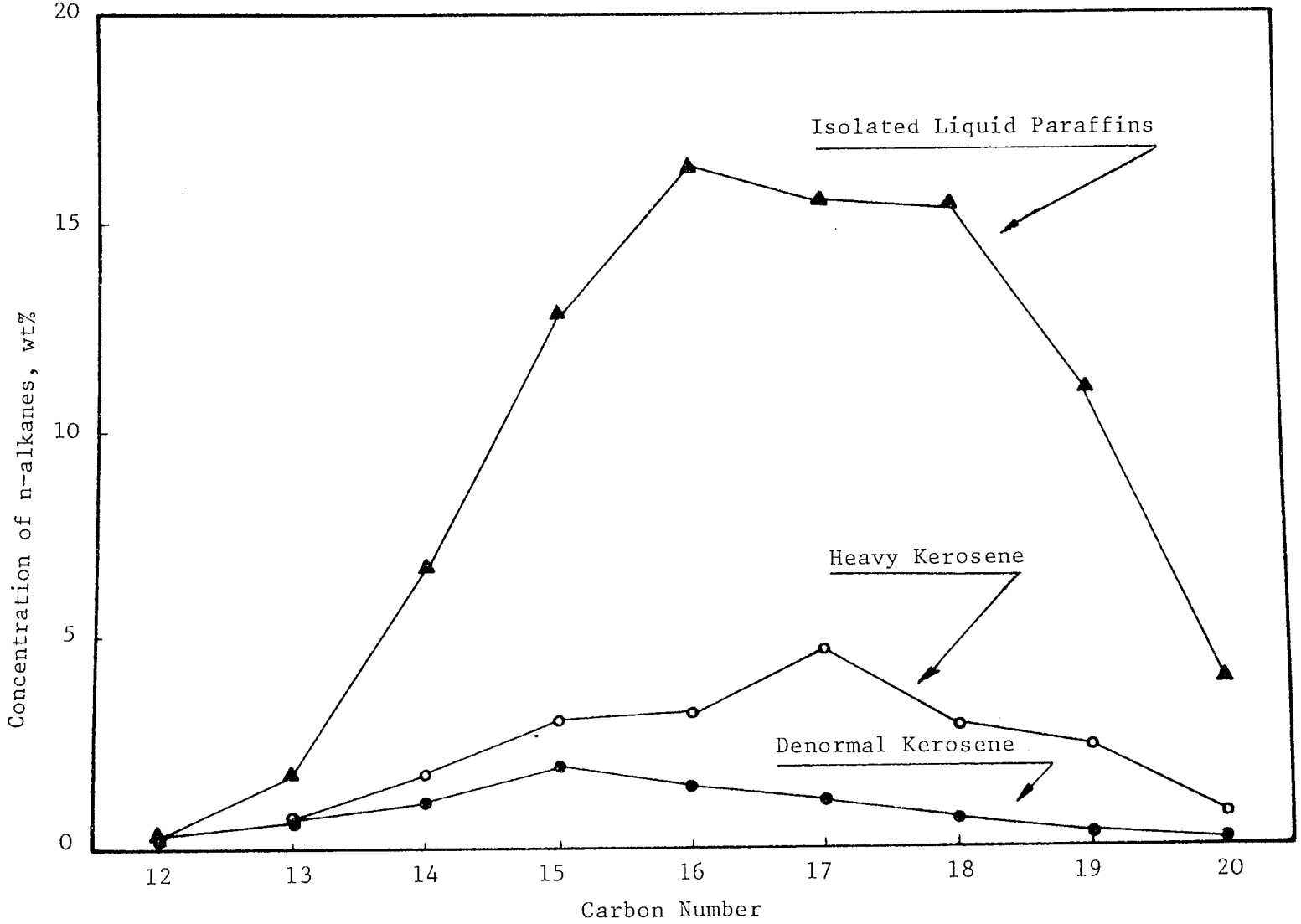

Table 9.16 Distribution of the normal alkanes presented in the original feed (Heavy Kerosene), isolated liquid paraffins and denormalized kerosene as determined by the Gas-Liquid Chromatography (GLC).*

N-Alkanes	H. Kerosene (Wt %)	Denormalized Kerosene (Wt %)	Isolated Liquid Paraffins (Wt %)
C_{12}	0.1360	0.1366	0.2340
C_{13}	0.6479	0.6088	1.6891
C_{14}	1.6224	1.1478	6.6284
C_{15}	2.9368	1.7769	12.7184
C_{16}	3.0083	1.3453	16.2350
C_{17}	4.5873	1.0426	15.5490
C_{18}	2.7093	0.6605	15.3379
C_{19}	2.3556	0.2547	10.9649
C_{20}	0.7416	0.1168	3.8850
Total	18.7457	7.0900	83.2417

* Conditions:

- Adsorption temperature = 643 K
- Zeolite particle size = $(1.0 - 2.0) \times 10^{-3}$m
- Kerosene flow rate = 33.33×10^{-9} m^3/s
- Desorption temperature = 643 K
- Desorbent = Steam at a flow rate of 41.6×10^{-6}kg/s

analytical results were obtained by conducting the adsorption run at the optimum condition, while the desorption run was conducted using steam as a desorbing agent ata flowrate of 41.6×10^{-6} kg/s and at a desorption temperature of 643 K. The heavy kerosene of Kuwait Petroleum Cut obtained from KNPC Refinery (Kuwait National Petroleum Company) contains about 18.75% by weight n-paraffins ranging from dodecane ($n\text{-}C_{12}$) to cosane ($n\text{-}C_{20}$) with varying concentration. As shown in Table 9.16 the maximum concentration was recorded for n-heptadecane ($n\text{-}C_{17}$) as 4.59 wt% of the total feed, while the minimum concentration was recorded for n-dodecane ($n\text{-}C_{12}$) as 0.136 wt%. The range of $n\text{-}C_{15}$ to $n\text{-}C_{18}$ constitutes more than 70% of the total n-paraffins that exist in the feed, 40.5% of which is represented by $n\text{-}C_{16}$ and $n\text{-}C_{17}$ only. The concentration of $n\text{-}C_{12}$, $n\text{-}C_{13}$, and $n\text{-}C_{20}$ is relatively small compared to the other n-paraffins, and they represent altogether only 8.1% of the total n-paraffins that exist in the feed. The total n-paraffins concentration found in the denormalized kerosene was 7.09 wt%. The range of $n\text{-}C_{14}$ to $n\text{-}C_{17}$ represented about 75 wt% of the totaln-paraffins that exist in the denormalized kerosene. In the case of the isolated liquid paraffins, the n-paraffins represented 83.24 wt% of the total material existing in the product. The range of $n\text{-}C_{15}$ to $n\text{-}C_{19}$ represented more than 85 wt% of the total n-paraffins content in the product, while n-dodecane and n-Tridecane existed in small concentration not exceeding 1.92 wt% of the total product and 2.31 wt% of the total n-paraffins that exist in the isolated liquid paraffins (product). Figure (9.33) through Fig. (9.35) show the charts of n-paraffins distribution as determined by

Fig. 9.3 3 The Peaks of n-Alkanes Content in the Heavy Kerosene as Determined by GLC at the Specified Conditions Mentioned in Table 8.1 .

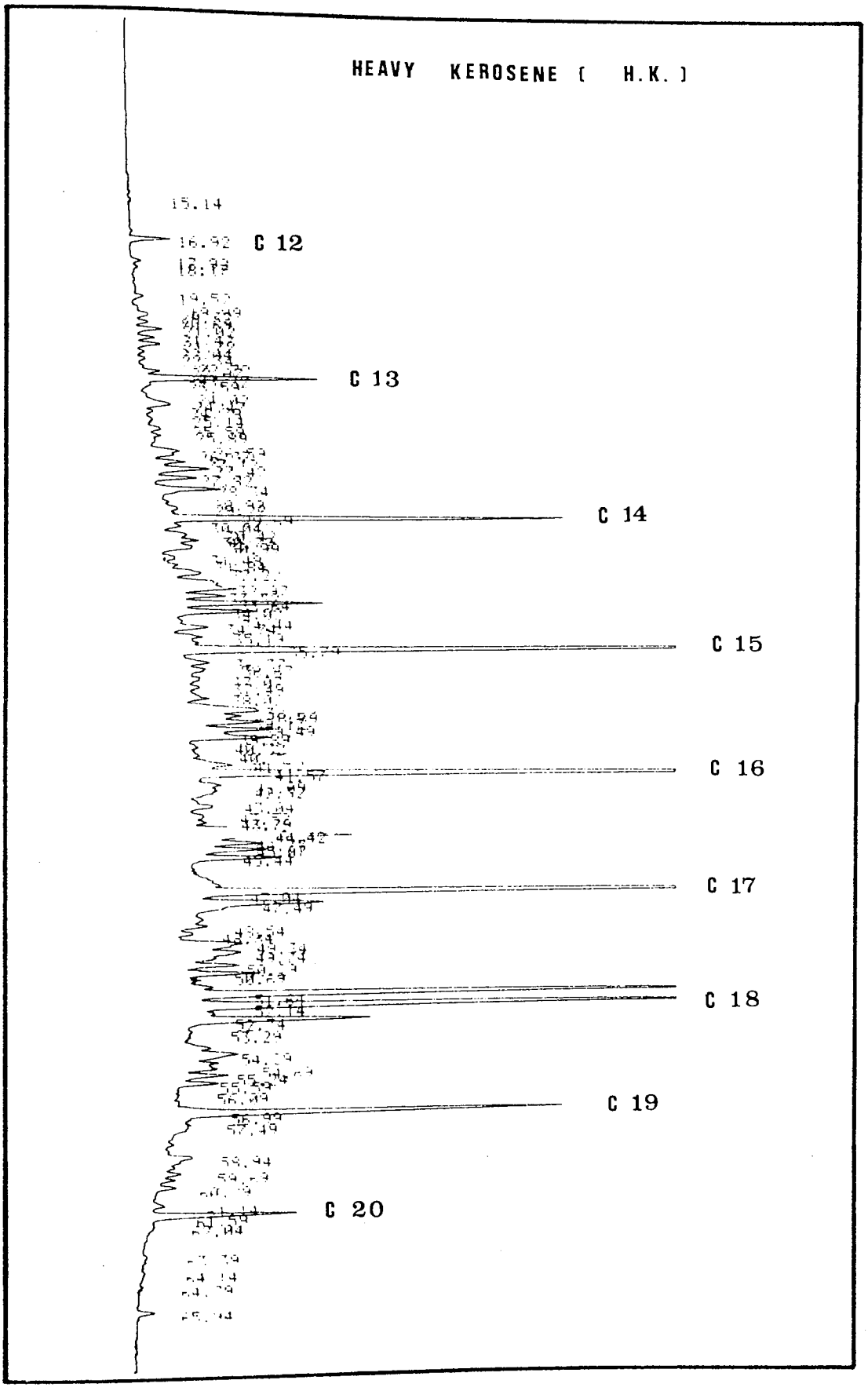

FIG. 9.34 The Peaks of n-Alkanes Content in Denormalized Kerosene as Determined by GLC at the Specified Conditions Mentioned in Table 8.1 .

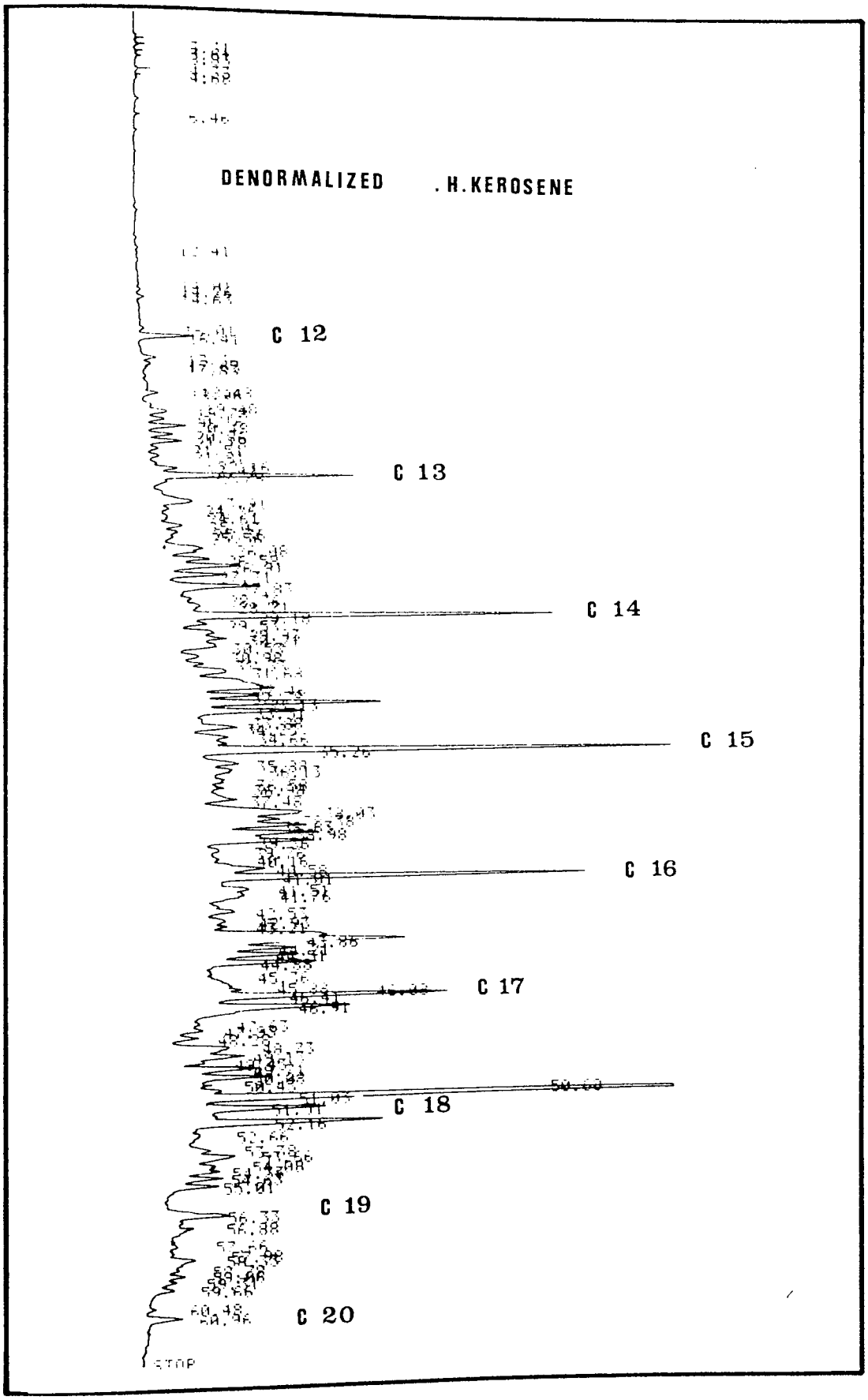

FIG. 9.35 The Peaks of n-Alkanes Content in Liquid Paraffins Product as Determined by GLC at the Specified Conditions Mentioned in Table 8.1 .

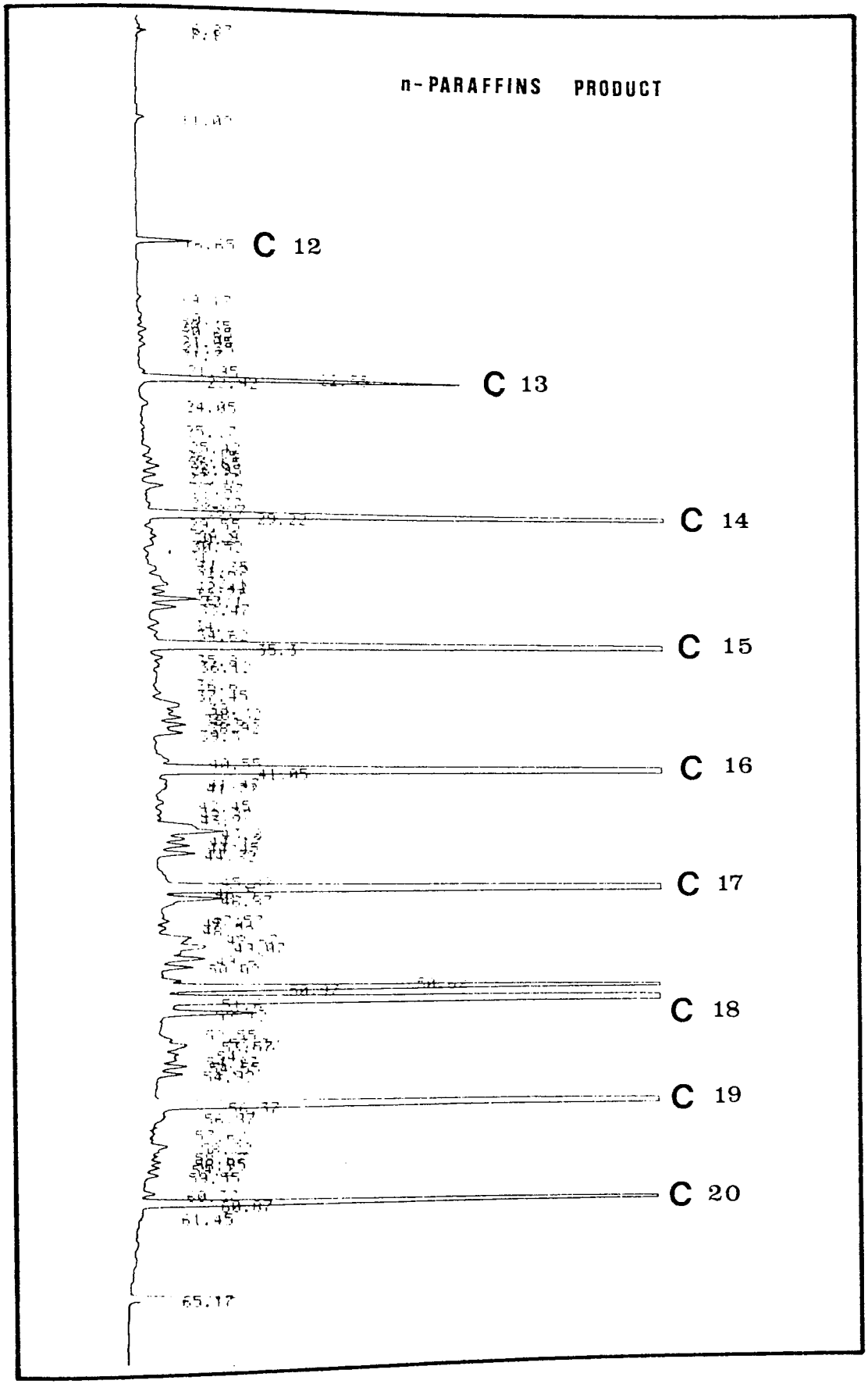

the GLC in the feed, the by-product, and in the product respectively. Table 9.17 shows the material balance of the adsorption separation of n-paraffins from HK on zeolite type-5A. The material losses as shown in this Table is mounted to 0.85 wt% which is acceptable. The total amount of n-alkanes adsorbed at any time Θ is given by: $G = QC_o \rho_{HK} \Theta$ where, Q is the feed volumetric flowrate (m^3/s), Co is the original concentration of n-alkanes in the feed (kg/kg), ρ_{HK} is the density of the feed (kg/m^3), and Θ is the time (s). For example at a feed flowrate of 33.33×10^{-9} m^3/s, the amount of n-alkanes adsorbed after 2400 s is 0.0124 kg. The calculated experimental value was 0.0062 kg. This difference in the amount adsorbed of n-alkanes can be discussed as follows. The weight of heavy kerosene occupying the intersticies between the particles of the bed was 0.0117 kg of which 0.0022 kg was occupied by n-alkanes. Finally the fluid inside the pores of the zeolite unadsorbed will be 50.07×10^{-6} m^3 x the concentration of n-paraffins in this fluid. This concentration will be less than that of the feed since it will have been reduced by the adsorption. It is assumed that the n-paraffins concentration in the fluid is half of that in the feed that will correspond to 0.0039 kg, then a mass balance would:

1. Input feed = 12.4×10^{-3} kg n-alkanes

2. Adsorbed on zeolite = 6.2×10^{-3} kg n-alkanes

3. Held up in intersticies = 2.2×10^{-3} kg n-alkanes

4. Held up in fluid in pores = 3.9×10^{-3} kg n-alkanes

Total = 12.3×10^{-3} kg n-alkanes.

This balance would appear to verify the distribution of n-paraffin within the system.

The aromatic hydrocarbons content of the original feed, the isolated liquid paraffins, and the denormalized kerosene were investigated, the results of which are shown in Table 9.18. These aromatics as determined by the Ultra-Violet (UV) technique were classified under three groups. The mono-aromatics (or the benzene compounds), the di-aromatics (or the naphthalene compounds), and the tri-aromatics (or the phenanthrene and anthracene compounds). The concentration of these groups and the total aromatics content differed from one stream to another. The total aromatics content determined in the original feed constituted 22.82 wt%, while it was reduced to 17.71 wt% in the denormalized kerosene, and to 5.5 wt% in the isolated liquid paraffin. The mono-aromatics or (the benzene compounds) were dominant in the different streams, where they represented 98.5%, 98.4%, and 92.3% of the total aromatic compounds in the feed, the by-product, and the product respectively. In general, the naphthalene compounds were more concentrated in the streams than the phenanthrene and the anthracene compounds except in the original feed, where the tri-aromatics were more concentrated than the di-aromatics. This distribution is shown in Table 9.18 where the tri-aromatics represent 0.3 wt% of the total aromatic compounds in the original feed, while the di-aromatics represent only 0.045 wt%.

Table 9.17 Total material balance of adsorption separation of n-paraffins from HK on zeolite Type-5A at a feed flow rate of $33.33 \times 10^{-9} m^3/s$, an adsorption temperature of 643 K and zeolite particle size of $(1.0 - 2.0) \times 10^{-3} m$.

Material	Wt (10^3 kg)	Wt (%)
Input, kg:		
* Total Feed	76.0012	100
Output, kg:		
* Liquid paraffins adsorbed on zeolite	7.8680	10.35
* Denormal Product	67.4924	88.80
* Total material output	75.3604	99.15
* Losses	0.6408	0.85

Table 9.18 Aromatic hydrocarbons content of original feed (Heavy Kerosene), isolated liquid paraffins and denormalized kerosene as determined by the U.V.*

Sample	Aromatic** Content by U.V. (Wt %)			
	Mono-aromatics	Di-aromatics	Tri-aromatics	Total aromatics
Original Feed (H.K.)	22.4756	0.0450	0.3000	22.8206
Isolated Liquid Paraffins	5.0750	0.2890	0.1335	5.4975
Denormalized Kerosene	17.4300	0.1700	0.1100	17.71

* Conditions:

- Adsorption temperature = 643 K
- Zeolite particle size = $(1.0 - 2.0) \times 10^{-3}$ m
- Kerosene flow rate = 33.33×10^{-9} m^3/s
- Desorption temperature = 643 K
- Desorbent = Steam at a flow rate of 41.6×10^{-6} kg/s

** Aromatic Content:

- Mono-Aromatics = Benzene compounds
- Di-Aromatics = Naphthalene compounds
- Tri-Aromatics = Phenanthrene and Anthracene compounds

Some important physico-chemical properties of the feed, the by-product, and the product were investigated. For example, the density measured at 288 K, the pour point, and the smoke point. The pour point of the HK was dropped from 261 K (-12°C) to 231 K (-42°C) in the denormalized kerosene by adsorbing the n-paraffins on zeolite Type-5A which is a desired property enabling the by-product of the adsorption process (denormalized kerosene) to be used as a fuel in the cold climates. The smoke point of the HK dropped from 0.024 m to 0.018 m in the denormalized kerosene which means that the HK loses about 25% of its smoke point value by the process of adsorption of n-paraffins by zeolite. The highest value of density was estimated as 913.1 kg/m^3 for the denormalized kerosene, while the lowest value was estimated as 791.5 kg/m^3 for the isolated liquid paraffins. Table 9.19 shows the variation of these properties with the different streams.

The surface area and the pore volume of the fresh zeolite Type-5A were investigated and compared with that of the reactivated and the used materials as shown in Table 9.20. The surface area of the fresh zeolite was found to be 512×10^3 m^2/kg. This area was reduced to 320×10^3 m^2/kg after reactivation of the zeolite (in the fifth cycle), while it was reduced sharply to 95×10^3 m^2/kg after the first adsorption run immediately without any reactivation step. In other words, the fresh zeolite lost 37.5% and 81.4% of its surface area after reactivation and one adsorption run respectively. The pore volume of the fresh zeolite was dropped from 0.32×10^{-3} m^3/kg to 0.161×10^{-3} m^3/kg for the reactivated zeolite, while this

Table 9.19 Physico-chemical properties of original feed (Heavy Kerosene), isolated liquid paraffins and denormalized kerosene. *

Properties	Heavy Kerosene	Denormalized Kerosene	Isolated Liquid Paraffins
Density @ 288 K, kg/m^3	826.1	913.1	791.5
Pour Point, K	261	231	269
Smoke Point, m	0.024	0.018	-
Total n-alkanes, % Wt	18.75	7.090	91.98
Total aromatics, % wt	22.82	17.71	5.50

* Conditions:

- Adsorption temperature = 643 K
- Zeolite particle size = $(1.0 - 2.0) \times 10^{-3}$ m
- Kerosene flow rate = 33.33×10^{-9} m^3/s
- Desorption temperature = 643 K
- Desorbent = Steam of a flow rate of 41.6×10^{-6} kg/s

Table 9.20 Surface area and pore volume data for fresh, used and reactivated zeolite Type-5A

Sample Description	Surface Area 10^{-3} x (m^2/kg)	Pore Volume 10^{3} x (m^3/kg)
Used Zeolite (after use)	95	0.082
Reactivated Zeolite	320	0.161
Fresh Zeolite (Before use)	512	0.32

volume was dropped sharply to 0.082×10^{-3} m^3/kg for the used zeolite after one adsorption run at the optimum adsorption conditions. It was noticed that the fresh zeolite lost 49.7% and 74.4% of its pore volume after reactivation and one adsorption run respectively.

9.5 Mathematical Modelling:

As discussed previously in Chapter 6, a material balance on the fluid and solid phases contained within the section dz shows that:

$$\frac{\partial c}{\partial t} + \frac{\rho_B}{\epsilon} \frac{\partial q}{\partial t} + V \frac{\partial t}{\partial z} = 0 \qquad (6.24)$$

and that $$\left[1 + \frac{\rho_B}{\epsilon} f'(c) \right] \frac{\partial c}{\partial t} + V \frac{\partial c}{\partial z} = 0 \qquad (6.25)$$

Equation (6.25) is a first order partial differential equation that is linear in the derivatives but has a variable coefficient because of f'(c). Such equations have remarkably simple geometrical properties as expressed by a solution procedure known as the method of characteristics [81].

Suppose a solution C = C (x, t) has been found and that the values of the two partial derivatives can be computed from Eq. 6.25 and from the solution itself. For this purpose, Eq. 6.25 can be solved simultaneously with:

$$\left(\frac{\partial c}{\partial t}\right) dt + \left(\frac{\partial c}{\partial z}\right) dz = dc \qquad (9.8)$$

The solution would be expressed by two equations, such as:

$$\frac{\partial c}{\partial t} = \frac{\begin{vmatrix} 0 & V \\ dc & dz \end{vmatrix}}{\begin{vmatrix} 1 + \frac{\rho_B}{\epsilon} f'(c) & V \\ dt & dz \end{vmatrix}} \qquad (9.9)$$

and a similar equation for $\partial c/\partial z$. There are certain ratios of dz to dt, i.e., certain charcteristic directions in the zt plane which make the denominator equal to zero. When this occurs, the numerator must also be zero if $\partial c/\partial t$ is to be finite. Then dc will be zero. Thus, C is constant along the "charcteristic lines" corresponding to:

$$\frac{dz}{dt} = \frac{V}{1 + \left(\frac{\rho_B}{\epsilon}\right) f'(c)} \qquad (9.10)$$

Since c is constant, f'(c) is constant and the characteristics are straight lines in the zt plane. When such a line crosses the line z = 0, for example, the specified concentration at the bed's entrance is maintained for all other values of z and t along the same characteristic.

The method of characteristics brings out an important aspect of fixed-bed behaviour; at least when there is efficient mass transfer between phases, fluid marked by a certain composition travels through the packing without a change in the concentration at a velocity

$$V^* = \frac{V}{1 + (\rho_B/\epsilon) f'(c)} \qquad (9.11)$$

called the concentration wave velocity.

The solvent fluid travels at velocity V, which is greater. The slower progress of the adsorbable molecules (n-alkanes) is owing to the fact that they spend a certain fraction of their time in a

fixed state while the fluid is moving past.

If depending on the shape of the equilibrium relationship and the range of concentrations involved, f'(c) is nearly constant, then the velocities will beequal for all concentrations and a wavefront will maintain its shape as it moves through the bed. On the other hand, if V* (c) varies, some concentrations will move faster than others and distortion of waveshapes will occur (81).

Consider the movement of a wavefront of concentration C_o, through a fixed adsorbent bed which is initially free of solute (n-alkanes), where C_o corresponds to a step change to concentration C_o at the bed's entrance at time zero. Figure 9.36 shows the characteristic lines corresponding to an equilibrium curve similar to that shown in Fig. 9.24. The horizontal axis represents the conditions at the entrance to the bed, where the concentration is constant ($C = C_o$) after $t = 0$. The characteristics, such as CD crossing the axis, all have the same steep slope corresponding to

$$V^* = \frac{V}{1 + (\rho_B/\epsilon)\ f'(c_o)} \qquad (9.12)$$

{Note that $f'(C_o)$ is smaller than f(0) on Fig. 9.24].

The line OA has a slope equal to the fluid velocity V. To the left of this line, fluid initially in the packing has not yet been displaced by feed. Immediately to the right, the feed fluid has arrived but the concentration has not yet changed and is still equal to zero.

All the characteristic lines, such as AB, crossing OA have a smaller slope,

$$V^* = \frac{V}{1 + (\rho_B/\epsilon)\ f'(0)} \qquad (9.13)$$

because f (0) is relatively large on Fig. 9.24.

The two families of characteristics cross each other on Fig. 9.36. At such a point of intersection, the concentration has two values, C_o and zero, and the solution of Eq. (6.25) is discontinuous. The concentration wave moves through the bed as a "shock wave" as in the upper part of Fig. 9.36. The velocity of translation of this wave is found from a material balance. During the time t required for the wave to emerge from the packing of depth z, the total amount of solute flowing in is $C_o v\ t$; non flows out. The quantity that accumulates in the bed is $\epsilon C_o z + \rho_B q_o^* z$. Equating the two quantities gives:

$$\frac{z}{t} = \frac{V}{1 + (\rho_B/\epsilon)(q_o^*/C_o)} \qquad (9.14)$$

The experimental breakthrough time for the adsorption of n-alkanes from HK on zeolite Type-5A at the optimum condition was reached after 2700 s. For the same condition, the breakthrough time is reached after 1200 s as predicted by the model using the method of characteristics (see Fig. 9.36).

It would appear that there is no local equilibrium exists in the dynamic flow system because of the short contact time between

the fluid and the solid phase, e.g. (volume of bed x ϵ /volumetric flowrate = 431 s).

The method of analysis (the calibration curve between n-alkanes content and the RI) (Fig. 9.2) may have affected the results.

It is noteworthy to say that the BET-equation is usually used for predicting the equilibrium isotherm of binary system, whereas a multicomponent system is being used in this study.

The equilibrium isotherm curve (Fig.9.24) which has been abstracted from the dynamic flow system (BT-curve) is inserted into this model, which is quite different than the equilibrium isotherm obtained from a batch system since the contact time in both cases is different.

This explanation reveals the difference in starting up the breakthrough time of the process between the experimental value and that predicted by the model.

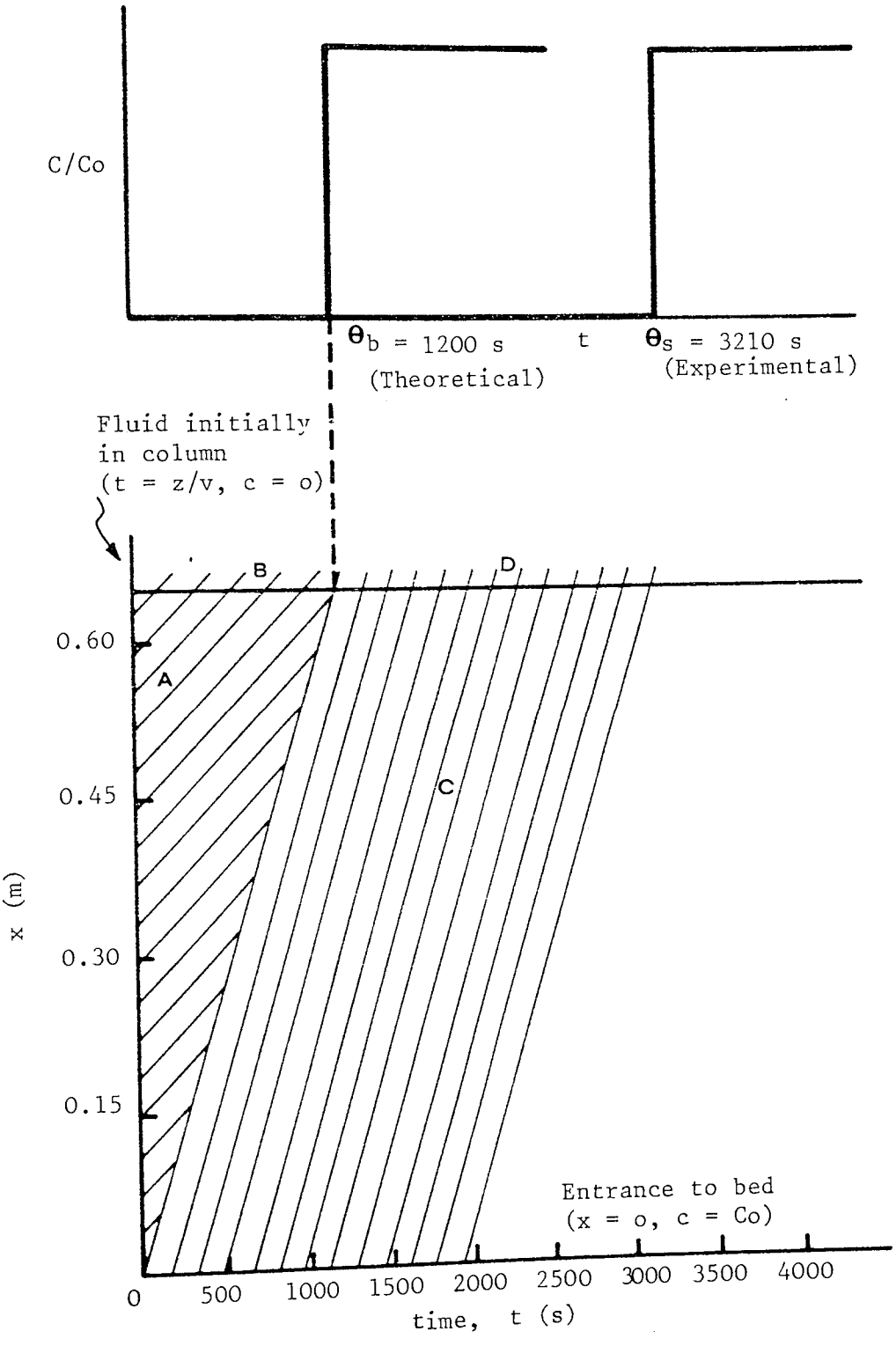

Fig. 36 Graphical solution of fixed-bed sorption problem using the BET-equilibrium.

CONCLUSIONS

CONCLUSIONS

1. The value of refractive index was found to be a useful indicator of the content of n-alkanes present in the denormalised kerosene. This has agreed very well with the n-alkanes concentration as determined by the GLC.

2. An optimum operating condition for multicomponent adsorption of n-alkanes on zeolite type-5A has been achieved corresponding to a feed flowrate of 33.33×10^{-9} m^3/s, a temperature of 643 K, and a pellet particle size of $1.0\text{-}2.0 \times 10^{-3}$m. This set of conditions yielded a height of mass transfer zone of 0.206 m and a dynamic capacity of 9.653×10^{-2} kg n-paraffins/kg of zeolite. The laboratory findings obtained could serve as a basis for design of a commercial plant.

3. The nitrogen flowrate was found to have a significant effect on the height of mass transfer zone but had less effect on the dynamic capacity of zeolite.

4. It has been possible to utilize the data of the dynamic flow system (breakthrough curve) to establish the equilibrium isotherm curve. This is based on the assumption that each point on the curve is considered to be at local equilibrium. The BET-equation has been used to predict the equilibrium isotherm theoretically and this was found to give a reasonable agreement with the experimental results.

5. The diffusion coefficients of n-alkanes were determined by Eltekov's Equation and were found to always give higher values than those predicted by the Barrer-Brooke's Equation for the same range of flowrates and adsorption temperatures. The diffusion coefficient was found to be directly proportional to the adsorbent pellet particle size as predicted by Eltekov's Equation.

6. When using steam as the desorbing agent without intermediate reactivation of zeolite, multicycle adsorption had a significant effect on reducing the dynamic capacity of the adsorbent and on increasing the height of mass transfer zone.

7. By reactivation, the zeolite adsorbent kept its efficiency, with no significant loss or change in the dynamic capacity.

8. When using steam as a desorbing agent, the amount of n-alkanes desorbed and the desorption efficiency were found to increase with the rise of the desorption temperature.

9. Normal-hexane was found to be the best desorbing agent compared with steam and n-pentane. The corresponding desorption efficiency was 88.2%. The amount desorbed by n-hexane was 6.938×10^{-3} kg n-alkanes.

10. The steam flowrate was found to have an effect on the equilibrium desorption time. For the same desorption cycle number, it was noticed that the desorption time increased as the steam flowrate increased.

11. The concentration of n-alkanes as determined by GLC was found to be 18.75 wt% in heavy kerosene, and 7.09 wt% in denormalized kerosene. The concentration of total aromatic hydrocarbon, determined by UV-analysis was 22.82 wt% in heavy kerosene, and 17.71 wt% in denormalized kerosene. Three types of aromatics were found. These included the alkyl benzene compounds, the naphthalene compounds, and the phenanthrene and anthracene compounds. Benzene compounds or the mono-aromatics represented the highest wt% among the others.

12. The purity of the n-paraffin product achieved using steam as the desorbing agent was 83.24 wt% N-alkanes in the range of n-C_{15} to n-C_{19} represented more than 85% of the total n-alkanes in the product. The total aromatic hydrocarbons found in the product was 5.5 wt%, of which 92 wt% was of the alkyl benzene compounds.

13. The pour point of HK dropped from -12°C to -42°C in the denormalized kerosene by the process of adsorption. The denormalized kerosene could be used as a fuel in cold climate conditions.

14. The surface area of the fresh zeolite was found to be 512 x $10^3 m^2/kg$. This area was reduced to 320 x $10^3 m^2/kg$ after reactivation, and was reduced sharply to 95 x $10^3 m^2/kg$ after the first adsorption run immediately without reactivation of zeolite.

RECOMMENDATION FOR FUTURE WORK

RECOMMENDATIONS FOR FUTURE WORK

1. The effect of feed composition and its variations on optimum operating conditions of adsorption should be evaluated for different kerosene cuts such as straight-run kerosene and kerosene-diesel.

2. The effect of adsorption column material, height, and diameter on the dynamic flow system should be investigated so that more quantitative design data could be obtained.

3. A study of the dynamic properties of multicomponent n-alkanes adsorption on zeolite in the liquid phase is recommended in order to compare the results obtained with those of vapor-phase adsorption. This can be carried out at temperatures not exceeding 503 K (230°C) since the initial boiling point of heavy kerosene (the feed used in this study) is 505.5 K (232.5°C). Prior to using clay-bound molecular sieves in a liquid-phase process, treatment with liquid water will be required at less than 175°C followed by drying to a moisture content of 1.8 wt% which increases the exchange rate for n-paraffins and desensitizes the sieves to surface poisons (84). This requires very high pressures Aromatics and oxygen containing impurities adversely affect the rate of adsorption by molecular sieves in liquid-phase operation. These should be removed by adsorption on silica gel, other molecular sieves, alumina, or activated carbon (84).

4. That the optimum normal paraffin content that could be removed without lowering the quality of the denormalized products should be tested. This study could be carried concurrently with the normal paraffin recovery study and should reveal the amount of economically recoverable normal paraffins from different petroleum fractions.

5. The performance of n-hexane was found to be superior to that of steam. However, if the molecular sieves can be modified to reduce the equilibrium loading of water at desorption temperatures, then steam can be recommended on the grounds of lower cost and easier separation from the product. Experimental work is required to find these optimum conditions.

APPENDIX (A)

Experimental Data of the Breakthrough Curves

Table A.1 Experimental data of the breakthrough-curve of n-paraffins adsorption from HK at 16.66 x 10^{-9} m^3/s, 643 K, and zeolite particle size of 1.0-2.0 x 10^{-3}m.

Sample No.	Time x 10^{-2}(s)	RI @ 298 K	Conc.(Wt%)	Vol. Collected x 10^6(m^3)
1	6	1.4652	0	2.2
2	12	1 4654	0	2.3
3	18	1.4656	0	2.5
4	24	1.4656	0	2.7
5	30	1.4656	0	2.8
6	36	1.4654	0	2.8
7	42	1.4654	0	2.8
8	48	1.4654	0	2.8
9	54	1.4652	0	2.8
10	60	1.4652	0	2.9
11	66	1.4651	0	2.9
12	72	1 4648	0	3.2
13	75	1.4643	0	1.6
14	78	1.4636	1.25	1.7
15	81	1.4627	4.06	1.7
16	84	1.4610	9.37	1.8
17	87	1.4598	13.13	1.6
18	90	1.4592	15.00	1.6
19	93	1.4588	16.25	1.5
20	96	1.4586	16.88	1.7
21	102	1.4582	18.13	3.5
22	108	1.4580	18.75	3.6
23	114	1.4580	18.75	3.6
24	120	1.4580	18.75	2.4
Total				59.3 x 10^{-6} m^3

Table A.2 Experimental data of the breakthrough-curve of n-paraffins adsorption from HK at 22.22 x 10^{-9} m^3/s, 643 K, and zeolite particle size of 1.0-2.0 x 10^{-3}m.

Sample No.	Time x 10^{-2}(s)	RI @ 298 K	Conc.(Wt%)	Vol. Collected x 10^6(m^3)
1	6	1.4646	0	2.4
2	12	1.4643	0	2.7
3	18	1.4646	0	2.9
4	24	1.4649	0	3.9
5	30	1.4646	0	6.0
6	36	1.4648	0	6.0
7	42	1.4648	0	4.9
8	48	1.4644	0	5.5
9	49.5	1.4635	1.56	1.6
10	51	1.4628	3.75	1.7
11	52.5	1.4615	7.81	1.6
12	54	1.4596	13.75	1.6
13	55.5	1.4592	15.0	1.5
14	57	1.4589	15.94	1.5
15	60	1.4585	17.19	2.9
16	66	1.4582	18.13	5.9
17	72	1.4580	18.75	6.3
18	78	1.4580	18.75	6.3
Total				65.2 x 10^{-6} m^3

Table A.3 Experimental data of the breakthrough-curve of n-paraffins adsorption from HK at 33.33 x 10^{-9} m^3/s, 643 K, and zeolite particle size of 1.0-2.0 x $10^{-3}m$.

Sample No.	Time x 10^{-2}(s)	RI @ 298 K	Conc.(Wt%)	Vol. Collected x 10^6(m^3)
1	6	1.4640	0	10.1
2	12	1.4642	0	10.0
3	18	1.4642	0	9.6
4	24	1.4640	0	10.1
5	30	1.4628	3.75	10.9
6	31.5	1.4608	10.00	2.8
7	33	1.4593	14.69	3.0
8	34.5	1.4586	16.88	2.7
9	36	1.4581	18.44	3.1
10	42	1.4580	18.75	12.0
11	48	1.4580	18.75	7.4
Total				81.7 x 10^{-6} m^3

Table A.4 Experimental data of the breakthrough-curve of n-paraffins adsorption from HK at 44.44 x 10^{-9} m^3/s, 643 K, and zeolite particle size of 1.0-2.0 x $10^{-3}m$.

Sample No.	Time x 10^{-2}(s)	RI @ 298 K	Conc.(Wt%)	Vol. Collected x $10^6(m^3)$
1	6	1.4646	0	12. 3
2	12	1.4646	0	12.2
3	18	1.4648	0	12.1
4	21	1.4643	0	6.0
5	22.5	1.4639	0.31	2.9
6	24	1.4632	2.50	2.8
7	25.5	1.4622	5.62	2.9
8	27	1.4604	11.25	3.1
9	28.5	1.4594	14.38	2.9
10	30	1.4587	16.56	2.8
11	36	1.4581	18.44	12.5
12	42	1.4580	18.75	12.6
Total				85.1 x $10^{-6}m^3$

Table A.5 Experimental data of the breakthrough-curve of n-paraffins adsorption from HK at 50.00 x 10^{-9} m^3/s, 643 K, and zeolite particle size of 1.0-2.0 x $10^{-3}m$.

Sample No.	Time x 10^{-2}(s)	RI @ 298 K	Conc.(Wt%)	Vol. Collected x $10^6(m^3)$
1	6	1.4641	0	15.0
2	12	1.4639	0.31	15.2
3	15	1.4631	2.81	7.5
4	16.5	1.4621	5.94	3.8
5	18	1.4593	14.69	3.7
6	19.5	1.4584	17.50	3.9
7	21	1.4583	17.81	3.8
8	24	1.4582	18.13	7.6
9	27	1.4580	18.75	7.7
10	30	1.4580	18.75	7.8
11	36	1.4580	18.75	15.0
Total				91.0 x $10^{-6}m^3$

Table A.6 Experimental data of the breakthrough-curve of n-paraffins adsorption from HK at 33.33 x 10^{-9} m^3/s, 603 K, and zeolite particle size of 1.0-2.0 x 10^{-3}m.

Sample No.	Time x 10^{-2}(s)	RI @ 298 K	Conc.(Wt%)	Vol. Collected x $10^6(m^3)$
1	6	1.4636	1.25	14.0
2	12	1.4635	1.56	12.3
3	15	1.4628	3.75	6.9
4	16.5	1.4621	5.94	3.3
5	18	1.4605	10.94	3.5
6	19.5	1.4597	13.44	3.6
7	21	1.4591	15.31	3.8
8	22.5	1.4587	16.56	3.7
9	24	1.4584	17.50	3.6
10	30	1.4581	18.44	12.8
11	36	1.4580	18.75	10.0
12	42	1.4580	18.75	16.8
Total				94.3 x $10^{-6}m^3$

Table A.7 Experimental data of the breakthrough-curve of n-paraffins adsorption from HK at 33.33 x 10^{-9} m^3/s, 623 K, and zeolite particle size of 1.0-2.0 x $10^{-3}m$.

Sample No.	Time x 10^{-2}(s)	RI @ 298 K	Conc.(Wt%)	Vol. Collected x $10^{6}(m^3)$
1	6	1.4647	0	9.1
2	12	1.4649	0	10.3
3	18	1.4650	0	10.6
4	24	1.4638	0.62	7.3
5	27	1.4623	5.31	5.8
6	28.5	1.4612	8.75	2.9
7	30	1.4599	12.81	2.9
8	33	1.4592	15.00	5.1
9	36	1.4588	16.25	5.2
10	42	1.4582	18.13	12.2
11	48	1.4582	18.13	17.1
12	54	1.4581	18.44	13.3
13	60	1.4581	18.44	10.6
14	66	1.4580	18.75	4.9
15	72	1.4580	18.75	5.9
Total				123.2 x $10^{-6}m^3$

Table A.8 Experimental data of the breakthrough-curve of n-paraffins adsorption from HK at 33.33 x 10^{-9} m^3/s, 643 K, and zeolite particle size of 1.0-2.0 x 10^{-3}m.

Sample No.	Time x 10^{-2}(s)	RI @ 298 K	Conc.(Wt%)	Vol. Collected x 10^6(m^3)
1	6	1.4640	0	10.1
2	12	1.4642	0	10.0
3	18	1.4642	0	9.6
4	24	1.4640	0	10.1
5	30	1.4628	3.75	10.9
6	31.5	1.4608	10.00	2.8
7	33	1.4593	14.69	3.0
8	34.5	1.4586	16.88	2.7
9	36	1.4581	18.44	3.1
10	42	1.4580	18.75	12.0
11	48	1.4580	18.75	7.4
Total				81.7 x 10^{-6} m^3

Table A.9 Experimental data of the breakthrough-curve of n-paraffins adsorption from HK at 33.33 x 10^{-9} m^3/s, 663 K, and zeolite particle size of 1.0-2.0 x $10^{-3}m$.

Sample No.	Time x 10^{-2}(s)	RI @ 298 K	Conc.(Wt%)	Vol. Collected x $10^{6}(m^3)$
1	6	1.4653	0	8.3
2	12	1.4655	0	2.5
3	18	1.4650	0	9.4
4	24	1.4647	0	8.4
5	25.5	1.4640	0	2.3
6	27	1.4634	1.87	2.3
7	28.5	1.4625	4.69	2.4
8	30	1.4613	8.44	2.2
9	31.5	1.4606	10.63	2.2
10	33	1.4600	12.50	2.3
11	34.5	1.4596	13.75	2.2
12	36	1.4590	15.63	2.3
13	39	1.4587	16.56	4.4
14	42	1.4584	17.50	4.5
15	48	1.4581	18.44	7.4
16	54	1.4580	18.75	7.0
17	60	1.4580	18.75	8.2
18	66	1.4580	18.75	7.8
Total				86.1 x $10^{-6}m^3$

Table A.10 Experimental data of the breakthrough-curve of n-paraffins adsorption from HK at 33.33 x 10^{-9} m^3/s, 683 K, and zeolite particle size of 1.0-2.0 x $10^{-3}m$.

Sample No.	Time x 10^{-2}(s)	RI @ 298 K	Conc.(Wt%)	Vol. Collected x $10^6(m^3)$
1	6	1.4647	0	8.2
2	12	1.4650	0	9.5
3	18	1.4653	0	9.9
4	21	1.4645	0	6.4
5	22.5	1.4639	0.31	3.1
6	24	1.4627	4.06	3.3
7	25.5	1.4602	11.88	3.2
8	27	1.4594	14.38	3.4
9	30	1.4588	16.25	6.6
10	33	1.4584	17.50	6.1
11	36	1.4583	17.81	6.3
12	42	1.4583	17.81	13.2
13	48	1.4581	18.44	13.0
14	54	1.4581	18.44	13.4
15	60	1.4580	18.75	13.9
16	66	1.4580	18.75	9.3
Total				128.8 x $10^{-6}m^3$

Table A.11 Experimental data of the breakthrough-curve of n-paraffins adsorption from HK at 33.33 x 10^{-9} m^3/s, 643 K, and zeolite particle size of <0.5 x 10^{-3}m.

Sample No.	Time x 10^{-2}(s)	RI @ 298 K	Conc.(Wt%)	Vol. Collected x 10^6(m^3)
1	6	1.4616	7.50	18.1
2	12	1.4620	6.25	17.8
3	18	1.4615	7.81	18.6
4	21	1.4608	10.00	9.2
5	22.5	1.4602	11.88	4.6
6	24	1.4590	15.63	4.6
7	25.5	1.4586	16.88	4.7
8	27	1.4583	17.81	4.8
9	30	1.4580	18.75	9.5
10	36	1.4580	18.75	19.1
11	42	1.4580	18.75	19.2
Total				130.2 x $10^{-6}m^3$

Table A.12 Experimental data of the breakthrough-curve of n-paraffins adsorption from HK at 33.33 x 10^{-9} m^3/s, 643 K, and zeolite particle size of 0.5-1.0 x 10^{-3}m.

Sample No.	Time x 10^{-2}(s)	RI @ 298 K	Conc.(Wt%)	Vol. Collected x 10^{6}(m^3)
1	6	1.4629	3.44	15.2
2	12	1.4632	2.50	15.6
3	18	1.4624	5.00	16.1
4	19.5	1.4617	7.19	4.0
5	21	1.4608	10.00	4.1
6	22.5	1.4593	14.69	4.0
7	24	1.4589	15.94	4.1
8	27	1.4585	17.19	8.3
9	30	1.4583	17.81	8.5
10	36	1.4581	18.44	17.0
11	42	1.4580	18.75	17.0
12	48	1.4580	18.75	15.9
Total				129.8 x $10^{-6}m^3$

Table A.13 Experimental data of the breakthrough-curve of n-paraffins adsorption from HK at 33.33 x 10^{-9} m^3/s, 643 K, and zeolite particle size of 1.0-2.0 x 10^{-3}m.

Sample No.	Time x 10^{-2}(s)	RI @ 298 K	Conc.(Wt%)	Vol. Collected x 10^{6}(m^3)
1	6	1.4640	0	10.1
2	12	1.4642	0	10.0
3	18	1.4642	0	9.6
4	24	1.4640	0	10.1
5	30	1.4628	3.75	10.9
6	31.5	1.4608	10.00	2.8
7	33	1.4593	14.69	3.0
8	34.5	1.4586	16.88	2.7
9	36	1.4581	18.44	3.1
10	42	1.4580	18.75	12.0
11	48	1.4580	18.75	7.4
Total				81.7 x 10^{-6} m^3

Table A.14 Experimental data of the breakthrough-curve of n-paraffins adsorption from HK at 33.33 x 10^{-9} m^3/s, 643 K, and zeolite particle size of 2.0-3.0 x 10^{-3}m.

Sample No.	Time x 10^{-2}(s)	RI @ 298 K	Conc.(Wt%)	Vol. Collected x 10^{6}(m^3)
1	6	1.4639	0.31	7.6
2	12	1.4640	0	8.2
3	18	1.4636	1.25	8.5
4	21	1.4630	3.12	4.1
5	22.5	1.4625	4.69	2.1
6	24	1.4617	7.19	2.1
7	25.5	1.4609	9.69	2.3
8	27	1.4601	12.19	2.3
9	28.5	1.4595	14.06	2.3
10	30	1.4591	15.31	2.4
11	33	1.4586	16.88	4.7
12	36	1.4583	17.81	4.8
13	42	1.4581	18.44	9.6
14	48	1.4580	18.75	9.7
15	54	1.4580	18.75	13.2
Total				83.9 x $10^{-6}m^3$

Table A.15 Effect of Nitrogen gas flowrate on the experimental results of breakthrough of n-paraffins sepration from HK by adsorption on zeolite type-5A at HK flowrate of 33.33 x $10^{-9}m^3/s$, 643 K, and zeolite particle size of 1.0 - 2.0 x $10^{-3}m$.

N2 - Flowrate		67 x 10^{-7} (m^3/s)		13.3 x 10^{-7} (m^3/s)	
Sample No.	Time 10^{-2}x (s)	Conc. (wt%)	Vol. Collected 10^6 x (m^3)	Conc. (wt%)	Vol. Collected 10^6 (m^3)
1	6	0	10.1	0.31	10.6
2	12	0	10.0	0	10.4
3	18	0	9.6	0.31	10.2
4	24	0	10.1	1.56	10.4
5	30	3.75	10.9	6.56	11.0
6	31.5	10.00	2.8	14.06	3.0
7	33	14.69	3.0	15.94	3.2
8	34.5	16.88	2.7	17.50	2.9
9	36	18.44	3.1	18.75	3.3
10	42	18.75	12.0	18.75	3.3
11	48	18.75	7.4	-	-

APPENDIX (B)

Calculation of the Dynamic Capacity of Zeolite

Table B.1 Calculation of the dynamic capacity of zeolite at $16.66 \times 10^{-9} m^3/s$, 643 K, and zeolite particle size of $1.0\text{-}2.0 \times 10^{-3} m$.

Volume Collected $\times 10^6$ (m^3)	W $\times 10^3$ (kg)	WCo $\times 10^3$ (kg)	WC $\times 10^3$ (kg)
2.2	1.8174	0.3408	0
2.3	1.9000	0.3563	0
2.5	2.0653	0.3872	0
2.7	2.2305	0.4182	0
2.8	2.3131	0.4337	0
2.8	2.3131	0.4337	0
2.8	2.3131	0.4337	0
2.8	2.3131	0.4337	0
2.8	2.3131	0.4337	0
2.9	2.3957	0.4492	0
2.9	2.3957	0.4492	0
3.2	2.6435	0.4957	0
1.6	1.3218	0.2478	0
1.7	1.4044	0.2633	0.0176
1.7	1.4044	0.2633	0.0570
1.8	1.4870	0.2788	0.1393
1.6	1.3218	0.2478	0.1736
1.6	1.3218	0.2478	0.1983
1.5	1.2392	0.2324	0.2014
1.7	1.4044	0.2633	0.2371
3.5	2.8914	0.5421	0.5241
3.6	2.9740	0.5576	0.5576
3.6	2.9740	0.5576	0.5576
2.4	1.9826	0.3717	0.3717
Total 59.3	48.9877	9.1386	3.0353

Amount adsorbed $= \Sigma WCo - \Sigma WC = (9.1386\text{-}3.0353) \times 10^{-3} = 6.1033 \times 10^{-3}$ kg n-Paraffins.

Ad $= 6.1033 \times 10^{-3} kg / 81.24 \times 10^{-3} kg = 7.513 \times 10^{-2}$ kg n-paraffins/kg of zeolite.

Table B.2 Calculation of the dynamic capacity of zeolite at 22.22 x $10^{-9}m^3/s$, 643 K, and zeolite particle size of 1.0-2.0 x $10^{-3}m$.

Volume Collected x 10^6 (m^3)	W x 10^3 (kg)	WCo x 10^3 (kg)	WC x 10^3 (kg)
2.4	1.9826	0.3717	0
2.7	2.2305	0.4182	0
2.9	2.3957	0.4492	0
3.9	3.2218	0.6041	0
6.0	4.9566	0.9294	0
6.0	4.9566	0.9294	0
4.9	4.0479	0.7590	0
5.5	4.5436	0.8520	0
1.6	1.3218	0.2478	0.0206
1.7	1.4044	0.2633	0.0527
1.6	1.3218	0.2478	0.1032
1.6	1.3218	0.2478	0.1817
1.5	1.2392	0.2324	0.1859
1.5	1.2392	0.2324	0.1975
2.9	2.3957	0.4492	0.4118
5.9	4.8740	0.9139	0.8834
6.3	5.2044	0.9758	0.9758
6.3	5.2044	0.9758	0.9758
Total 65.2	53.8	10.0992	3.9884

Amount adsorbed = $\Sigma WCo - \Sigma WC = (10.0992-3.9884)^{x\ 10^{-3}} = 6.1108 \times 10^{-3}$ kg n-Paraffins.

Ad = $6.1108 \times 10^{-3}kg/81.512 \times 10^{-3}kg = 7.497 \times 10^{-2}$ kg n-paraffins/kg of zeolite.

Table B.3 Calculation of the dynamic capacity of zeolite at $33.33 \times 10^{-9} m^3/s$, 643 K, and zeolite particle size of $1.0\text{-}2.0 \times 10^{-3} m$.

Volume Collected x 10^6 (m^3)	W x 10^3 (kg)	WCo x 10^3 (kg)	WC x 10^3 (kg)
10.1	8.3436	1.5644	0
10.0	8.2610	1.5489	0
9.6	7.9306	1.4870	0
10.1	8.3436	1.5644	0
10.9	9.0045	1.6883	0.3377
2.8	2.3131	0.4337	0.2313
3.0	2.4783	0.4647	0.3641
2.7	2.2305	0.4182	0.3765
3.1	2.5609	0.4802	0.4722
12.0	9.9132	1.8587	1.8587
7.4	6.1131	1.1462	1.1462
Total 81.7	67.4924	12.6547	4.7867

Amount adsorbed $= \Sigma WCo - \Sigma WC = (12.6547\text{-}4.7867) \times 10^{-3} = 7.868 \times 10^{-3}$ kg n-Paraffins.

Ad $= 7.868 \times 10^{-3} kg / 81.512 \times 10^{-3} kg = 9.653 \times 10^{-2}$ kg n-paraffins/kg of zeolite.

Table B.4 Calculation of the dynamic capacity of zeolite at 44.44 x $10^{-9}m^3/s$, 643 K, and zeolite particle size of 1.0-2.0 x $10^{-3}m$.

Volume Collected x 10^6 (m^3)	W x 10^3 (kg)	WCo x 10^3 (kg)	WC x 10^3 (kg)
12.3	10.1610	1.9052	0
12.2	10.0784	1.8897	0
12.1	9.9958	1.8742	0
6.0	4.9566	0.7807	0
2.9	2.3957	0.4492	0.0074
2.8	2.3131	0.4337	0.0578
2.9	2.3957	0.4492	0.1346
3.1	2.5609	0.4802	0.2881
2.9	2.3957	0.4492	0.3445
2.8	2.3131	0.4337	0.3830
12.5	10.3263	1.9362	1.9042
12.6	10.4089	1.9517	1.9517
Total 85.1	70.3011	13.1815	5.0713

Amount adsorbed = $\Sigma WCo - \Sigma WC = (13.1815-5.0713)^{x\ 10^{-3}} = 8.1102 \times 10^{-3}$ kg n-Paraffins.

Ad = 8.1102 x 10^{-3}kg/84.4 x 10^{-3}kg = 8.145 x 10^{-2} kg n-paraffins/kg of zeolite.

Table B.5 Calculation of the dynamic capacity of zeolite at 50.00 x $10^{-9}m^3/s$, 643 K, and zeolite particle size of 1.0-2.0 x $10^{-3}m$.

Volume Collected x 10^6 (m^3)	W x 10^3 (kg)	WCo x 10^3 (kg)	WC x 10^3 (kg)
15.0	12.3915	2.3234	0
15.2	12.5567	2.3544	0.0389
7.5	6.1958	1.1617	0.1741
3.8	3.1392	0.5886	0.1865
3.7	3.0566	0.5731	0.4490
3.9	3.2218	0.6041	0.5638
3.8	3.1392	0.5886	0.5591
7.6	6.2784	1.1772	1.1383
7.7	6.3610	1.1927	1.1927
7.8	6.4436	1.2082	1.2083
15.0	12.3915	2.3234	2.3234
Total 91.0	75.1751	14.0954	7.8340

Amount adsorbed = $\Sigma WCo - \Sigma WC = (14.0954-7.8340)^{x\ 10^{-3}} = 6.2614 \times 10^{-3}$ kg n-Paraffins.

Ad = $6.2614 \times 10^{-3}kg/81.568 \times 10^{-3}kg = 7.676 \times 10^{-2}$ kg n-paraffins/kg of zeolite.

Table B.6 Calculation of the dynamic capacity of zeolite at 33.33 x $10^{-9}m^3/s$, 603 K, and zeolite particle size of 1.0-2.0 x $10^{-3}m$.

Volume Collected x 10^6 (m^3)	W x 10^3 (kg)	WCo x 10^3 (kg)	WC x 10^3 (kg)
14.0	11.5654	2.1685	0.1446
12.3	10.1610	1.9052	0.1585
6.9	5.7001	1.0688	0.2138
3.3	2.7261	0.5111	0.1619
3.5	2.8914	0.5421	0.3163
3.6	2.9740	0.5576	0.3997
3.8	3.1392	0.5886	0.4806
3.7	3.0566	0.5731	0.5062
3.6	2.9740	0.5576	0.5205
12.8	10.5741	1.9826	1.9500
10.0	8.2610	1.5490	1.5490
16.8	13.8785	2.6022	2.6022
Total 94.3	77.9012	14.6064	9.0033

Amount adsorbed = $\Sigma WCo - \Sigma WC = (14.6064-9.0033)^{x\ 10^{-3}} = 5.6031 \times 10^{-3}$ kg n-Paraffins.

Ad = 5.6031 x 10^{-3}kg/84.68 x 10^{-3}kg = 6.617 x 10^{-2} kg n-paraffins/kg of zeolite.

Table B.7 Calculation of the dynamic capacity of zeolite at $33.33 \times 10^{-9} m^3/s$, 623 K, and zeolite particle size of $1.0\text{-}2.0 \times 10^{-3} m$.

Volume Collected x 10^6 (m^3)	W x 10^3 (kg)	WCo x 10^3 (kg)	WC x 10^3 (kg)
9.1	7.5175	1.4095	0
10.3	8.5088	1.5954	0
10.6	8.7567	1.6419	0
7.3	6.0305	1.1307	0.0374
5.8	4.7914	0.8984	0.2544
2.9	2.3957	0.4492	0.2096
2.9	2.3957	0.4492	0.3069
5.1	4.2131	0.7900	0.6320
5.2	4.2957	0.8054	0.6981
12.2	10.0784	1.8897	1.8272
17.1	14.1263	2.6487	2.5611
13.3	10.9871	2.0601	2.0260
10.6	8.7567	1.6419	1.6147
4.9	4.0471	0.7590	0.7590
5.9	4.8740	0.9139	0.9139
Total 123.2	101.7755	19.0830	11.8403

Amount adsorbed = $\Sigma WCo - \Sigma WC = (19.0830\text{-}11.8403) \times 10^{-3} = 7.2427 \times 10^{-3}$ kg n-Paraffins.

Ad = $7.2427 \times 10^{-3} kg / 87.592 \times 10^{-3} kg = 8.269 \times 10^{-2}$ kg n-paraffins/kg of zeolite.

Table B.8 Calculation of the dynamic capacity of zeolite at $33.33 \times 10^{-9} m^3/s$, 643 K, and zeolite particle size of $1.0\text{-}2.0 \times 10^{-3} m$.

Volume Collected x 10^6 (m^3)	W x 10^3 (kg)	WCo x 10^3 (kg)	WC x 10^3 (kg)
10.1	8.3436	1.5644	0
10.0	8.2610	1.5489	0
9.6	7.9306	1.4870	0
10.1	8.3436	1.5644	0
10.9	9.0045	1.6883	0.3377
2.8	2.3131	0.4337	0.2313
3.0	2.4783	0.4647	0.3641
2.7	2.2305	0.4182	0.3765
3.1	2.5609	0.4802	0.4722
12.0	9.9132	1.8587	1.8587
7.4	6.1131	1.1462	1.1462
Total 81.7	67.4924	12.6547	4.7867

Amount adsorbed = $\Sigma WCo - \Sigma WC = (12.6547\text{-}4.7867)^{x\ 10^{-3}} = 7.868 \times 10^{-3}$ kg n-Paraffins.

Ad = $7.868 \times 10^{-3} kg / 81.512 \times 10^{-3} kg = 9.653 \times 10^{-2}$ kg n-paraffins/kg of zeolite.

Table B.9 Calculation of the dynamic capacity of zeolite at 33.33 x $10^{-9}m^3/s$, 663 K, and zeolite particle size of 1.0-2.0 x $10^{-3}m$.

Volume Collected x 10^6 (m^3)	W x 10^3 (kg)	WCo x 10^3 (kg)	WC x 10^3 (kg)
8.3	6.8566	1.2856	0
2.5	2.0653	0.3872	0
9.4	7.7653	1.4560	0
8.4	6.9392	1.3011	0
2.3	1.9000	0.3563	0
2.3	1.9000	0.3563	0.0355
2.4	1.9826	0.3717	0.0930
2.2	1.8174	0.3408	0.0852
2.2	1.8174	0.3408	0.1534
2.3	1.9000	0.3563	0.2020
2.2	1.8174	0.3408	0.2272
2.3	1.9000	0.3563	0.2613
4.4	3.6348	0.6815	0.5681
4.5	3.7175	0.6970	0.6156
7.4	6.1131	1.1462	1.0698
7.0	5.7827	1.0843	1.0843
8.2	6.7740	1.2701	1.2701
7.8	6.4436	1.2082	1.2082
Total 86.1	71.1270	13.3365	6.8737

Amount adsorbed = $\Sigma WCo - \Sigma WC = (13.3365-6.8737) \times 10^{-3} = 6.4628 \times 10^{-3}$ kg n-Paraffins.

Ad = $6.4628 \times 10^{-3}kg / 83.16 \times 10^{-3}kg = 7.772 \times 10^{-2}$ kg n-paraffins/kg of zeolite.

Table B.10 Calculation of the dynamic capacity of zeolite at 33.33 x $10^{-9}m^3/s$, 683 K, and zeolite particle size of 1.0-2.0 x $10^{-3}m$.

Volume Collected x 10^6 (m^3)	W x 10^3 (kg)	WCo x 10^3 (kg)	WC x 10^3 (kg)
8.2	6.7740	1.2701	0
9.5	7.8480	1.4715	0
9.9	8.1784	1.5335	0
6.4	5.2870	0.9913	0
3.1	2.5609	0.4802	0.0079
3.3	2.7261	0.5111	0.1107
3.2	2.6435	0.4957	0.3140
3.4	2.8087	0.5266	0.4039
6.6	5.4523	1.0223	0.8860
6.1	5.0392	0.9449	0.8819
6.3	5.2044	0.9758	0.9269
13.2	10.9045	2.0446	1.9421
13.0	10.7393	2.0136	1.9803
13.4	11.0697	2.0756	2.0413
13.9	11.4828	2.1530	2.1530
9.3	7.6827	1.4405	1.4405
Total 128.8	106.4015	19.9503	13.0885

Amount adsorbed = $\Sigma WCo - \Sigma WC = (19.9503-13.0885) \times 10^{-3} = 6.8618 \times 10^{-3}$ kg n-Paraffins.

Ad = $6.8618 \times 10^{-3}kg / 84.187 \times 10^{-3}kg = 8.151 \times 10^{-2}$ kg n-paraffins/kg of zeolite.

Table B.11 Calculation of the dynamic capacity of zeolite at $33.33 \times 10^{-9} m^3/s$, 643 K, and zeolite particle size of $< 0.5 \times 10^{-3} m$.

Volume Collected x 10^6 (m^3)	W x 10^3 (kg)	WCo x 10^3 (kg)	WC x 10^3 (kg)
18.1	14.9524	2.8036	1.1214
17.8	14.7046	2.7571	0.9190
18.6	15.3655	2.8810	1.2000
9.2	7.6001	1.4250	0.7600
4.6	3.8001	0.7125	0.4515
4.6	3.8001	0.7125	0.5940
4.7	3.8827	0.7280	0.6554
4.8	3.9653	0.7435	0.7062
9.5	7.8480	1.4715	1.4715
19.1	15.7785	2.9585	2.9585
19.2	15.8611	2.9740	2.9740
Total 130.2	107.5584	20.1672	13.8115

Amount adsorbed = $\Sigma WCo - \Sigma WC = (20.1672-13.8115) \times 10^{-3} = 6.3557 \times 10^{-3}$ kg n-Paraffins.

Ad = $6.3557 \times 10^{-3} kg / 85.32 \times 10^{-3} kg = 7.449 \times 10^{-2}$ kg n-paraffins/kg of zeolite.

Table B.12 Calculation of the dynamic capacity of zeolite at $33.33 \times 10^{-9} m^3/s$, 643 K, and zeolite particle size of $0.5\text{-}1.0 \times 10^{-3} m$.

Volume Collected $\times 10^6$ (m^3)	W $\times 10^3$ (kg)	WCo $\times 10^3$ (kg)	WC $\times 10^3$ (kg)
15.2	12.5567	2.3544	0.4320
15.6	12.8872	2.4164	0.3322
16.1	13.3002	2.4938	0.6650
4.0	3.3044	0.6196	0.2376
4.1	3.3870	0.6351	0.3387
4.0	3.3044	0.6196	0.4854
4.1	3.3870	0.6351	0.5399
8.3	6.8566	1.2856	1.1786
8.5	7.0219	1.3166	1.2506
17.0	14.0437	2.6332	2.5897
17.0	14.0437	2.6332	2.6332
15.9	13.1350	2.4628	2.4628
Total 129.8	107.2278	20.1054	13.1357

Amount adsorbed $= \Sigma WCo - \Sigma WC = (20.1054\text{-}13.1357) \times 10^{-3} = 6.9695 \times 10^{-3}$ kg n-Paraffins.

Ad $= 6.9695 \times 10^{-3} kg / 84.13 \times 10^{-3} kg = 8.284 \times 10^{-2}$ kg n-paraffins/kg of zeolite.

Table B.13 Calculation of the dynamic capacity of zeolite at 33.33 x $10^{-9}m^3/s$, 643 K, and zeolite particle size of 1.0-2.0 x $10^{-3}m$.

Volume Collected x 10^6 (m^3)	W x 10^3 (kg)	WCo x 10^3 (kg)	WC x 10^3 (kg)
10.1	8.3436	1.5644	0
10.0	8.2610	1.5489	0
9.6	7.9306	1.4870	0
10.1	8.3436	1.5644	0
10.9	9.0045	1.6883	0.3377
2.8	2.3131	0.4337	0.2313
3.0	2.4783	0.4647	0.3641
2.7	2.2305	0.4182	0.3765
3.1	2.5609	0.4802	0.4722
12.0	9.9132	1.8587	1.8587
7.4	6.1131	1.1462	1.1462
Total 81.7	67.4924	12.6547	4.7867

Amount adsorbed = $\Sigma WCo - \Sigma WC = (12.6547-4.7867)^{x\ 10^{-3}} = 7.868 \times 10^{-3}$ kg n-Paraffins.

Ad = $7.868 \times 10^{-3}kg/81.512 \times 10^{-3}kg = 9.653 \times 10^{-2}$ kg n-paraffins/kg of zeolite.

Table B.14 Calculation of the dynamic capacity of zeolite at 33.33 x $10^{-9}m^3/s$, 643 K, and zeolite particle size of 2.0-3.0 x $10^{-3}m$.

Volume Collected x 10^6 (m^3)	W x 10^3 (kg)	WCo x 10^3 (kg)	WC x 10^3 (kg)
7.6	6.2784	1.1772	0.0195
8.2	6.7740	1.2701	0
8.5	7.0219	1.3166	0.0878
4.1	3.3870	0.6351	0.1057
2.1	1.7348	0.3253	0.0814
2.1	1.7348	0.3253	0.1247
2.3	1.9000	0.3563	0.1841
2.3	1.9000	0.3563	0.2316
2.3	1.9000	0.3563	0.2671
2.4	1.9826	0.3717	0.3035
4.7	3.8827	0.7280	0.6554
4.8	3.9653	0.7435	0.7062
9.6	7.9306	1.4870	1.4624
9.7	8.0132	1.5025	1.5025
13.2	10.9045	2.0446	2.0446
Total 83.90	69.3098	12.9958	7.7765

Amount adsorbed = ΣWCo - ΣWC = $(12.9958-7.7765) \times 10^{-3} = 5.2191 \times 10^{-3}$ kg n-Paraffins.

Ad = 5.2191×10^{-3}kg/84.19×10^{-3}kg = 6.199×10^{-2} kg n-paraffins/kg of zeolite.

APPENDIX (C)

Prediction of the Equilibrium Isotherm of n-Paraffins Adsorption on Zeolite Type-5A from the BT-Data

Using the local-equilibrium theory for the adsorption curve, the method of characteristic shows that at each point

$$\frac{t}{Z} = \frac{1}{V^*} = \frac{1}{V}\left(1 + \frac{\rho_B}{\epsilon}\,\frac{dq^*}{dc}\right)$$

$$\text{or} \quad f'(c) = \frac{dq^*}{dc} = \frac{\epsilon}{\rho_B}\left(\frac{Vt}{Z} - 1\right) \qquad (6.25)$$

$$= \frac{0.109}{0.624}\left[\frac{34}{65}\,t - 1\right]$$

$$= 0.0914\,t - 0.175 \quad \text{(gmole) (cm}^3\text{) / (gm) (gmole)}$$

The breakthrough data ha·tbeen applied at a feed flowrate of 33.33×10^{-9} m^3/s, and a temperature of 643 K. As a sample calculation, take the point at t = 3000 s, where $C = 0.2\,C_o = 0.2 \times \frac{18.75 \times 0.8261}{100 \times 215} = 1.441 \times 10^{-4}$ gmole/cm^3 ; $dq^*/dc = 274.025$ cm^3/gm.

Similar values of the slope of the equilibrium line ha ve been calculated at all the concentrations. Starting at $\overline{C} = 0$, where $q^* = 0$, values of q* (c) were found by numerical integration (see Table C.1). The following Table presents the results.

C, gmole/cm^3 x 10^4	q*, gmole/gm
0	0
0.721	0.0355
2.642	0.1030
4.743	0.1561
6.065	0.1820
6.786	0.2013
7.145	0.2055

Table C.1 Prediction of the Equilibrium Values of Adsorption at Different Concentrations at a Feed Flowrate of 33.33 x 10^{-9} m^3/s, and a Temperature of 643 K.

t	C	ΔC	$\frac{dq^*}{dc}$	$\frac{dq}{dm}$	$q^* = q_n + \frac{dq}{dm}\Delta C$	$\overline{C}$
s	gmole/cm^3 x 10^4	gmole/cm^3 x 10^4	cm^3/gm	cm^3/gm	gmole/gm x 10^4	gmole/cm^3 10_4
0	0		-0.175			
		0		109.505	0	0
2400	0		219.185			
		1.441		246.605	355.36	0.721
3000	1.441		274.025			
		2.401		280.880	1029.75	2.642
3150	3.842		287.735			
		1.802		294.590	1560.60	4.743
3300	5.644		301.445			
		0.842		308.300	1820.19	6.065
3450	6.486		315.155			
		0.599		322.010	2013.07	6.786
3600	7.085		328.865			
		0.119		356.285	2055.47	7.145
4200	7.204		383.705			

★ Notes:

$\Delta C = C_{n+1} - C_n$

$\frac{dq^*}{dc}$ = is found from Eq. (6.25)

$$\frac{dq}{dm} = \left[\left(\frac{dq^*}{dc} \right)_{n+1} + \left(\frac{dq^*}{dc} \right)_n \right] / 2$$

$$\overline{C} = \left(C_{n+1} + C_n \right) / 2$$

APPENDIX (D)

Calculation of the Diffusion Coefficients and the Superficial Velocity of the Vapor Mixture

Table D.1 Calculation of the diffusion coefficient for n-paraffins separation from HK by adsorption on zeolite type-5A at different flow rates, 643 K, and particle size of 1.0-2.0 x 10^{-3}m, using Barrer-Brook's equation.

Flowrate x 10^3 (m^3/s)	($\pi/4\tau$) x 10^4 (s^{-1})	$(V/S_{ex})^2$ x 10^8 (m^2)	$\left(\frac{Ad}{Am}\right)^2$	De x 10^{10} (m^2/s)
16.66	2.469	25	0.6433	0.397
22.22	5.233	25	0.7708	1.008
33.33	7.850	25	0.7068	1.387
44.44	6.382	25	0.6270	1.000
50.00	11.894	25	0.6052	1.800

Table D.2 Calculation of the diffusion coefficient for n-paraffins separation from HK by adsorption on zeolite type-5A at different adsorption temperatures, 33.33 x $10^{-9}m^3/s$, and particle size of 1.0-2.0 x $10^{-3}m$, using Barrer-Brook's equation.

Adsorption Temp. (K)	$(\pi/4\tau) \times 10^4$ (s^{-1})	$(V/S_{ex})^2 \times 10^8$ (m^2)	$\left(\frac{Ad}{Am}\right)2$	De x 10^{10} (m^2/s)
603	7.072	25	0.5520	0.976
623	4.220	25	0.5200	0.549
643	7.850	25	0.7068	1.387
663	3.584	25	0.4649	0.417
683	5.131	25	0.5676	0.728

Table D.3 Calculation of the diffusion coefficient for n-paraffins separation from HK by adsorption on zeolite type-5A at different particle sizes of zeolite pellets, $33.33 \times 10^{-9} m^3/s$ and 643 K, using Barrer-Brook's equation.

Particle Size x 10^3 (m)	$(\pi/4\tau) \times 10^4$ (s^{-1})	$(V/S_{ex})^2 \times 10^8$ (m^2)	$\left(\frac{Ad}{\overline{Am}}\right)^2$	De x 10^{10} (m^2/s)
<0.5	7.696	25	0.4932	0.949
0.5 - 1.0	6.230	25	0.7133	1.111
1.0 - 2.0	7.850	25	0.7068	1.387
2.0 - 3.0	4.673	25	0.4957	0.579

Table D.4 Calculation of the superficial-velocity of the vapor mixture in the adsorption column at different flowrates, 643 K, and zeolite particle size of 1.0-2.0 x 10^{-3} m.

Flowrate x 10^9 (m^3/s)	M_{N_2} x 10^5 (mole/s)	M_K x 10^5 (mole/s)	M_T x 10^5 (mole/s)	V_T x 10^7 (m^3/s)	V_b x 10^6 (m^3)	Vads x 10^6 (m^3)	V_v x 10^6 (m^3)	A x 10^6 (m^2)	Super. Velocity (m/s)	Linear Velocity (m/s)
16.66	2.727	5.735	8.462	44.65	130.62	116.06	14.56	22.4	0.20	0.022
22.22	2.727	7.648	10.375	54.74	130.62	116.45	14.17	21.8	0.25	0.027
33.33	2.727	11.472	14.199	74.92	130.62	116.45	14.17	21.8	0.34	0.037
44.44	2.727	15.297	18.024	95.10	130.62	116.53	14.09	21.7	0.44	0.047
50.00	2.727	17.210	19.937	105.20	130.62	120.57	10.05	15.5	0.68	0.052

Table D.5 Calculation of the superficial-velocity of the vapor mixture in the adsorption column at different adsorption temperatures, 33.33×10^{-9} m^3/s, and zeolite particle size of $1.0\text{-}2.0 \times 10^{-3}$ m.

Ads. Temp. (K)	$M_{N_2} \times 10^5$ (mole/s)	$M_K \times 10^5$ (mole/s)	$M_T \times 10^5$ (mole/s)	$V_T \times 10^7$ (m^3/s)	$V_b \times 10^6$ (m^3)	Vads $\times 10^6$ (m^3)	$V_v \times 10^6$ (m^3)	$A \times 10^6$ (m^2)	Super. Velocity (m/s)	Linear Velocity (m/s)
603	2.727	11.472	14.199	70.26	130.62	120.92	9.65	14.9	0.47	0.035
623	2.727	11.472	14.199	72.59	130.62	125.13	5.49	8.5	0.85	0.036
643	2.727	11.472	14.199	74.92	130.62	116.45	14.17	21.8	0.34	0.037
663	2.727	11.472	14.199	77.25	130.62	118.80	11.82	18.2	0.42	0.038
683	2.727	11.472	14.199	79.58	130.62	120.27	10.35	15.9	0.50	0.039

Table D.6 Calculation of the superficial-velocity of the vapor mixture in the adsorption column at different zeolite particle sizes, 643 K, and 33.33 x 10^{-9} m^3/s.

Particle Size 10^3(m)	M_{N_2} x 10^5 (mole/s)	M_K x 10^5 (mole/s)	M_T x 10^5 (mole/s)	V_T x 10^7 (m^3/s)	V_b x 10^6 (m^3)	Vads x 10^6 (m^3)	V_v x 10^6 (m^3)	A x 10^6 (m^2)	Super. Velocity (m/s)	Linear Velocity (m/s)
0.5	2.727	11.472	14.199	74.92	130.62	121.89	8.73	13.4	0.56	0.037
0.5-1.0	2.727	11.472	14.199	74.92	130.62	120.19	10.43	16.0	0.47	0.037
1.0-2.0	2.727	11.472	14.199	74.92	130.62	116.45	14.17	21.8	0.34	0.037
2.0-3.0	2.727	11.472	14.199	74.92	130.62	120.27	10.35	15.9	0.47	0.037

APPENDIX (E)

Sample Calculation

E.1. Calculation of the Vapor-Mixture Velocity:

By calculating the vapor-mixture velocity, two points should be taken into consideration.

1) The velocity of importance is the superficial velocity and not the linear velocity.
2) The vapor-mixture includes the kerosene vapor in admixture with nitrogen gas. As an example, let us consider the following operating condition.

- A feed flowrate of 16.66×10^{-9} m^3/s (60 cm^3/hr)
- An adsorption temperature of 643 K.
- An adsorbent pellet particle size of $(1.0\text{-}2.0) \times 10^{-3}$ m and
- A nitrogen flowrate of 40 cm^3/min @ 298 K and atmospheric pressure.

The calculation procedures are as follows:

$$\text{No. of moles of } N_2 = \frac{1 \text{ atm} \times 40 \text{ cm}^3/\text{min}}{82.06 \text{ cm}^3 \text{ atm/gmole K} \times 298 \text{ K}}$$

$$= 1.636 \times 10^{-3} \text{ gmole/s}$$

$$\text{i.e. No. of Moles of } N_2 = 2.727 \times 10^{-5} \text{ gmoles/s}$$

$$\text{No. of moles of kerosene vapor mixture} = \frac{16.66 \times 10^{-9} \text{ m}^3/\text{s} \times 0.8261 \text{ gm/cm}^3}{240 \text{ gm/gmole}}$$

$$= 5.735 \times 10^{-5} \text{ gmole/s}$$

$$\text{Total molar flow} = (2.727 + 5.735) \times 10^{-5} = 8.462 \times 10^{-5} \text{ gmole/s}$$

$$\text{Total volume} = \frac{8.462 \times 10^{-5} \text{ gmole/s} \times 82.06 \text{ cm}^3 \text{ atm} \times 643 \text{ K}}{\text{gmole K} \times \text{atm}}$$

$$= 44.65 \times 10^{-7} \text{ m}^3/\text{s}$$

Volume of the adsorption column $= \pi D^2 L/4 = 130.624 \times 10^{-6}$ m^3

Volume of adsorbent = Weight of adsorbent / bulk density of adsorbent

V_{ads} = 81.24 gm / 0.7 (gm/cm^3)

= 116.059×10^{-6} m^3

Volume of voids V_v = $(130.624 - 116.057) \times 10^{-6} = 14.567 \times 10^{-6}$ m^3

This voids volume corresponds to a cross-section area) = 14.567×10^{-6} $m^3/0.65$ m.

A = 22.411×10^{-6} m^2

The superficial velocity of the vapor mixture) = 44.65×10^{-7} (m^3/s) x $22.41 \times 10^{-6} m^2$

V = 1.992×10^{-1} m/s

= 0.2 m/s

E.2. Calculation of the Dynamic Capacity of Zeolite:

Let us consider the same operating condition as mentioned in E.1.

The procedure of calculation proceed as follows:

The first fraction of effluent collected from the adsorption process has a volume of 2.2 cm^3 of denormalized kerosene.

The weight of this volume = 2.2 cm^3 x 0.8261 gm/cm^3)

= 1.8174×10^{-3} kg

The original concentration of n-alkanes in the fraction = 18.75 wt%

hence,

The original weight of n-alkanes in the fraction before adsorption

= $0.1875 \times 1.8174 \times 10^{-3}$

= 0.3408×10^{-3} kg

The concentration of n-alkanes in the fraction after adsorption = 0 wt%

i.e. the weight of n-alkanes in the fraction = $0 \times 1.8174 \times 10^{-3} = 0$

This means that all the n-alkanes in the fractions have been adsorbed.

If the same procedures are repeated for the other collected fractions upto the saturation point, then as seen in Table B.1. of Appendix B:

The total volume collected up to the saturation point = 59.3×10^{-6} m^3

The weight of this volume = 48.9877×10^{-3} kg

The weight of n-alkanes in this volume before adsorption = 9.1386×10^{-3} kg

The weight of n-alkanes in this volume after adsorption = 3.0353×10^{-3} kg

The weight of n-alkanes adsorbed =$(9.1386 - 3.0353) \times 10^{-3} = 6.1033 \times 10^{-3}$ kg

This weight is adsorbed in 81.24×10^{-3} kg of zeolite adsorbent

This means the dynamic capacity of zeolite = 7.513×10^{-2} kg n-alkanes/kg of zeolite.

i.e. 7.513 gm n-alkanes / 100 gm of zeolite.

E.3 Calculation of the Diffusion Coefficient:

A) By Eltekov's Equation:

For the same operating condition mentioned in E.1, the diffusion coefficient is calculated as follows:

The superficial velocity = 0.2 m/s

The dynamic capacity is found as 7.513×10^{-2} kg of n-alkanes/ kg of zeolite

The efficiency of the adsorption column = 80.62% (Table 9.4)

The maximum adsorption capacity q_m $= 7.513 \times 10^{-2} / 0.8062$

$= 9.319 \times 10^{-2}$ kg n-alkanes/ kg of zeolite

Converting this capacity to mmole/cm^3

A_m = (9.319 gm n-alkanes/100 gm zeolite) x (0.7 gm zeolite/cm^3 zeolite) x (mole n-alkane/215 gm n-alkane) x (1000 mmole n-alkane/mole n-alkane)

= 0.303 mmole n-alkanes/cm^3 zeolite

The original concentration of n-alkanes in the feed C_o = 18.75 wt%

By converting this concentration to mmole of n-alkanes/cm^3 kerosene

then C_o = 0.720 mmole n-alkanes

$\tau = \theta_E - \theta_B$ = 9780 - 6600 = 3180 sec (Table 9.1)

Porosity of adsorbent = 43% = ϵ

Adsorbent radius = r = 0.075 cm (using size 1.0 - 2.0 x 10^{-3}m)

Then by substituting in Eltekov's Equation:

$$\text{Diffusion coefficient } De^{-1} = \frac{6\ \tau\ (1-\epsilon)}{r^2} - \frac{12\ A_m}{rvC_o}$$

De^{-1} = 1933440 - 338.9

De^{-1} = 1933101.1 s/cm^2

De = 5.172 x 10^{-7} cm^2/s

= 5.172 x 10^{-11} m^2/s

B) By Barrer-Brook's Equation:

$$De = \left(\frac{\pi}{4\tau}\right) \left(\frac{V}{S_{ex}}\right)^2 \left(\frac{A_d}{A_m}\right)^2$$

The detailed calculation is illustrated in Table D.1 through D.3 of Appendix D.

APPENDIX (F)

Prediction of the Equilibrium Isotherm of n-Paraffins Adsorption on Zeolite Type-5A by the BET-Equation

The BET equation predicts the value of adsorption (q)

where,

$$q = \frac{q_m \beta (f-1) X (1-X)}{1 + (\beta f - 1) X} \qquad (F.1)$$

and β is an unknown parameter

By rearranging,

$$\frac{X (I-X)}{q} = \frac{1}{\beta q_m (f-1)} + \frac{1}{q_m} X \qquad (F.2)$$

and solving equation F.2 for trial values of β such that the value of q_m obtained coincide with the experimental value.

The successful trial $\beta = 1.0$, gives :

$$\frac{X (I-X)}{q} = \frac{1}{q_m (f-1)} + \frac{1}{q_m} X \qquad (F.3)$$

i.e. the intercept $b = \frac{1}{q_m (f-1)}$, and

$$\tan \alpha = \frac{1}{q_m}$$

From Table F.1 and Fig. F.1 in Appendix F :

$b = 0.44 \times 10^{-4}$ g/mmole

$$\tan \alpha = \frac{1.12 \times 10^{-4}}{0.08} = 14 \times 10^{-4} \text{ g/mmole}$$

i.e., $14 \times 10^{-4} = \frac{1}{q_m}$ or $q_m = 714.28$ mmole/g

and $0.44 \times 10^{-4} = \frac{1}{714.28 (f-1)}$

gives $f = 30.817$

Then, the BET quation becomes as :

$$q = \frac{21297.7\ x\ (1 - x)}{1 + 29.817\ x} \qquad (F.4)$$

Insertion of values into eq. (F.4) predicts the theoretical value of adsorption (q). The result is shown in Fig. (9.24)

Table F.1 The equilibrium relationship between the concentration of n-alkanes in the vapor-phase and the value of adsorption (q) at a feed flowrate of 33.33 x 10^{-9} m^3/s, a temperature of 643 K, and a zeolite particle size of (1.0 - 2.0) x 10^{-3} m.

Concentration (C) $(gmole/cm^3).10^4$	Concentration (X) (mole fraction)	X (1 - X)/q $(g/mmole).10^4$	q_{exp} (mmole/g)	$q_{theor.}$ (mmole/g)
0	0	0	0	0
0.721	0.0188	5.2	35.5	251.7
2.642	0.0688	6.2	103.0	447.2
4.743	0.1234	6.9	156.1	492.3
6.065	0.1578	7.3	182.0	496.1
6.786	0.1766	7.2	201.3	494.3
7.145	0.1860	7.4	205.5	492.6

FIG. F.1 Prediction of the constants in the BET-equation.

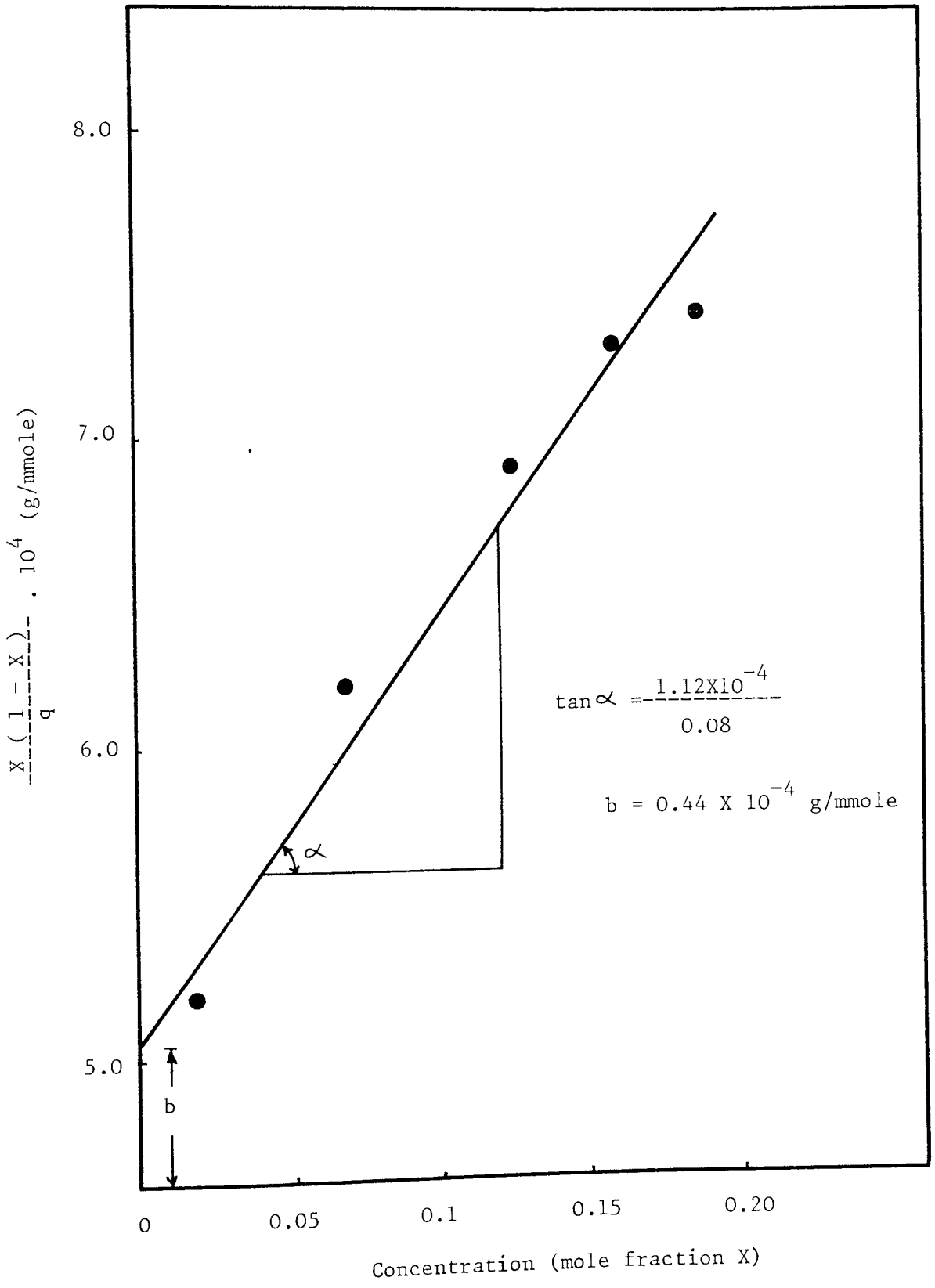

APPENDIX (G)

A Regression Program Used for the Adsorption Isotherm Determination

```
 30 INPUT "DEGREE OF EQUATION: ";D
 39 REM DIMENSION A(*),R(*,*),T(*) ACCORDING TO DEGREE OF EQUATION
 40 DIM A(2 * D + 1),R(D + 1,D + 2),T(D + 2)
 60 INPUT "NUMBER OF KNOWN POINTS:";N
 80 A(1) = N
 89 REM ENTER COORDINATES OF DATA POINTS
 90 FOR I = 1 TO N
100 PRINT "X,Y  OF POINT ";I;
110 INPUT " :";X,Y
119 REM LINES 120-200 POPULATE MATRICES WITH A SYSTEM OF EQUATION
120 FOR J = 2 TO 2 * D + 1
130 A(J) = A(J) + X ^ (J - 1)
140 NEXT J
150 FOR K = 1 TO D + 1
160 R(K,D + 2) = T(K) + Y * X ^ (K - 1)
170 T(K) = T(K) + Y * X ^ (K - 1)
180 NEXT K
190 T(D + 2) = T(D + 2) + Y ^ 2
200 NEXT I
209 REM LINES 210-480 SOLVE THE SYSTEM OF EQUATION IN THE MATRICES
210 FOR J =1 TO D + 1
220 FOR K = 1 TO D + 1
230 R(J,K) = A(J +K - 1)
240 NEXT K
250 NEXT J
260 FOR J =1 TO D + 1
270 K = J
280 IF R(K,J) < 0 OR R(K,J) > 0 THEN 320
290 K = K + 1
295 IF K < D + 1 THEN 280
300 PRINT CHR$ (7);"NO UNIQUE SOLUTION"
310 GO TO 790
320 FOR I = 1 TO D + 2
330 S = R(J,I)
340 R(J,I) = R(K,I)
350 R(K,I) = S
360 NEXT I
370 Z = 1 / R(J,J)
380 FOR I = 1 TO D + 2
390 R(J,I) = Z * R(J,I)
400 NEXT I
410 FOR K = 1 TO D + 1
```

```
420 IF K = J THEN 470
430 Z = - R(K,J)
440 FOR I = 1 TO D + 2
450 R(K,I) = R(K,I) + Z * R(J,I)
460 NEXT I
470 NEXT K
480 NEXT J
495 PRINT TAB( 13)"CONSTANT = ";R(1,D + 2)
499 REM PRINT EQUATION COEFFICIENTS
500 FOR J = 1 TO D
510 PRINT J;"DEGREE COEFFICIENT =" ;R(J + 1,D + 2)
520 NEXT J
530 PRINT
539 REM COMPUTE REGRESSION ANALYSIS
540 P= 0
550 FOR J = 2 TO D + 1
560 P = P + R(J,D + 2) * (T(J) - A(J) * T(1) / N )
570 NEXT J
580 Q = T(D + 2) - T(1) ^ 2 / N
590 Z = Q - P
600 I = N - D - 1
620 PRINT
630 J = P / Q
640 PRINT "COEFFICIENT OF": PRINT "DETERMINATION (R^2) = ";J
650 PRINT "COEFFICIENT OF" : PRINT "CORRELATION = ";SQR (J)
660 PRINT "STANDERD ERROR OF ESTIMATE = "; SQR (Z / I)
670 PRINT
679 REM COMPUT Y-COORDINATE FROM ENTERED X-COORDINATE
680 PRINT "INTERPOLATION (0 TO END PROGRAM)"
690 P = R(1,D + 2)
700 INPUT "VALUE OF X:";X
720 IF X = 0 THEN 790
730 FOR J = 1 TO D
740 P = P + R(J + 1,D + 2 ) * X ^ J
750 NEXT J
760 PRINT TAB( 10)"Y = ";P
770 PRINT
780 GOTO 680
790 END
```

```
>RUN
DEGREE OF EQUATION: ?2
NUMBER OF KNOWN POINTS:?6
X,Y  OF POINT 1 :?0.0000721,0.035536
X,Y  OF POINT 2 :?0.0002642,0.102975
X,Y  OF POINT 3 :?0.0004743,0.156060
X,Y  OF POINT 4 :?0.0006065,0.1821019
X,Y  OF POINT 5 :?0.0006786,0.201307
X,Y  OF POINT 6 :?0.0007145,0.205547
            CONSTANT = 9.8767893E-3
         1DEGREE COEFFICIENT =382.532081
         2DEGREE COEFFICIENT =-153042.901


COEFFICIENT OF
DETERMINATION (R^2) = 0.998745269
COEFFICIENT OF
CORRELATION = 0.999372438
STANDERD ERROR OF ESTIMATE = 3.03664638E-3




INTERPOLATION (0 TO END PROGRAM)
VALUE OF X:?0.0000721
          Y = 3.66617726E-2

INTERPOLATION (0 TO END PROGRAM)
VALUE OF X:?0.0002642
          Y = 0.10025912

INTERPOLATION (0 TO END PROGRAM)
VALUE OF X:?0.0004743
          Y = 0.156883149

INTERPOLATION (0 TO END PROGRAM)
VALUE OF X:?0.0006065
          Y = 0.185586851

INTERPOLATION (0 TO END PROGRAM)
VALUE OF X:?0.0006786
          Y = 0.198987116

INTERPOLATION (0 TO END PROGRAM)
VALUE OF X:?0.0007145
          Y = 0.205065991

INTERPOLATION (0 TO END PROGRAM)
VALUE OF X:?0
```

APPENDIX (H)

A Paper on : " Optimal Separation of n-Paraffins From Kuwait Kerosene Using a Molecular Sieve Adsorbent ".

TO BE PUBLISHED IN THE

JOURNAL OF APPLIED CHEMISTRY AND BIOTECHNOLOGY

Aston University

Content has been removed for copyright reasons

Aston University

Content has been removed for copyright reasons

NOMENCLATURE

NOMENCLATURE

Å	:	Angstrom
A_z	:	Cross-sectional area of the adsorbent bed, m^2.
A_d	:	Dynamic capacity of zeolite, kg n-alkanes/100 kg of zeolite.
A	:	Cross-sectional area of the adsorbent column equivalent to a volume of V_v, m^2.
A_m	:	Maximum dynamic capacity of zeolite and found as Ad/γ , kg n-alkanes/100 kg of zeolite.
a	:	The total surface in a unit volume of packed space used in Eq.6.21, m^2.
ABS	:	Alkylbenzene sulfonate.
BT-Curve	:	Breakthrough Curve.
b	:	A constant found in Appendix F and equal to $\{q_m (F-1)\}^{-1}$.
C	:	Concentration of adsorbate in effluent, kg adsorbate/kg of feed.
C_o	:	Original concentration of adsorbate in the feed, kg adsorbate/kg of feed.
c	:	Concentration of adsorbate in the fluid stream, moles/m^3.
Ca_b, Ca_n, Ca_f	:	The content of benzene, naphthalene and phenanthrene nuclei respectively (wt%), found from Eq.8.1 to 8.3.
C_b, C_n, C_f	:	The content of benzene, naphthalene and phenanthrene hydrocarbons found from Eq. 8.4 to 8.6.
D	:	Diameter of the adsorbent bed, m.
$\overline{D}$	:	Optical density of the paraffin test sample {Eq.8.7}.
D_e	:	Diffusion coefficient, m^2/s.
d	:	Density used in Eq. 2.1.
F	:	The adsorption coefficient found from Appendix F.
f	:	Fractional saturation of the adsorbent within the MTZ at the breakthrough point.
G	:	Superficial mass velocity of fluid, $kg/m^2.s$.

$\overline{G}$: The total amount of adsorbate adsorbed at any time θ, kg.

HMTZ : Height of mass transfer zone, m.

HK : Heavy kerosene.

K_A : Adsorption equilibrium constant.

K_{200}, K_{230}, K_{255} : Specific extinction coefficients of sample adsorption in ranges 200, 230 and 255 nm wavelength and can be calculated from Eq.8.7.

k : A factor based on a unit of exterior particle surface used in Eq.6.21.

LAB : Linear alkylbenzene or linear detergent alkyllate.

LAS : Linear alkylbenzene sulfonates.

LES : Length of equivalent equilibrium section, m.

LUB : Length of unused bed, m.

MS-5A : Linde molecular sieve Type-5A.

L_s : Position of stoichiometric front, distance from inlet end of bed, m.

ΔL : Increase in length of the equivalent equilibrium section, m.

M : Molecular weight.

$\overline{M}$: A symbol for an alkali metal such as Na and K, or alkaline earth metals like Ca, Mg, Sr. {used in the unit cell formula of zeolite}.

M_{N_2} : Molar flowrate of nitrogen gas, moles/s.

M_K : Molar flowrate of kerosene, moles/s.

M_T : Total molar flowrate ($M_{N_2} + M_K$), moles/s.

M_r : Molar refraction used in Eq. 2.1.

MTZ : Mass Transfer Zone.

M.S. : Molecular Sieves.

m_a : The weight of adsorbent, kg {Eq.9.2}.

m : The weight of solution, kg {Eq.9.2}.

NMR : Nulcear magnetic resonance.

$\overline{n}$: Refractive index used in Eq.2.1.

n- : Normal-

n : The valence of the cation used in the formula for a unit cell of zeolite.

PVC	:	Polyvinylchloride.
Q	:	The feed volumetric flowrate, m^3/s.
q	:	Solid-phase concentration of adsorbed material, moles/kg of adsorbent.
q*	:	The equilibrium number of moles of adsorbate per unit mass of solid, moles/kg of adsorbent.
q_m	:	The capacity of the adsorbent corresponding to complete coverage of the surface, moles/kg of adsorbent.
q^*_o	:	The equilibrium number of moles of adsorbate per unit mass of solid corresponding to C_o, moles/kg of adsorbent.
R	:	Radius of the adsorbent bed, m.
RI	:	Refractive index.
r	:	Equilibrium constant used in Eq.6.22 and equal to $(k + K_A C_o^{-1})$.
$\bar{r}$	:	Radius of the adsorbent particle, m.
(S_{ex}/V)	:	The ratio of the external surface of a granule to its total volume taken as $20\ cm^2/cm^3$.
SCP	:	Single cell protein.
SFA	:	Synthetic fatty acids.
t	:	Time, s.
δt	:	Time interval, s.
U	:	Front velocity, $(G\Delta Y / \rho_B \Delta X)$, m/s.
UV	:	Ultra-Violet.
V	:	Velocity of fluid in interstices of bed, m/s.
V*	:	Concentration propagation or wave velocity, m/s.
V_{ads}	:	Volume of the adsorbent, m^3.
V_b	:	Volume of the adsorbent column, m^3.
V_T	:	Total volumetric flowrate of kerosene and nitrogen, m^3/s.
V_v	:	Volume of the voids in the adsorbent column, m^3.
W_{SB}	:	Weight of the adsorbent in a short bed, kg.
W_{MTZ}	:	Weight of the adsorbent in a steady-state mass transfer zone, kg.
WES	:	Weight of adsorbent in equivalent equilibrium section, kg.

WUB	:	Weight of unused bed, kg.
w	:	Weight of adsorbate, kg.
$\overline{X}$	:	Adsorbent loading, kg/100 kg of activated adsorbent.
X_e	:	Equilibrium zone, or upstream, adsorbate loading, kg/100 kg of activated adsorbent.
X_o	:	Initial, or downstream, adsorbate loading, kg/100 kg of activated adsorbent.
ΔX	:	Delta loading, $X_e - X_o$, kg/100 kg of activated carbon.
ΔX_{MTZ}	:	Average delta loading in steady-state mass transfer zone, kg/100 kg of activated adsorbent.
ΔX_{SB}	:	Average delta loading in a short bed, kg/100 kg of activated adsorbent.
X	:	Mole fraction used in Eq. 9.5, moles of adsorbate/moles of feed.
x	:	An integer used in the formula for a unit cell of zeolite.
Y_o	:	Effluent, or downstream, concentration of adsorbable component, kg/kg of feed.
Y_e	:	Inlet, or upstream, concentration of adsorbable component, kg/kg of feed.
ΔY	:	Change in concentration of adsorbable component in fluid, $Y_e - Y_o$, kg/100 kg of feed.
y	:	An integer used in the formula for a unit cell of zeolite.
$\overline{Z}$	:	The number of moles of water of crystalization, used in the formula for zeolite unit cell.
Z	:	Distance from the base of the adsorbent column, m.
δz	:	Thickness of an element of the adsorbent bed, m.

Greek letters:

θ	:	Time, s.
θ_o	:	Initial time, s.
θ_B or θ_b	:	Time at which breakthrough occurs, s.
θ_E or θ_e	:	Time at which the adsorbent bed reaches saturation, or the exhaustion time, s.
θ_s	:	Time at which the stoichiometric front exists from the adsorbent bed, s.
$\theta_{b_{SB}}$	:	Breakthrough time for a bed whose length is shorter than a steady-state transfer zone, s.
$\Delta\theta$	:	Time increment, s.
τ	:	The time difference between and $_B$, s.
β	:	The coefficient of mutual displacement, defined as the ratio of molar volumes of components 1 and 2.
γ	:	Effective efficiency of the adsorbent column, %.
ρ_B	:	Bulk density of the adsorbent, kg/m^3.
ρ_{HK}	:	Density of heavy kerosene, 826.1 kg/m^3.
ϵ	:	Fractional void volume of the packed-bed.

LIST OF REFERENCES

1. Al-Ameeri, R.S.; Owaysi, F.A., Ind. Eng. Chem. Prod. Res. Dev., 23 (4), 634 (1984).

2. Chandra, D.; Sodhi, J.S.; Gulati, J.B., Chem. Age India, 22, 282 (1971).

3. Mahta, J.N.; Saraf, D.N.; Singhal, A.K., Petroleum & Hydrocarbons, 7 (4), 257 (1973).

4. Shukla, R.P.; Singhal, A.K.; Saraf, D.N., Indian Chemical Engineer, XXI (2), 13 (1979).

5. Barrer, R.M.; Belchetz, L., Transactions of the Faraday Society, XL, 195-216 (1944).

6. Ruthren, D.M., AIChE J., 22, 753 (1976).

7. Ruthren, D.M., Loughlin, K.F.; Halborow, K.A., Chem. Eng. Sci., 28, 701 (1973).

8. Sundstrom, D.W.; Krautz, F.G., J. Chem. Eng. Data, 13 (2), 223 (1968).

9. Benachrelli, E.M., Rep. Acad. Sci. USSR, 50 (2), 345 (1968)

10. Avery, W.F., U.S. Patent 3422005, January 14, 1969.

11. Freund, M. & et al., "Paraffin Products", Elsevier Scientific Publishing Company, N.Y. (1982).

12. Owaysi, F.A., "Proposal on Isolation and Purification of Liquid Paraffin", KISR, Nov. (1982).

13. Igenim, P.G., Chemistry & Technology of Fuels & Oils, No.2, 18 (1974).

14. Igenim, P.G., Chemistry & Technology of Fuels & Oils, No.6, 26 (1962).

15. Michielova, I.A.; Lulova, N.I.; Postonov, V.V., Chemistry & Technology of Fuels & Oils, No.2, 15 (1975).

16. Symoniak, M.F., Chemical Engineering, 76, 172 (1969).

17. Peterson, D.L., Redlich, O., J. of Chem. Eng. Data, 7 (4), 570 (1962).

18. Brooks, K.W., Oil & Gas J., 58 (35), 89 (1960).

19. Corano, Z., "Cagaky Cosi.", 14 (8), 434 (1970) (Japan).

20. Trafford, J.E.; Quartano, R.N., Hydrocarbon Processing, 48 (1), 134 (1969).

21. Owaysi, F.A., "Proposal on Isolation and Purification of Liquid Paraffin", KISR, March (1981).

22. Nayer, B.C. & et al., Chem. Eng. World, XV (11), 37 (1980).

23. Allen, J.L., "The Kinetics of Adsorption of Pure Hydrocarbons by Synthetic Zeolites", Ph.D. Thesis, Clarkson College of Technology (1964).

24. Sodhi, J.S.; Chandra, D., Petroleum & Hydrocarbons, 4 (4), 1970.

25. Hirsch, C.K., "Molecular Sieves", Reinhold Publishing Corp., N.Y. (1961).

26. Barrer, R.M., J. Am. Chem. Soc., 82, 1041 (1960).

27. Breck, D.M., "Zeolite Molecular Sieves", Wiley Interscience, N.Y. (1974).

28. Tsurvizumi, A., Bull. Chem. Soc., 34, 1457 (1961) (Japan).

29. Breck, D.W. & et al., J. Am. Chem. Soc., 78 (23) 5963-5967 (1956).

30. Griesmer & et al., Chem. Eng. Prog. Symp. Ser., 24 (55), 45-50 (1959).

31. Turkevich, J., Catalysis Reviews, 1 (1), 1-35 (1967).

32. Breck, D.W., J. Chem. Educ., 41, 678 (1964).

33. Reed, T.B.; Breck, D.W., J. Am. Chem. Soc., 78, 5972 (1956).

34. Hassan, A.M., "The Adsorption of Straight Chain Hydrocarbons From Ternary Liquid Salution by 5A-Molecular Sieves Crystals", Ph.D. Thesis, Carnell University (1975).

35. Norman,N.L. , " Recent Developments in Separation Science" , Chemeical Rubber Company Press, New Jersey (1976).

36. Myers, H.S.; Hipkin, H.G., Petroleum Refiner, 35 (7), 175 (1956).

37. Roberts, P.V.; Yosk, R., Ind. Eng. Chem. Proc. Des. Dev., 6 (4), 516 (1967).

38. Rabo, J.A., "Zeolite Chemistry & Catalysis", American Chemical Society, Washington, D.C. (1971).

39. Meier, W.M., "Molecular Sieves Zeolites", American Chemical Society, Washgington, D.C. (1973).

40. Broughton, D.B. & et al., Chem. Eng. Prog., 66, 70 (1970).

41. Neuzil, R.W., U.S. Patent 3,558,732 (Jan. 26, 1971).

42. Dorodnova, V.S.; Korzhov, Y.A.; Martynenku, A.G., Chemistry and Technology of Fuels and Oils, 18 (8), 395 (1972).

43. Owaysi, F.A.; Al-Ameeri, R.S.; Abu-Naba'a, I., "Proposal on Selection of the Best Feed of Different Types of Kerosene Cuts", KISR, Nov. (1983).

44. Asher, W.J. & et al., Hydrocarbon Processing, 48 (1), 134 (1969).

45. Avery, W.F.; Lee, W.N., Oil & Gas J., 60, 23 (1962).

46. Industrial & Engineering Chemistry, 54 (5), 12 (1962).

47. Griesmer, G.J.; Avery, W.F.; Lee, M.N., Hydrocarbon Processing, 44 (6), 147 (1965).

48. Scott, K.A., Petroleum Refiner, 43 (3), 1964.

49. Yeo, A.A. & et al., Sixth World Petroleum Congress IV, 15, 161 (1963).

50. Ritzer, H. & et al., Erdole and Kohle, 22 (3), 132 (1969) (Germany).

51. Carson, D.B.; Broughten, D.B., Petroleum Refiner, 38 (4), 130 (1959).

52. Carson, D.B.; Broughton, D.B., Oil & Gas J., 57 (15), (1959).

53. Sterba, M.J.; Hydrocarbon Processing, 44 (6), 151 (1965).

54. Petroleum Refiner, 41 (9), 244 (1962).

55. Broughten, D.B.; Lickus, A.G., Petroleum Refiner, 40 (5), 173 (1961).

56. Franz, W.F. & et al., Oil & Gas J., 57 (15), 116 (1959).

57. Franz, W.F. & et al., Petroleum Refiner, 38 (4), 125 (1959).

58. Wehner, K. & et al., Ropa a White, 6, 289 (1968) (Czech.).

59. Wehner, K. & et al., Chem. Tech., 19 (7), 385 (1967).

60. Wehner, K.; Kaufman, H.; Seidel, G., "Conference on the Chemistry & Chemical Processing of Petroleum & Natural Gas", 452 (1965) (Germany).

61. Grebbel, J., British Patent 1510705, May 17, 1978.

62. Anstey, R.H.; Macnab, R.M., British Patent 1026116, April 14, 1966.

63. Turnbull, J.N.; Gilbert, R.J., British Patent 1110494, April 18, 1968.

64. Wanlers, G.J., U.S. Patent 3922218, November 25, 1975.

65. Perry, R.H.; Chilton, C.H., "Chemical Engineers' Handbook", 5th Edition, McGraw-Hill, N.Y., 1973.

66. Powers, J.M.; Corer, D.E., U.S. Patent 3378486, April 16, 1968.

67. Lauder, B.T.; Rolfe, J.R., U.S. Patent 4069142, January 17, 1978.

68. Savage, D.W. & et al., U.S. Patent 3418235, December 24, 1968.

69. Philips, J.R., Ind. Eng. Chem. Proc. Des. Dev., 9 (3), 484 (1970).

70. Philips, J.R., Chem. Eng. Prog. Symp. Series, 65 (96), 109 (1981).

71. O'Connor, J.G.; Norris, M.S., Analytical Chemistry, 32 (6), 701 (1960).

72. Flank, W.H., "Adsorption & Ion Exchange with Synthetic Zeolite, American Chemical Society, Washington, D.C. (1980).

73. Sinha, S.K.; Saraf, D.N.; Kunzru, D., ZEOLITES, 2, 175-178 (1982).

74. Michaels, A.S., Ind. Eng. Chem., 44 (8), 1922 (1952).

75. Lukchis, G.M., Chem. Eng., 111-116 (June 11, 1973).

76. Collins, J.J., Chem. Eng. Prog. Symp. Series, 63 (74), 31 (1980).

77. Rosen, J.B., Ind. Eng. Chem., 46, 1590 (1954).

78. Kehat, E.; Rosenktanz, Z., Ind. Eng. Chem. Proc. Des. Dev., 4, 217 (1965).

79. Siryuk, A.G. & et al., Translated from Khimiya i Tekhnologiya Topliv i Masel, No. 2, 58-61, February, 1975.

80. Fal'kovich, M.I.; El'tekov, Y.A.; Chernozhukov, N.I., Translated from Khimiya Technologiya Topliv i Masel, No. 12, 11-14 December, 1968.

81. Sherwood, T.K., Rigford, R.L.; Wilke, C.P., "Mass Transfer, McGraw-Hill Chemical Engineering Series, N.Y. (1975).

82. Hougen, O.A.; Watson, K.M.; Ragatz, R.A., "Chemical Process Principle - Part I - Material and Energy Balances", 2nd Ed., John Wiley & Son Inc., N.Y. (1943).

83. Fatkhi, A. & et al., Translated from Khimiya Tekhnologiya Topliv i Masel, No.2, 39-42, February, 1981.

84. Sterba, M.J., "Recovery of Normal Paraffins by the Molex Process", Proc. Am. Petrol. Inst., Sect. III, 45, 3 (1966).